BULLETIN OF THE UNIVERSITY OF UTAH

Volume 52 October 1961 No. 29

Bulletin No. 108

of the

UTAH ENGINEERING EXPERIMENT STATION

GRAVITY FLOW OF BULK SOLIDS

by

A. W. Jenike

Salt Lake City, Utah

PREFACE

There is hardly an industry in existence which does not use solid materials in bulk form. Where the volume of the solids is substantial, gravity is usually relied upon to cause the solids to flow. Such materials as ores, coal, cement, flour, cocoa, soil, to which the general term of bulk solids is applied, flow by gravity or are expected to flow by gravity in thousands of installations and by the billions of tons annually. Mining relies on gravity flow in block-caving and in ore passes; subsidence is a case of gravity flow of solids. Agriculture relies on gravity flow of its products in storage silos, in feed plants and on the farms. Every type of processing industry depends on gravity flow of some solid, often of several solids.

Although vast quantities of bulk solids have been handled for many years, the author believes that this is the first comprehensive study of the subject. The fact that this work appears at this time is not accidental, but stems from the progress achieved during the past fifteen years in the mathematical theory of plasticity and in the techniques of numerical calculation. On the basis of recently developed and refined principles of plasticity, the problem of flow of bulk solids has been set up in mathematical terms. A few years ago, this would not have been possible; just as a few years ago the mathematically formulated problem would have been practically insoluble because there were no computers to carry out the necessary

calculations.

The careful reader of the author's previous reports and papers on the subject of flow of bulk solids will notice substantial modifications in the design formulae. No apology is offered for these seeming inconsistencies; the author has always approached the subject from the standpoint of the engineer who has had to provide definite recommendations on the basis of information at hand, at the time. Hence, as the volume of experience increased, the theory was developed, and the numerical data were computed, the design methods improved and changed - at times, radically.

The work is presented in six parts. In Part I, the yield function applicable to bulk solids is described, and the flow properties of bulk solids are defined. The solids are assumed to be rigid-plastic, isotropic, frictional, and cohesive. During incipient failure, the solids expand (dilate), during steady state flow, they may expand or contract. The yield function is consistent with the principle of normality [7] which is specifically applied in incipient failure.

Part II contains the theory of steady state gravity flow of solids in converging and vertical channels. The equations are first derived in a general form, applicable to problems of extrusion as well as gravity flow, in plane strain and in axial symmetry. Some of the derivations are more general than they need to be for this work. They will be referred to in other publications which are now in preparation [22, 23]. It is shown that, provided the slopes of the walls of a converging channel are sufficiently steep and mathematically

continuous, the stress pattern in the neighborhood of the vertex of the channel is, primarily, a function of the slope and of the frictional conditions of the walls at the vertex, with the influence of the top boundary of the channel vanishing at the vertex. The particular stress field which develops at the vertex is called the radial stress field, because it is the field which can lead to a radial velocity field.

Since the radial stress field is closely approached in the vicinity of the vertex, that field represents the stresses at the outlet of a channel. The region of the outlet of a channel is most important because it is there that obstructions to flow originate. The radial stress field thus provides a basis for a general solution of flow in this important region of the channels.

In Part III, the conditions leading to incipient failure are considered. General equations of stress are derived in plane strain and in axial symmetry. The conditions following incipient failure are discussed, and it is suggested that the velocity fields usually computed for conditions of failure are meaningless and that only initial acceleration fields can be computed. Two cases of incipient failure are analyzed: doming across a flow channel, and piping (which refers to a state of stress around a vertical, empty hole of circular cross-section).

Part IV describes the flow criteria. The material developed in the previous three parts is brought together to relate the slopes of channels and the size of the outlets necessary to maintain the flow of

a solid of given flowability on walls of given frictional properties.

Part V describes the testing apparatus and the method which has been developed to measure the flowability of solids, their density, and the angle of friction between a solid and a wall.

Finally, Part VI contains the application of the theory to the design of storage installations and flow channels, and discusses flow promoting devices, feeders, segregation, blending, structural problems, the flow of ore, as well as aspects of block-caving and miscellaneous items related to the gravity flow of solids. All these topics are approached from the standpoint of flow: their effect on flow and vice-versa.

The reader will soon realize that many of the bins now in operation have been designed to fill out an available space at a minimum cost of the structure rather than to satisfy the conditions of flow. The result has been a booming business for manufacturers of flow promoting devices. While there are, and always will be, solids which are not suitable for gravity flow, the vast majority of them will flow if the bins and feeders are designed correctly. However, a correct bin will usually be taller and more expensive. It is up to the engineer to decide whether the additional cost of the correct bin will be balanced by savings in operation.

This part is made as self-contained as possible to facilitate its reading to the engineer who has neither time nor inclination to study the theoretical parts.

The reader versed in soil mechanics should note that the magnitude

of the stresses discussed here is 100 to 1000 times smaller than that encountered in soil mechanics. Hence, some phenomena which may not even be observable in soil mechanics assume critical importance in the gravity flow of solids. For instance, the curvature of the yield loci (Mohr envelopes) in the (σ,τ) coordinates is seldom detectable in soil mechanics, but in gravity flow the curvature assumes an important role in the determination of the flowability of a solid. By the terminology of soil mechanics, solids possessing a cohesion of 50 pounds per square foot are cohesionless: standard soil mechanics tests do not measure such low values. But a solid with that value of cohesion, an angle of internal friction of 30°, and a weight of 100 pounds per cubic foot can form a stable dome across a 3-foot-diameter channel and prevent flow from starting. In gravity flow, it is of interest to be able to predict whether or not flow will take place through a 6-inch-diameter orifice. This involves values of cohesion down to 8 pounds per square foot and even less for lighter solids.

ACKNOWLEDGEMENTS

The work described in this report has been carried out over a period of some nine years, and during that time the author has become indebted to a number of persons who have contributed of their time and skills, and to a number of institutions which for the past five years have given financial support to the project.

The author is particularly grateful to Dr. P. J. Elsey of the Utah Engineering Experiment Station for his constant and sympathetic interest in the project, and to Dr. Elsey and Professor R. H. Woolley for their assistance in setting up the Bulk Solids Flow Laboratory at the University of Utah; to Professor R. T. Shield of Brown University for the many long discussions of the topics of plasticity and for his critical revues of the work at various stages of advancement. The author is very much in debt to his students: Joseph L. Taylor, who has contributed of his mathematical skill, and, especially, Jerry R. Johanson, whose constant assistance in every facet of the work has been most useful. Mr. Johanson, a Ph.D. candidate, also carried out all of the numerical calculations which this work required.

The cost of this project has been substantial and the author wishes to acknowledge the initial support which he received from the American Institute of Mining Mineralogical and Petroleum Engineers, whose Mineral Beneficiation and Research Committees promptly recommended the author's application for AIME sponsorship. This was followed by a grant of money from Engineering Foundation and by the further support from research funds of the Utah Engineering Experiment Station.

The AIME and the Engineering Foundation have remained sponsors of the project.

Sincere thanks are due to Dr. Carl J. Christensen, director of the Utah Engineering Experiment Station, for his help in keeping the project alive through times of financial difficulty.

The main support for the applied part of the project, entitled "Bulk Solids Flow", has come from the American Iron and Steel Institute, to whom the author is most grateful.

The mathematical concepts described in this report, as well as other work which is appearing separately, have been developed under a 1959 grant from the National Science Foundation to a project entitled: "Flow of rigid-plastic solids in converging channels under the action of body forces".

Andrew W. Jenike
October, 1961

CONTENTS

PART I

THE YIELD FUNCTION

Introduction

In gravity flow of solids, as in soil mechanics, it is convenient to assume pressures and compressive strain rates as positive, and tensions and expansive strain rates as negative. This convention is adopted throughout the work.

The solids which are considered in this work are rigid-plastic. In the plastic regions, the solids are assumed to be isotropic, frictional, cohesive and compressible. During incipient failure an element of a solid expands, while during steady state flow, the element either expands or contracts as does the pressure along the streamline.

While many problems of continuous plastic flow have been solved for isotropic, non-work-hardening solids with a zero angle of friction [e.g., 1,2,3,4,5], attempts to work out solutions of continuous flow of solids, which exhibit an angle of friction greater than zero, have not been successful. The cause of the difficulty has lain in the yield function ascribed to these solids. The yield function was a generalization of the criterium of either Tresca or von Mises into a function dependent on the hydrostatic stress. In the principal stress space such a generalization transformed the prism of Tresca and the cylinder of von Mises into, respectively, a pyramid and a cone,

which were assumed to be of constant size and to extend without a bound in the direction of the hydrostatic pressure. As a result, the principle of plastic potential [6], or normality [7], required the solid to dilate continuously during flow while at the same time retaining its strength properties. Continuous dilation is not supported by physical observations. Dilation implies a reduction in density which in turn causes a loss of strength and a shrinking of the yield surface.

There is ample evidence obtained from shear and triaxial tests to the effect that a solid may flow without a change of density as well as with an increase of density, and that during flow the yield surface of an element of the solid at a generic point is remarkably independent of the history of stress and strain [8].

In this work a yield surface recently proposed by Jenike and Shield [9] is used. This surface is shown in Fig. 1, in principal stress space. The abscissa $\sigma_1\sqrt{2} = \sigma_2\sqrt{2}$ is in the σ_1,σ_2-plane and bisects the angle between the σ_1,σ_2-axes. This surface is the Shield's pyramid [10] with three modifications: the pyramid is bounded on the pressure side (after Drucker [11])by a flat hexagonal base perpendicular to the octahedral axis; the size of the pyramid is a function of the density, the time interval of consolidation at rest, the temperature, and the moisture content of the solid; and the vertex of the pyramid is rounded off.

During flow, the time interval of consolidation is zero, while the temperature and moisture content are assumed constant; density is variable and is assumed a function of the major pressure at a generic

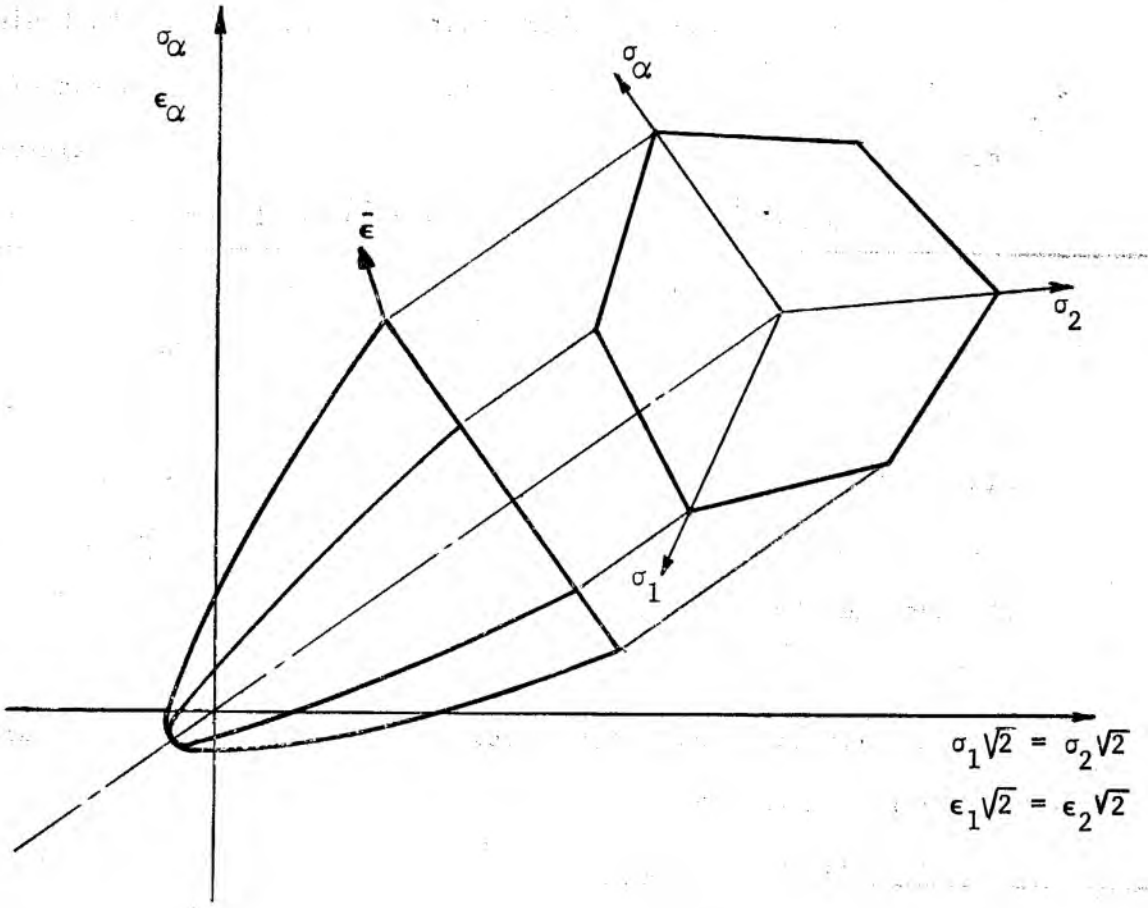

Fig. 1

Yield surface

point. In consequence, the size of the yield surface during flow is a function of the major pressure only, while the change in the size of the yield surface (and in density) of an element becomes a function of the gradient of the major pressure along the path of that element.

A change of density is measured by the normal component of the strain rate vector, which thus must be free to assume a positive or a negative direction depending on the sign of the pressure gradient, and independently of the state of stress at the generic point. The adopted yield surface allows this freedom to the strain rate vector because, during flow, the vector is located at a corner between the side walls of the pyramid and its flat, hexagonal base, as shown in Fig. 1. In the plane strain flow of an incompressible solid, normality locates the stresses on a straight side of the hexagonal base of the yield surface. In the plane strain flow of a compressible solid and in axi-symmetric flow, which involve three dimensional deformations, normality locates the stresses at a corner of the hexagonal base.

It will thus be observed that in axial symmetry the principles of isotropy and plastic potential enforce the Haar and von Karman hypothesis [12] for the adopted yield function, except possibly when the principal stresses in the meridian plane are either both major or both minor. However, the latter conditions exclude all fields with body force*, hence are useless in this work. The Haar and

* Assume the meridian pressures to be both minor, then equations (14) - (16) and (20) - (22) become

$$\sigma_x = \sigma_y = \sigma_2 = \sigma(1 - \sin\delta), \quad \tau_{xy} = 0, \quad \sigma_\alpha = \sigma_1 = \sigma(1 + \sin\delta)$$

von Karman hypothesis states that in axial symmetry the circumferential stress is equal to either the major of the minor stress of the meridian plane.

The relationship between the size of the yield surface and the major pressure during flow is described by the effective yield locus [9]. The remarkable feature of this yield function is that not only does it not complicate the analysis of the stress fields but for steady state flow it leads to a pseudo-static system without pseudo-cohesion even though the solid may be cohesive.

In the analysis of incipient failure, it will be necessary to assume a constant yield surface throughout the plastic region. This is not a serious limitation because the considered plastic regions are of small size. The stresses of incipient failure are located on the side of the yield pyramid, not on the base, and dilation accompanies failure.

The coordinate systems

In order to handle problems of plane strain and of axial symmetry with one set of equations, combined coordinates are introduced with a

and the solution of the equations of equilibrium (48) and (49), with $m = 1$, is of the form

$$\gamma = 0, \quad \sigma = \sigma_o (y/y_o)^{\frac{2 \sin \delta}{1-\sin \delta}}.$$

This requires the absence of body forces. Similar functions are obtained for two major meridian pressures, and for the conditions of incipient failure.

coefficient m to distinguish between the two systems. Coefficient

$$m = 0 \tag{1}$$

applies to plane strain, and

$$m = 1 \tag{2}$$

applies to axial symmetry.

Two systems of coordinates will be found useful: a plane-Cartesian/polar-cylindrical system x, y, α, and a polar/spherical system r, θ, α, as shown in Fig. 2. Axis x is vertical and when the problems have symmetry they are symmetric with respect to this axis. The circumferential coordinate α appears only in the problems of axial symmetry and by virtue of that symmetry all the derivatives with respect of α are zero.

The positive directions of the stresses are shown in the Figure 2. It will be noted that pressures are assumed positive. The direction of the major pressure σ_1 with respect to the axis x is measured by angle ω.

Evidently

$$\omega = \theta + \psi, \tag{3}$$

where ψ is the angle between the directions of σ_1 and of the ray r.

Two kinds of stresses are recognized:

Consolidating stresses which occur during steady state flow and are denoted by letters σ and τ, and yield stresses which occur during incipient failure and are denoted by letters $\bar{\sigma}$ and $\bar{\tau}$. In both cases the principal pressures σ_1 and σ_2 ($\bar{\sigma}_1$ and $\bar{\sigma}_2$) act in the meridian plane (x,y) or (r,θ), while the principal pressure σ_α ($\bar{\sigma}_\alpha$) is the circumferential pressure. The principal pressures are ordered as follows

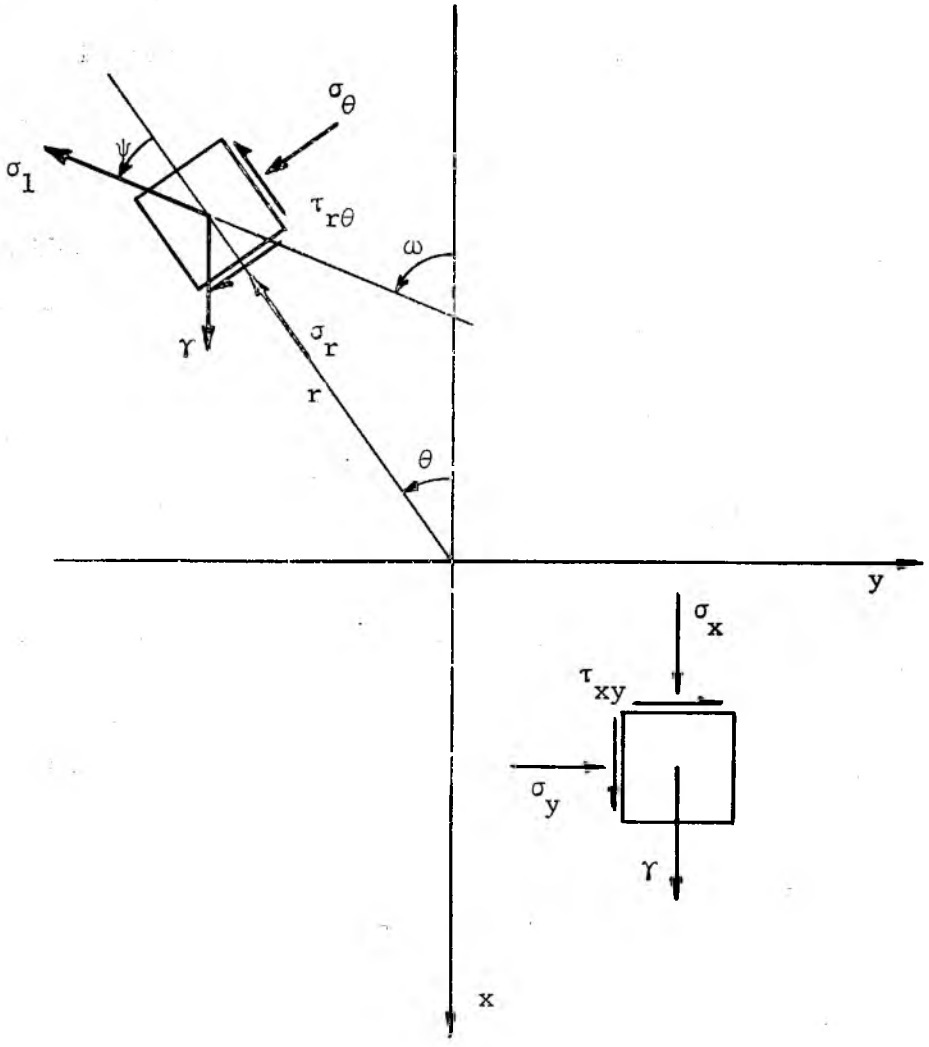

Fig. 2

Coordinate systems in plane strain

and in the meridian plane of axial symmetry

$$\sigma_1 > \sigma_2, \quad \sigma_\alpha = \sigma_1 \text{ or } \sigma_\alpha = \sigma_2. \tag{4}$$

The assumed yield function is of the following general form

$$f(\bar{\sigma}_1, \bar{\sigma}_2) = F(\gamma, t, T, H), \tag{5}$$

where γ is the bulk density of the solid, t the time interval of consolidation at rest, T its temperature, and H its surface moisture content.

It should be noted that the method by which a solid is consolidated to the given density γ may affect the yield function. For instance, a solid may be consolidated by vibration, or pounding; it may be consolidated by the application of a hydrostatic pressure, as well as by the application of pressures which are different in magnitude but whose deviator components are insufficient to cause shear. Then, and this is of main interest in our study, a solid may be consolidated under a set of pressures which cause a continuous deformation of the solid: this is the condition of flow. Finally, flow may be stopped for an interval of time t with the consolidating pressures remaining practically unchanged and with the solid undergoing additional consolidation at rest.

The bulk density of a solid is assumed to be a function of the majore consolidating pressure σ_1, as well as of the time t, the temperature T, and the moisture content H, thus

$$\gamma = \gamma(\sigma_1, t, T, H). \tag{6}$$

Effective yield locus (EYL) [9]

During steady state flow, within the regions of non-zero velocity, the solid deforms continuously without abrupt changes in bulk density, and the plastic region is uniformly at yield with yield planes passing through every point of the region. In these regions, the time interval of consolidation at rest is zero, while the temperature and moisture content can usually be assumed constant,

$$t = 0, \quad T = \text{constant}, \quad H = \text{constant}. \tag{7}$$

Density then becomes a single-valued function of the major consolidating pressure σ_1 while the yield function, eq. (5), reduces to

$$f(\bar{\sigma}_1, \bar{\sigma}_2) = F(\sigma_1). \tag{8}$$

Experimental data show that the ratio between the major and the minor consolidating pressures during flow approaches a constant value*,

$$\frac{\sigma_1}{\sigma_2} = \frac{1 + \sin \delta}{1 - \sin \delta}. \tag{9}$$

This function is called the effective yield locus (EYL), and δ is referred to as the effective angle of friction. In general, δ is a function of the temperature T and the moisture content H of the solid,

$$\delta = \delta(T,H), \tag{10}$$

but, under conditions of flow and with relations (7) in force, δ is constant.

The equation of the effective yield locus (9) can also be expressed by means of the stress components as follows

* See also reference [13], Fig. 1.2.2.

$$\sin\delta = \frac{\sqrt{(\sigma_x - \sigma_y)^2 + 4\tau_{xy}^2}}{\sigma_x + \sigma_y}, \tag{11}$$

or

$$\sin\delta = \frac{\sqrt{(\sigma_r - \sigma_\theta)^2 + 4\tau_{r\theta}^2}}{\sigma_r + \sigma_\theta}. \tag{12}$$

In principal stress space, function (9) is represented by the side OAB of Shield's pyramid [10] with its vertex at the origin, Fig. 3. This pyramid is also of hexagonal cross-section but, unlike the yield function, Fig. 1, extends into the direction of hydrostatic pressure without a base. In the (σ,τ) coordinates this function is represented by two straight lines, EYL passing through the origin and inclined at the angle δ to the σ-axis, Fig. 4. These lines are envelopes of Mohr stress circles determining the consolidating pressures σ_1 and σ_2.

Stresses and density during flow

It is convenient to introduce a mean pressure

$$\sigma = \frac{\sigma_1+\sigma_2}{2} = \frac{\sigma_x+\sigma_y}{2} = \frac{\sigma_r+\sigma_\theta}{2}. \tag{13}$$

The component stresses can now be expressed in the plane-Cartesian/polar-cylindrical coordinates by

$$\sigma_x = \sigma(1 + \sin\delta \cos 2\omega), \tag{14}$$

$$\sigma_y = \sigma(1 - \sin\delta \cos 2\omega), \tag{15}$$

$$\tau_{xy} = \sigma \sin\delta \sin 2\omega; \tag{16}$$

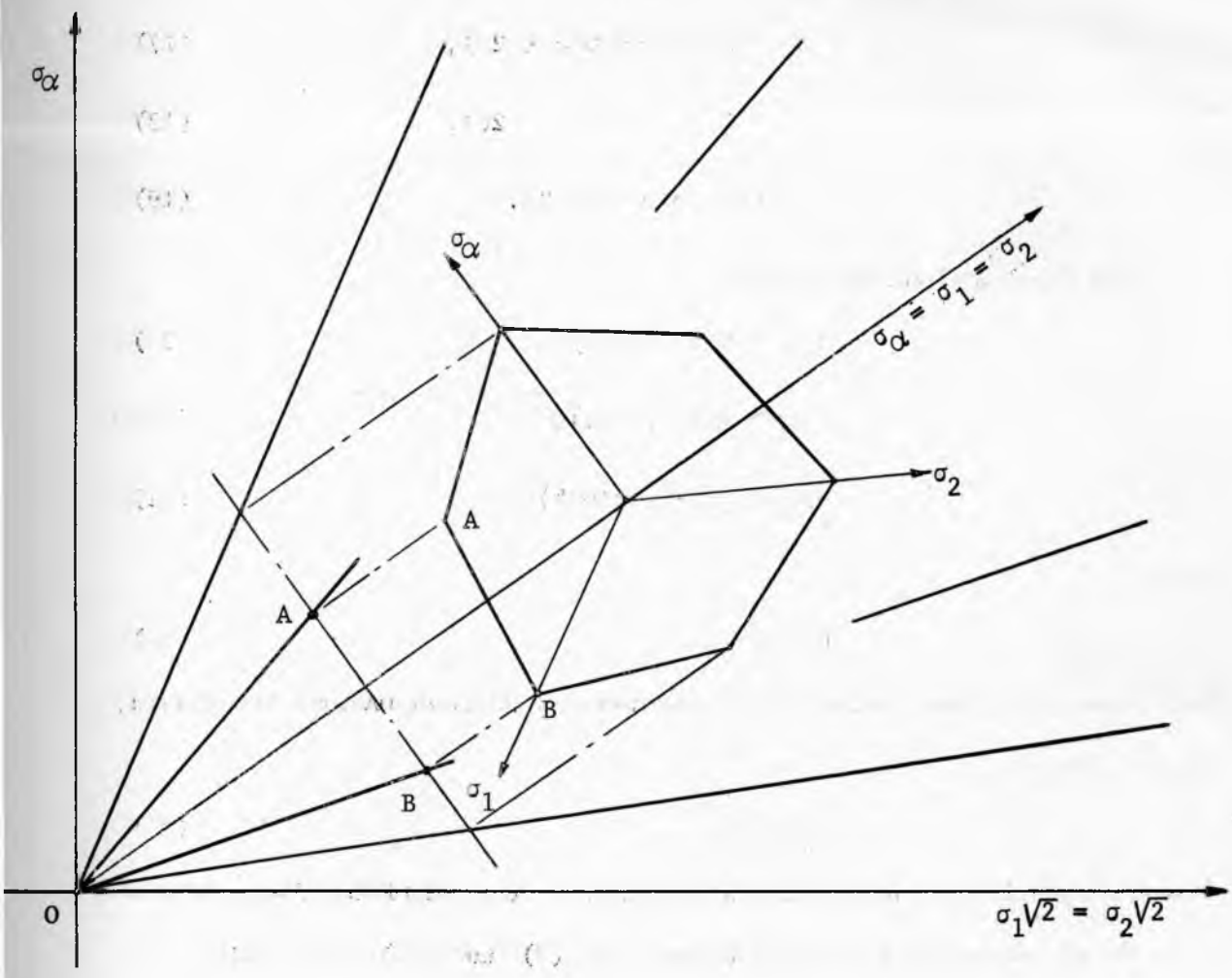

Fig. 3

Effective yield surface

and in the polar/spherical coordinates by

$$\sigma_r = \sigma(1 + \sin\delta \cos 2\psi), \tag{17}$$

$$\sigma_\theta = \sigma(1 - \sin\delta \cos 2\psi), \tag{18}$$

$$\tau_{r\theta} = \sigma \sin\delta \sin 2\psi. \tag{19}$$

The principal pressures are

$$\sigma_1 = \sigma(1 + \sin\delta), \tag{20}$$

$$\sigma_2 = \sigma(1 - \sin\delta), \tag{21}$$

$$\sigma_\alpha = \sigma(1 + k \sin\delta), \tag{22}$$

where

$$k = +1, \tag{23}$$

for converging flow, locates the stresses on the edge OA of the pyramid, Fig. 3, while

$$k = -1, \tag{24}$$

for diverging flow, locates the stresses on the edge OB of the pyramid.

On the strength of the relations (6), (7) and (20), the bulk density during flow becomes of the form

$$\gamma = \gamma(\sigma). \tag{25}$$

This relation has been found experimentally to be well represented by the equation

$$\gamma = \gamma_o(1 + \sigma)^\beta, \tag{26}$$

where γ_o and β are constant under conditions of flow. Tests show that for σ measured in pounds per square foot, β does not exceed .10. The method of measuring β is described in reference [14] and the results of

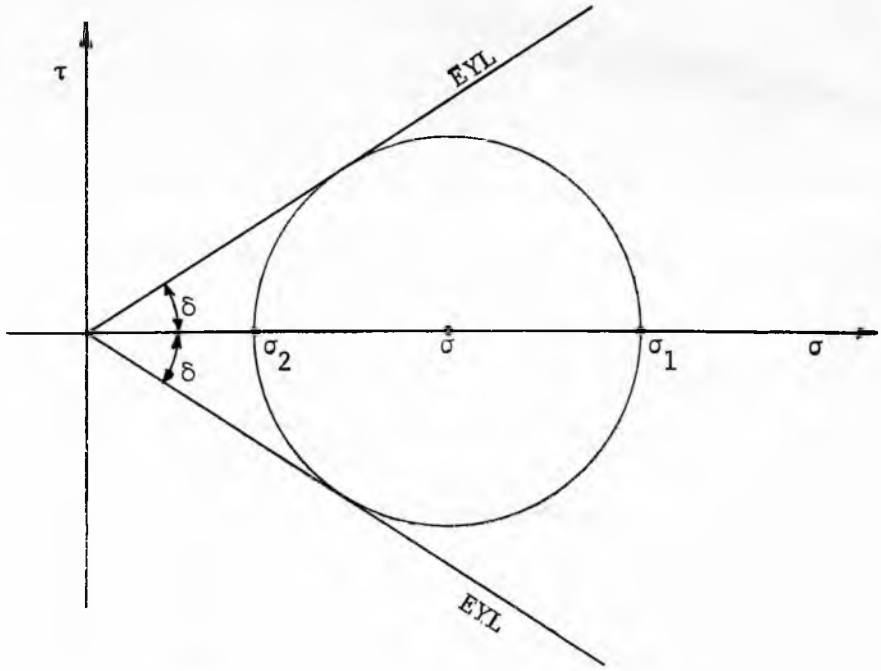

Fig. 4

Effective yield locus

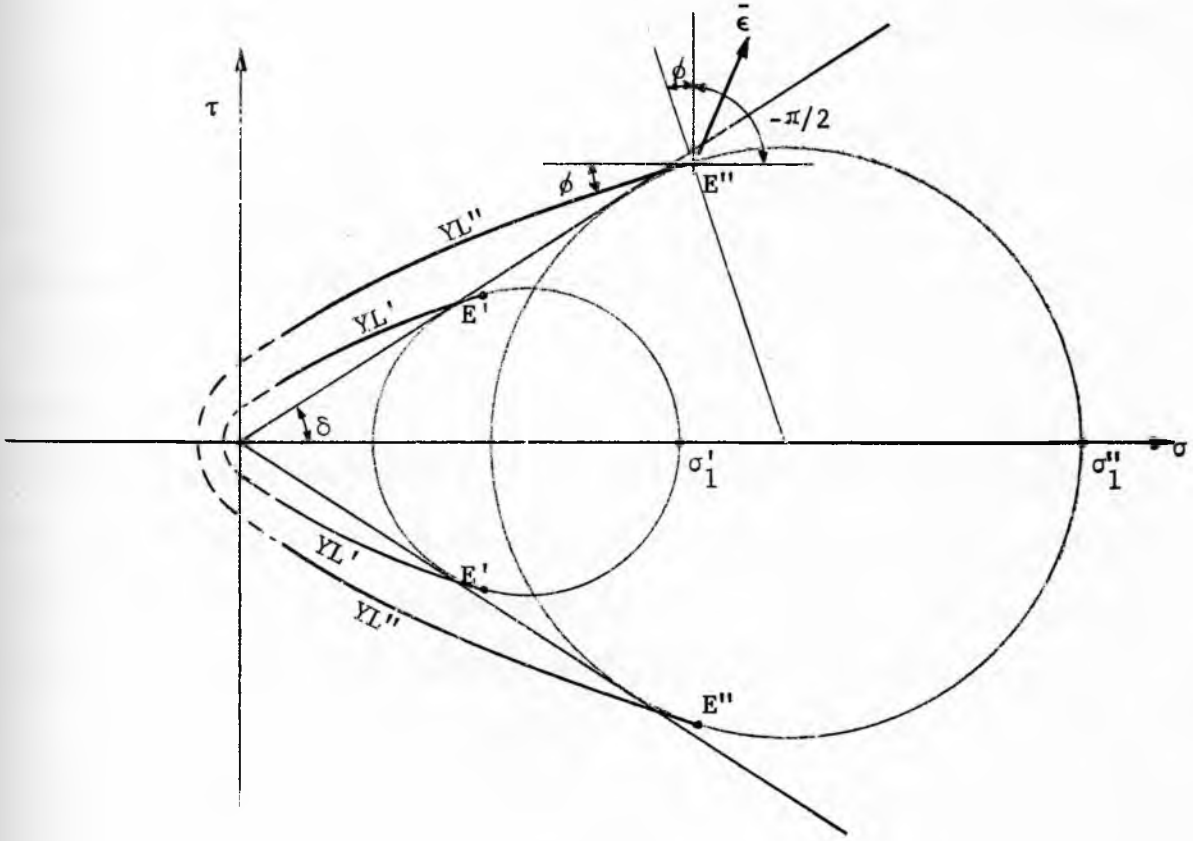

Fig. 5

Yield loci

tests for several solids for a range of major pressure σ_1 from 150 to 2,500 pounds per square foot are shown in Table 1.

Table 1

Solid	β
Adipic acid	.026
Soybean oil meal (dry)	.010
Cocoa powder	.096
Light soda ash	.017
Foundry sand	.009
Iron ore (6% H_2O)	.076
Taconite concentrate	.029
Taconite concentrate	.036
Copper concentrate (dry)	.009
Copper concentrate (5% H_2O)	.055
Feed granules	.017
Feed granules	.020

Eq. (26) leads to awkward mathematical expressions and in parts of the analysis will be replaced by

$$\gamma = \gamma_o \sigma^{\beta}. \tag{27}$$

This is justified by the fact that, in many interesting parts of a field, σ is large compared to unity, and eq. (27) is practically equivalent to eq. (26). It should be noted that with the assumption of incompressibility, $\beta = 0$, and both equations (26) and (27) yield $\gamma = \gamma_o$.

Yield locus (YL)

The yield function defined by conditions (7) and eq. (8) is represented by a family of yield loci in the (σ,τ) coordinates. The major consolidating pressure σ_1 is the parameter of the family. In Fig. 5 two yield loci denoted YL' and YL" are shown; these yield loci were generated by the major consolidating pressures σ_1' and σ_1''.

The properties of a yield locus, Fig. 6, will now be discussed in some detail. The stresses acting in a cross-section of a solid are described by a stress vector whose component are: the normal pressure $\bar{\sigma}$ and the shear stress $\bar{\tau}$. The yield locus is the locus of the values of $(\bar{\sigma},\bar{\tau})$ at which permanent deformation, or yield, occurs. In plasticity, the equations of equilibrium are assumed satisfied, therefore, the stresses described by the yield locus cannot be exceeded. This implies that the yield locus is the envelope of the Mohr stress circles at yield.

For any stress condition represented by a Mohr circle A, not touching the yield locus, the solid is rigid (or elastic). When the stress condition changes so that the corresponding Mohr circle A' comes in contact with the yield locus, yield stresses, described by the points B, develop in the two planes of the solid inclined at angles $\pm(\pi/4 - \phi/2)$ to the direction of the major pressure $\bar{\sigma}_1$, and the solid deforms. These two planes are called the slipplanes, and are represented by two sliplines in the principal, physical plane x-y, Fig. 7. Angle ϕ is the angle of friction of the solid.

The strain rate which accompanies a yield stress is described by

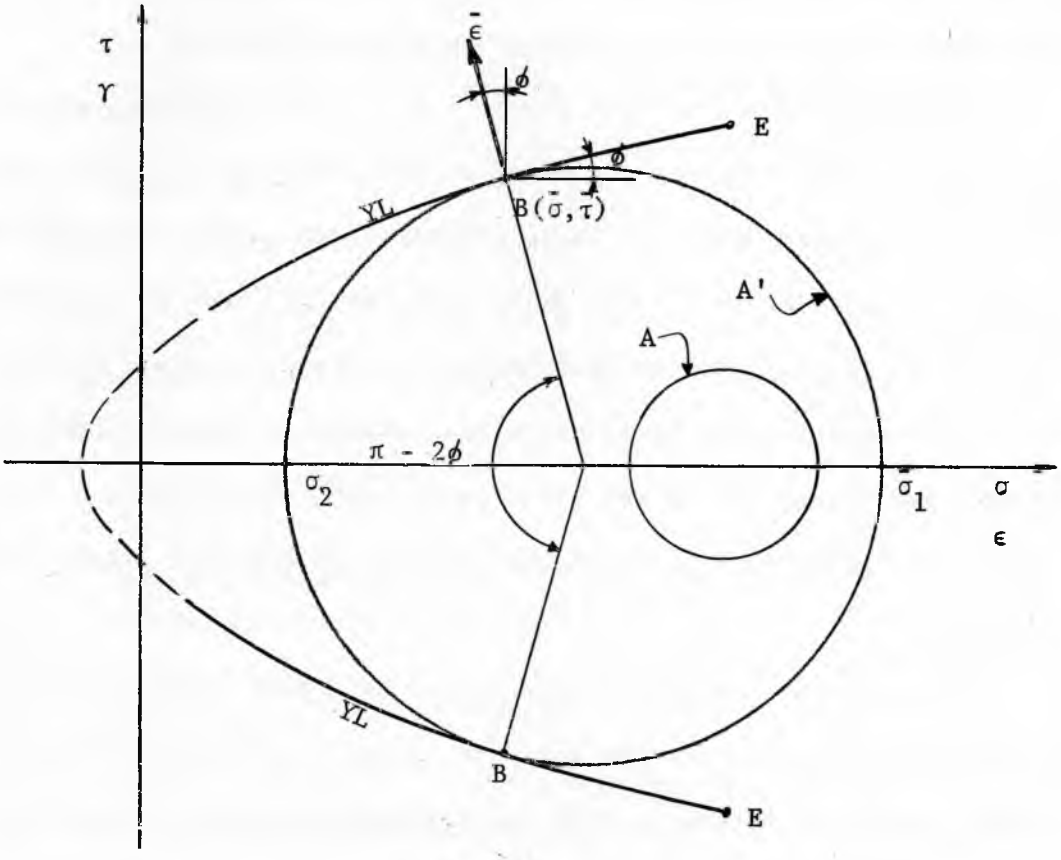

Fig. 6

Yield locus

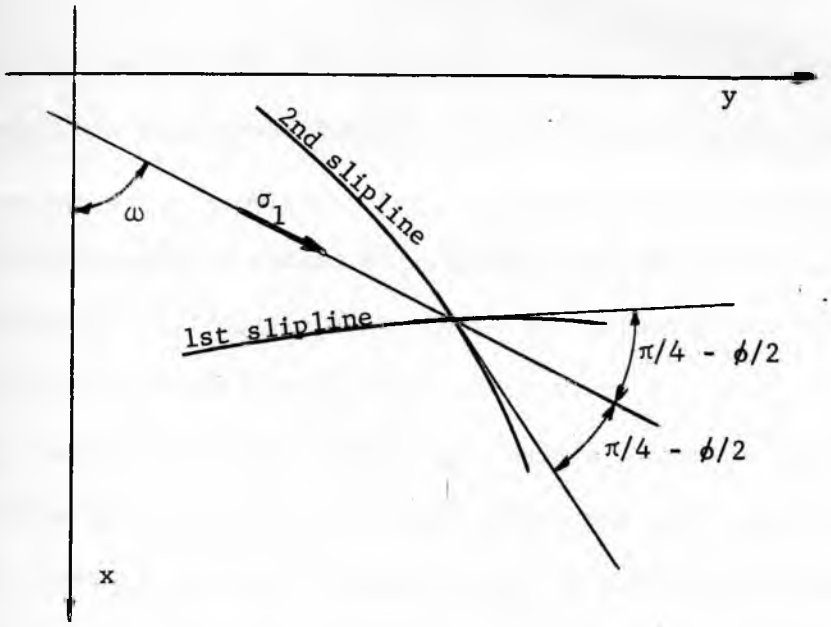

Fig. 7

Sliplines

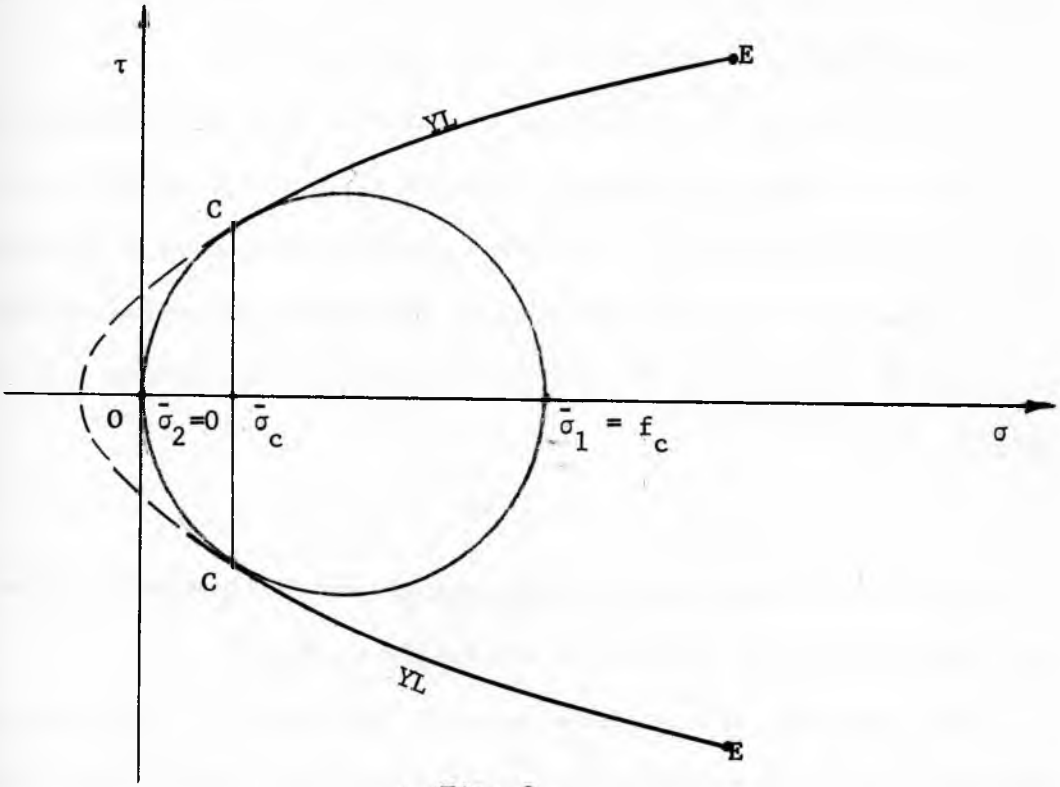

Fig. 8

Unconfined yield pressure, f_c

the strain rate vector $\bar{\epsilon}$, whose components are: the normal strain rate ϵ and the shear strain rate γ. If the coordinates (ϵ,γ) are superimposed over the coordinates (σ,τ), Figures 5 and 6, then by the principle of normality [7], the strain rate vector $\bar{\epsilon}$ is normal to the yield locus at the point of contact with the Mohr stress circle. It is evident from Fig. 6 that any point of contact, B, enforces a direction of the strain rate vector which contains a negative, hence expansive, normal component of strain rate and, therefore, implies dilation of the solid. The only exception is point E, the terminus of the yield locus, at which normality only restricts the direction of the strain rate vector to within a sector ϕ, $-\pi/2$, shown in Fig. 5. When the Mohr circle is tangential to the yield locus at point E, normality allows the solid either to dilate, or to contract, or to deform without change of density. This is the condition which occurs during steady flow.

It is observed that the angle of friction ϕ is not constant along the yield locus but varies from a minimum at points E to $\pi/2$ at the intercept with the σ-axis. The shape of the yield locus at low values of $\bar{\sigma}$ is important in this work because it affects the value of the major pressure f_c which causes failure at a traction free surface. f_c is defined thus

$$\bar{\sigma}_2 = 0, \qquad \bar{\sigma}_1 = f_c. \tag{28}$$

f_c is called the unconfined yield pressure and is obtained by inscribing a Mohr yield circle through the origin O, Fig. 8.

The curvature of the yield locus at low values of $\bar{\sigma}$ is not generally recognized and lacking complete experimental verification, the following

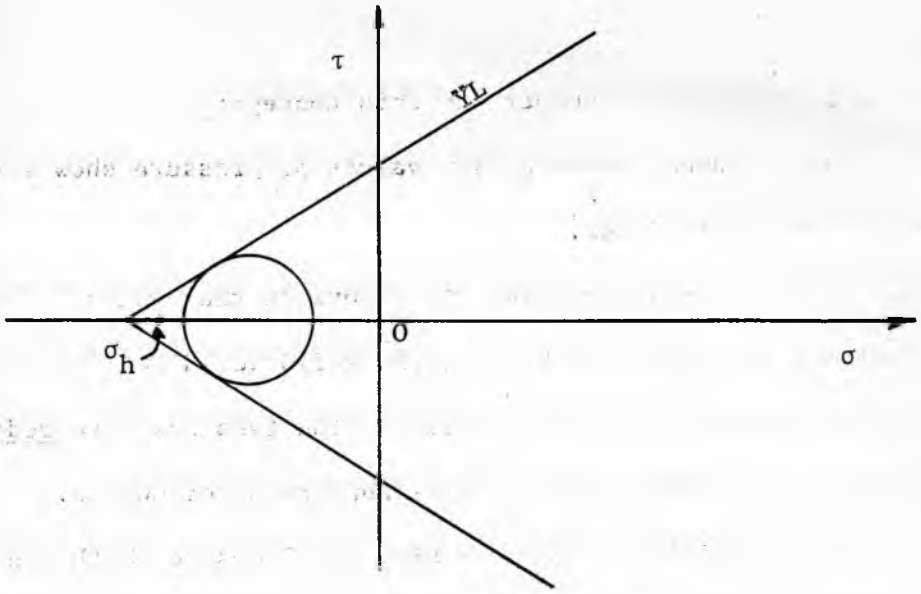

Fig. 9

Unlikely shape of the yield locus

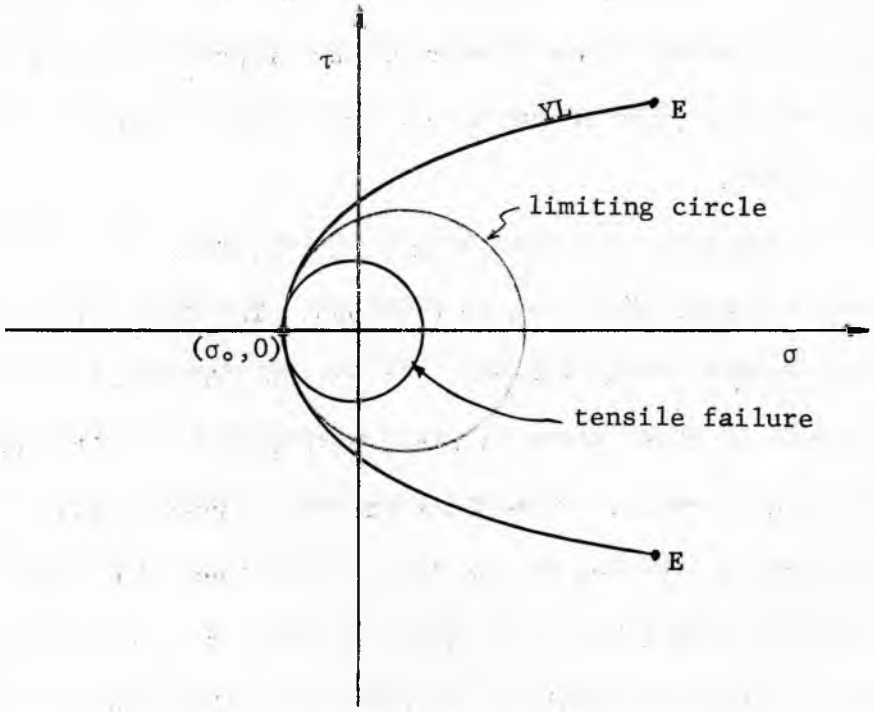

Fig. 10

Tensile (brittle) failure

arguments are offered in support of this concept:

(a) Direct shear tests at low values of pressure show a downward curving of the yield locus.

(b) If the yield locus were to intersect the σ-axis at an angle other than $\pi/2$, as shown in Fig. 9, the solid would be stable under a hydrostatic tension $\bar{\sigma}_h$ but would fail if the tensions were reduced to those given by the Mohr circle. This appears unreasonable.

(c) The yield locus shown in Fig. 10 allows for both, tensile (brittle) failure, and shearing failure of the solid. Namely, there exists a limiting circle of a radius equal to the radius of curvature of the yield locus at point $(\bar{\sigma}_o, 0)$ such that all stress conditions represented by circles within the limiting circle approach the yield locus at point $(\bar{\sigma}_o, 0)$, where the shear stress is zero, causing failure in tension; all other stress conditions are represented by Mohr circles which approach the yield locus at non-zero values of shear, causing failure in shear.

(d) The failure of a dome over a cavity, Fig. 11, often proceeds in successive stages which can be observed. The domes are usually smooth and rounded off at the top. At the two abutments of a dome, failure occurs in shear along slipines belonging to a different family at each abutment. From observations it appears that these sliplines merge at the top of the dome. Sliplines of different families are inclined to each other at an angle of $\pi/2 - \phi$. In order for these sliplines to merge, the angle of friction ϕ at the point of mergence must equal $\pi/2$. It seems that, at the top of the dome, failure does

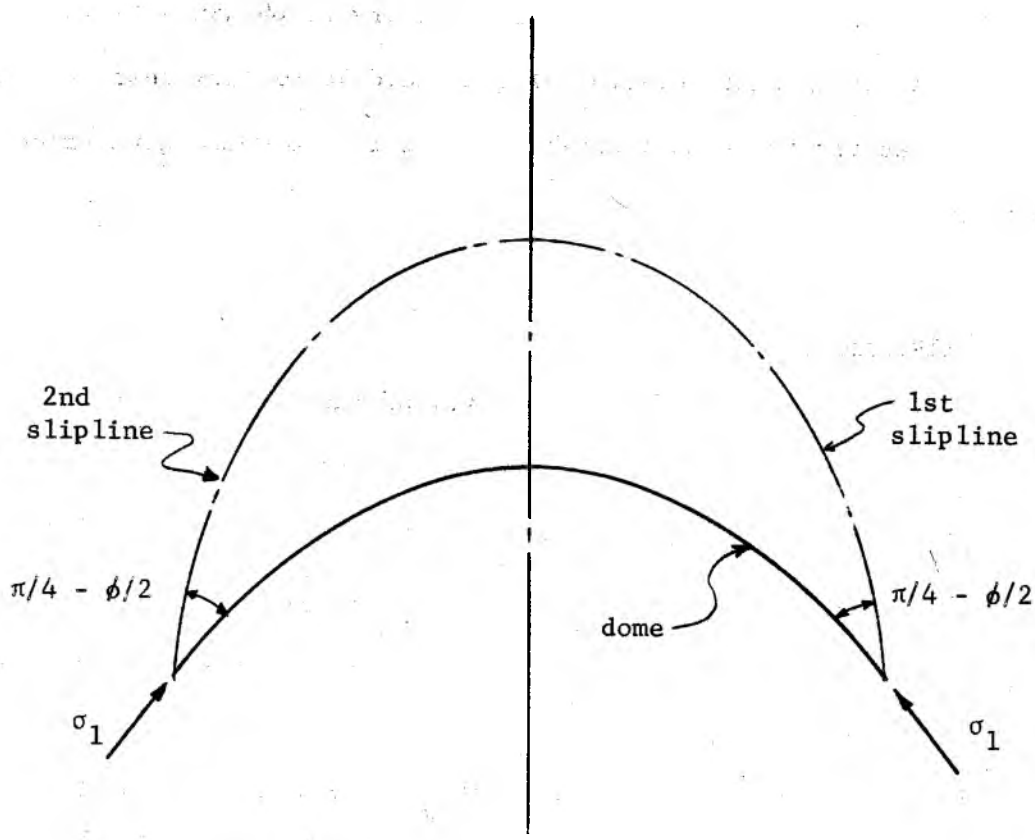

Fig. 11

Failure of a dome

occur in tension, and $\phi = \pi/2$.

It is evident that an accurate determination of the value of the yield locus at point C, Fig. 8, is necessary to obtain a reliable value of f_c. A linear extrapolation of the yield locus from test values obtained at pressures considerably higher than C would give erroneous results.

Time yield locus (TYL)

If flow is stopped for an interval of time t, the consolidating pressures remain practically unchanged and the solid undergoes further consolidation at rest. This may cause an expansion of the yield loci throughout the solid. The new yield loci are called time yield loci. A typical time yield locus (TYL), together with a yield locus (YL), is shown in Fig. 12.

It should be remembered that both, temperature and moisture content, are parameters in the yield function (5) and, if either of them should change during the time of consolidation, the position of the time yield locus may be affected.

Stresses during failure

In order to express the stresses during failure in a tractable form, the yield locus of Fig. 6 is linearized as shown in Fig. 13. In linearization, the value of f_c and the size and position of the consolidating stress circle are left unchanged. The stresses can now be expressed in the plane-Cartesian/cylindrical-polar coordinates

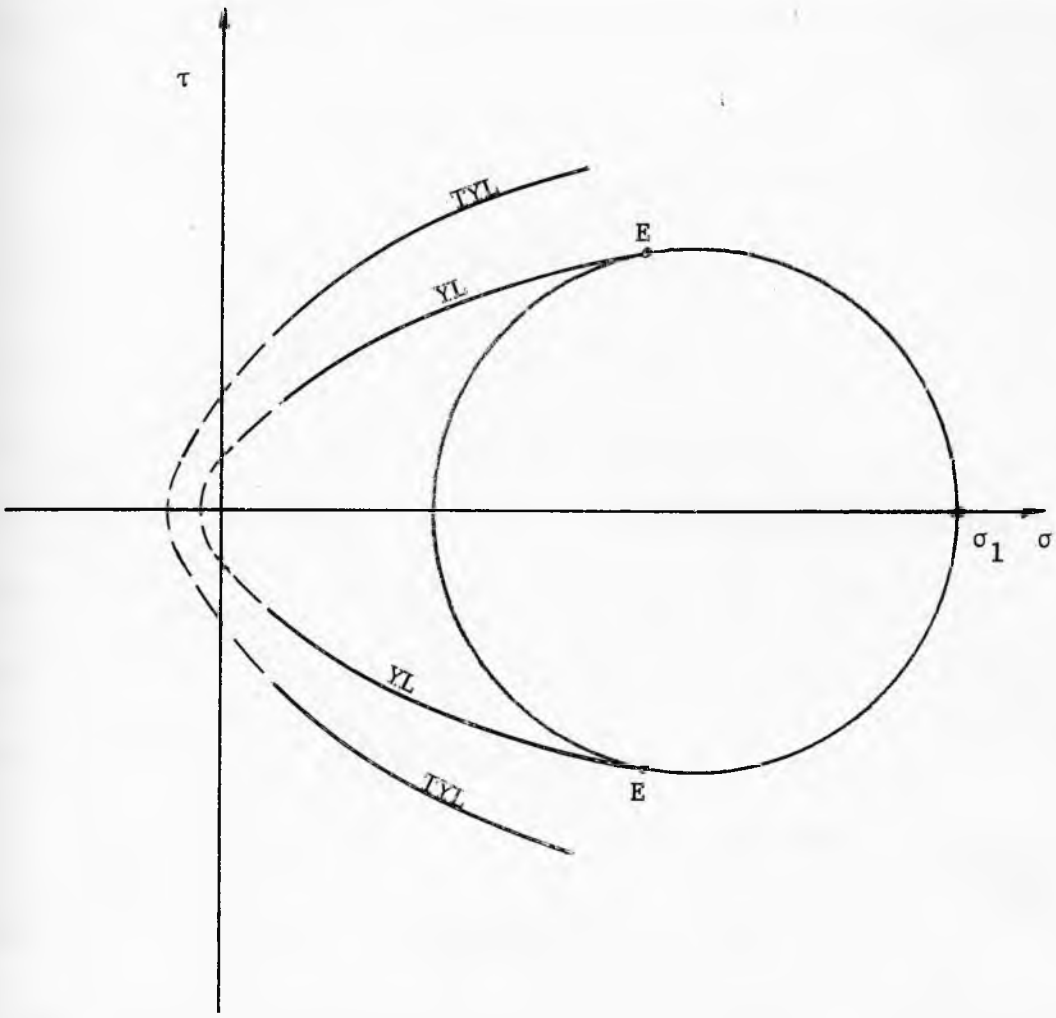

Fig. 12

Time yield locus

by

$$\bar{\sigma}_x = \bar{\sigma}(1 + \sin\phi \cos 2\omega) - f_c \frac{1 - \sin\phi}{2 \sin\phi}, \tag{29}$$

$$\bar{\sigma}_y = \bar{\sigma}(1 - \sin\phi \cos 2\omega) - f_c \frac{1 - \sin\phi}{2 \sin\phi}, \tag{30}$$

$$\bar{\tau}_{xy} = \bar{\sigma} \sin\phi \sin 2\omega; \tag{31}$$

and in the polar/spherical coordinates, by

$$\bar{\sigma}_r = \bar{\sigma}(1 + \sin\phi \cos 2\psi) - f_c \frac{1 - \sin\phi}{2 \sin\phi}, \tag{32}$$

$$\bar{\sigma}_\theta = \bar{\sigma}(1 - \sin\phi \cos 2\psi) - f_c \frac{1 - \sin\phi}{2 \sin\phi}, \tag{33}$$

$$\bar{\tau}_{r\theta} = \bar{\sigma} \sin\phi \sin 2\psi. \tag{34}$$

The principal pressures are

$$\bar{\sigma}_1 = \bar{\sigma}(1 + \sin\phi) - f_c \frac{1 - \sin\phi}{2 \sin\phi}, \tag{35}$$

$$\bar{\sigma}_2 = \bar{\sigma}(1 - \sin\phi) - f_c \frac{1 - \sin\phi}{2 \sin\phi}, \tag{36}$$

$$\bar{\sigma}_\alpha = \bar{\sigma}(1 + k \sin\phi) - f_c \frac{1 - \sin\phi}{2 \sin\phi}. \tag{37}$$

In the above equations

$$\bar{\sigma} = \frac{\bar{\sigma}_1 + \bar{\sigma}_2}{2} + f_c \frac{1 - \sin\phi}{2 \sin\phi}, \tag{38}$$

and $k = +1$ for converging failure, and $k = -1$ for diverging failure, the same as for flow.

Flow-function

The concept of the flow-function is introduced as a measure of the flowability of solids. This concept is obtained by substituting relation (6) for γ in eq. (5), and by placing the minor yield pressure

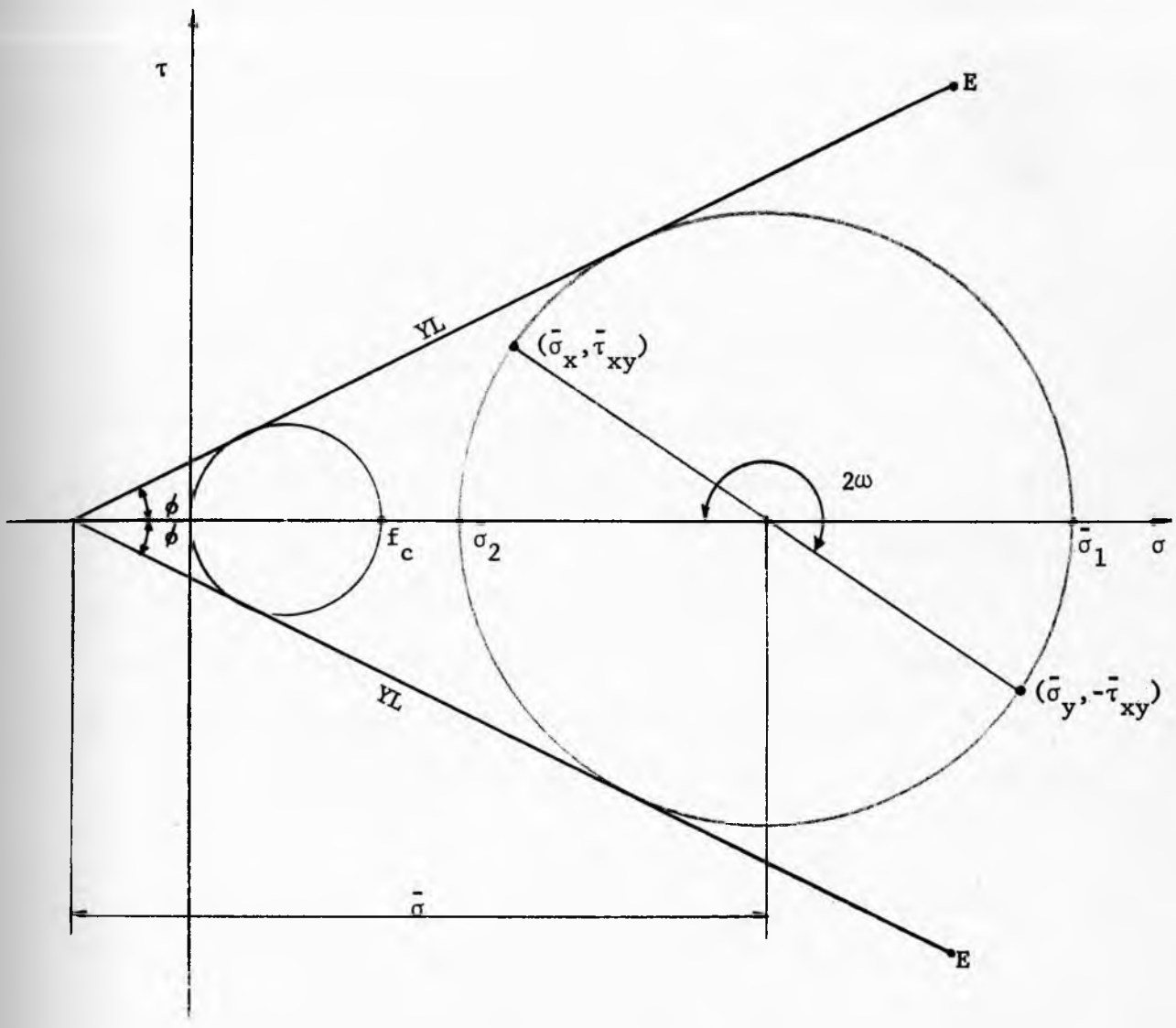

Fig. 13

Linearized yield locus

$\bar{\sigma}_2 = 0$. The corresponding value of the major pressure is the unconfined yield pressure f_c, eq. (28). Eq. (5) then assumed the form

$$f_c = G(\sigma_1, t, T, H), \tag{39}$$

and this relation is called the flow-function of a solid. It is usually plotted as

$$f_c = f_c(\sigma_1), \tag{40}$$

Fig. 14, with t, T and H as parameters.

A flow-function measured without consolidation at rest (t = 0) is referred to as the instantaneous flow-function, while a flow-function measured with consolidation at rest ($t \neq 0$) is referred to as the time flow-function.

Low values of f_c indicate a high flowability of the solid, and vice versa. In particular, a perfectly free flowing solid is one whose f_c is zero for all values of the major consolidating pressure σ_1. In Fig. 14 such a flow-function line coincides with the σ_1-axis.

Flowfactor ff

The concept of the flowfactor is introduced as a measure of the flowability of channels. The flowfactor ff is defined as the ratio

$$ff = \frac{\sigma_1}{f_c}, \tag{41}$$

and represented by a straight line in the (σ_1, f_c) coordinates, Fig. 15. In the design for no-piping an instantaneous flowfactor and a time flowfactor are used. The former applies to solids which are not

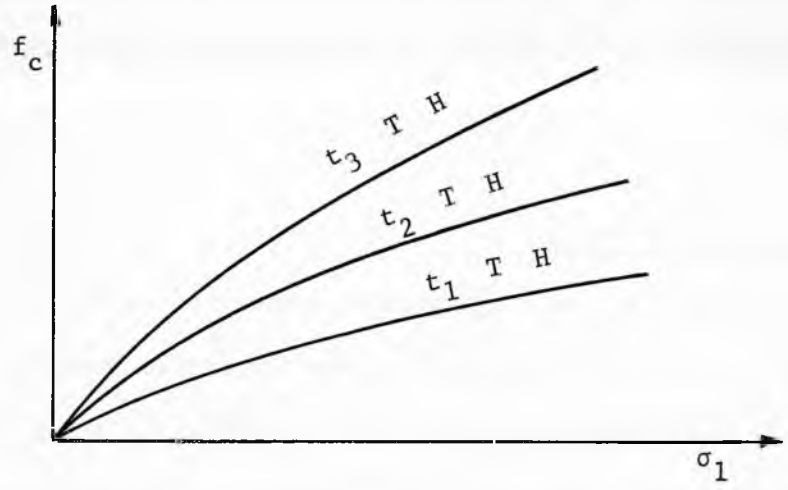

Fig. 14

Flow-function

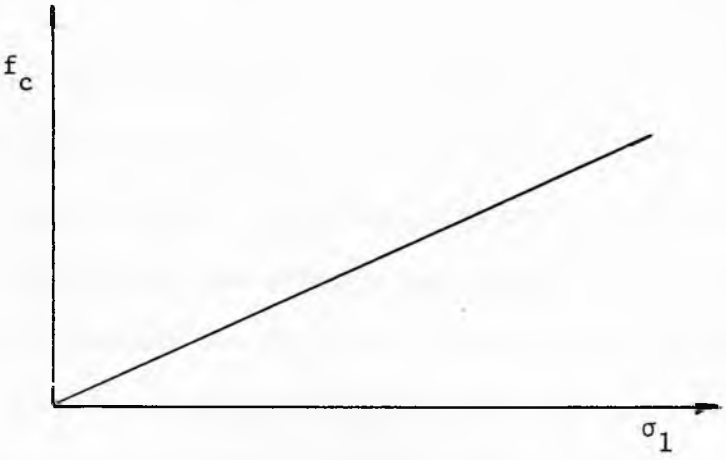

Fig. 15

Flowfactor

affected by consolidation at rest, while the latter applies to those whose time flow-function exceeds the instantaneous flow-function by, say, 20%.

Wall yield locus (WYL)

A side boundary between a region in a plastic state of stress and a rigid (or elastic) stationary region is called a wall. In general, there is a velocity discontinuity along a wall, the wall frictional strength is fully mobilized, and the stresses acting on the wall lie on a wall yield locus, which is represented by a line WYL in the (σ,τ) coordinates, Fig. 16. Since the solid is in a plastic state, the stresses at the wall lie at one of the points of intersection W of the wall yield locus with a Mohr stress circle tangential to the yield locus of the solid, YL. During flow, the circle is tangential to the yield locus at the points E and is also tangential to the effective yield locus (not shown in Fig. 16).

The position of the wall yield locus depends on the frictional conditions at the wall. These conditions may range from perfectly smooth (in concept, at least) to the full strength of the flowing solid. In the former case, the wall yield locus is represented by the positive part of the σ-axis, the stresses at the wall are defined by one of the points M, and the wall can transfer no shear stress. In the latter case, the wall yield locus merges with the yield locus of the solid and the stresses at the walls are given by one of the points E (or points B in incipient failure). Such a wall will be referred to as a

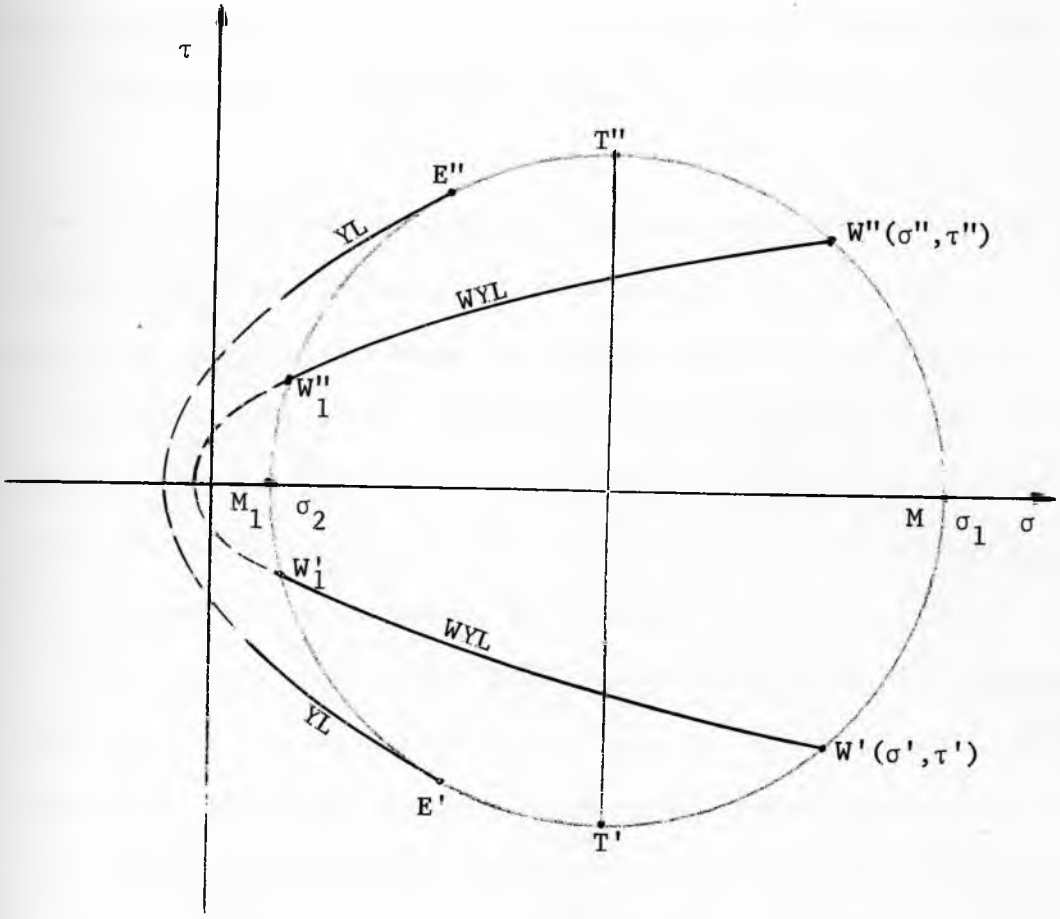

Fig. 16

Wall yield locus

"rough wall". A rough wall is a slipline.

The wall yield locus shown by line WYL in Fig. 16 denotes a degree of weakness of the wall as compared to a rough wall and such a wall will be referred to as a "weak wall".

In this work, the stresses at the walls assume values which lie on the arc E'ME", hence the stresses at a weak wall are represented either by point W' or W".

Observations of flow patterns in models and measurements of wall yield loci indicate that the introduction of a wall made of an extraneous material, even a coarse material, causes a significant drop in the cohesive and frictional forces at the wall. There seems to be no practical way of gradually decreasing the weakness of a wall by, say, increasing its coarseness until the wall yield locus merges with the yield locus of the solid. Experiments indicate that for weak walls the points W locate within the arc T'MT" of the Mohr stress circle, and that the wall yield locus can be linearized without a significant loss of accuracy. Since linearization reduces the amount of testing necessary to define the wall yield locus, and greatly simplifies the analysis, it will be adopted in this work. The position of a wall yield locus becomes thus fully determined by the magnitude of the angle of friction ϕ' between a solid and a wall.

In plane strain the channel may be asymmetric and the frictional conditions at each wall may be different, as shown in Fig. 17. In this case, the relations have to be developed separately for each wall. The values relating to a point of a wall inclined at angle θ' to the

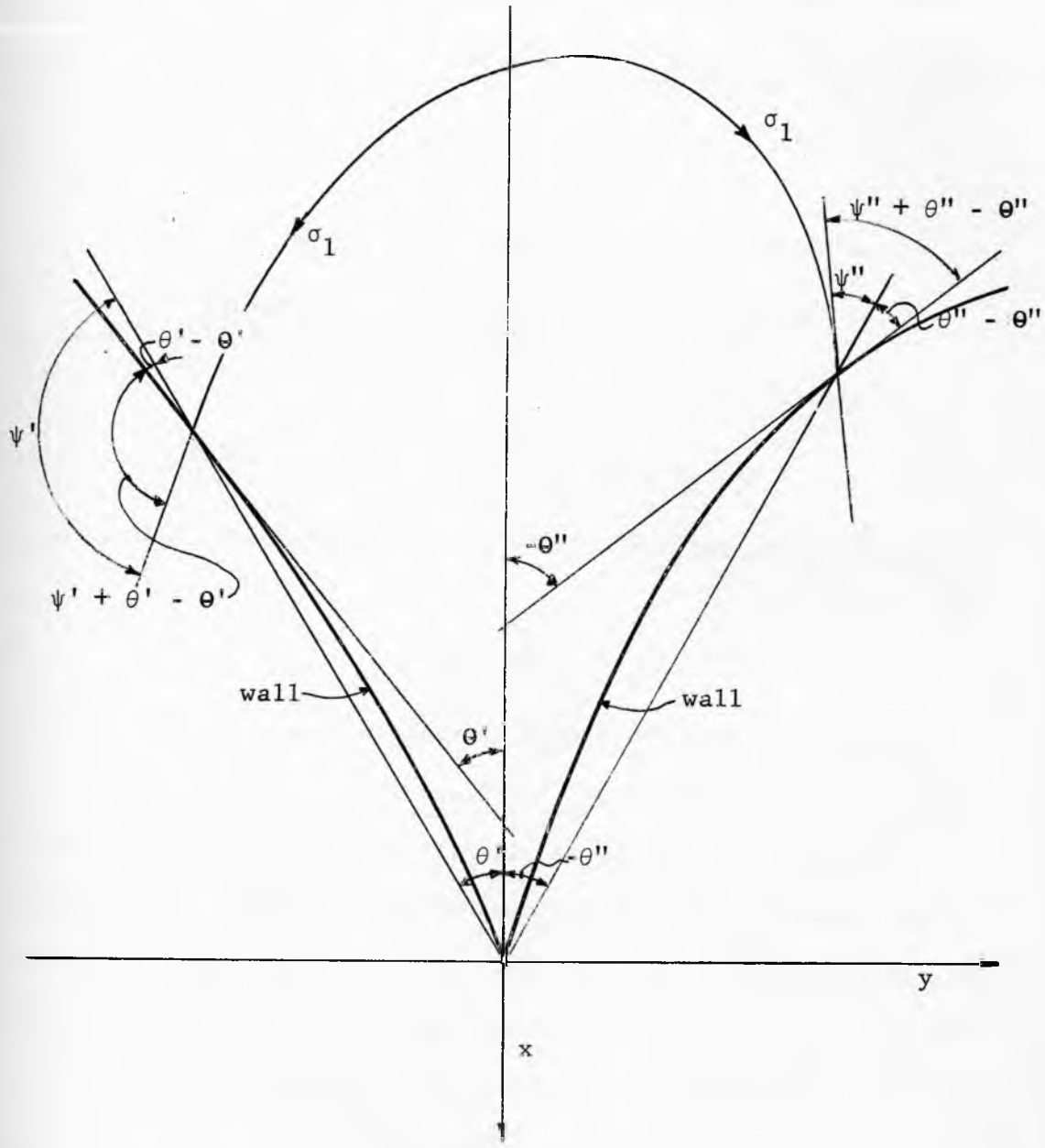

Fig. 17

Wall conditions

x-axis are denoted by primes. The corresponding part of the Mohr stress circle and the yield loci are shown in Fig. 18 (a), the wall yield locus is determined by the angle of friction ϕ'. The relation between the stresses at the wall are

$$\frac{\tau'}{\sigma'} = \tan \phi' . \tag{42}$$

From the geometry of the Mohr circle it follows that

$$\sin[2(\psi' + \theta' - \Theta') - \phi' - \pi] = \frac{\sin \phi'}{\sin \delta},$$

and the significant solution for ψ' is

$$\psi' + \theta' - \Theta' = \frac{\pi}{2} + \frac{1}{2}(\phi' + \text{Arc sin} \frac{\sin \phi'}{\sin \delta}) . \tag{43}$$

For rough walls, point W' merges with point E' and it is evident from Fig. 18 (a) that

$$\psi' + \theta' - \Theta' = \frac{3}{4}\pi + \frac{\phi}{2}, \tag{44}$$

or, noting that π is the period of angle ψ', eq. (44) can also be written $\psi' + \theta' - \Theta' = -\pi/4 + \phi/2$.

Similarly, the values relating to the wall inclined at angle $-\Theta''$ to the x-axis are denoted by double-primes, and the corresponding part of the Mohr stress circle and the yield loci are shown in Fig. 18 (b). The wall yield locus is located by the angle of friction ϕ'' between the solid and the wall. Relations (42) to (44) now become

$$\frac{\tau''}{\sigma''} = \tan \phi'' \tag{45}$$

$$\psi'' + \theta'' - \Theta'' = \frac{\pi}{2} - \frac{1}{2}(\phi'' + \text{Arc sin} \frac{\sin \phi''}{\sin \delta}), \tag{46}$$

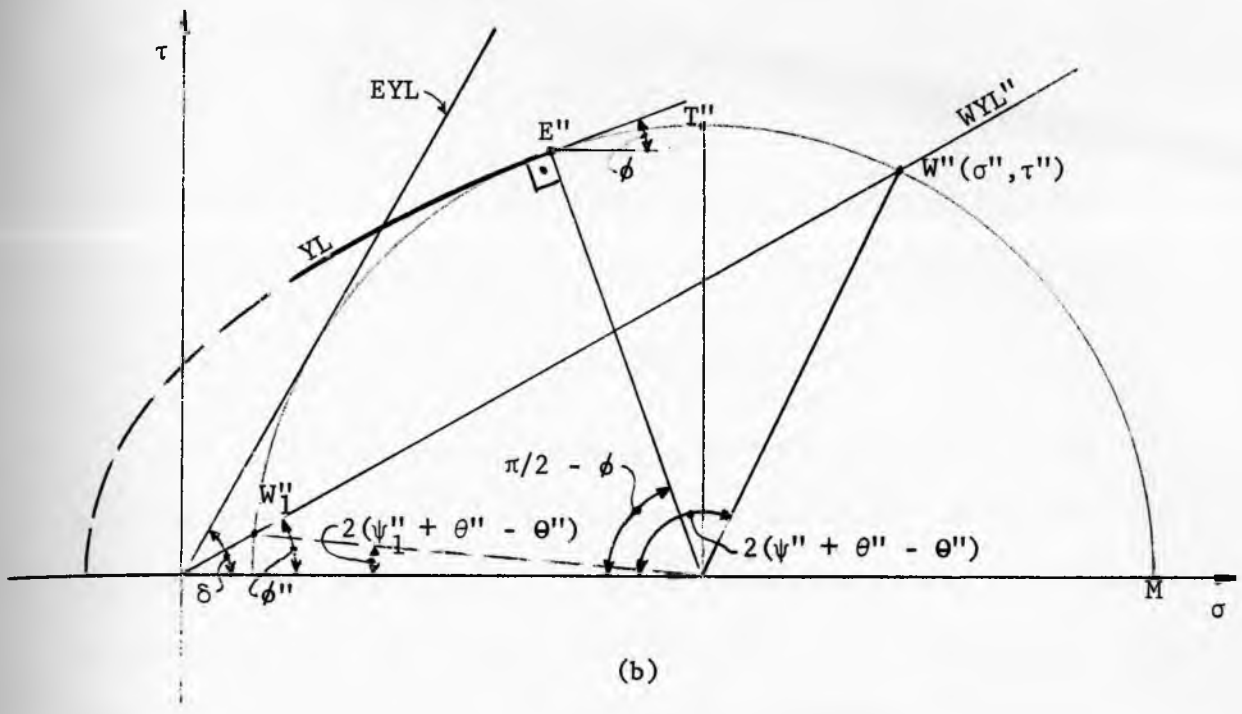

(b)

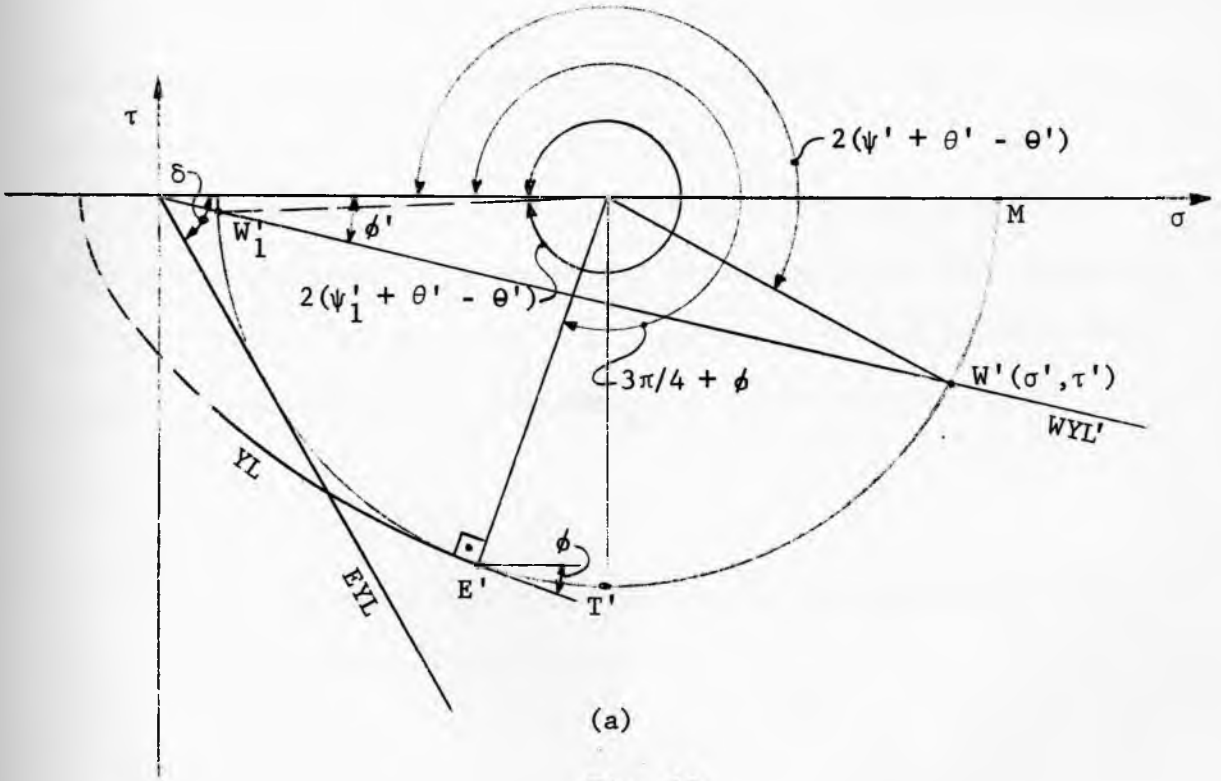

(a)

Fig. 18

Linearized wall yield loci

$$\psi'' + \theta'' - \theta'' = \frac{\pi}{4} - \frac{\phi}{2}. \qquad (47)$$

PART II

STEADY STATE FLOW

General equations

In this section the differential equations required for the solution of the stress and velocity fields in steady state flow are presented. The adopted yield function allows the stress equations to be uncoupled from the velocity equations and to be solved first. The solution of the stress field produces the direction of the major pressure $\omega(x,y)$ and the value of density $\gamma(x,y)$ throughout the field, and suitable velocity fields can then be computed.

The boundary conditions have to be satisfied in both, the stress and velocity fields and certain physical conditions imposed on the stress and velocity fields have to be met.

All the differential equations are hyperbolic and each field requires the solution of a set of two partial differential equations of first order. The equations are presented in a form suitable for numberical calculations by the method of characteristics.

Stress field.

In the plane-Cartesian/cylindrical-polar coordinates x, y, α, Fig. 2, the equations of equilibrium are

$$\frac{\partial \sigma_x}{\partial x} + \frac{\partial \tau_{xy}}{\partial y} + m \frac{\tau_{xy}}{y} = \gamma, \tag{48}$$

$$\frac{\partial \tau_{xy}}{\partial x} + \frac{\partial \sigma_y}{\partial y} + m \frac{\sigma_y - \sigma_\alpha}{y} = 0. \tag{49}$$

These two equations together with the equation of the effective yield locus (11) and the empirical relation for density (26) can be solved for the four dependent variables (σ_x, σ_y, τ_{xy}, γ) in plane strain. In axial symmetry, the fifth dependent variable σ_α is taken care of by the additional equation (22).

The equations of equilibrium are first expressed in terms of σ and ω by means of equations (14) - (16) and (22), thus

$$(1 + \sin\delta \cos 2\omega)\frac{\partial \sigma}{\partial x} + \sin\delta \sin 2\omega \frac{\partial \sigma}{\partial y} - 2\sigma \sin\delta \sin 2\omega \frac{\partial \omega}{\partial x} +$$

$$+ 2\sigma \sin\delta \cos 2\omega \frac{\partial \omega}{\partial y} = \gamma_o (1 + \sigma)^\beta - m \frac{\sigma}{y} \sin\delta \sin 2\omega,$$

$$\sin\delta \sin 2\omega \frac{\partial \sigma}{\partial x} + (1 - \sin\delta \cos 2\omega) \frac{\partial \sigma}{\partial y} + 2\sigma \sin\delta \cos 2\omega \frac{\partial \omega}{\partial x} +$$

$$+ 2\sigma \sin\delta \sin 2\omega \frac{\partial \omega}{\partial y} = m \frac{\sigma}{y} \sin\delta (k + \cos 2\omega).$$

Now the following abbreviation is introduced [15]

$$S = \frac{\cot\delta}{2} \ln \frac{\sigma}{\sigma_o}, \tag{50}$$

where σ_o is an arbitrary constant. The differential equations then reduce to the following form

$$\frac{\partial (S + \omega)}{\partial x} + \frac{\partial (S + \omega)}{\partial y} \tan(\omega + \frac{\pi}{4} - \frac{\delta}{2}) = A, \tag{a}$$

$$\frac{\partial (S - \omega)}{\partial x} + \frac{\partial (S - \omega)}{\partial y} \tan(\omega - \frac{\pi}{4} + \frac{\delta}{2}) = B, \tag{b}$$

where

$$A = -\frac{\gamma_o(1+\sigma)^{\beta}\sin(\omega - \frac{\pi}{4} + \frac{\delta}{2})}{2\sigma \sin\delta \cos(\omega + \frac{\pi}{4} - \frac{\delta}{2})} + m\frac{\cos(\omega + \frac{\pi}{4} - \frac{\delta}{2}) + k\cos(\omega - \frac{\pi}{4} + \frac{\delta}{2})}{2y \cos(\omega + \frac{\pi}{4} - \frac{\delta}{2})}, \quad (51)$$

$$B = \frac{\gamma_o(1+\sigma)^{\beta}\sin(\omega + \frac{\pi}{4} - \frac{\delta}{2})}{2\sigma \sin\delta \cos(\omega - \frac{\pi}{4} + \frac{\delta}{2})} - m\frac{\cos(\omega - \frac{\pi}{4} + \frac{\delta}{2}) + k\cos(\omega + \frac{\pi}{4} - \frac{\delta}{2})}{2y \cos(\omega - \frac{\pi}{4} + \frac{\delta}{2})}. \quad (52)$$

In the first characteristic direction,

$$\frac{dy}{dx} = \tan(\omega + \frac{\pi}{4} - \frac{\delta}{2}), \quad (53)$$

the left hand side of eq.(a) is a total derivative

$$\frac{d(S + \omega)}{dx} = A. \quad (54)$$

Similarly, in the second characteristic direction,

$$\frac{dy}{dx} = \tan(\omega - \frac{\pi}{4} + \frac{\delta}{2}), \quad (55)$$

the left hand side of eq.(b) is a total derivative

$$\frac{d(S - \omega)}{dx} = B. \quad (56)$$

It will be observed that the two stress characteristics intersect at an angle $\pi/2 - \delta$, and form angles $\pm (\pi/4 - \delta/2)$ with the direction of the major pressure.

Velocity field.

The velocity field is computed with the assumption of continuity and isotropy. The equation of continuity in steady flow can be

written as follows

$$\frac{\partial}{\partial x}(\gamma\, u\, y^m) + \frac{\partial}{\partial y}(\gamma\, v\, y^m) = 0, \tag{57}$$

where u and v are the components of the velocity vector in the directions of the coordinate axes x and y, respectively, Fig. 19. Density γ is eliminated by means of eq. (26), yielding

$$\frac{\partial}{\partial x}\left[(1+\sigma)^{\beta} u y^m\right] + \frac{\partial}{\partial y}\left[(1+\sigma)^{\beta} v y^m\right] = 0,$$

which expands into

$$\frac{\partial u}{\partial x} + \frac{\partial v}{\partial y} + e = 0, \tag{58}$$

where

$$e = m\,\frac{v}{y} + \frac{\beta}{1+\sigma}\left(\frac{\partial \sigma}{\partial x}\, u + \frac{\partial \sigma}{\partial y}\, v\right). \tag{59}$$

The principle of isotropy states that the directions of the principal strain rates coincide with the directions of the principal stresses. The normal, compressive strain rates ϵ_x and ϵ_y, and the shear strain rate γ_{xy} are expressed in terms of the velocity components as follows

$$\epsilon_x = -\frac{\partial u}{\partial x}, \quad \epsilon_y = -\frac{\partial v}{\partial y}, \quad \gamma_{xy} = -\frac{\partial u}{\partial y} - \frac{\partial v}{\partial x}. \tag{60}$$

The equation of isotropy then can be written

$$\tan 2\omega = \frac{\dfrac{\partial u}{\partial y} + \dfrac{\partial v}{\partial x}}{\dfrac{\partial u}{\partial x} - \dfrac{\partial v}{\partial y}}. \tag{61}$$

In order to find the characteristic directions and the relations

which hold along the characteristics, equations (58) and (61), together with the equations of the total derivatives

$$\frac{\partial u}{\partial x}\,dx + \frac{\partial u}{\partial y}\,dy = du, \qquad \frac{\partial v}{\partial x}\,dx + \frac{\partial v}{\partial y}\,dy = dv,$$

are solved for $\partial u/\partial x$ to yield

$$\frac{\partial u}{\partial x} = -\frac{dy}{dx}\,\frac{\frac{du}{dy} + \frac{dv}{dx} + e\left(\frac{dy}{dx} - \tan 2\omega\right)}{\left[\frac{dy}{dx} - \tan\left(\omega + \frac{\pi}{4}\right)\right]\left[\frac{dy}{dx} - \tan\left(\omega - \frac{\pi}{4}\right)\right]}. \tag{c}$$

The characteristic directions are

$$\frac{dy}{dx} = \tan\left(\omega \pm \frac{\pi}{4}\right). \tag{62}$$

Hence, the velocity characteristics are orthogonal and do not coincide with the stress characteristics.

In the directions of the characteristics, the numerator of eq.(c) is zero and, with the substitution of the appropriate expression (62) for dy/dx, reduces to

$$\frac{du}{dy} + \frac{dv}{dx} \pm \frac{e}{\cos 2\omega} = 0. \tag{63}$$

In both equations (62) and (63) the top sign applies along the first characteristic and the bottom sign along the second characteristic.

Sometimes it is more convenient to have the velocity vector expressed in terms of its projections v_1 and v_2, Fig. 19, on the directions of the characteristics. A substitution for

$$\begin{aligned} u &= -v_1 \sin(\omega - \pi/4) + v_2 \sin(\omega + \pi/4), \\ v &= v_1 \cos(\omega - \pi/4) - v_2 \cos(\omega + \pi/4) \end{aligned} \tag{64}$$

in eq.(63) leads to the following relations:

along the 1st characteristic: $\frac{dy}{dx_1} = \tan\left(\omega + \frac{\pi}{4}\right)$, (65)

$$\frac{dv_1}{dy_1} + v_2 \frac{d\omega}{dy_1} + \frac{m}{2y}\left(v_1 + v_2 \frac{dy}{dx_2}\right) + \frac{\beta v_1}{2(1+\sigma)} \frac{d\sigma}{dy_1} + \frac{\beta v_2}{2(1+\sigma)} \frac{d\sigma}{dx_2} = 0. \quad (66)$$

In the above equations, as well as in the two equations below, the derivatives are taken in the direction of the 1st or the 2nd characteristic as indicated by the subscript.

Along the 2nd characteristic: $\frac{dy}{dx_2} = \tan\left(\omega - \frac{\pi}{4}\right)$, (67)

$$\frac{dv_2}{dy_2} - v_1 \frac{d\omega}{dy_2} + \frac{m}{2y}\left(-v_1 \frac{dy}{dx_1} + v_2\right) - \frac{\beta v_1}{2(1+\sigma)} \frac{d\sigma}{dx_1} + \frac{\beta v_2}{2(1+\sigma)} \frac{d\sigma}{dy_2} = 0. \quad (68)$$

Superposition. Since both, the equation of continuity (58) and of isotropy (61), are linear and homogeneous, a linear combination of two (or more) solutions of a velocity field is also a solution. This property of the velocity field is very convenient in the development of physical solutions.

Physical conditions

The following conditions are imposed on the stress and velocity fields on physical grounds:

A. Stresses are positive (tension not allowed) and bounded.

B. Along a line of infinite shear strain rate, frictional and cohesive forces are fully mobilized. This implies that stresses along such a line lie either on the yield locus or on the wall yield locus, hence, such a line is either a slipline or a weak wall.

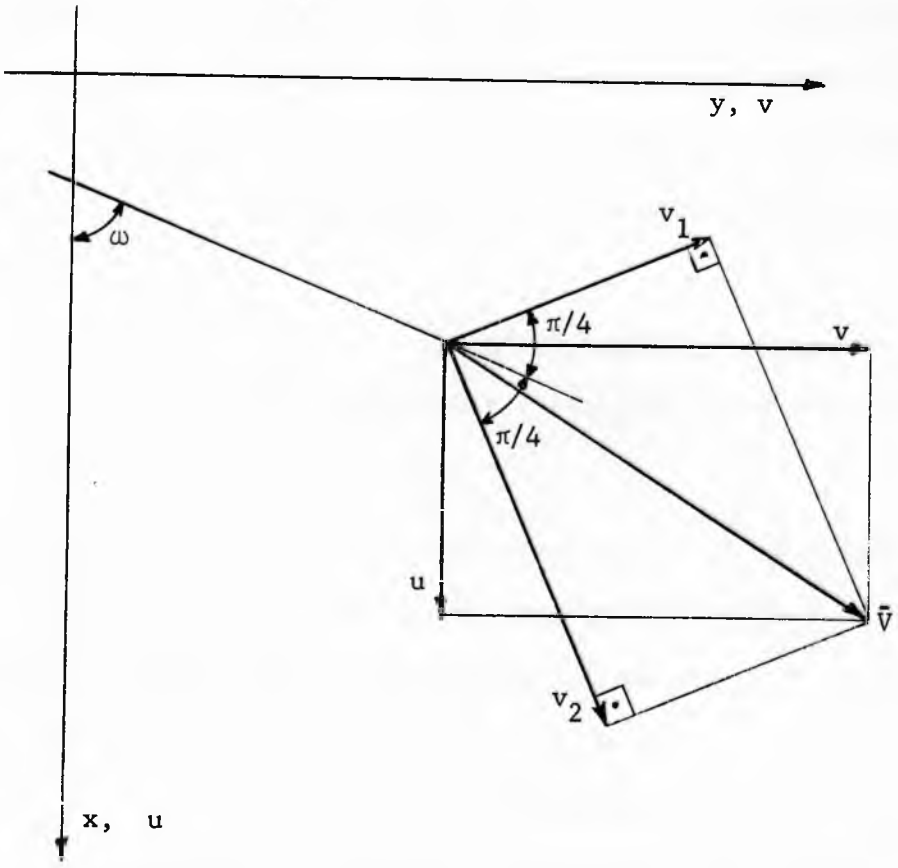

Fig. 19

Projections of the velocity vector

on the characteristic directions

C. The velocity $\bar{V}$ of an element of a solid is bounded.

D. The acceleration of an element,

$$\frac{d\bar{V}}{dt} = \frac{dV}{dt}\,\bar{s} + \frac{V^2}{\rho_s}\,\bar{n} \tag{69}$$

along the path of its travel, Fig. 20, is bounded. This implies that dV/dt is bounded everywhere, and $1/\rho_s$ is bounded everywhere with the exception of points at which $\bar{V} = 0$.

E. Singularities in density are inadmissible.

Grids, special lines and regions

The solution of a stress field defines the function

$$\omega = \omega(x,y), \tag{70}$$

where $\tan \omega = dy/dx$ is the direction of the major pressure σ_1. Eq.(70) thus is the differential equation of a grid of lines of action of pressure σ_1, Fig. 21. While the solution of flow does not require the determination of this grid, eq.(70) is used to locate the following grids, special lines and regions.

1. Stress characteristics. The slope of the stress characteristics, Fig. 22, is given by

$$\omega \pm (\pi/4 - \delta/2). \tag{71}$$

The fields shown in Figures 22 to 24 assume that the walls are rough.

2. Velocity characteristics. The slope of these lines, Fig. 23, is

$$\omega \pm \pi/4. \tag{72}$$

It will be ovserved that the velocity characteristics form two bunches whose stalks are located at the vertex of the channel. The stalks are

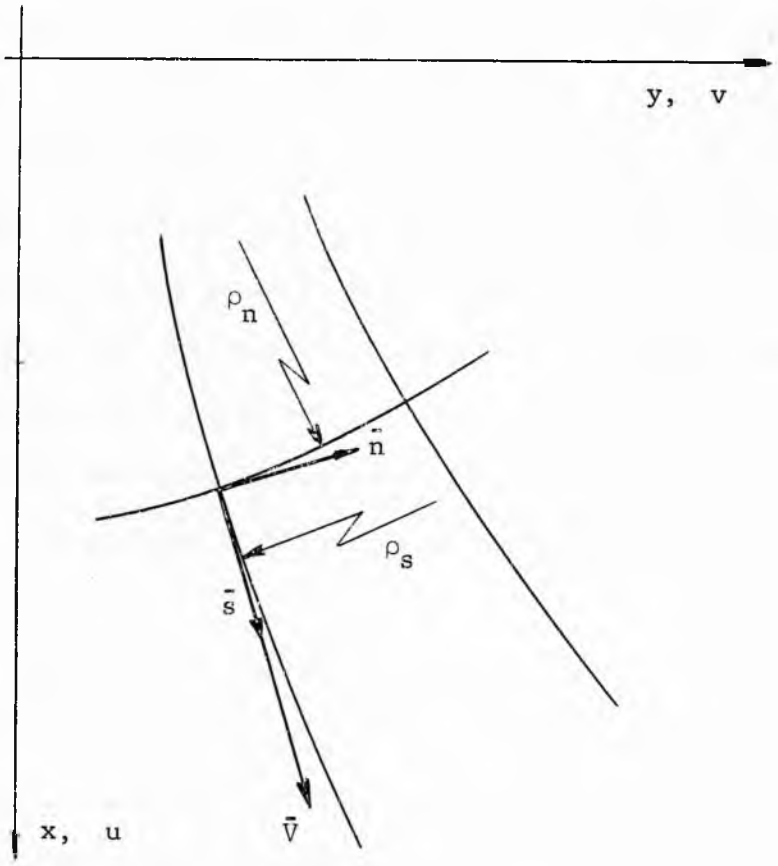

Fig. 20

Velocity along a streamline in (s,n) coordinates

within the walls of the channel because the walls are rough. The stresses at the walls are given by the points E, Fig. 18. If the walls were weak in such a degree that the stresses at the walls were given by the points T (T = W), Fig. 18, then the wall on each side of the channel would aline with a velocity characteristic. The stalks would be at the walls. If the walls were weaker yet, so that the stresses at the walls were given by the points W, as shown in Fig. 18, the stalks of the velocity characteristics would be cut off by the walls.

3. Lines of maximum shear strain rate. These lines are inclined at angles $\pm \pi/4$ to the lines of the principal strain rates and, with the assumption of isotropy, also to the lines of the principal stresses. Therefore, the slope of these lines is $\omega \pm \pi/4$ and they coincide with the velocity characteristics, Fig. 23. The lines of maximum shear strain rate are important because some of them can be observed through a transparent wall of a model and thus provide an experimental check of the analysis.

4. Sliplines. Under conditions of flow, the sliplines, Fig. 24, do not coincide with either the stress or the velocity characteristics.

However, sliplines are significant because by the physical condition B a line of infinite shear strain rate across a solid can occur only along a slipline. A slipline has the slope of either of the two angles

$$\omega \pm (\pi/4 - \phi/2). \tag{73}$$

From Fig. 24, it is evident that the sliplines, like the velocity characteristics, form two bunches with stalks at the vertex of the channel. Since the walls are rough, they aline with the sliplines and, therefore,

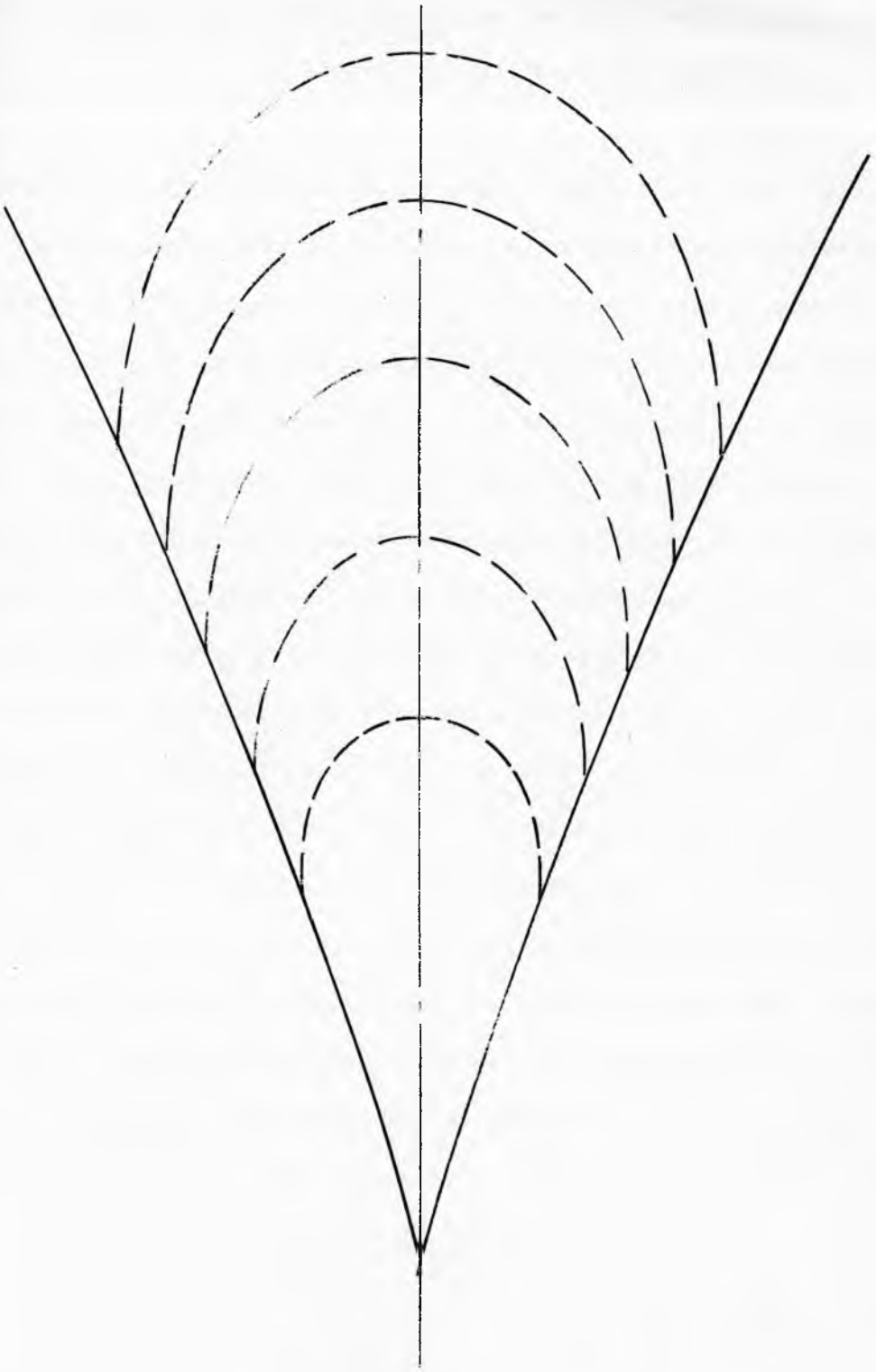

Fig. 21

Lines of action of the major pressure σ_1

the stalks of the sliplines are at the walls. Any weakness at the walls would cut off the stalks of the sliplines.

During flow, angle ϕ is measured at the points E of the Mohr stress circle, Fig. 5. At these points angle ϕ is always smaller than δ: this follows from the condition of convexity of the yield locus [7]. Angle ϕ is also greater than zero: this can be demonstrated by means of models in which the lines of maximum shear strain rate can be observed through a transparent front wall. If ϕ were zero, then eq. (73) would be identical with eq. (72) and, in a channel with rough walls, the walls would coincide with the lines of maximum shear strain rate. The stalks of the latter lines would lie at the walls while, in fact, these stalks are observed in the positions shown in Fig. 23. Another illustration of $\phi > 0$ is provided in the section "Flow in vertical channels".

5. Streamlines. In steady state flow the paths of flowing elements of the solid are independent of time and are called streamlines.

Streamlines have the following two properties: they cannot have cusps, (except at points where $V = 0$), and they cannot intersect each other. The former follows from the physical condition D which requires that $1/\rho_s$ be bounded. The latter is demonstrated from the consideration of the equation of continuity in the orthogonal, curvilinear coordinates (s,n), Fig. 20. This equation is of the form

$$\frac{\partial(\gamma\, V\, \rho_n\, y^m)}{\partial s} = 0,$$

and it follows that

$$\gamma\, V\, \rho_n\, y^m = f(n).$$

It is easy to show that at the intersection of two streamlines $\rho_n \to 0$,

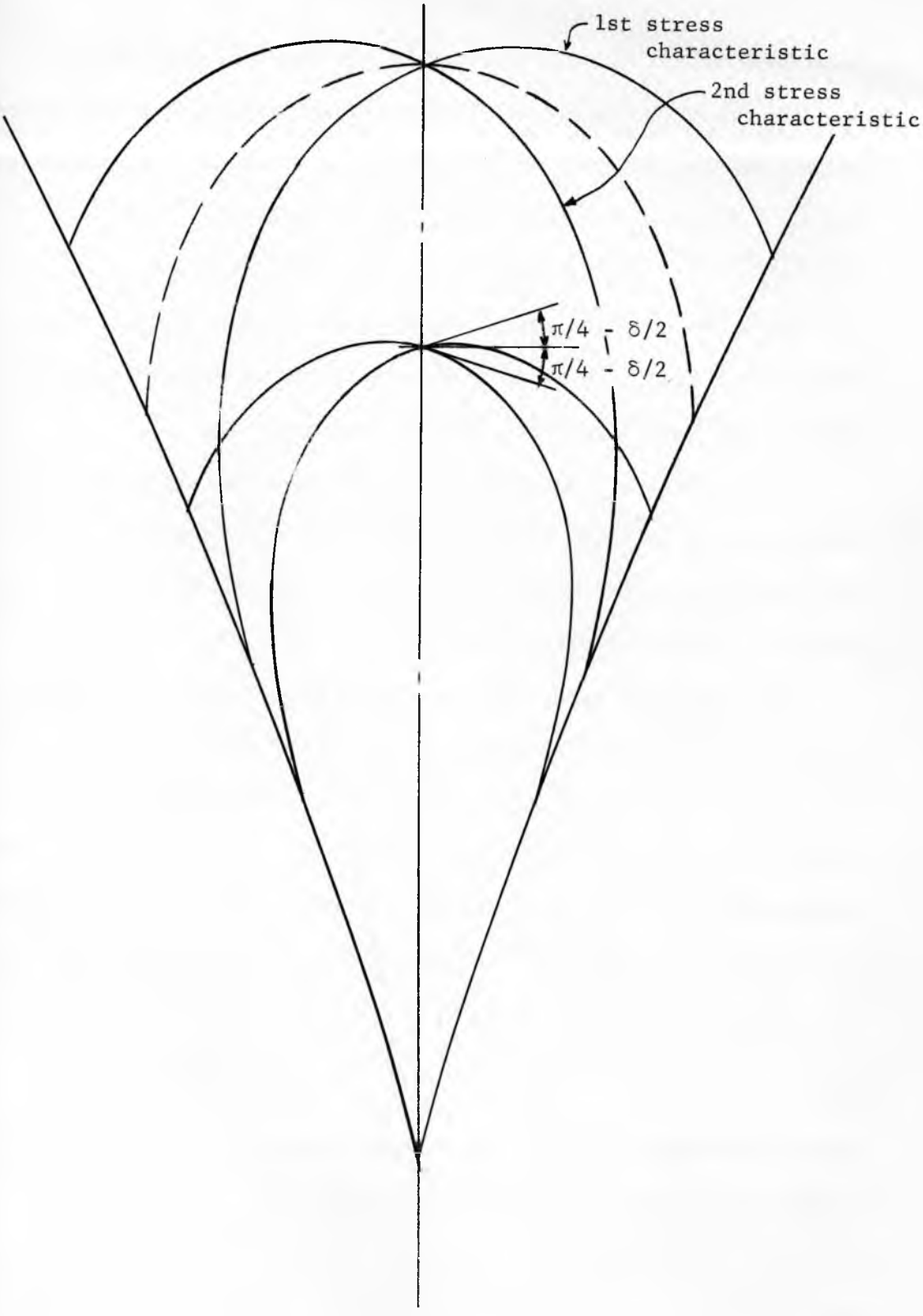

Fig. 22

Stress Characteristics

hence $V \to \infty$, which is not permitted by the physical condition C.

6. Coincidence of a velocity characteristic with a streamline. Suppose the 1st velocity characteristic coincides with a streamline, then $v_1 = V$ and $v_2 = 0$ in eq. (66), which integrates into

$$V^2 \, y^m \, (1 + \sigma)^\beta = c. \tag{74}$$

Since the constant c may be set equal to zero, velocity may be zero along such a line. In plane strain, velocity is either constant or, allowing for compressibility, almost constant.

7. Velocity discontinuities. Any line along which the shear strain rate is infinite will be referred to as a velocity discontinuity. This term thus covers both, jumps in the magnitude of velocity and infinitely large velocity gradients.

Two conditions need to be satisfied along a line of discontinuity. First, a velocity discontinuity has to follow either a slipline or a weak wall: this follows from the physical condition B. Second, a velocity discontinuity can occur only along a streamline. The latter is demonstrated as follows: Along a line of infinite shear strain rate, γ_{xy}, eq. (60), is infinite. In the (s,n) system of coordinates, Fig. 20, the strain rates are given by

$$\epsilon_s = -\frac{\partial V}{\partial s}, \quad \epsilon_n = -\frac{V}{\rho_n}, \quad \gamma_{sn} = -\frac{\partial V}{\partial n} + \frac{V}{\rho_s}. \tag{75}$$

and the relevant relation between these expressions and the strain rates in the (x,y), coordinates, equations (60), is

$$(\epsilon_s - \epsilon_n)^2 + \gamma_{sn}^2 = (\epsilon_x - \epsilon_y)^2 + \gamma_{xy}^2$$

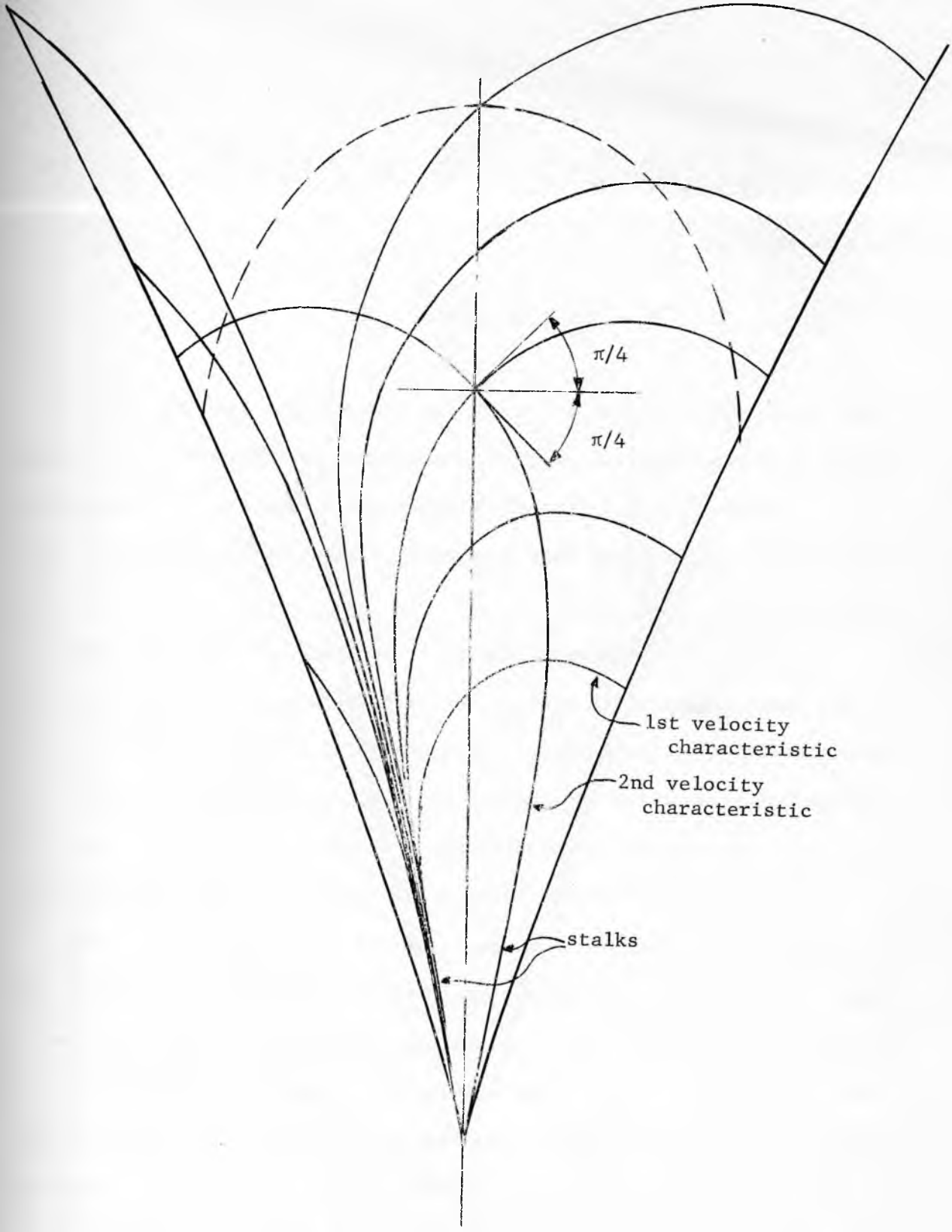

Fig. 23

Velocity characteristics

or

$$\left(\frac{\partial V}{\partial s} - \frac{V}{\rho_n}\right)^2 + \left(\frac{\partial V}{\partial n} + \frac{V}{\rho_s}\right)^2 = \left(\frac{\partial u}{\partial x} - \frac{\partial v}{\partial y}\right)^2 + \left(\frac{\partial u}{\partial y} + \frac{\partial v}{\partial x}\right)^2 . \qquad (d)$$

In this equation

$$\frac{\partial V}{\partial s} = \frac{\frac{dV}{dt} - \frac{\partial V}{\partial n}\frac{dn}{dt}}{\frac{ds}{dt}} = \frac{\frac{dV}{dt}}{V},$$

since $ds/dt = V$ and $dn/dt = 0$. All the terms on the left hand side of eq.(d) with the exception of $\partial V/\partial n$ are bounded by the physical conditions C and D. Hence, along a line of velocity discontinuity, it is necessary that $\partial V/\partial n \to \infty$, which means that a velocity discontinuity follows a streamline.

A velocity discontinuity, though it is a line of infinite shear strain rate, does not, in general, coincide with a line of maximum shear strain rate; the latter strain rate being bounded. A velocity discontinuity separates two regions which may be both plastic, both rigid (or elastic), or one plastic and the other rigid (or elastic).

A velocity discontinuity often originates at the top boundary of a channel. In channels with rough walls all the sliplines enter the stalks at the vertex, and discontinuities can extend from the top to the bottom of the channel. In all practical channels with weak walls the walls cut off the stalks of the sliplines. A velocity discontinuity cannot continue to an intersection with a wall, since that would involve an intersection of the streamline, which coincides with the discontinuity, with the wall, which itself is a streamline. A velocity discontinuity

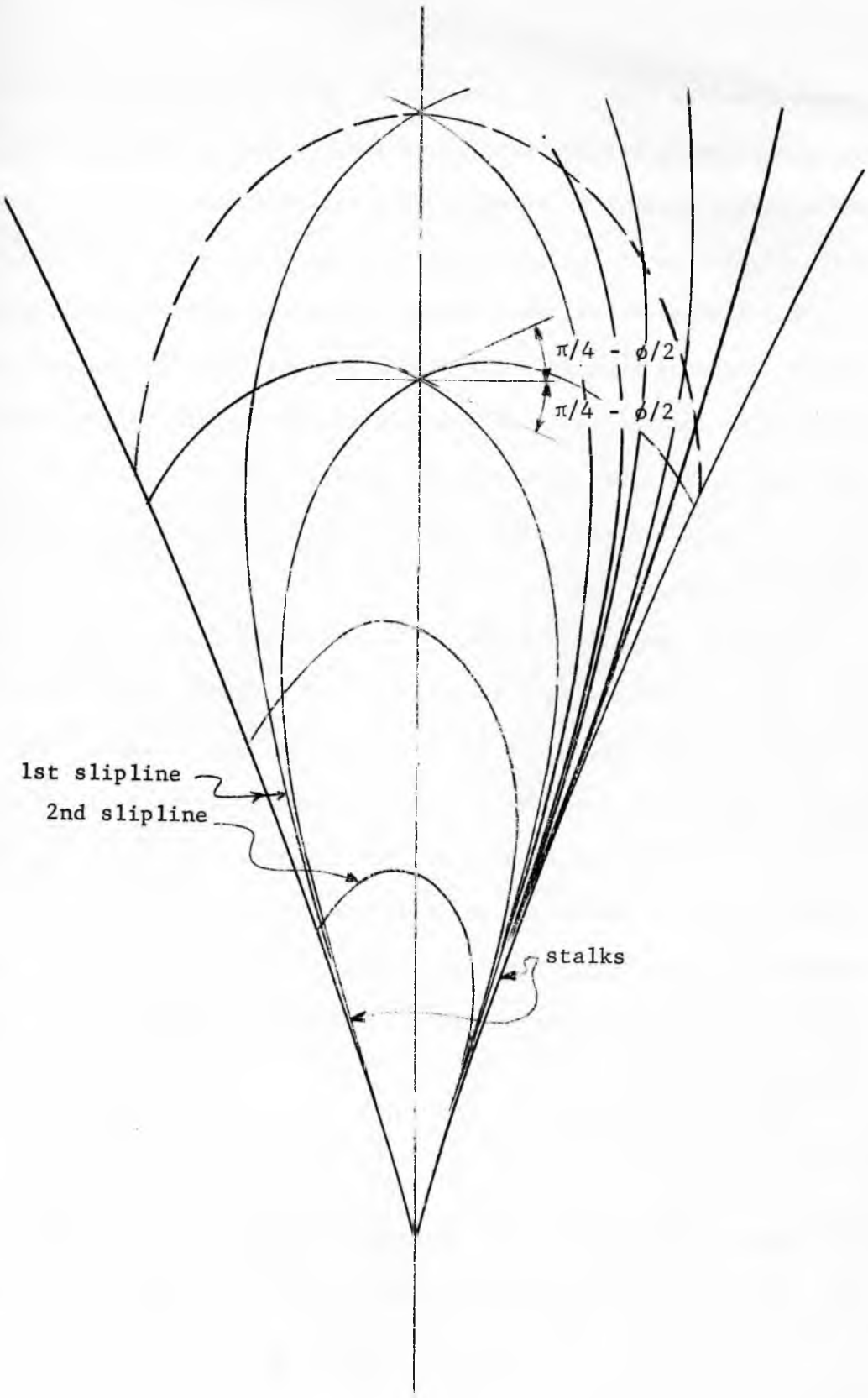

Fig. 24

Sliplines

cannot transfer from a slipline of one family to another slipline of the other family because that would imply a cusp in the streamline at the transfer point. In channels with weak walls a velocity discontinuity which originates at the top boundary dampens out within the field.

8. A straight velocity characteristic in incompressible plane strain. Suppose that in plane strain a first velocity characteristic is straight and the solid is incompressible, it then follows from eq. (66) that v_1 is constant along that characteristic.

9. Walls. A wall separates a plastic region from a stationary rigid (or elastic) region.

Usually, there is a velocity discontinuity along a wall. The wall then coincides with a streamline, and stresses along the wall are defined by either the yield locus or the wall yield locus. When the solid flows within rough walls, the walls coincide with sliplines and the stalks of the bunches of sliplines intersect the lower boundary of the channel. Therefore, any slipline which intersects the top boundary of the channel may form a wall. In consequence, the walls can shift readily in the upper part of the channel, adjusting to the top boundary conditions.

In accordance with eq.(3), at the walls, Fig. 17, there is

$$\psi' + \theta' = \omega' \quad \text{and} \quad \psi'' + \theta'' = \omega''. \tag{76}$$

For rough walls ψ' and ψ'' are eliminated by means of equations (44) and (47) leading to the following expressions for the slopes of the walls

$$\theta' = \omega' - \frac{3}{4}\pi - \frac{\phi}{2}, \tag{77}$$

$$\theta'' = \omega'' - \frac{\pi}{4} + \frac{\phi}{2}. \tag{78}$$

It will be noted that, since π is the period of angle ω, eq.(77) can also be written $\Theta' = \omega' + \pi/4 - \phi/2$.

When the solid flows within weak walls, the slopes of the walls are found from expressions (43) and (46) with appropriate substitutions of (76), thus

$$\Theta' = \omega' - [\frac{\pi}{2} + \frac{1}{2}(\phi' + \text{Arc sin } \frac{\sin \phi'}{\sin \delta})], \tag{79}$$

$$\Theta'' = \omega'' - [\frac{\pi}{2} - \frac{1}{2}(\phi'' + \text{Arc sin } \frac{\sin \phi''}{\sin \delta})]. \tag{80}$$

For straight walls intersecting at the origin, $\Theta' = \theta'$ and $\Theta'' = \theta''$.

When a velocity characteristic coincides with a wall along which there is a velocity discontinuity, the wall is weak to such a degree that the wall yield locus passes through the point T of the Mohr circle. For the linearized wall yield locus, Fig. 18 (a), this implies

$$\tan \phi' = \sin \delta. \tag{81}$$

In this case, the velocity discontinuity also coincides with a streamline and that enforces the restriction on the magnitude of the velocity along the wall expressed by eq.(74).

When there is no velocity discontinuity along a wall, the wall need not be a streamline and the stresses along the wall need not lie on a yield locus or on a wall yield locus. If such a wall coincides with a velocity characteristic then the velocity boundaries at the top and at the bottom of the channel have to be continuous at the walls. In practice, this is seldom attained and these conditions lead to non-steady flow. This is prevalent in axi-symmetric flow within rough walls. If such a wall does not coincide with a velocity characteristic then a

zero velocity region is enforced. This is discussed below.

10. Zero velocity regions within a plastic field. This concept is very useful in the development of fields in channels with sharp changes in cross-section, as shown in Fig. 25, because it allows the use of a continuous stress field. The stress characteristics of the 2nd family have to intersect the wall at an angle of 40° (in this example) to satisfy the wall yield locus and allow a velocity discontinuity along the wall. The stress characteristics above point A and below point B do so satisfy the WYL. Between the points A and B, the stress characteristics bend in gradually and the stresses at the wall are below yield values, hence no velocity discontinuity can occur along AB. Since AB is not a velocity characteristic, zero velocity along AB enforces a zero velocity region ABC where C is the intersection of two velocity characteristics (heavy lines) through A and B, respectively. Since, further, there can be no velocity discontinuity along the line ACB (not a slipline) that line is not a streamline. Streamlines develop smoothly around ACB. Zero velocity regions can be observed in a model with a transparent wall. Indeed, it was from observations of models that this concept arose.

In a bin, zero velocity regions occur at the transition from the vertical portion to the hopper. They have the effect of narrowing down the channel at the transition and explain the drop of the vertical pressure along the axis of symmetry. This drop was measured by the author several years ago, Fig. 26, and was reported in references [16, 17].

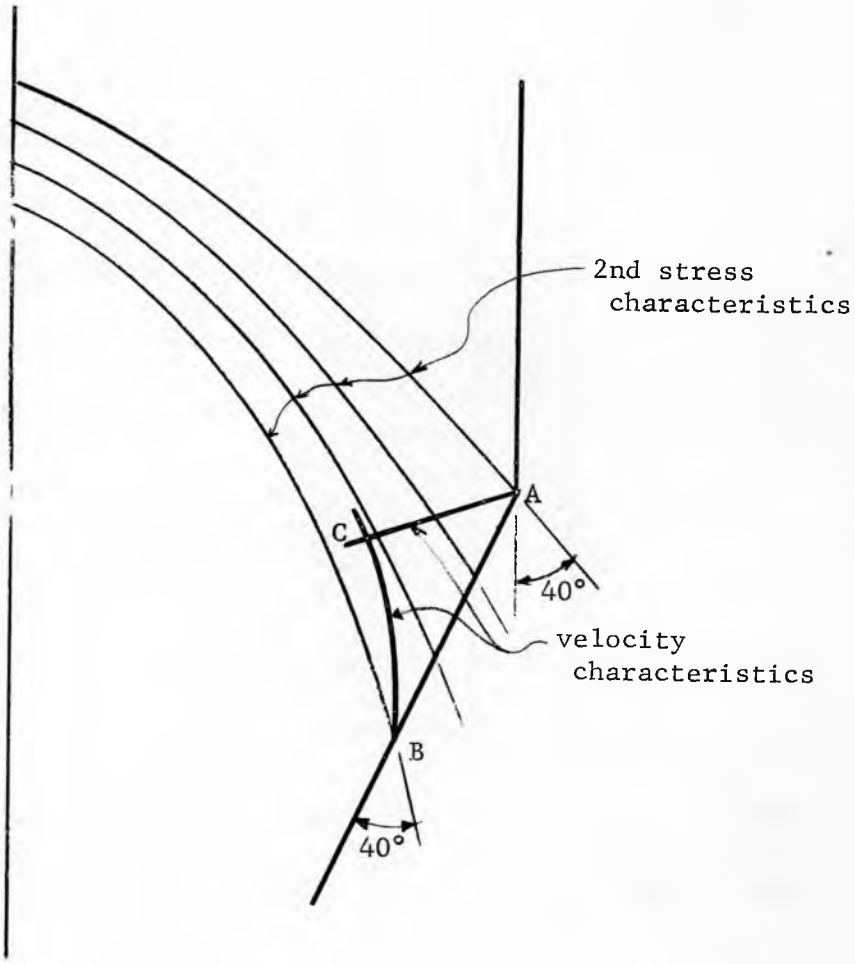

Fig. 25

Zero velocity region

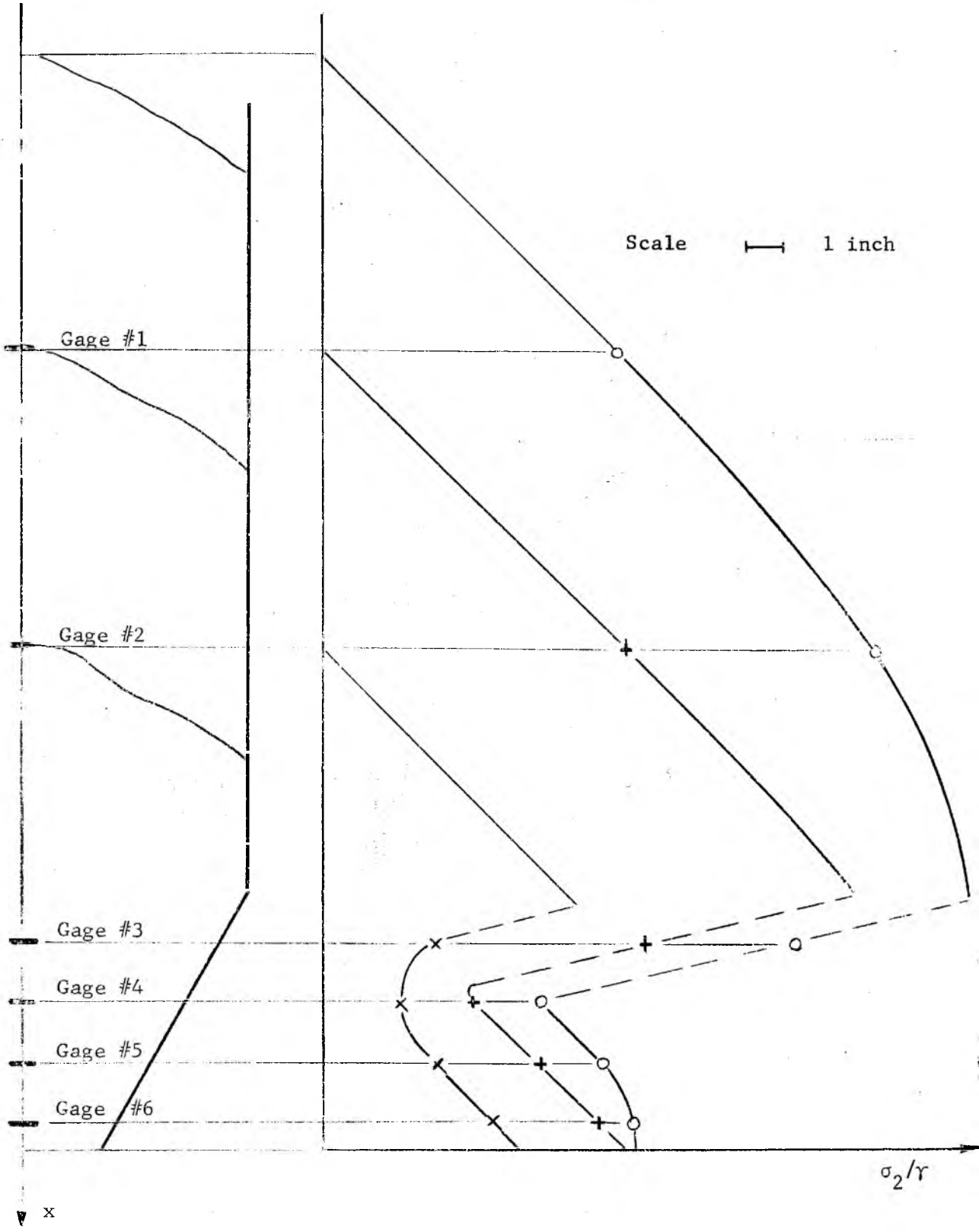

Fig. 26

Drop of vertical pressure at a transition

11. Stress discontinuities may occur only along streamlines. This follows from the fact that all real materials are compressible, and a discontinuity in stress implies a discontinuity in density. An element of solid flowing across a stress discontinuity would undergo a discontinuity of density and, therefore, an infinite acceleration, which is contrary to the physical condition D. Since the lines along which stress discontinuities might be expected to arise usually cross the streamline field, the existence of discontinuities is unlikely.

12. Stress singularities are inadmissible, because they would imply singularities in density which in a real solid are not acceptable by the physical condition E.

Converging channels

Equations of stress

In this section it will be advantageous to use the polar/spherical coordinates r, θ, α. The equations of equilibrium in these coordinates are

$$\frac{\partial \sigma_r}{\partial r} + \frac{1}{r}\frac{\partial \tau_{r\theta}}{\partial \theta} + \frac{1}{r}[\sigma_r - \sigma_\theta + m(\sigma_r - \sigma_\alpha) + m\,\tau_{r\theta}\cot\theta] + \gamma\cos\theta = 0, \tag{82}$$

$$\frac{\partial \tau_{r\theta}}{\partial r} + \frac{1}{r}\frac{\partial \sigma_\theta}{\partial \theta} + \frac{1}{r}[m(\sigma_\theta - \sigma_\alpha)\cot\theta + (2+m)\tau_{r\theta}] - \gamma\sin\theta = 0. \tag{83}$$

These equations are now transformed as follows: first, expressions (17), (18), (19) and (20) (with k = +1), and their appropriate derivatives are substituted for the component stresses; second, the substitution

$$\sigma = r\,\gamma(r,\theta)\; s(r,\theta) \tag{84}$$

is made; third, the derivatives $\partial s/\partial\theta$ and $\partial s/\partial r$ are separated, leading to the two equations

$$\frac{\partial s}{\partial\theta} + s\, f(r,\theta) + g(r,\theta) = 0, \tag{85}$$

$$r\,\frac{\partial s}{\partial r} + s\, h(r,\theta) + j(r,\theta) = 0, \tag{86}$$

where

$$f(r,\theta) = 2\left(\frac{\partial\psi}{\partial\theta} + 1\right)\frac{\sin\delta}{\cos^2\delta}\sin 2\psi + 2r\,\frac{\partial\psi}{\partial r}\,\frac{\sin\delta}{\cos^2\delta}(\sin\delta + \cos 2\psi) +$$

$$+ \frac{1}{\gamma}\,\frac{\partial\gamma}{\partial\theta} + m\,\frac{\sin\delta}{\cos^2\delta}(1 + \sin\delta)[\sin 2\psi - \cot\theta(1 + \cos 2\psi)], \tag{87}$$

$$g(r,\theta) = -\,\frac{\sin\delta}{\cos^2\delta}\sin(\theta + 2\psi) - \frac{\sin\theta}{\cos^2\delta}, \tag{88}$$

$$h(r,\theta) = 1 + 2\left(\frac{\partial\psi}{\partial\theta} + 1\right)\frac{\sin\delta}{\cos^2\delta}(\cos 2\psi - \sin\delta) - 2r\,\frac{\partial\psi}{\partial r}\,\frac{\sin\delta}{\cos^2\delta}\sin 2\psi +$$

$$+ \frac{r}{\gamma}\,\frac{\partial\gamma}{\partial r} + m\,\frac{\sin\delta}{\cos^2\delta}(1 + \sin\delta)(\cot\theta\,\sin 2\psi + \cos 2\psi - 1), \tag{89}$$

$$j(r,\theta) = -\,\frac{\sin\delta}{\cos^2\delta}\cos(\theta + 2\psi) + \frac{\cos\theta}{\cos^2\delta}. \tag{90}$$

The converging channels under consideration will be assumed to possess a vertex at which the extensions of the walls intersect. It will be shown that, with some continuity conditions satisfied, stress fields in all converging channels, irrespective of their top boundary and walls away from the vertex, approach a unique and relatively simple stress field at the vertex. That unique stress field will be called the "radial stress field," because it is the stress field compatible with a radial velocity field. The radial stress field is fully defined by the slopes of the tangents to the walls at the vertex (θ', $-\theta''$) and

the physical parameters of the solid and the walls (δ, ϕ', ϕ'').

While a physical channel can never be brought to a vertex, it is expected that the radial stress field is closely approached within a substantial region of the vertex, a region which will usually include the outlet of the channel. Since the knowledge of the stress field at the outlet of the channel is required in the derivation of flow criteria, the uniqueness and the simplicity of the radial stress field are of a great advantage in this derivation.

In the considerations which follow the origin of the coordinates will be located at the vertex of the channel.

Radial stress field.

Derivation. If it is assumed that

$$\psi = \psi(\theta) \tag{91}$$

and

$$\gamma = \text{const.} \tag{92}$$

Then the coefficients of the equations (85) and (86) assume the simplified form

$$f(\theta) = 2\left(\frac{d\psi}{d\theta} + 1\right) \frac{\sin \delta}{\cos^2 \delta} \sin 2\psi +$$

$$+ m \frac{\sin \delta}{\cos^2 \delta} (1 + \sin \delta)[\sin 2\psi - \cot \theta(1 + \cos 2\psi)], \tag{93}$$

$$g(\theta) = - \frac{\sin \delta}{\cos^2 \delta} \sin(\theta + 2\psi) - \frac{\sin \theta}{\cos^2 \delta}, \tag{94}$$

$$h(\theta) = 1 + 2\left(\frac{d\psi}{d\theta} + 1\right) \frac{\sin\delta}{\cos^2\delta} (\cos 2\psi - \sin\delta) +$$

$$+ m \frac{\sin\delta}{\cos^2\delta}(1 + \sin\delta)(\cot\theta \sin 2\psi + \cos 2\psi - 1), \qquad (95)$$

$$j(\theta) = - \frac{\sin\delta}{\cos^2\delta} \cos(\theta + 2\psi) + \frac{\cos\theta}{\cos^2\delta}. \qquad (96)$$

Equations (85) and (86) now become

$$\frac{\partial s}{\partial\theta} + s\, f(\theta) + g(\theta) = 0, \qquad (a)$$

$$r \frac{\partial s}{\partial r} + s\, h(\theta) + j(\theta) = 0, \qquad (b)$$

and integrate into

$$s = c(r)\, e^{-\int f(\theta)d\theta} - e^{-\int f(\theta)d\theta} \int g(\theta)\, e^{\int f(\theta)d\theta} d\theta,$$

$$s = k(\theta)\, r^{-h} - \frac{j(\theta)}{h(\theta)}. \qquad (c)$$

Hence

$$\frac{j(\theta)}{h(\theta)} = e^{-\int f(\theta)d\theta} \int g(\theta)\, e^{\int f(\theta)d\theta}, \qquad (d)$$

and there are two alternatives: either

$$k(\theta) \equiv c(r) \equiv 0, \qquad (e)$$

or

$$k(\theta) = e^{-\int f(\theta)d\theta}, \quad \text{and} \quad c(r) = r^{-h}.$$

Consider the latter case. Evidently h = const. $\neq 0$. Eq. (d) is differentiated, thus

$$g(\theta)\, h = f(\theta)\, j(\theta) + \frac{dj}{d\theta}. \qquad (f)$$

Now differentiation of eq.(96) yields

$$\frac{dj}{d\theta} = \frac{\sin\delta}{\cos^2\delta}\sin(\theta + 2\psi)(1 + 2\frac{d\psi}{d\theta}) - \frac{\sin\delta}{\cos^2\delta}.$$

In this equation and in eq. (93), the derivative $d\psi/d\theta$ is eliminated by means of eq.(95) to yield

$$\frac{dj}{d\theta} = \frac{\sin(\theta + 2\psi)\left[(h - 1)\cos^2\delta - \sin\delta(\cos 2\psi - \sin\delta)\right]}{\cos^2\delta(\cos 2\psi - \sin\delta)} - \frac{\sin\theta}{\cos^2\delta} +$$

$$- m\frac{\sin\delta(1 + \sin\delta)\sin(\theta + 2\psi)(\cot\theta \sin 2\psi + \cos 2\psi - 1)}{\cos^2\delta(\cos 2\psi - \sin\delta)},$$

and

$$f(\theta) = \frac{(h - 1)\sin 2\psi}{\cos 2\psi - \sin\delta} + m\frac{\sin\delta[\sin 2\psi - \cot\theta(1 + \cos 2\psi)]}{\cos 2\psi - \sin\delta}.$$

These expressions and expressions (94) and (96) are now substituted for the appropriate functions in eq.(f), which after transformations becomes

$$h = 1 + m\{\sin\delta[\cos 2\psi + \cos 2(\theta + 2\psi)] - \sin^2(\theta + 2\psi) +$$

$$- \cos 2(\theta + \psi) - \cos^2\theta\}/\cos^2\delta[\cos 2(\theta + \psi) - \cos 2\psi]. \quad (g)$$

In plane strain $h = 1$ and eq.(95) yields $d\psi/d\theta = -1$. This implies an elementary field with rectilinear characteristics, which enforce a constant velocity throughout the channel. This does not provide a solution to converging flow.

In axial symmetry, it follows from eq.(95) that, at the axis, for $\theta = 0$, ψ equals either 0 or $\pi/2$. Any other value would enforce $d\psi/d\theta = \infty$ at the axis, and that is inadmissible since it would imply an unbounded strain rate. Consider the initial condition $\theta = 0$, $\psi = \pi/2$. For these values, the numerator and denominator of eq. (g) vanish and the limit is

established by twice applying l'Hospital's rule, yielding

$$h = 1 + \frac{\sin\delta}{1+\sin\delta}\,\frac{3[(\frac{d\psi}{d\theta})^o]^2 + 4(\frac{d\psi}{d\theta})^o + 1}{2(\frac{d\psi}{d\theta})^o + 1},$$

because, from eq.(95), $d^2\psi/d\theta^2$ is bounded except, possibly, for $\cos 2\psi - \sin\delta = 0$. Eq.(95) at the axis of symmetry evaluates at

$$h = 1 - \frac{4\sin\delta}{1-\sin\delta}\,[(\frac{d\psi}{d\theta})^o + 1].$$

Elimination of h yields a quadratic in $d\psi/d\theta$, whose roots are both netative,

$$(\frac{d\psi}{d\theta})^o = -1 \quad \text{and} \quad (\frac{d\psi}{d\theta})^o = -\frac{5+3\sin\delta}{11+5\sin\delta}.$$

This produces two particlar solutions. These solutions have been checked out numerically and found not to lead to useful boundary conditions.

The solution to radial flow is then provided by the first alternative, eq.(e) which reduces eq.(c) to

$$s = s(\theta) = -\frac{j(\theta)}{h(\theta)}. \tag{97}$$

Equations (a) and (b) now become

$$\frac{ds}{d\theta} + s\,f(\theta) + g(\theta) = 0, \tag{98}$$

$$s\,h(\theta) + j(\theta) = 0. \tag{99}$$

They are solved for the derivatives

$$\frac{d\psi}{d\theta} = F(\theta,\psi,s) =$$

$$= -1 - [m\,s\sin\delta(1+\sin\delta)(\cot\theta\sin 2\psi + \cos 2\psi - 1) + \cos\theta +$$

$$- \sin\delta\cos(\theta+2\psi) + s\cos^2\delta]/2\,s\sin\delta(\cos 2\psi - \sin\delta), \tag{h}$$

$$\frac{ds}{d\theta} = F(\theta,\psi,s) =$$

$$= \frac{s \sin 2\psi + \sin(\theta + 2\psi) + m\, s \sin\delta[\cot\theta(1 + \cos 2\psi) - \sin 2\psi]}{\cos 2\psi - \sin\delta}. \quad \text{(i)}$$

These equations are equivalent to the integral equations

$$\psi(\theta) = \psi(\theta^o) + \int_{\theta^o}^{\theta} F[t,\psi(t),s(t)]\, dt, \tag{100}$$

$$s(\theta) = s(\theta^o) + \int_{\theta^o}^{\theta} G[t,\psi(t),s(t)]\, dt, \tag{101}$$

which are solved for a given set of boundary conditions, $\psi^o = \psi(\theta^o)$ and $s^o = s(\theta^o)$. σ may then be determined from the eq.(84) which now reduces to

$$\sigma = r\,\gamma\, s(\theta). \tag{102}$$

Solutions of the radial stress field. One conclusion which is evident from the eq.(102) is that a radial stress field cannot extend upward to a traction-free top boundary. In gravity flow, the top boundary is usually traction-free and, therefore, the actual field in the upper part of a channel deviates significantly from a radial stress field. The radial stress fields are computed from the equations (100) and (101). It will be observed that these equations contain boundary conditions given along a single ray $\theta = \theta^o$. In a physical channel the boundary conditions are different, they are given by the slopes of the wall θ' and θ'' ($\Theta' = \theta'$ and $\Theta'' = \theta''$ in a radial stress field, since the walls are straight and pass through the origin) and by the angles of friction ϕ' and ϕ'' between the solid and the walls ($\phi' = \phi'' = \phi$ for rough walls). It follows from Fig. 18 that two angles: ψ' and ψ_1', measured at the points W' and W_1', respectively, correspond to one value

of ϕ''. Thus, mathematically, the boundary conditions are not uniquely defined. The location of these points is shown in Fig. 27, in the (θ,ψ) coordinates for plane strain. In axial symmetry, $\theta' = -\theta''$ and $\psi' = \pi - \psi''$, while $\psi_1' = -\psi_1''$, and the boundary points are located symmetrically relative to either the point $(0,\pi/2)$ or $(0,0)$, Fig. 28.

In the (θ,ψ) coordinates, a solution is expressed by a line $\psi = \psi(\theta)$ which connects two boundary points. It is easy to show that a solution $\psi = \psi(\theta)$ cannot cross a line $\cos 2\psi - \sin\delta = 0$. This follows from the analysis of equations (h) and (i). Along that line, the derivative $d\theta/d\psi$ is zero, while the second derivative $d^2\theta/d\psi^2 \neq 0$. Hence the inverse function $\theta = \theta(\psi)$ reaches an extremum when passing the line $\cos 2\psi - \sin\delta = 0$ and the field backtracks into the same physical region. Thus, only solutions connecting either the point (θ',ψ') with $(-\theta'',\psi'')$, or the point (θ',ψ_1') with $(-\theta'',\psi_1'')$ are physically acceptable. Further, also on physical grounds, solutions connecting the points (θ',ψ_1') with $(-\theta'',\psi_1'')$ are rejected because they are not observed in practice.

Thus, only solutions connecting the points (θ',ψ') and $(-\theta'',\psi'')$ will be considered in this work. In axial and in plane symmetry these boundary values imply $\psi = \pi/2$ at the axis, i.e. for $\theta = 0$.

There is no direct way of finding a solution connecting two boundary points. The method adopted in this work is to compute a sufficient number of randomly spaced solutions from a boundary $\theta^o = 0$, ψ^o, s^o and to interpolate the required functions. To assist in the interpolation, contours of constant values of s are drawn in the (θ,ψ) coordinates,

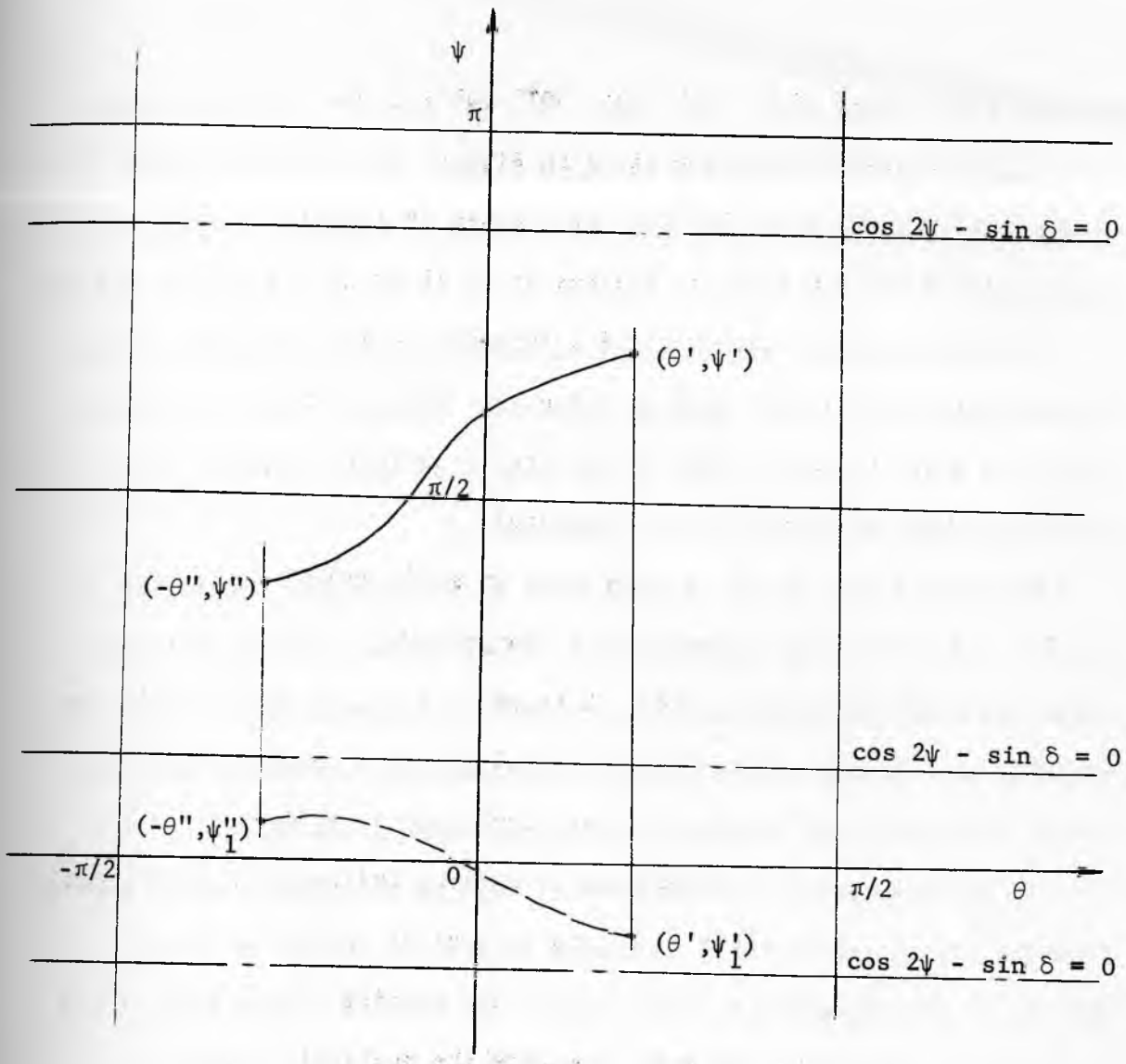

Fig. 27

Solutions of the radial stress field in plane strain

for the five values of δ: 30°, 40°, 50°, 60° and 70°. The solutions for symmetric plane strain are shown in Figures 29 to 33, for axial symmetry in Figures 34 to 38, and three cases of asymmetric plane strain at $\delta = 50°$ are shown in Figures 39 to 41 for $\phi' = 20°$, 30° and 40°.

In axial symmetry mathematical solutions are also available with a discontinuity in ψ at the axis of symmetry. However, these solutions imply $s = 0$ at the axis. This is physically unlikely to occur and, therefore, these solutions are not computed.

While no formal proof of uniqueness of solution for boundaries (θ', ψ') and $(-\theta'', \psi'')$ is submitted, the large number of numerical calculations which has been carried out seems to indicate that, within the range of application to the physical problems under consideration, the radial flow solutions obtained by the above method are unique.

In the discussion of Boundaries it will be indicated that in gravity flow the fields are unlikely to extend outside of the $j = 0$ lines. Therefore, all the plots in plane strain are bounded by the lines $j = 0$ and $\cos 2\psi - \sin \delta = 0$. In axial symmetry the available solutions cover more restricted regions in the (θ, ψ) coordinates and do not reach the above specificied lines. Indeed, in axial symmetry, for solutions with velocity discontinuities at the walls to exist, the walls must be sufficiently weak. For instance, it is most unlikely that axi-symmetric converging flow can occur within sliplines. However, flow without velocity discontinuity is possible within rough walls. In such flow, the walls are velocity characteristics, which means that $\psi' = 3\pi/4$ and $\psi'' = \pi/4$. A value of $\psi' - 90° = 45°$ cuts across the regions of solution

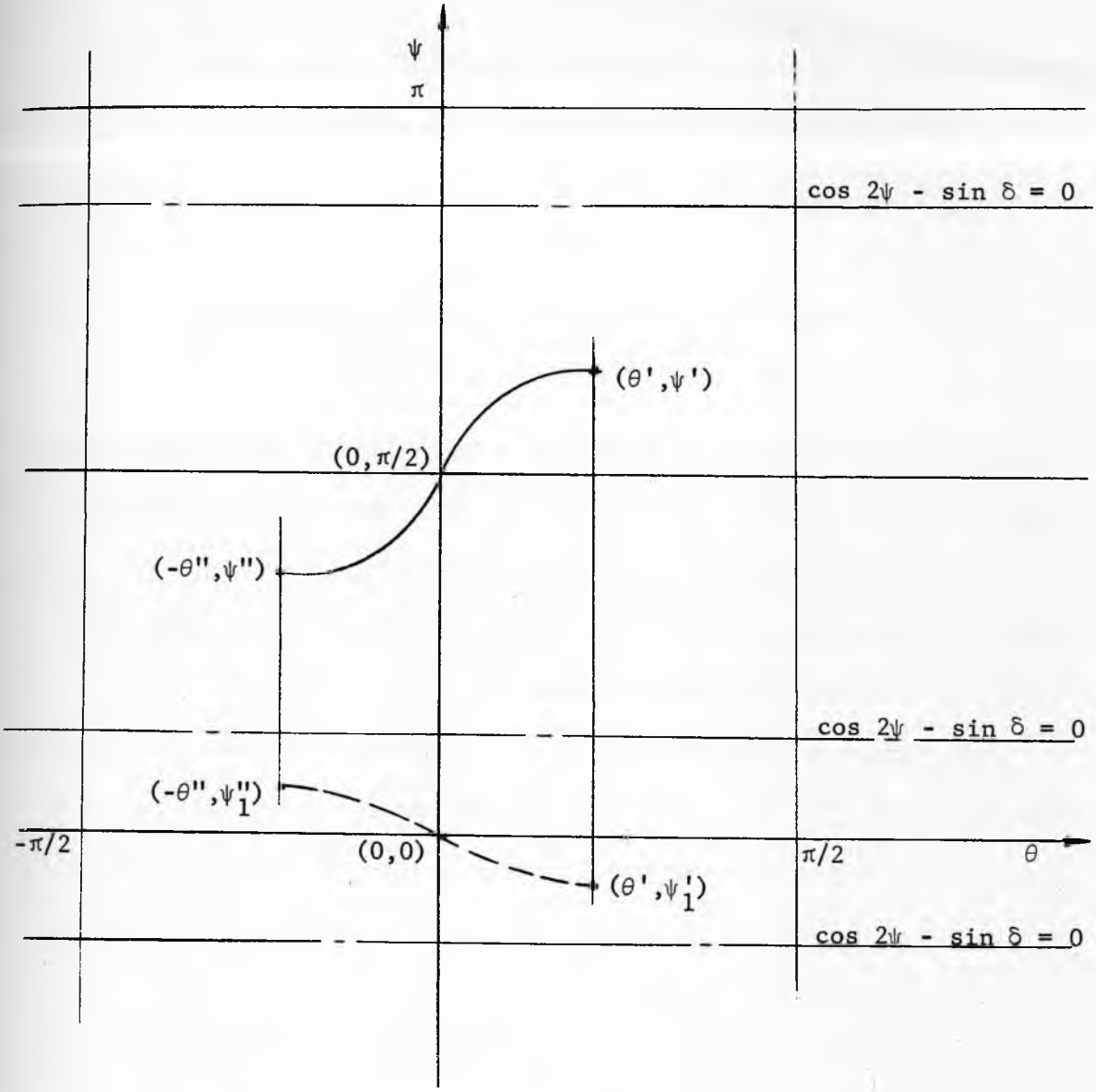

Fig. 28

Solutions of the radial stress field in axial symmetry

and indicates the largest possible value of θ' within rough walls. These values of θ' are listed in Table 2 as a function of δ.

Table 2

δ	30°	40°	50°	60°	70°
Max. θ'	15°	8.1°	4.4°	2.2°	.5°

Especially, for the larger values of δ, an axi-symmetric channel can open out but very little. In addition, this type of flow implies a continuous velocity profile at the top and at the bottom of the channel and is, in practice difficult to attain. As a result, this type of flow, if it occurs, is usually unsteady.

Resultant vertical force. It is of practical interest to know the resultant vertical force Q acting at a horizontal cross-section of a channel. An expression for this force will now be derived. The horizontal cross-section is of width $B = 2y'$, and is elevated a distance $-x_o$ above the wertex, Fig. 42.

The vertical pressure σ_x is found from eq.(14) with substitutions (3) and (102) for ω and σ, thus

$$\sigma_x = r\,\gamma\,s\,[1 + \sin\delta\,\cos 2(\psi + \theta)]\ .$$

The total vertical force is

$$Q = 2\pi^m\, L^{1-m} \int_o^{y'} \sigma_x y^m\, dy, \qquad (j)$$

where L is the length of the channel in plane strain. To compute Q it is necessary to express y as a function of x_o and the angles θ and ψ.

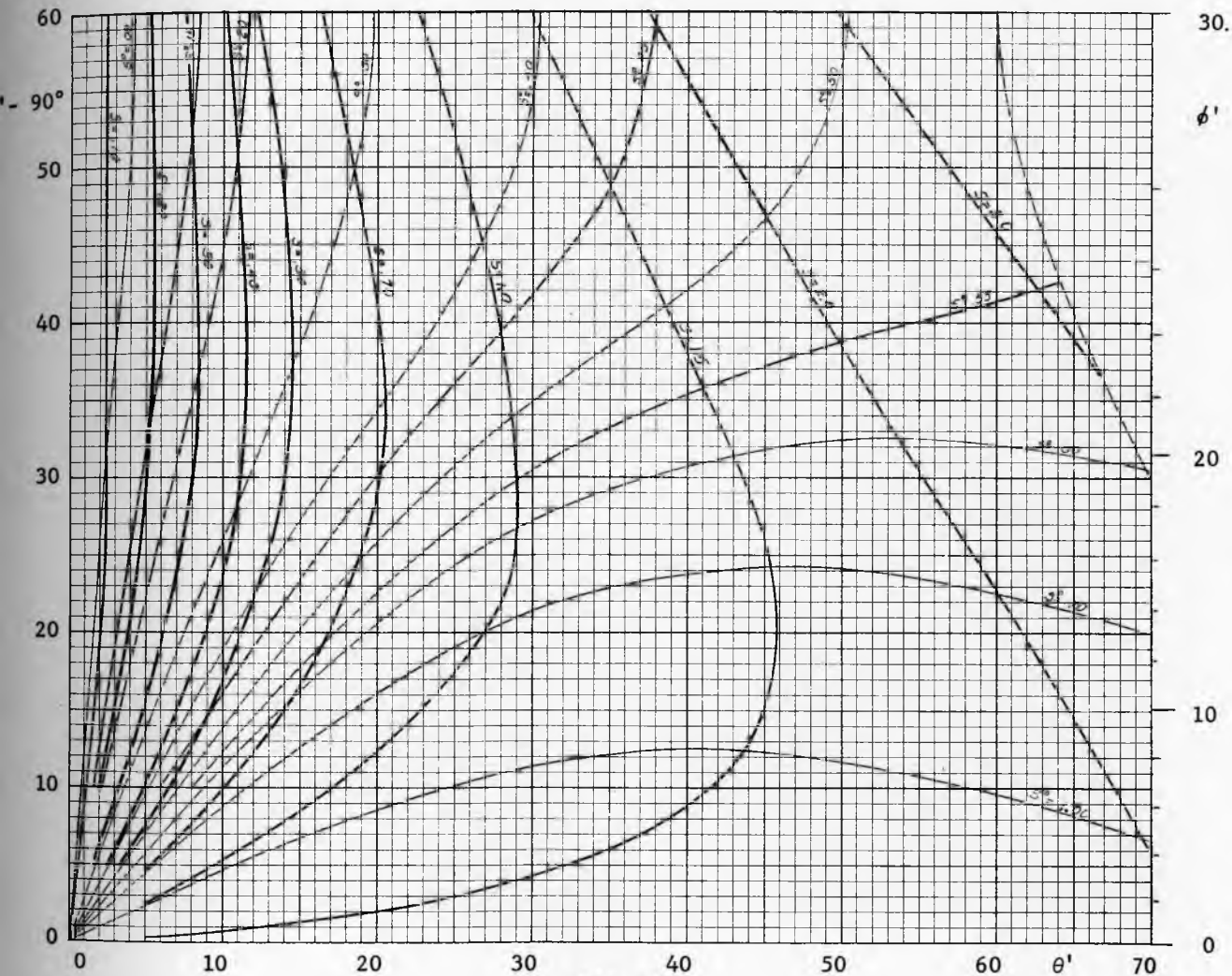

Fig. 29

Function s, $\delta = 30°$

Plane symmetry (symmetric plane flow)

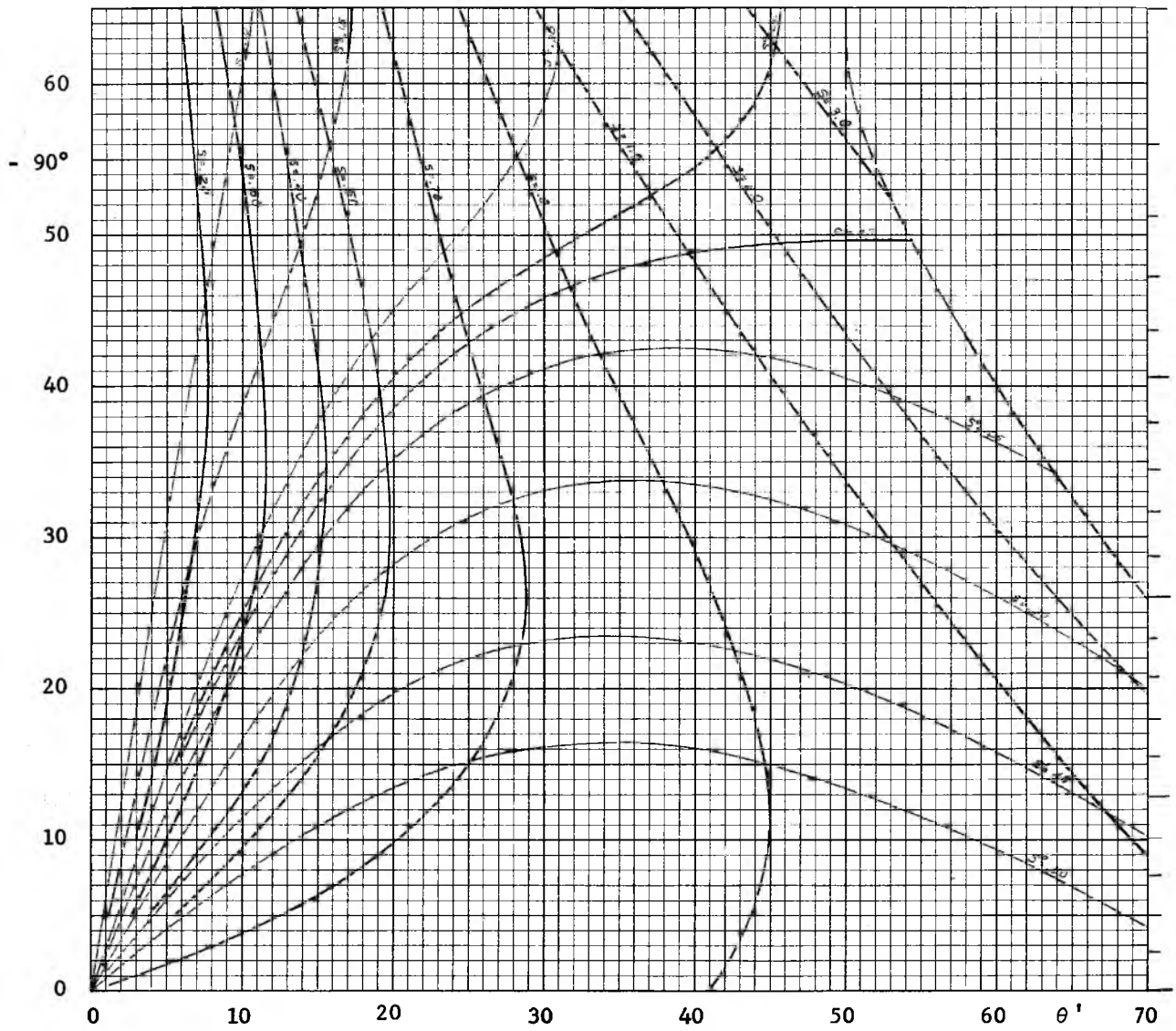

Fig. 30

Function s, $\delta = 40°$

Plane symmetry (symmetric plane flow)

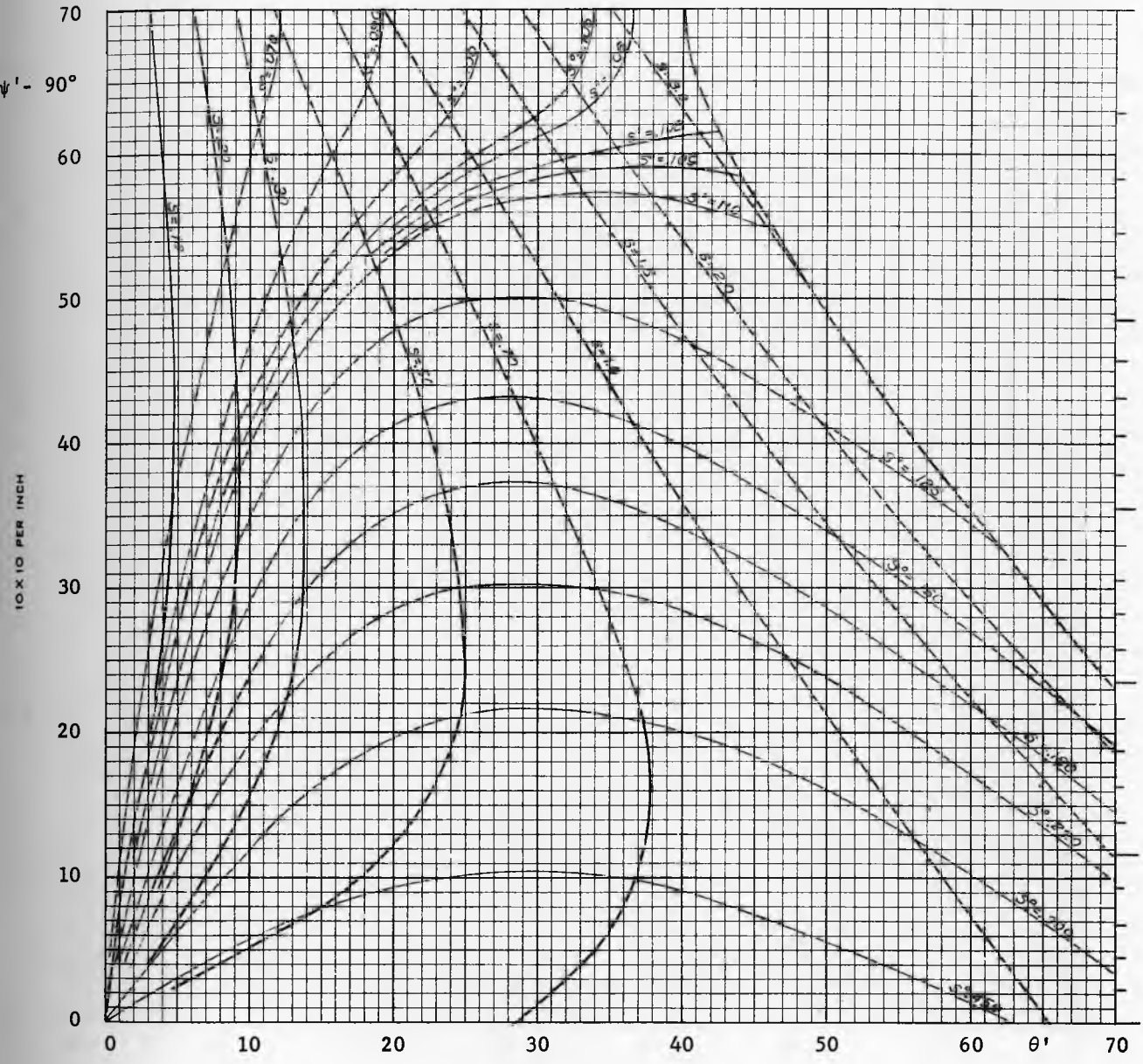

Fig. 31

Function s, $\delta = 50°$

Plane symmetry (symmetric plane flow)

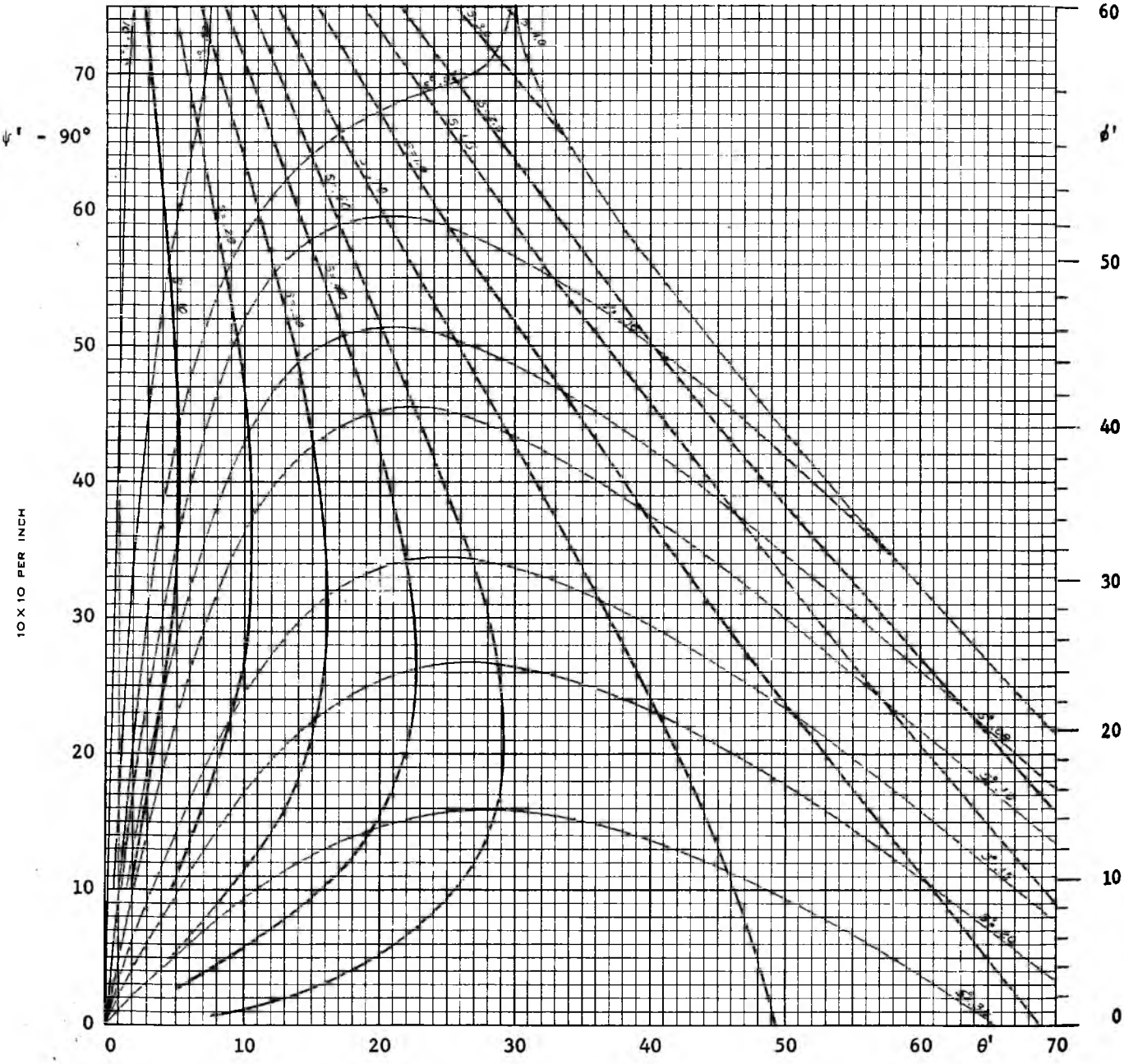

Fig. 32

Function s, $\delta = 60°$

Plane symmetry (symmetric plane flow)

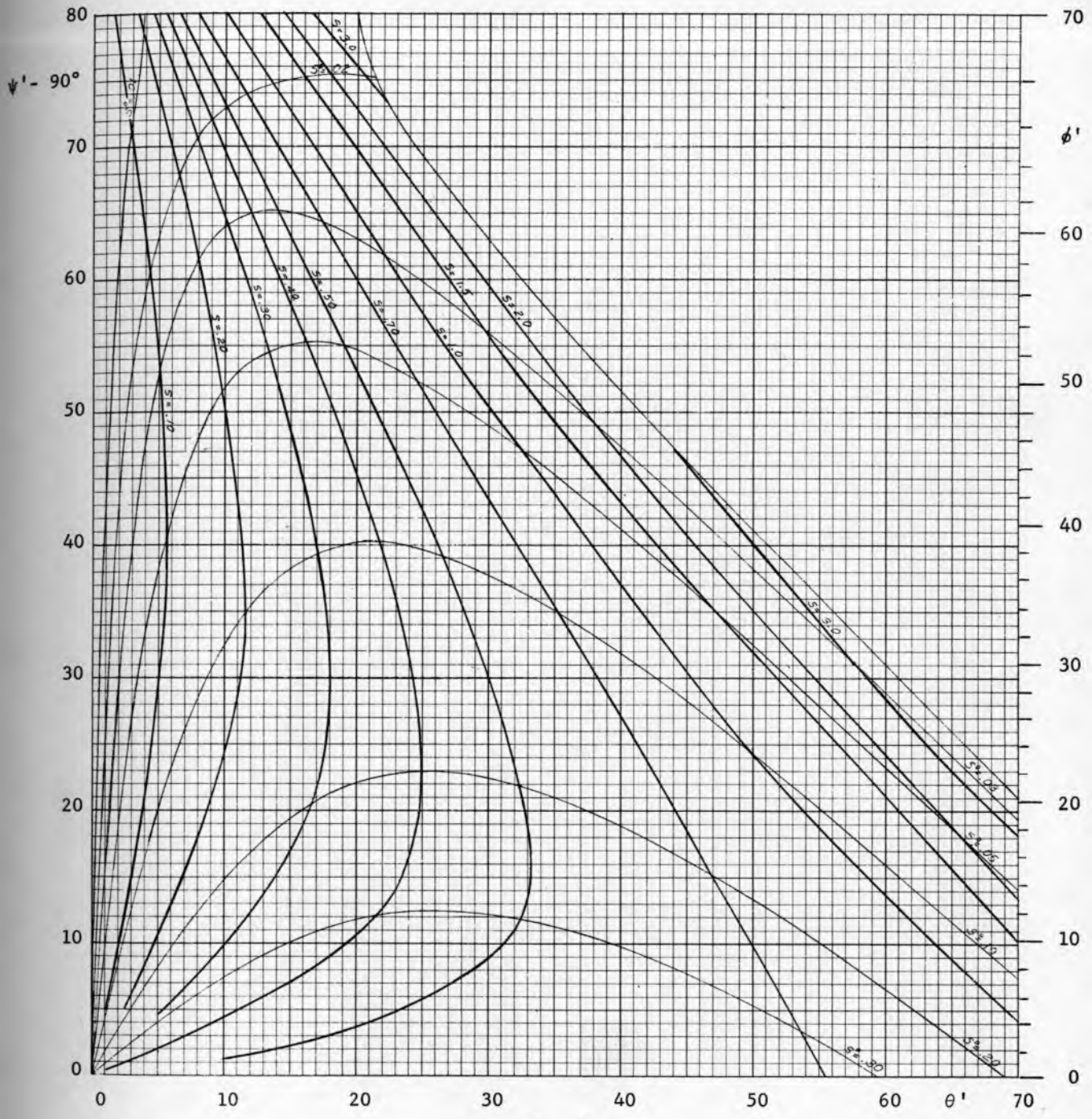

Fig. 33

Function s, $\delta = 70°$

Plane symmetry (symmetric plane flow)

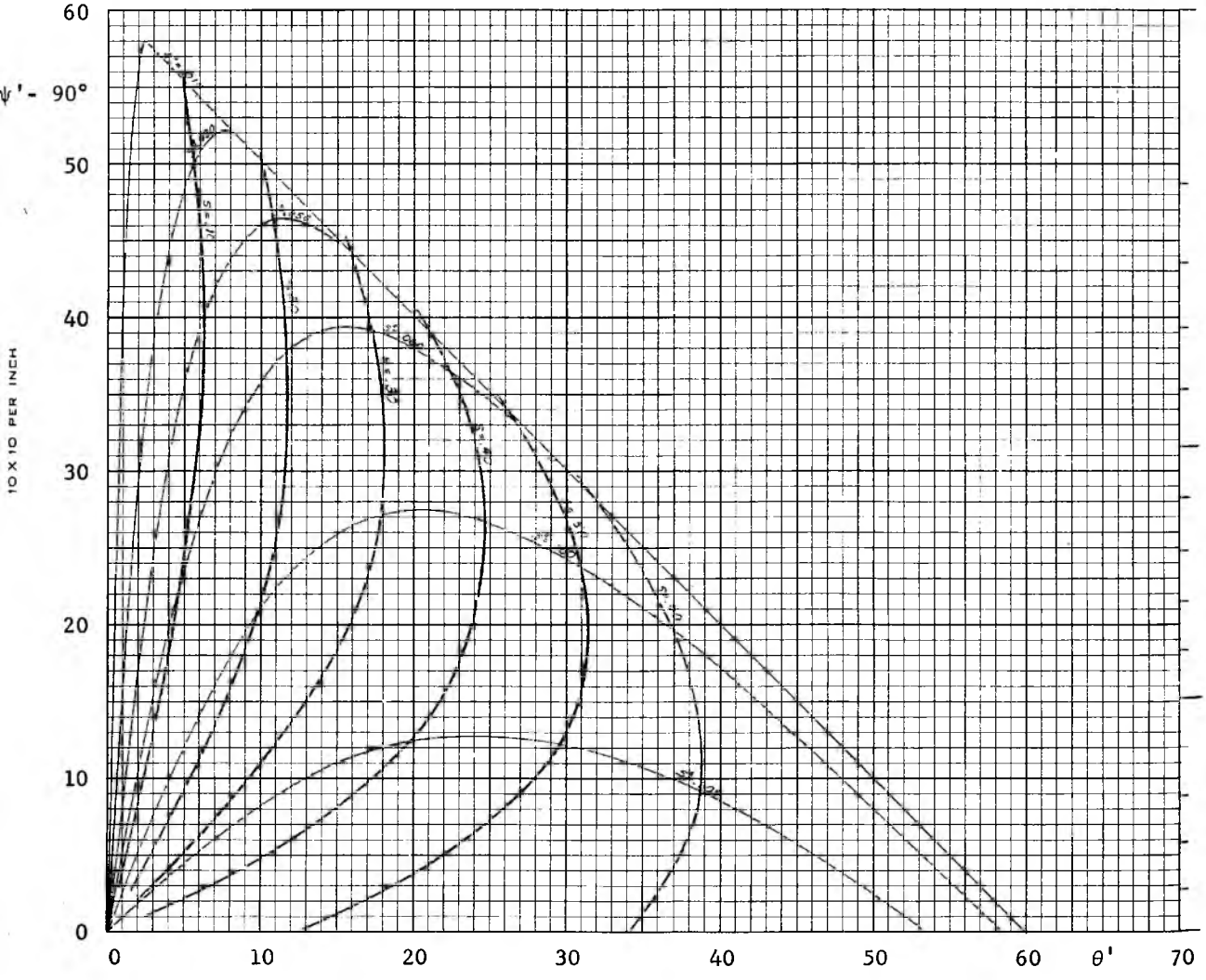

Fig. 34

Function s, $\delta = 30°$

Axial symmetry (conical flow)

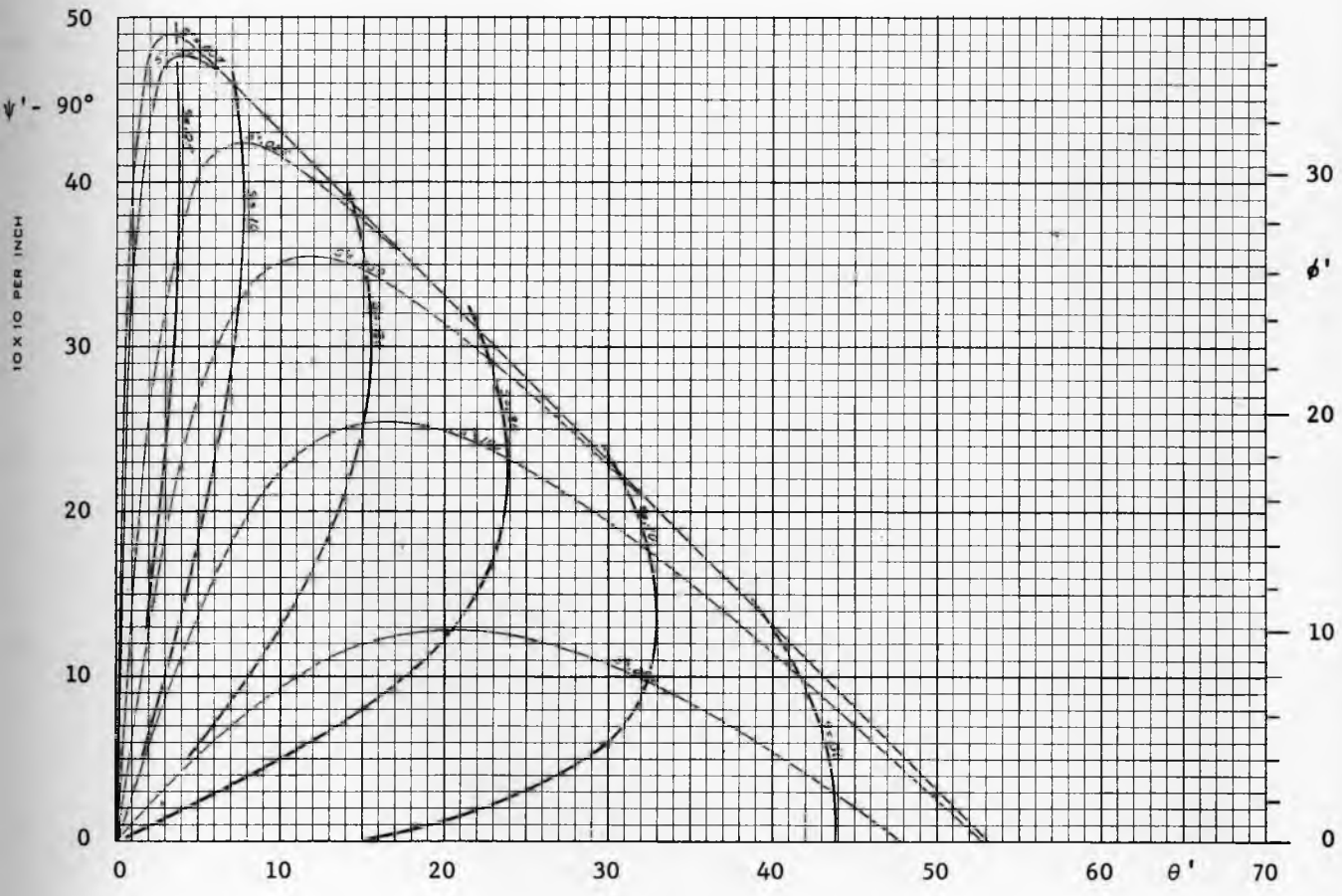

Fig. 35

Function s, $\delta = 40°$

Axial symmetry (conical flow)

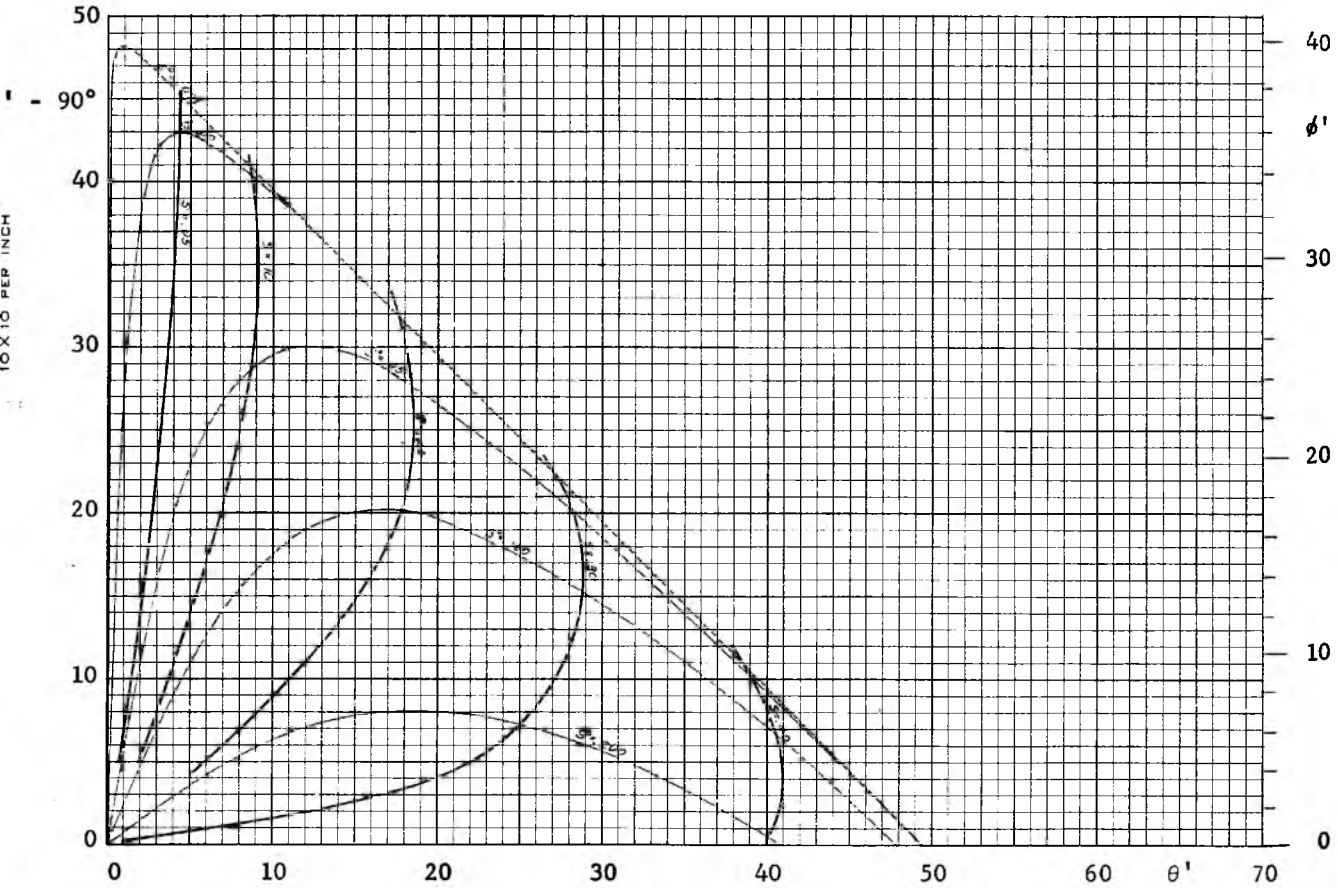

Fig. 36

Function s, $\delta = 50°$

Axial symmetry (conical flow)

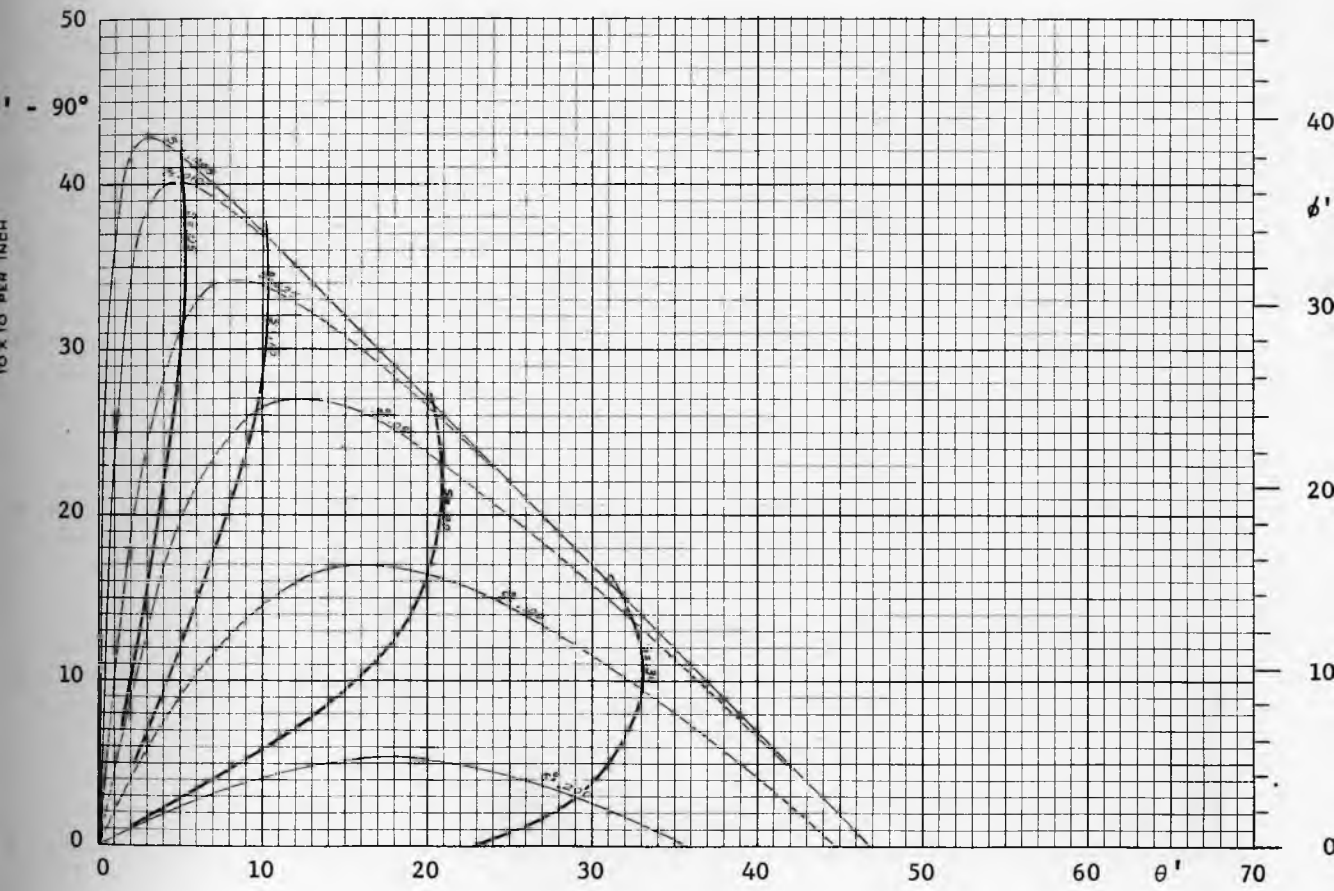

Fig 37

Function s, $\delta = 60°$

Axial symmetry (conical flow)

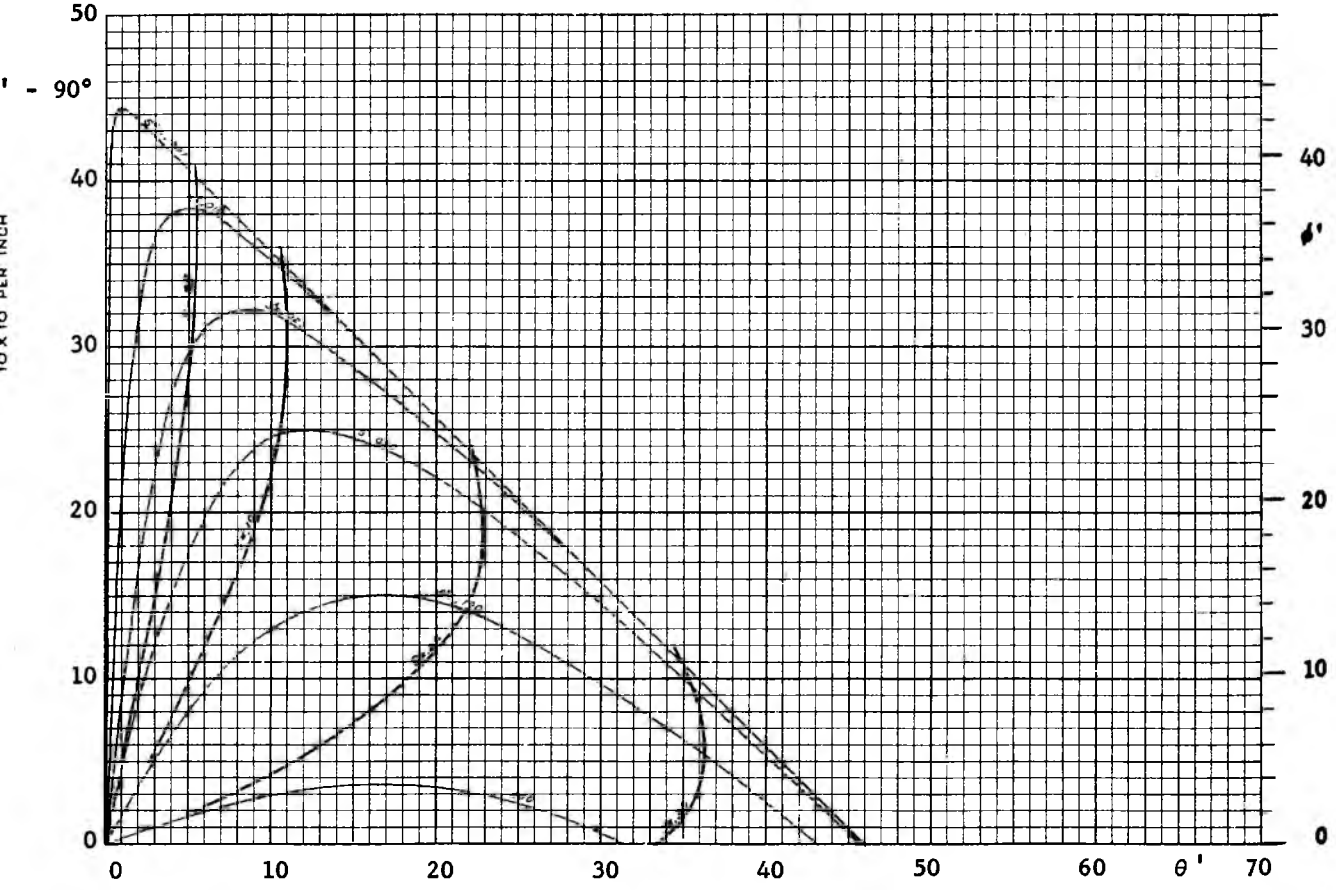

Fig. 38

Function s, $\delta = 70°$

Axial symmetry (conical flow)

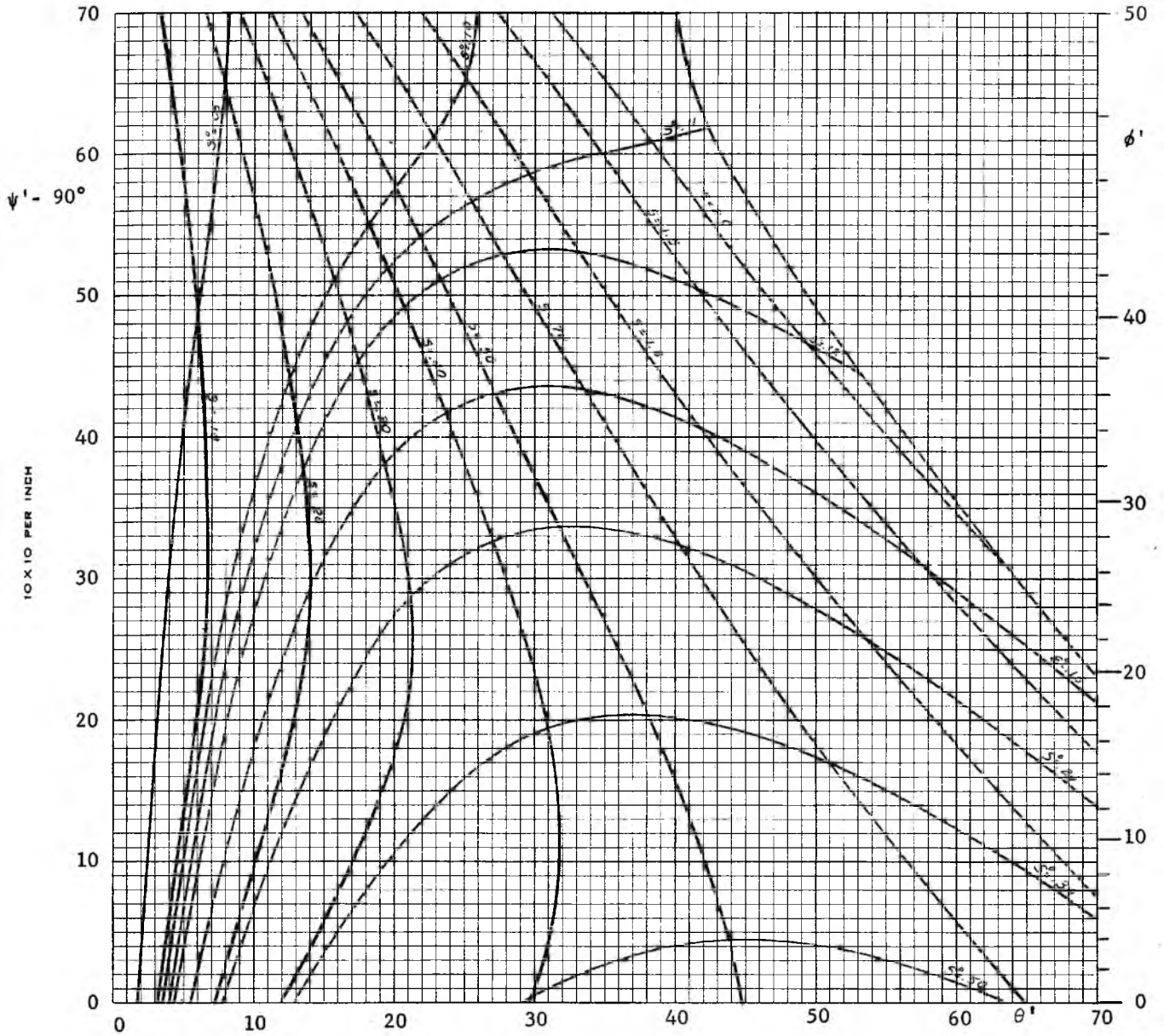

Fig. 39

Function s, $\delta = 50°$, $\phi^V = 20°$

Plane asymmetry (Plane flow - one vertical wall)

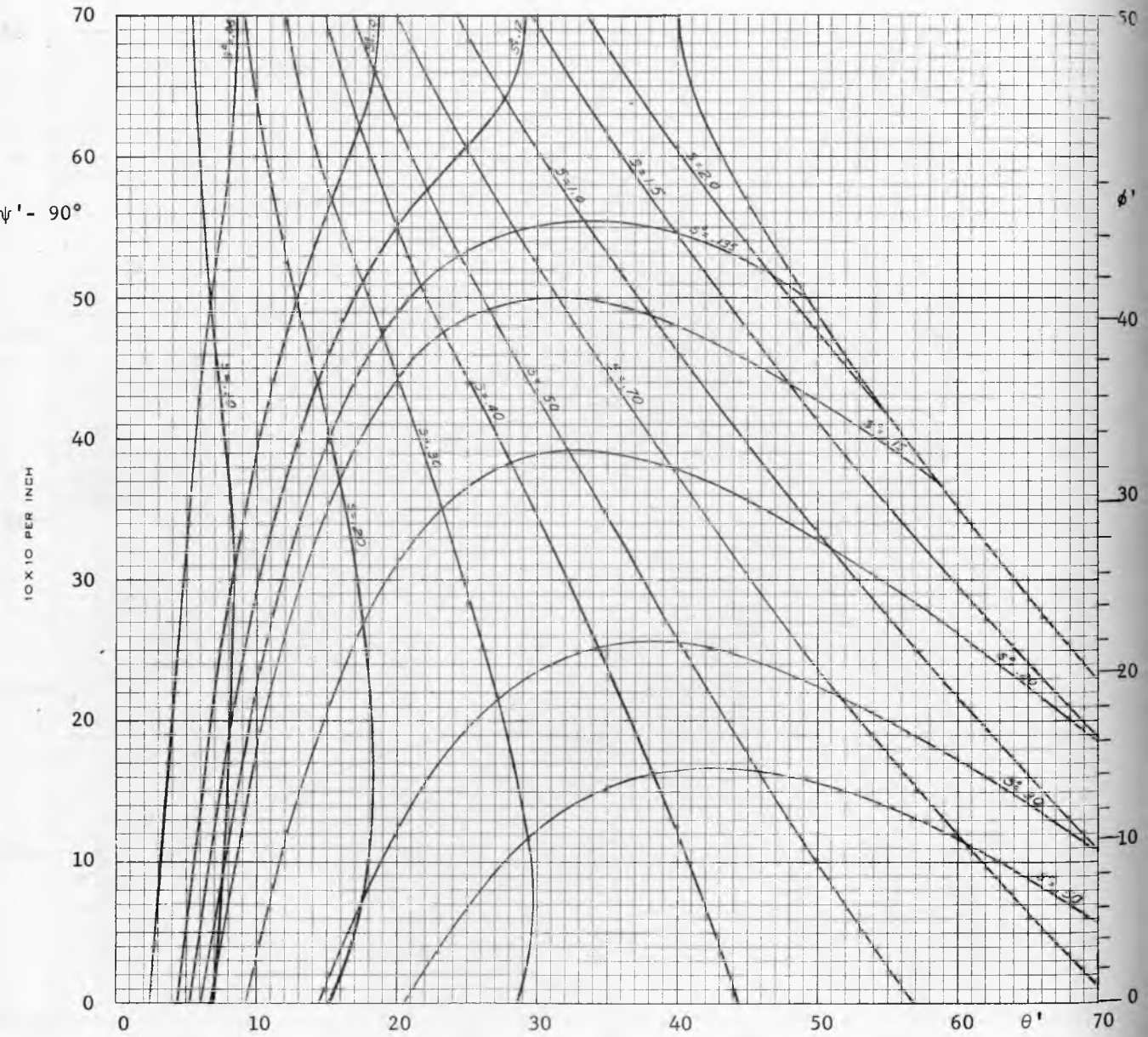

Fig. 40

Function s, $\delta = 50°$, $\phi^v = 30°$

Plane asymmetry (Plane flow - one vertical wall)

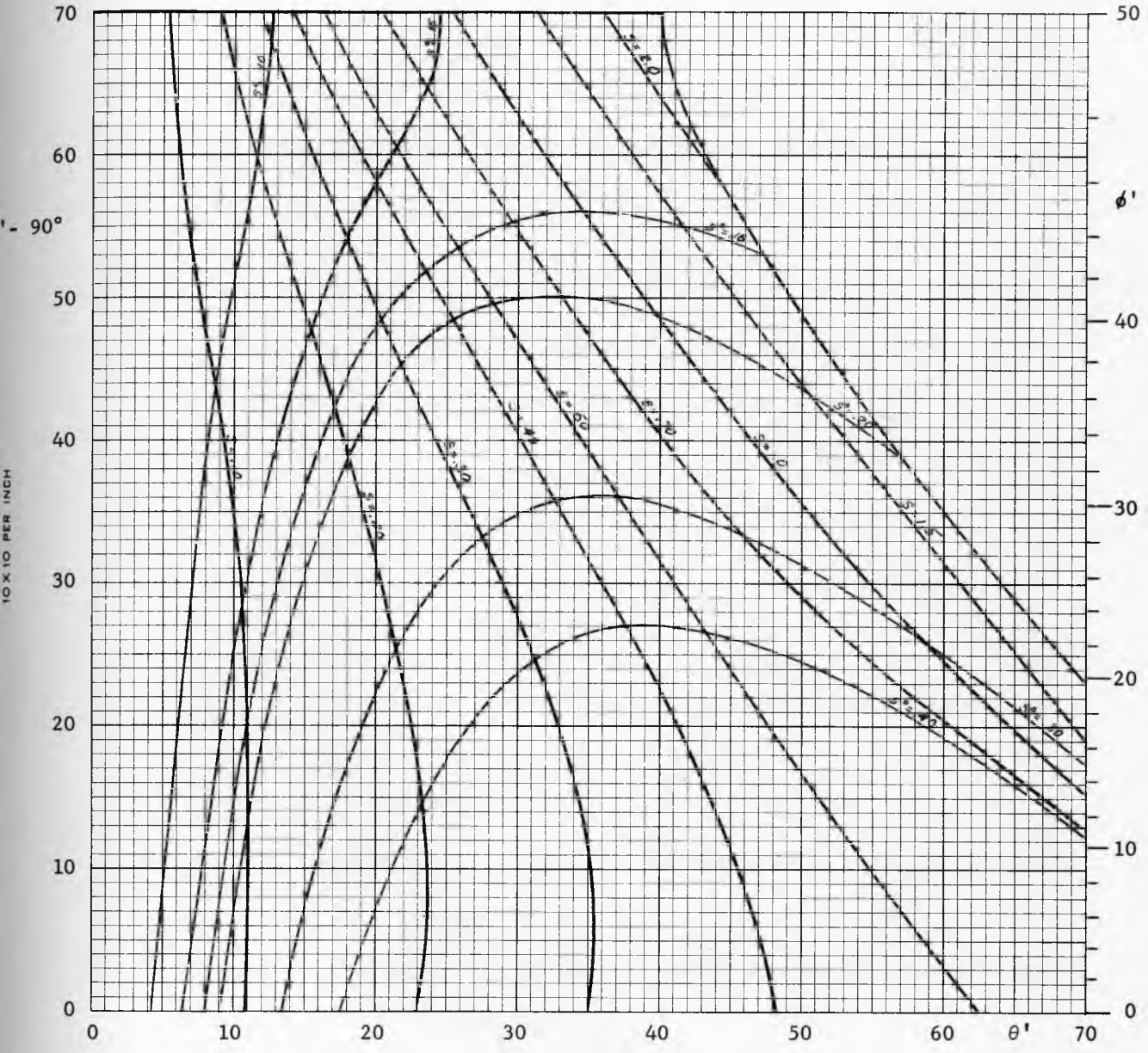

Fig. 41

Function s, $\delta = 50°$, $\phi^V = 40°$

Plane asymmetry (Plane flow - one vertical wall)

The relations between the (x,y) and (r,θ) coordinates are, (Fig. 2),

$$\left.\begin{aligned} x &= - r \cos \theta, \\ y &= - r \sin \theta. \end{aligned}\right\} \quad (k)$$

The total derivatives are:

$$dx = -\cos \theta \, dr + r \sin \theta \, d\theta,$$

$$dy = - \sin \theta \, dr - r \cos \theta \, d\theta.$$

For x_o constant, dx = 0 and elimination of dr between the above two equations leads to

$$dy = - \frac{r \, d\theta}{\cos \theta}. \qquad (1)$$

From conditions at the wall, Fig. 42, there is

$$x_o = y' \cot \theta'.$$

Within the channel

$$r = - \frac{x_o}{\cos \theta},$$

or, eliminating x_o,

$$r = - \frac{y' \cot \theta'}{\cos \theta}.$$

Hence expression (1) for dy becomes

$$dy = y' \cot \theta' \frac{d\theta}{\cos^2 \theta}.$$

Elimination of r in the second of equations (k) yields

$$y = y' \cos \theta' \tan \theta.$$

Substitutions for σ_x, r, y and dy in eq.(j) transform it into

$$Q = q \, \gamma \, L^{1-m} \, B^{2+m}, \qquad (103)$$

where

$$q = 2\pi^m \left(\frac{\cot \theta'}{2}\right)^{2+m} \int_o^{\theta'} s \frac{\tan^m \theta}{\cos^3 \theta} \left[1 + \sin \delta \cos 2(\theta + \psi)\right] d\theta. \qquad (104)$$

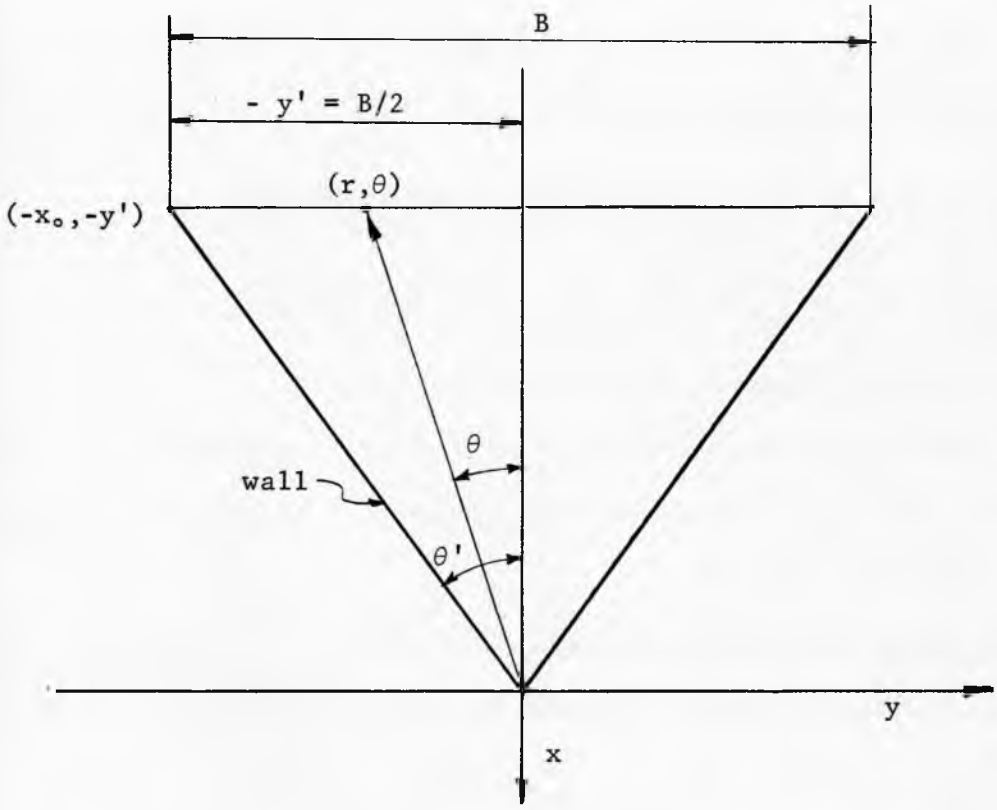

Fig. 42

Resultant vertical force

Lines of constant values of q are plotted in Figures 43 to 48 for $\delta = 30°$, $40°$ and $50°$ in symmetric plane strain and in axial symmetry.

Stresses at the walls. The normal and shearing stresses σ' and τ' which act between a flowing solid and the walls are computed from equations (18) and (19): $\sigma' = \sigma_\theta$ and $\tau' = -\tau_{r\theta}$, respectively. In these equations, σ is replaced by expression (102) with

$$r = \frac{B}{2 \sin \theta},$$

in accordance with Fig. 49, leading to

$$\frac{\sigma'}{\gamma B} = \frac{\sigma''}{\gamma B} = s' \frac{1 - \sin \delta \cos 2\psi'}{2 \sin \theta'}, \tag{105}$$

$$-\frac{\tau'}{\gamma B} = \frac{\tau''}{\gamma B} = s' \frac{\sin \delta \sin 2\psi'}{2 \sin \theta'}. \tag{106}$$

These equations apply in plane and axial symmetry.

Lines of constant values of $\sigma'/\gamma B$ and $\tau'/\gamma B$ are plotted in figures 50 to 61 for plane strain and axial symmetry in (θ', o') coordinates for $\delta = 30°$, $40°$ and $50°$.

Influence of compressibility. The influence of compressibility on the solutions of radial flow can be estimated by using the expression (27)

$$\gamma = \gamma_o \sigma^\beta$$

with σ eliminated by means of eq.(102) to yield

$$\gamma = (r^\beta \gamma_o s^\beta)^{\frac{1}{1-\beta}}, \tag{107}$$

and the derivatives

$$\frac{1}{\gamma}\frac{\partial \gamma}{\partial \theta} = \frac{\beta}{1-\beta}\frac{1}{s}\frac{ds}{d\theta}, \quad \frac{r}{\gamma}\frac{\partial \gamma}{\partial r} = \frac{\beta}{1-\beta}. \tag{108}$$

With these substitutions, and $\psi = \psi(\theta)$ for the radial field, the coefficients (87) to (90) of the differential equations (85) and (86)

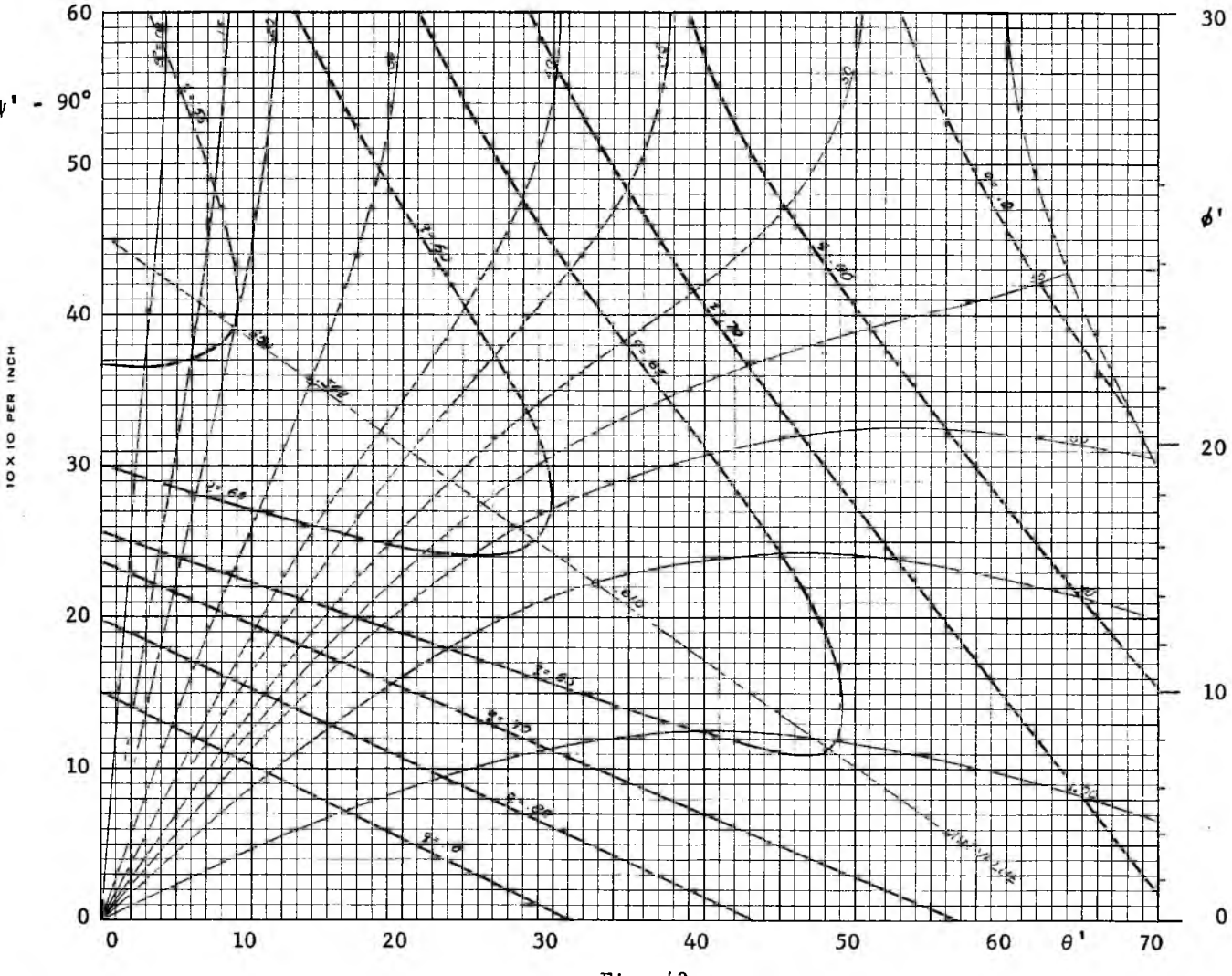

Fig. 43

Vertical force q, $\delta = 30°$

Plane symmetry (symmetric plane flow)

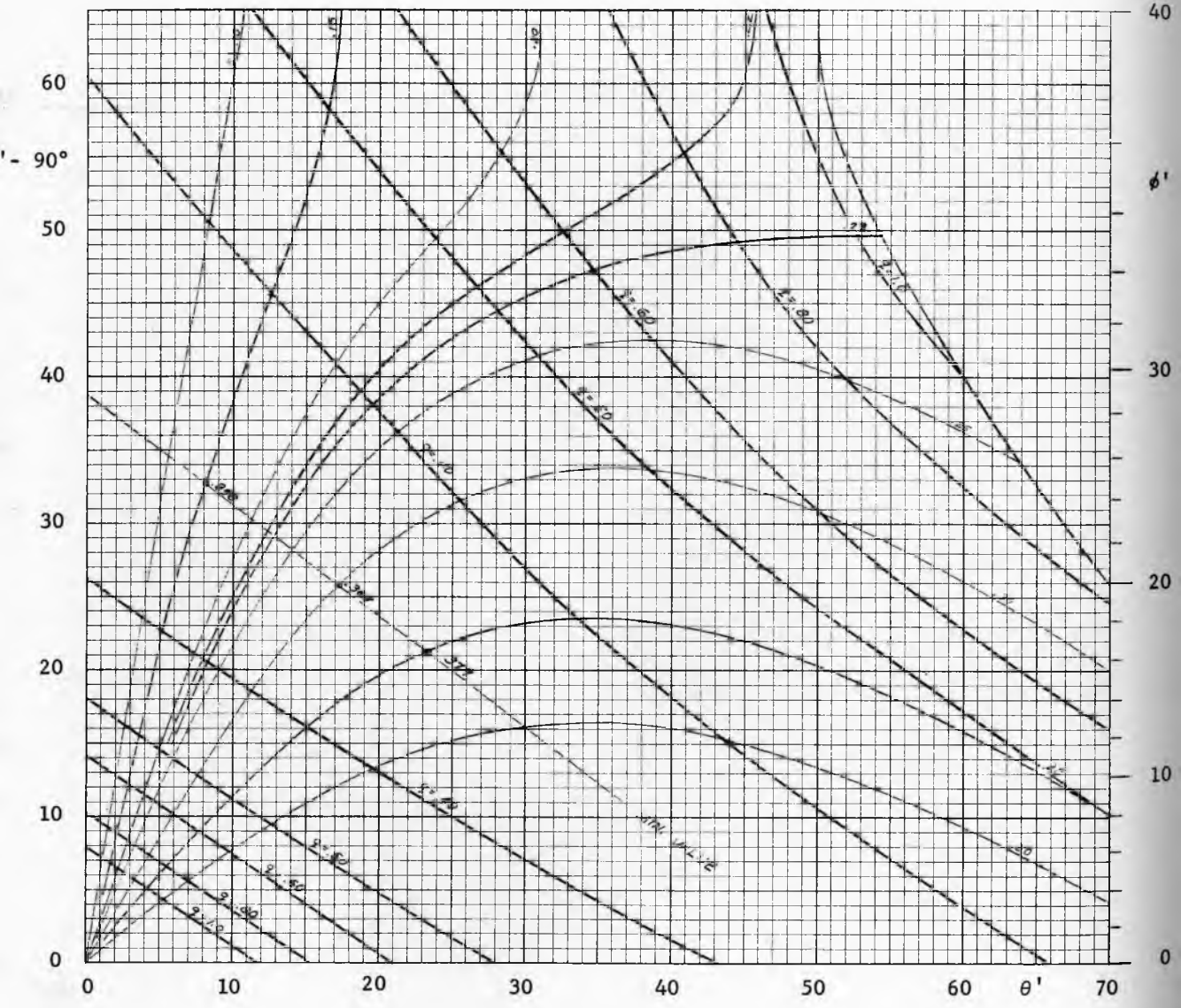

Fig. 44

Vertical force q, $\delta = 40°$

Plane symmetry (symmetric plane flow)

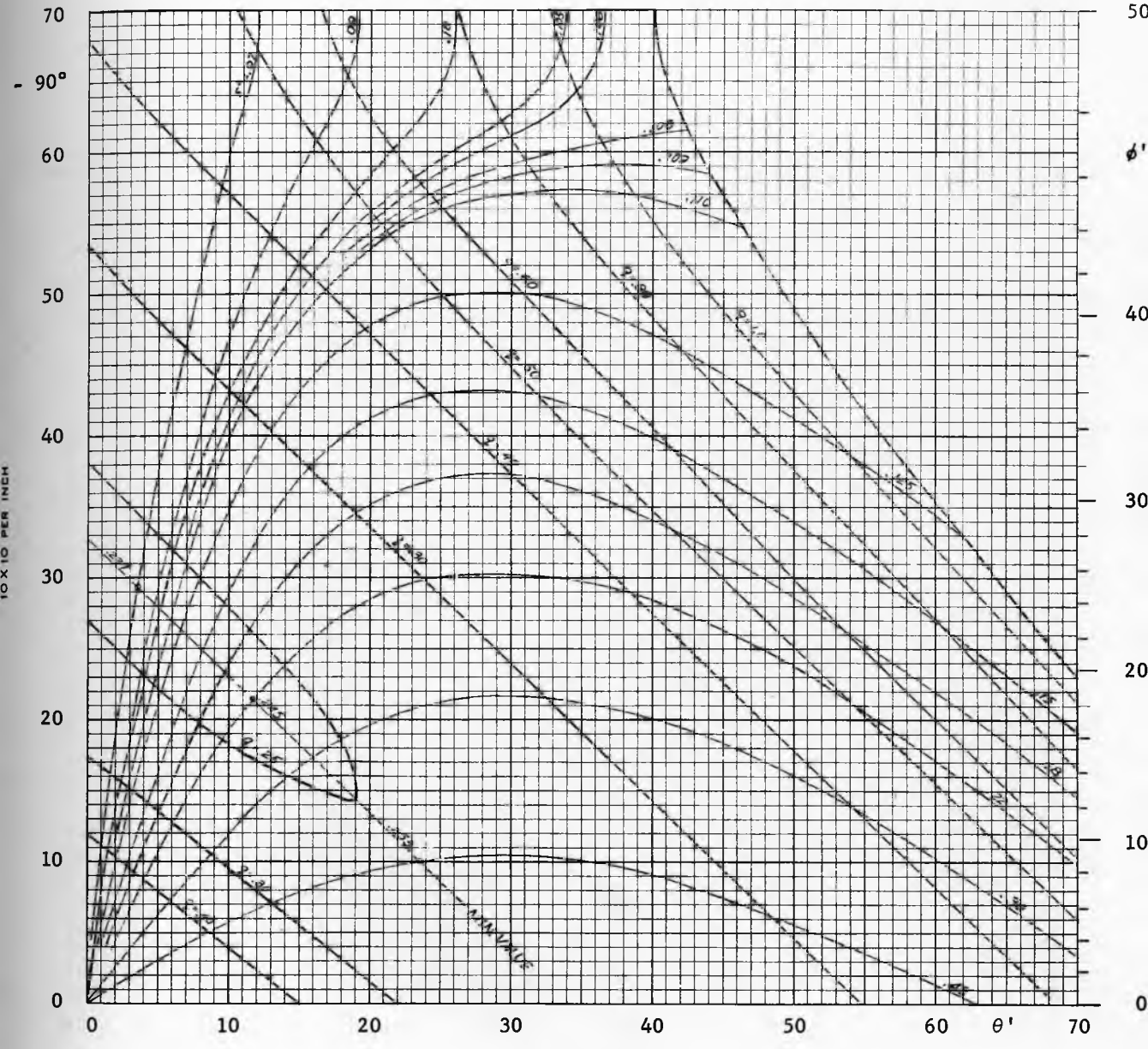

Fig. 45

Vertical force q, $\delta = 50°$

Plane symmetry (symmetric plane flow)

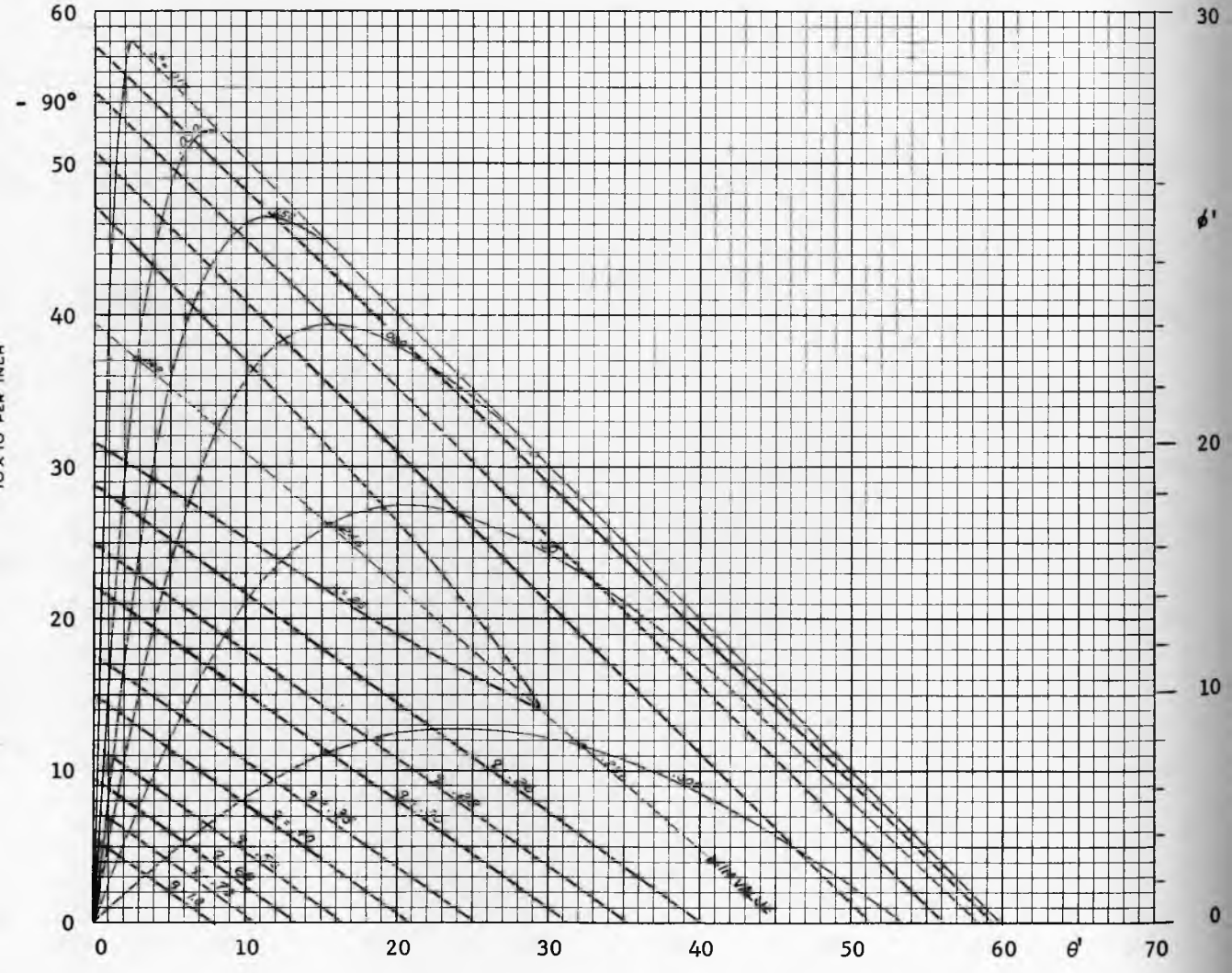

Fig. 46

Vertical force q, $\delta = 30°$

Axial symmetry (conical flow)

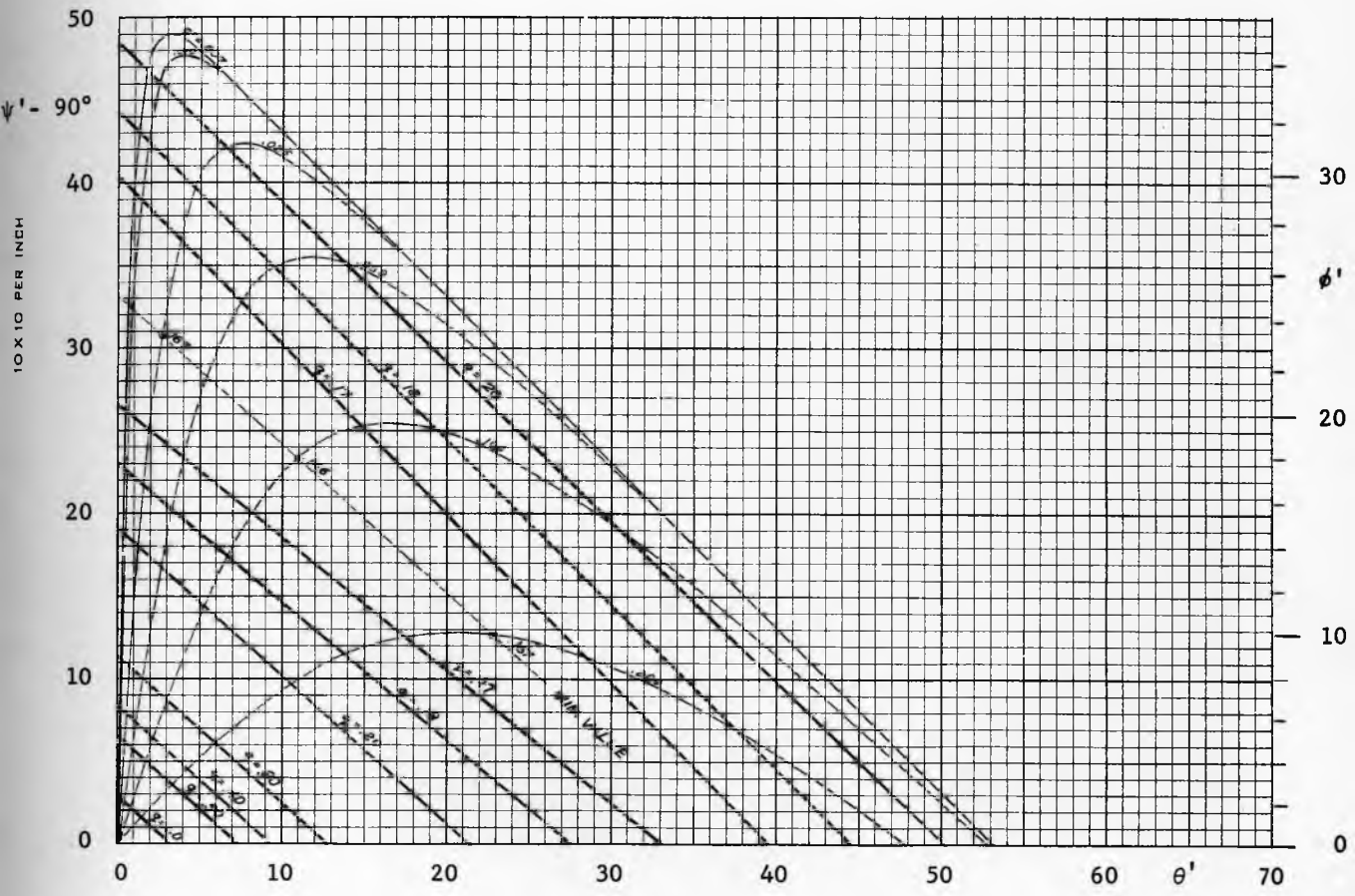

Fig. 47

Vertical force q, $\delta = 40°$

Axial symmetry (conical flow)

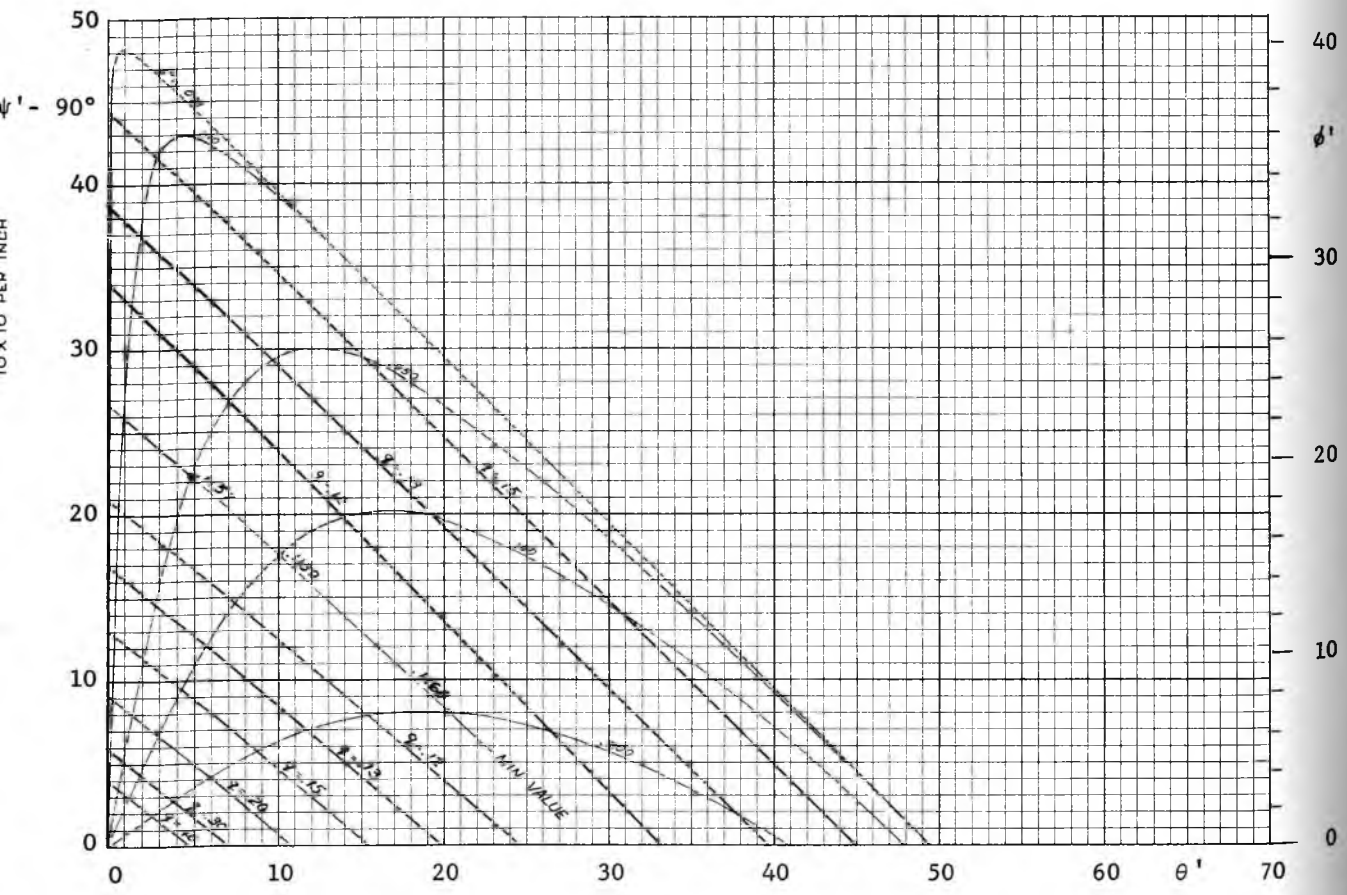

Fig. 48

Vertical force q, $\delta = 50°$

Axial symmetry (conical flow)

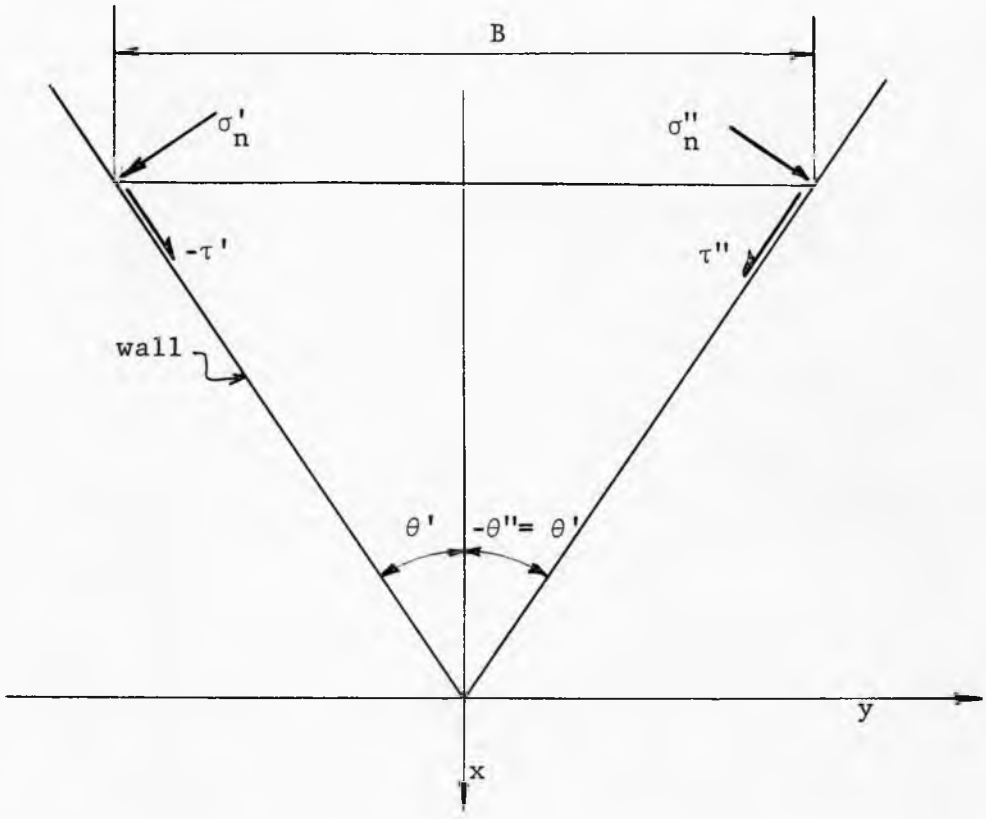

Fig. 49

Stresses at the walls

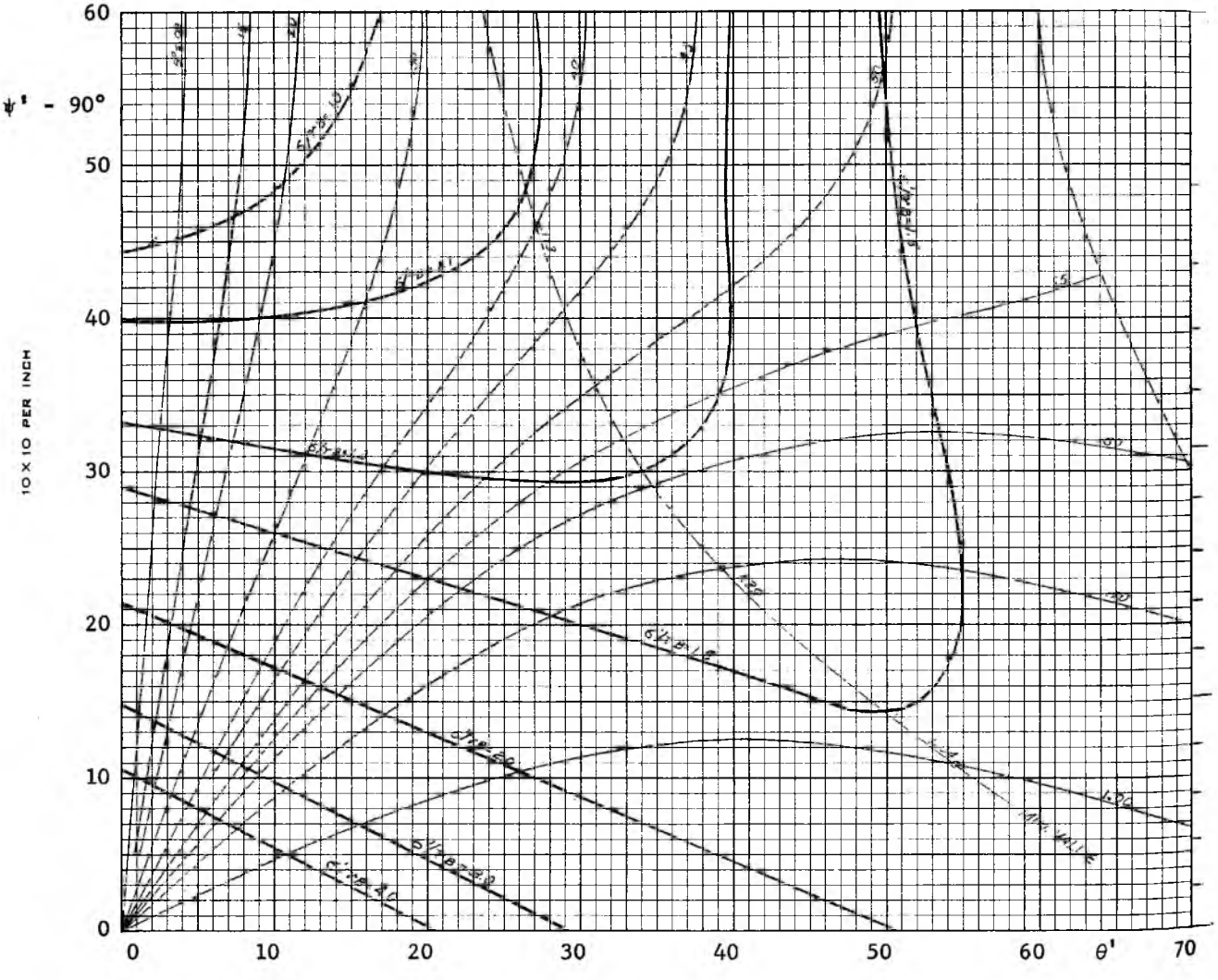

Fig. 50

Function σ'/γ B, $\delta = 30°$

Plane symmetry (symmetric plane flow)

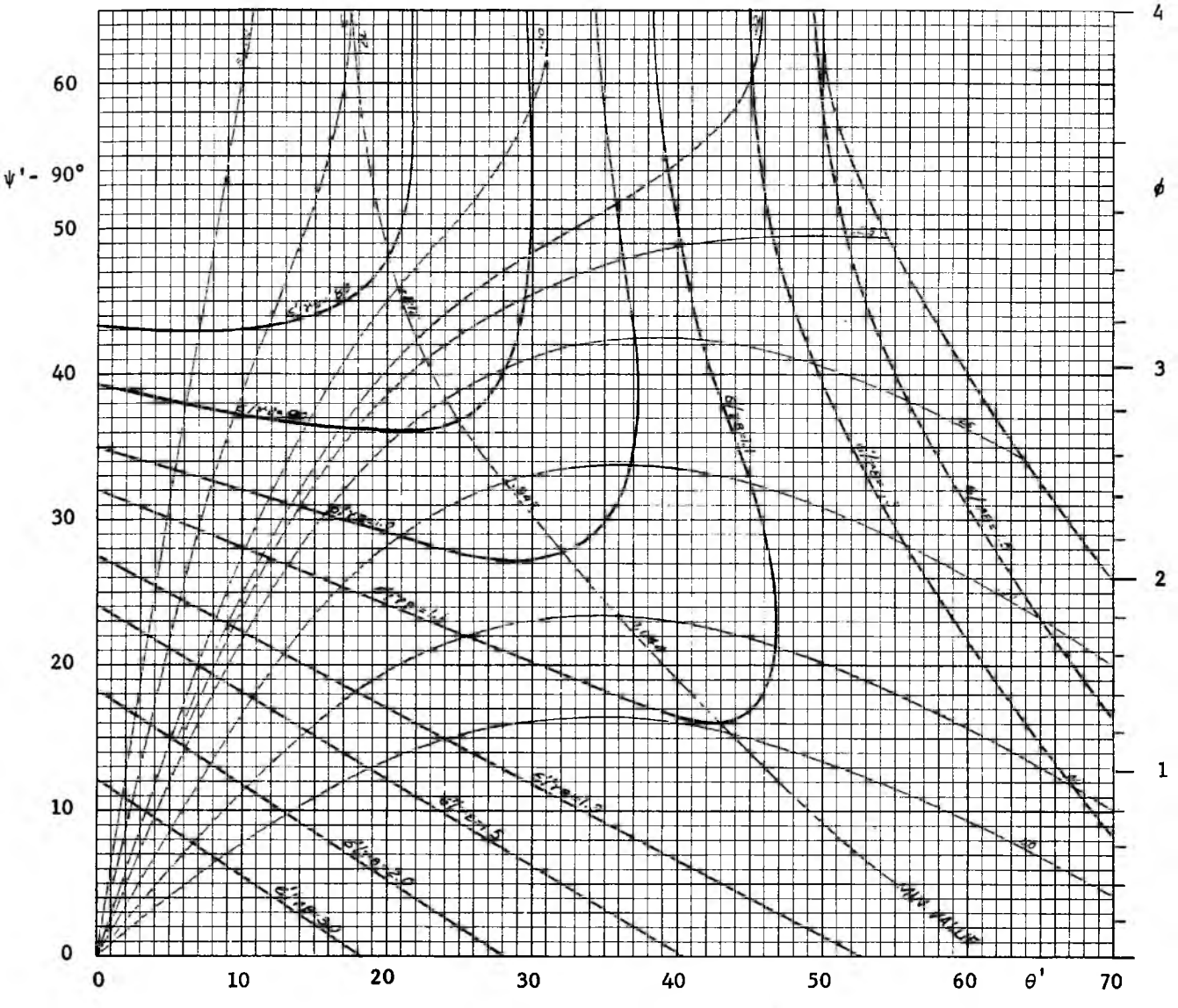

Fig. 51

Function σ'/γ B, $\delta = 40°$

Plane symmetry (symmetric plane flow)

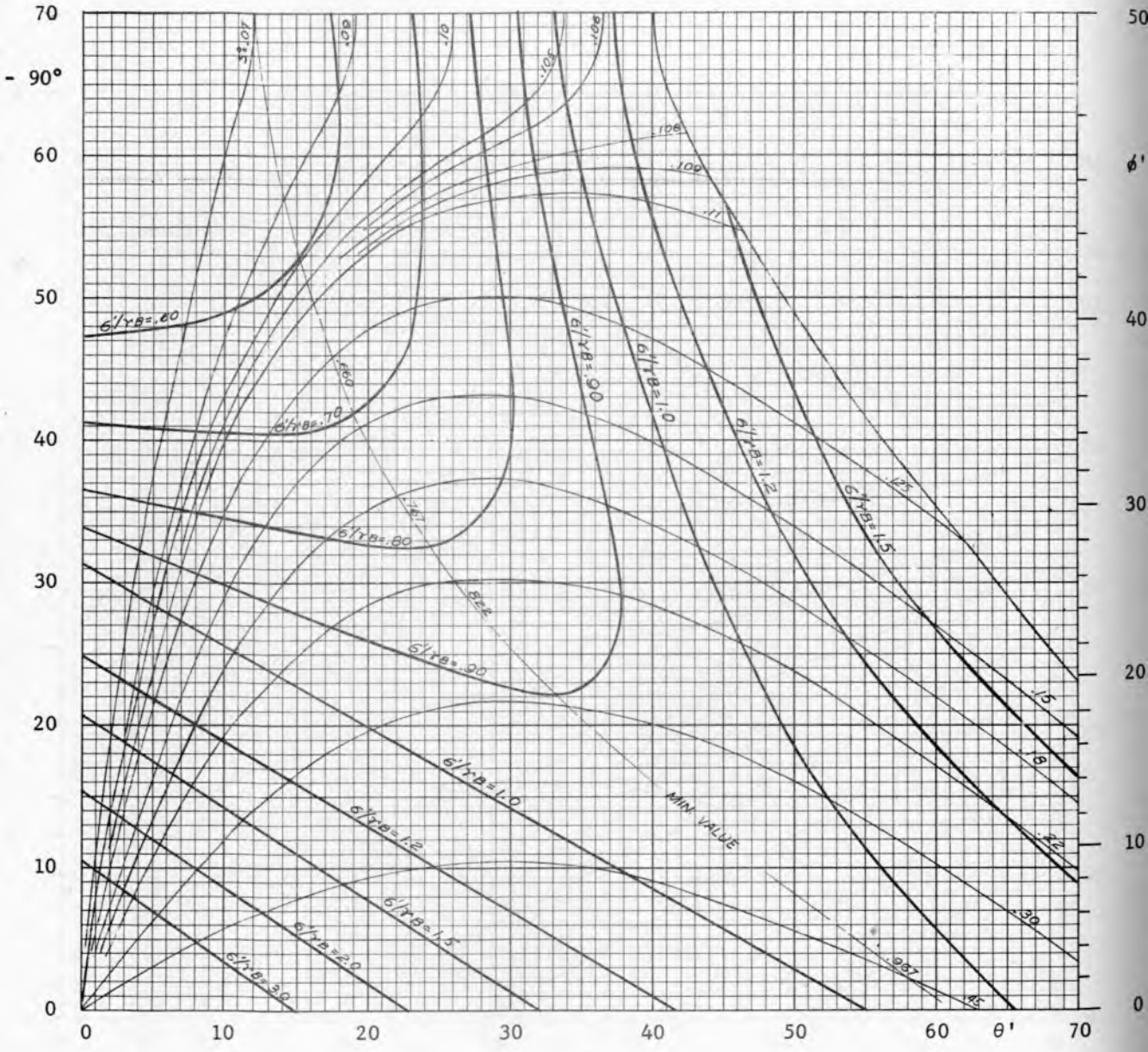

Fig. 52

Function $\sigma'/\gamma B$, $\delta = 50°$

Plane symmetry (symmetric plane flow)

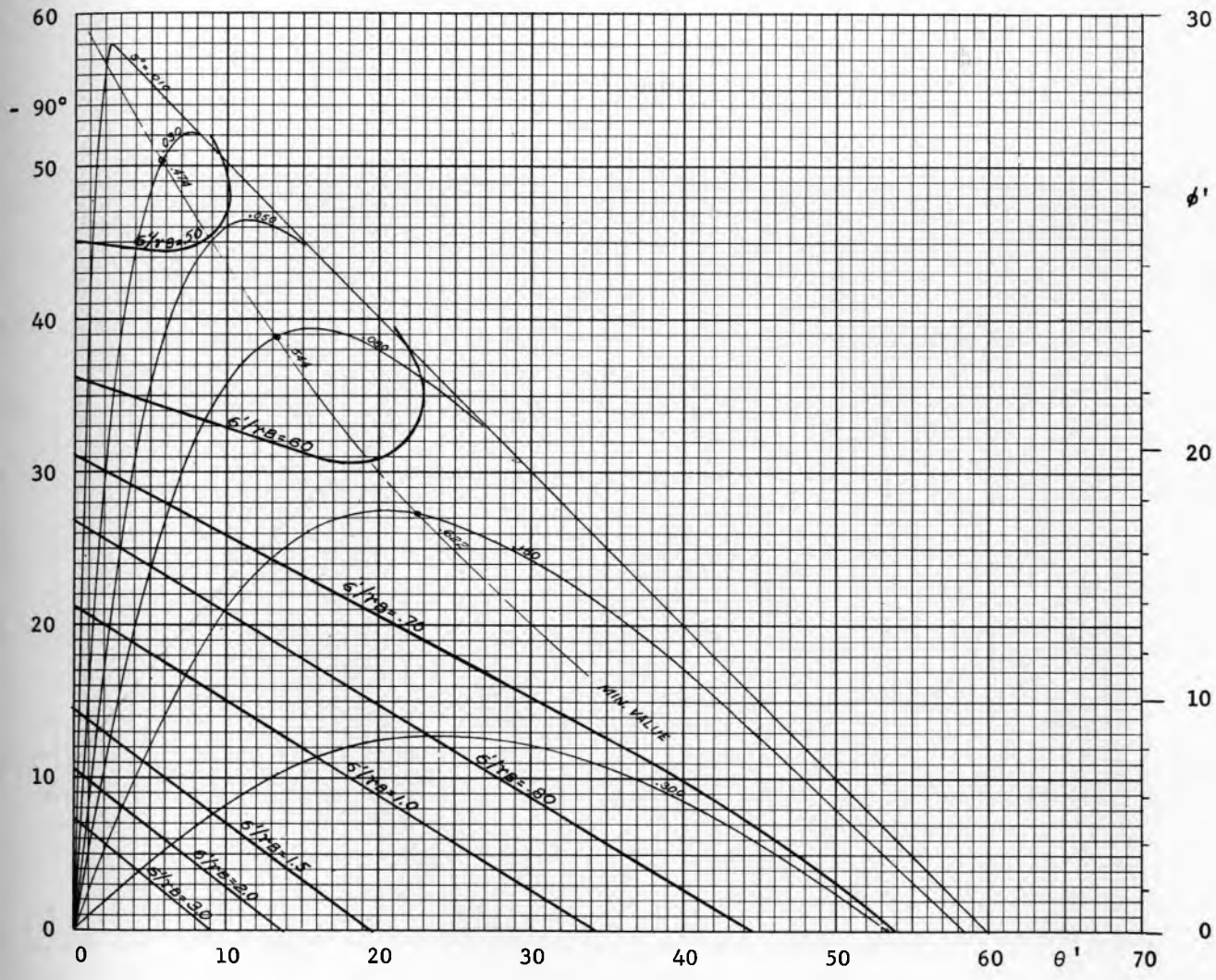

Fig. 53

Function $\sigma'/\gamma B$, $\delta = 30°$

Axial symmetry (conical flow)

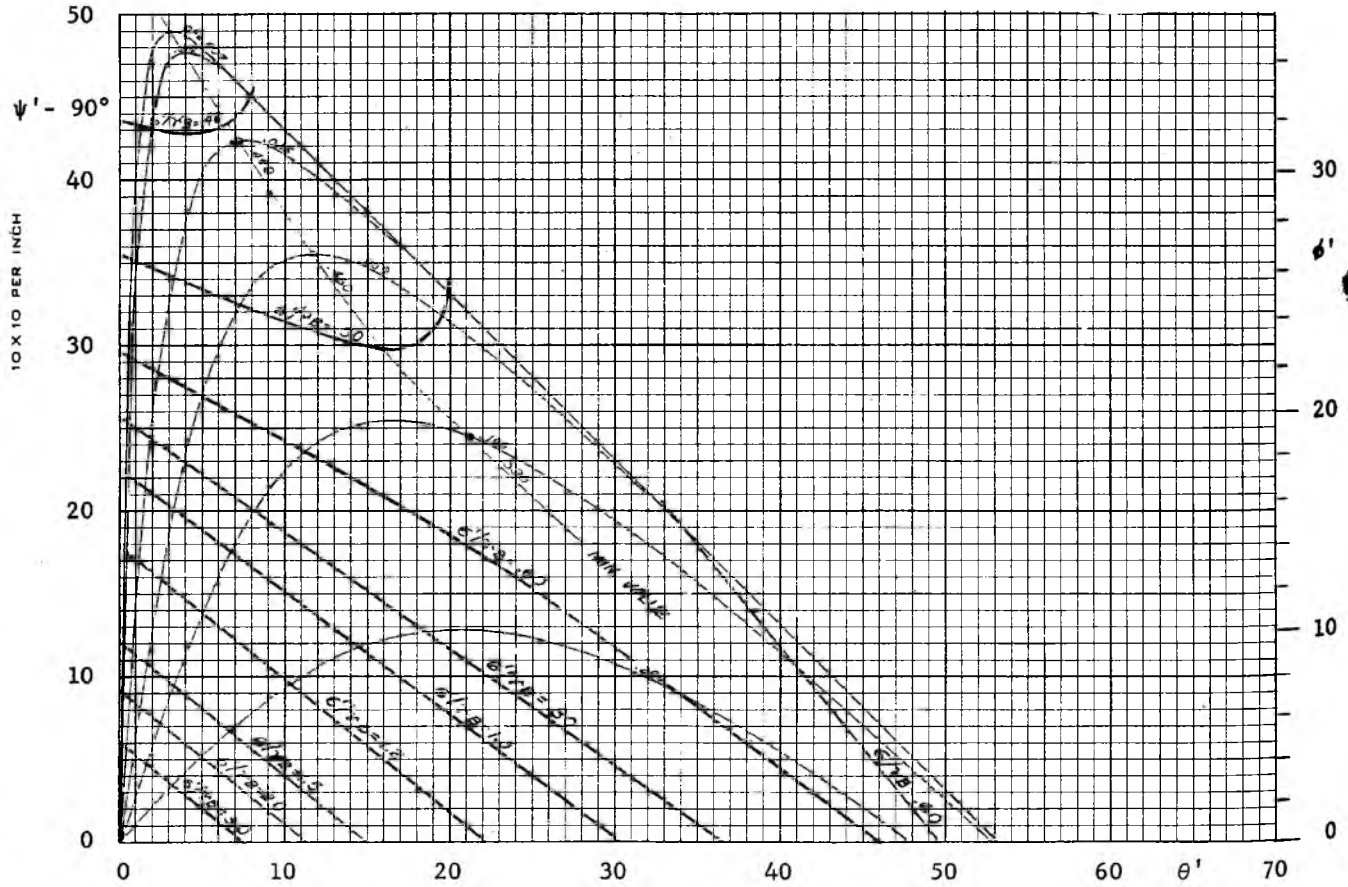

Fig. 54

Function σ'/γ B, $\delta = 40°$

Axial symmetry (conical flow)

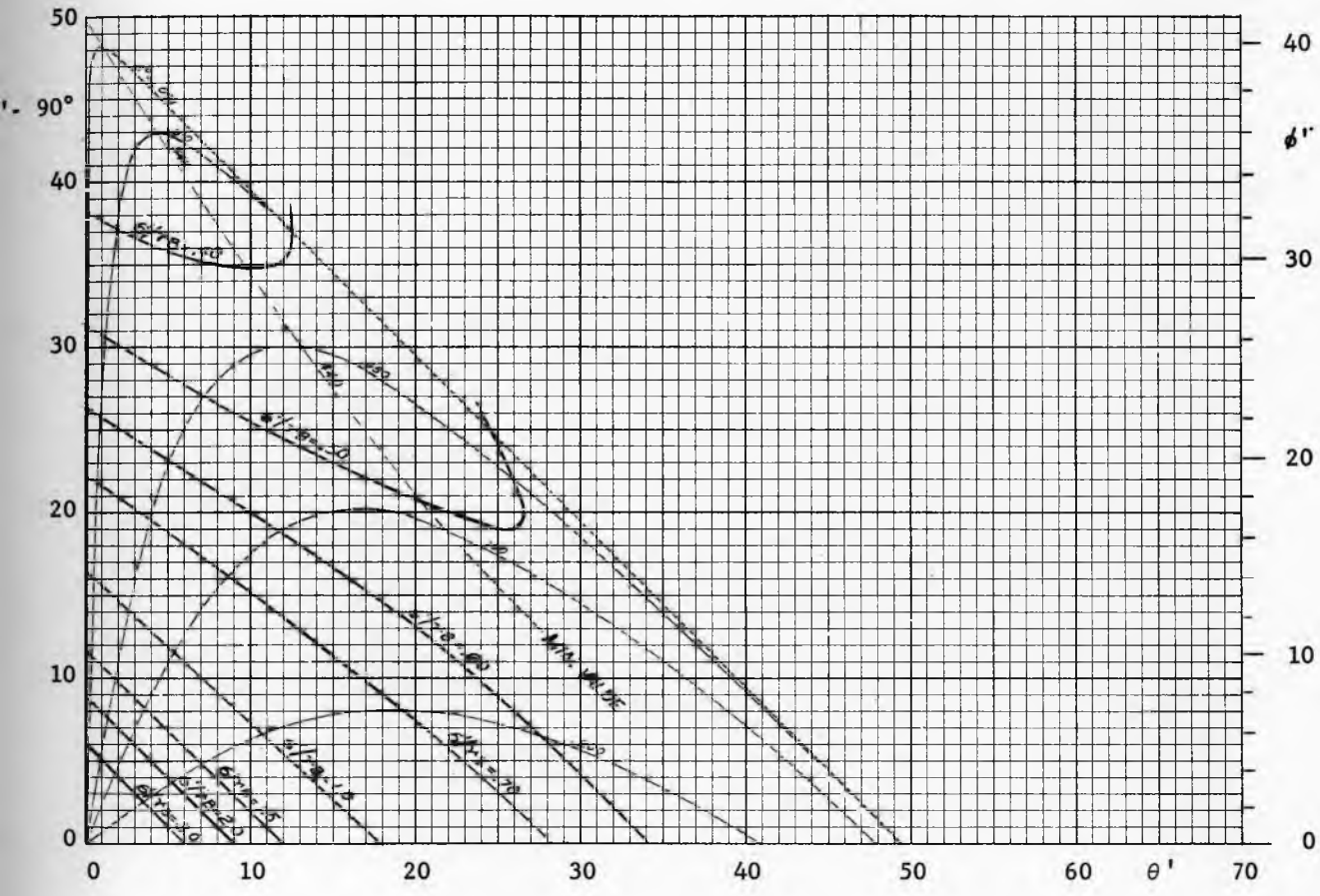

Fig. 55

Function σ'/γ B, $\delta = 50°$

Axial symmetry (conical flow)

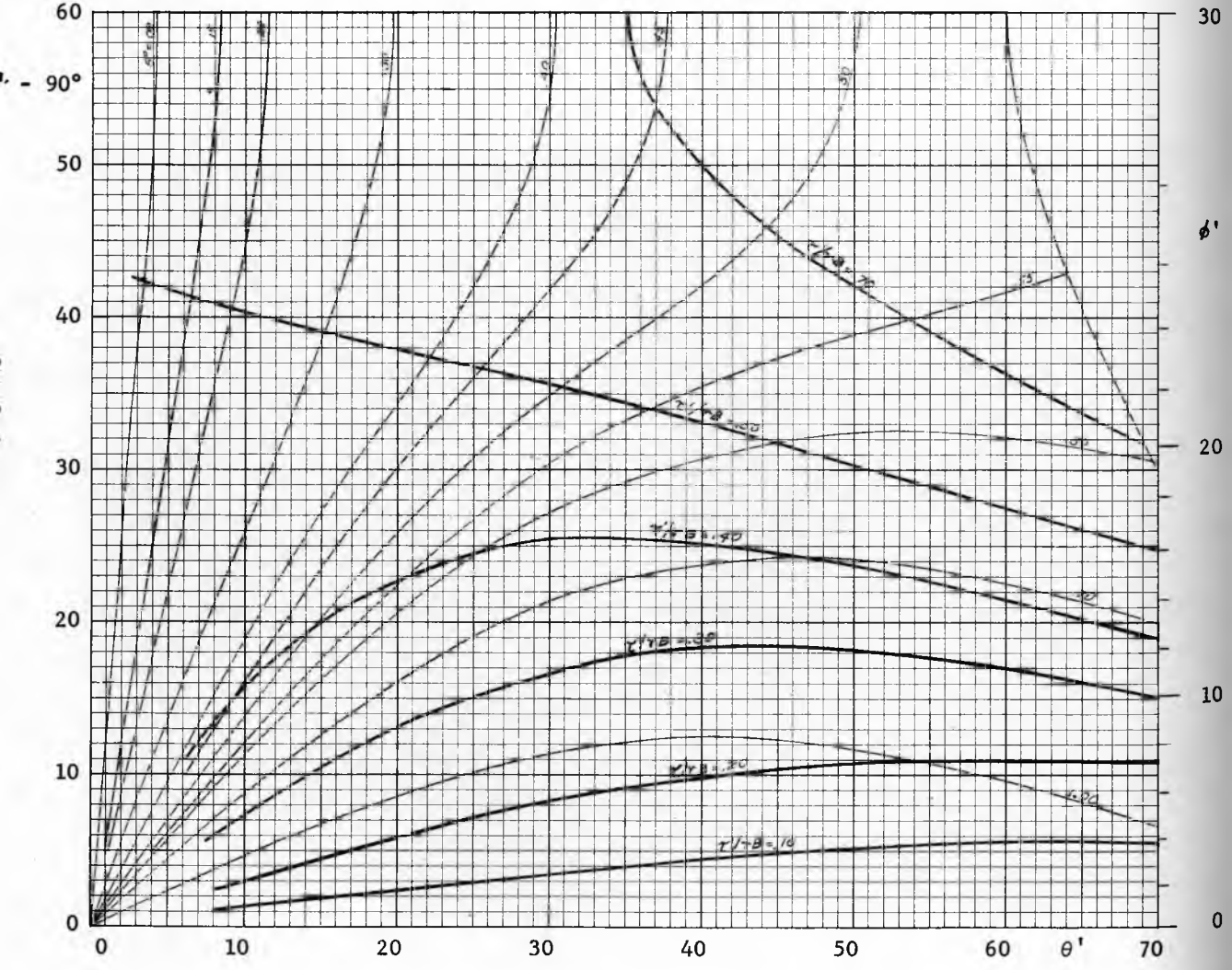

Fig. 56

Function τ'/γ B, $\delta = 30°$

Plane symmetry (symmetric plane flow)

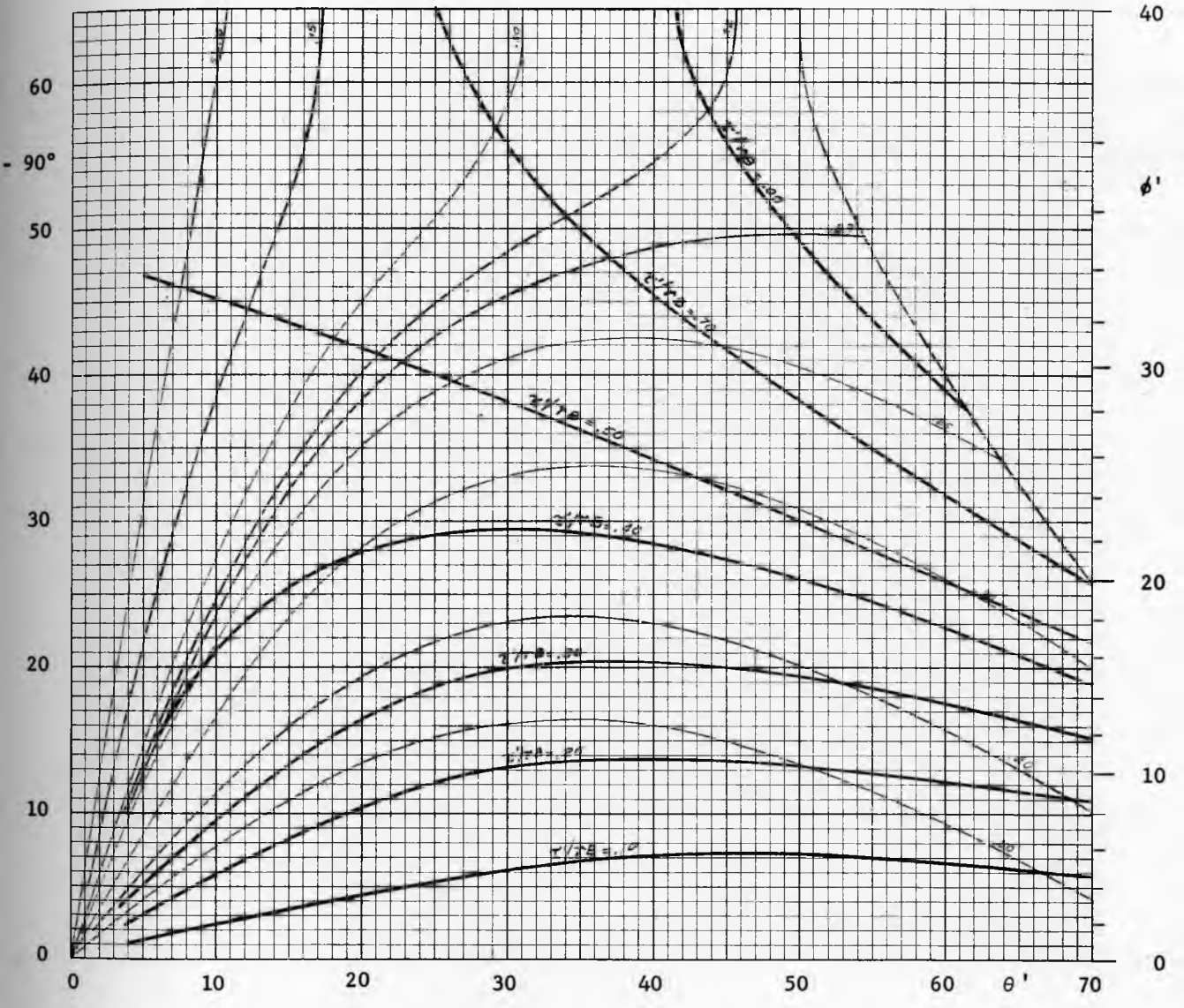

Fig. 57

Function τ'/γ B, $\delta = 40°$

Plane symmetry (symmetric plane flow)

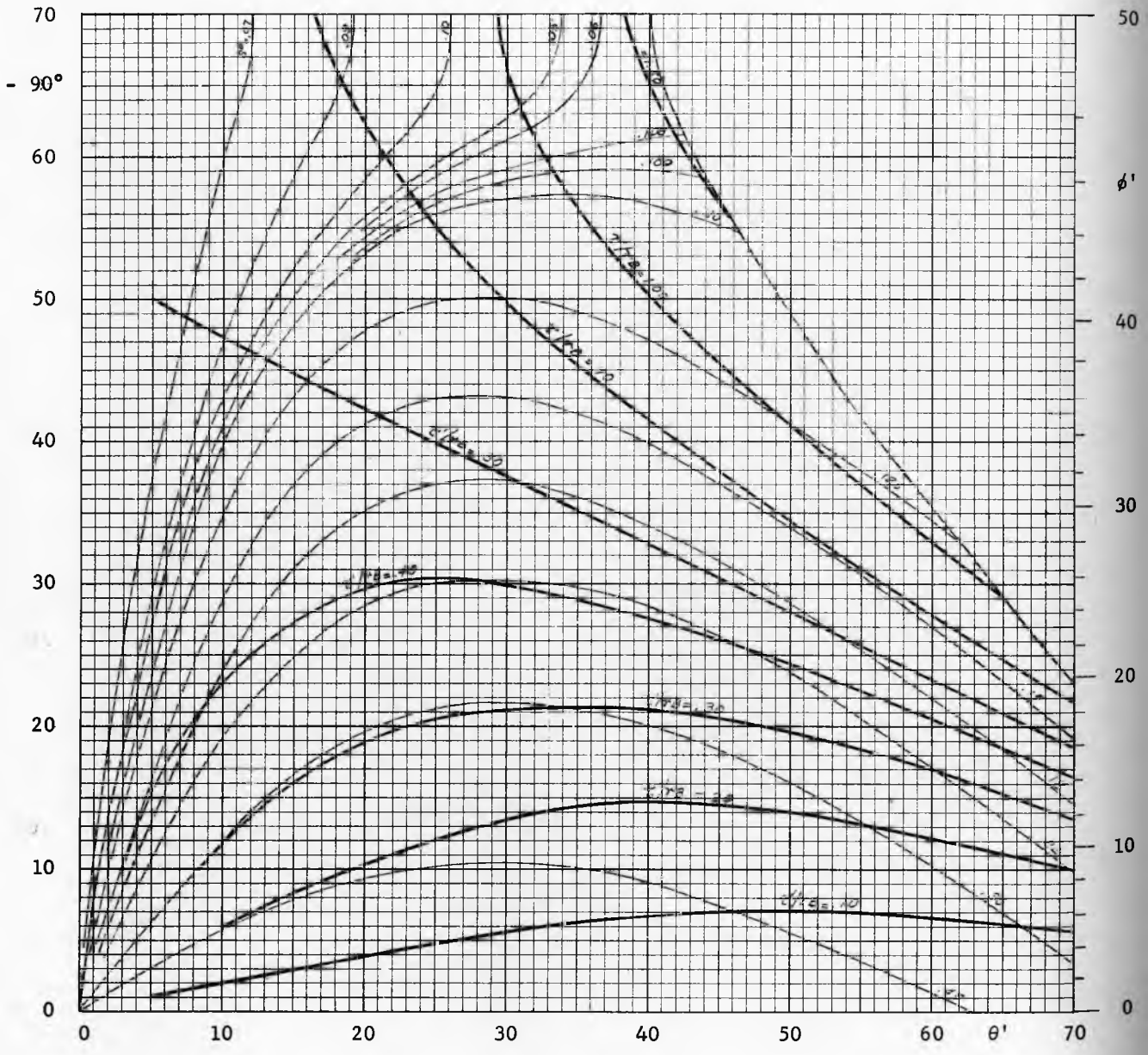

Fig. 58

Function τ'/γ B, $\delta = 50°$

Plane symmetry (symmetric plane flow)

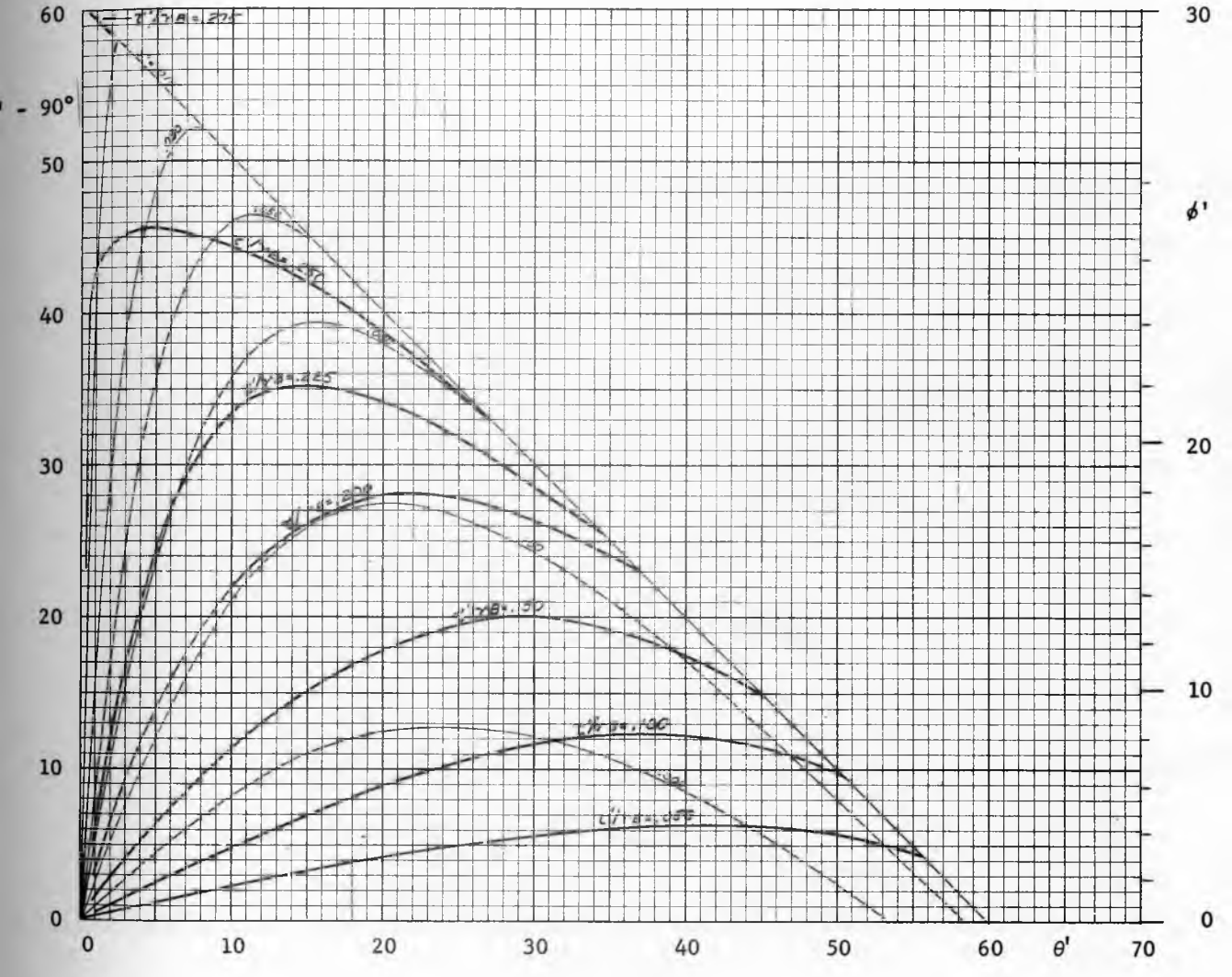

Fig. 59

Function $\tau'/\gamma B$, $\delta = 30°$

Axial symmetry (conical flow)

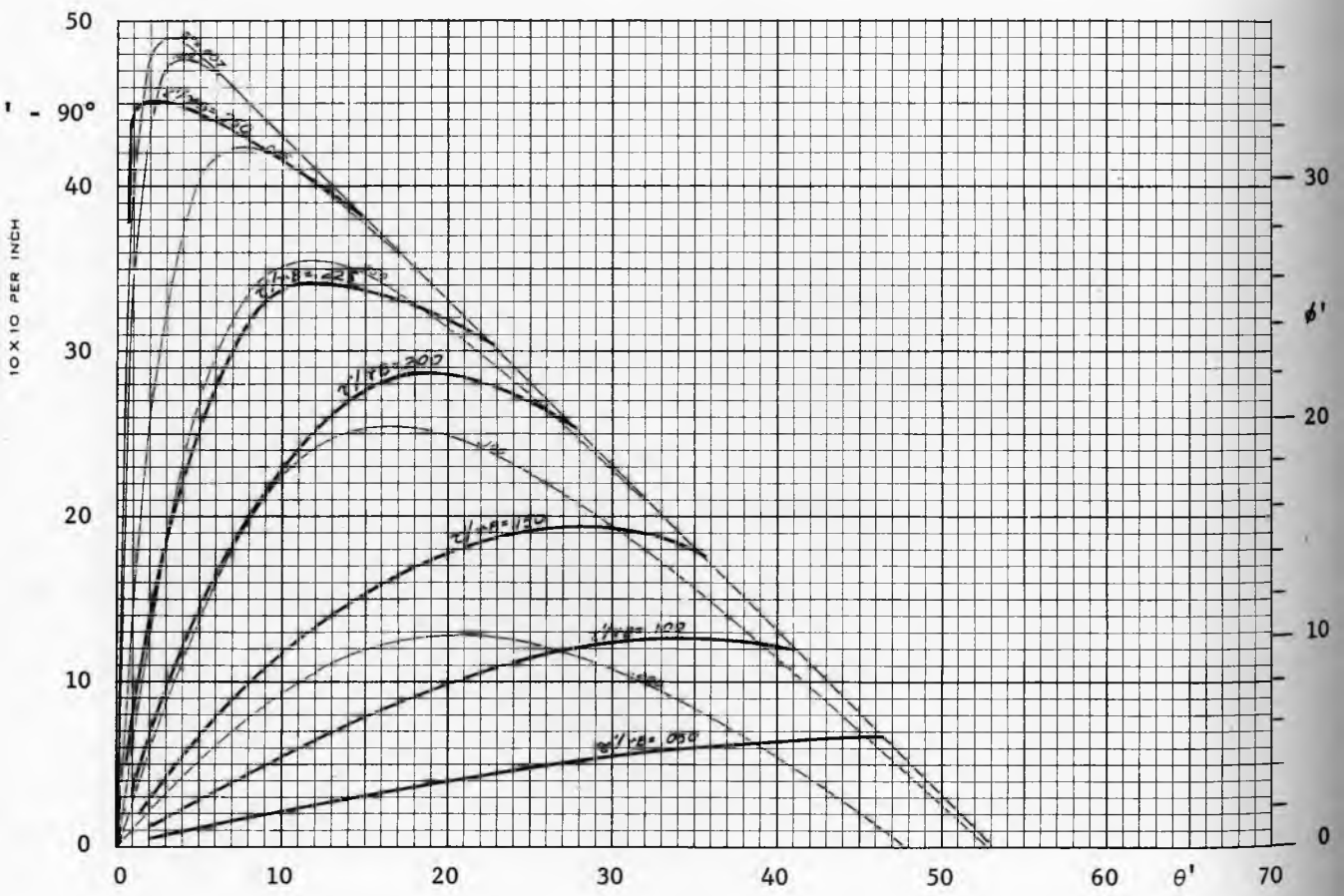

Fig. 60

Function τ'/γ B, $\delta = 40°$

Axial symmetry (conical flow)

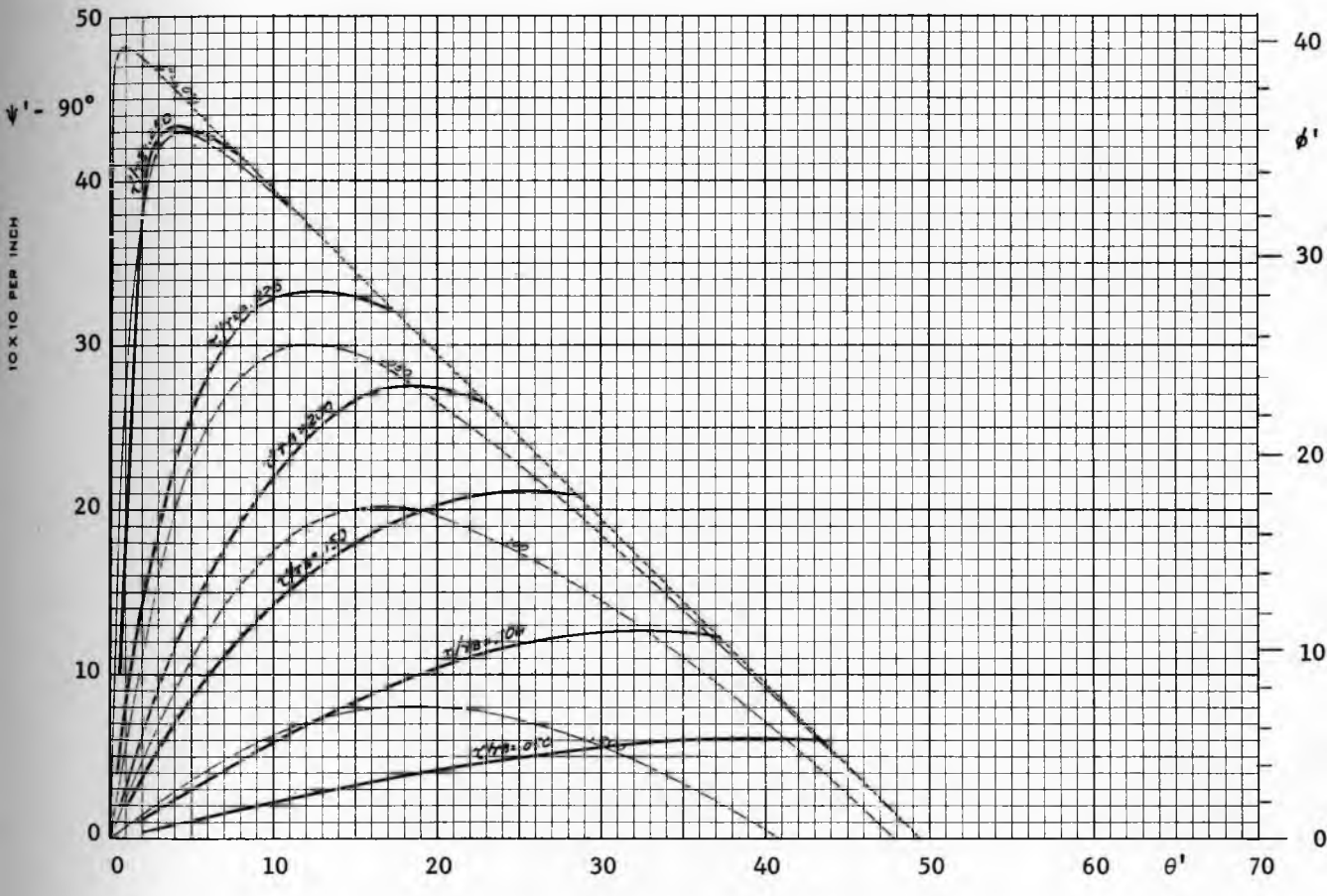

Fig. 61

Function τ'/γ B, $\delta = 50°$

Axial symmetry (conical flow)

become

$$f(\theta) = (1 - \beta)\left\{2\left(\frac{d\psi}{d\theta} + 1\right)\frac{\sin\delta}{\cos^2\delta}\sin 2\psi + \right.$$

$$\left. + m\,\frac{\sin\delta}{\cos^2\delta}(1 + \sin\delta)[\sin 2\psi - \cot\theta(1 + \cos 2\psi)]\right\}, \tag{109}$$

$$g(\theta) = -(1 - \beta)\left[\frac{\sin\delta}{\cos^2\delta}\sin(\theta + 2\psi) + \frac{\sin\theta}{\cos^2\delta}\right], \tag{110}$$

$$h(\theta) = \frac{1}{1 - \beta} + 2\left(\frac{d\psi}{d\theta} + 1\right)(\cos 2\psi - \sin\delta)\frac{\sin\delta}{\cos^2\delta} +$$

$$+ m\,\frac{\sin\delta}{\cos^2\delta}(1 + \sin\delta)(\cot\theta\,\sin 2\psi + \cos 2\psi - 1), \tag{111}$$

$$j(\theta) = -\frac{\sin\delta}{\cos^2\delta}\cos(\theta + 2\psi) + \frac{\cos\theta}{\cos^2\delta}, \tag{112}$$

and the differential equations reduce to the form (98) and (99) as for an incompressible solid. Equations (98) and (99) with the above coefficients are now solved for the derivatives

$$\frac{d\psi}{d\theta} = \Phi(\theta,\psi,s) =$$

$$= -1 - \left\{m\,s\,\sin\delta(1 + \sin\delta)(\cot\theta\,\sin 2\psi + \cos 2\psi - 1) + \cos\theta + \right.$$

$$\left. - \sin\delta\,\cos(\theta + 2\psi) + s\,\cos^2\delta/(1 - \beta)\right\}/2s\,\sin\delta(\cos 2\psi - \sin\delta), \tag{m}$$

$$\frac{ds}{d\theta} = \Gamma(\theta,\psi,s) =$$

$$= \left\{\frac{s\,\sin 2\psi}{1 - \beta} + \sin(\theta + 2\psi) + \right.$$

$$\left. + m\,s\,\sin\delta\,[\cot\theta\,(1 + \cos 2\psi) - \sin 2\psi]\right\}\frac{1 - \beta}{\cos 2\psi - \sin\delta} \tag{n}$$

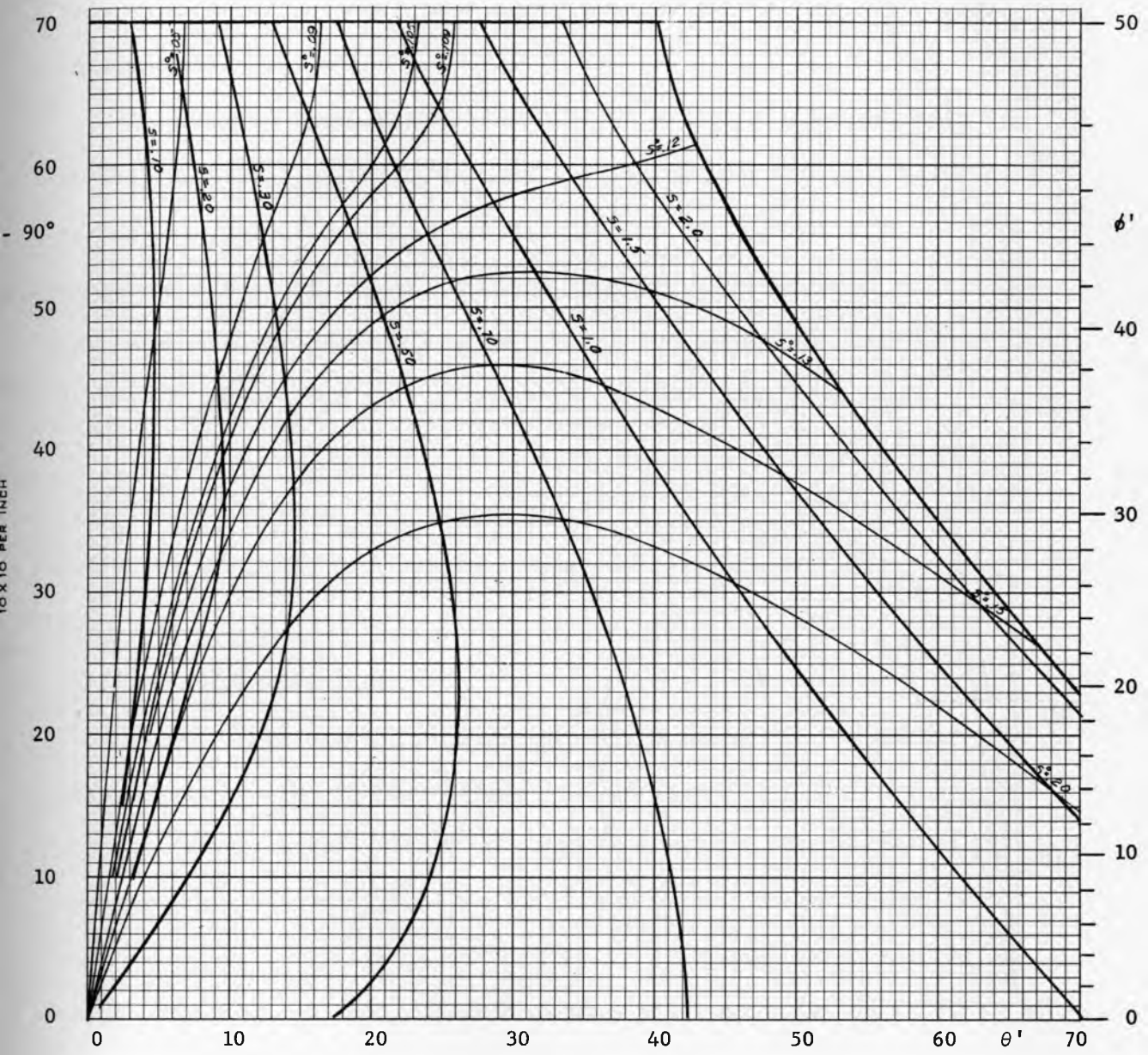

Fig. 62

Function s, $\beta = 0.10$, $\delta = 50°$

Plane symmetry (symmetric plane flow)

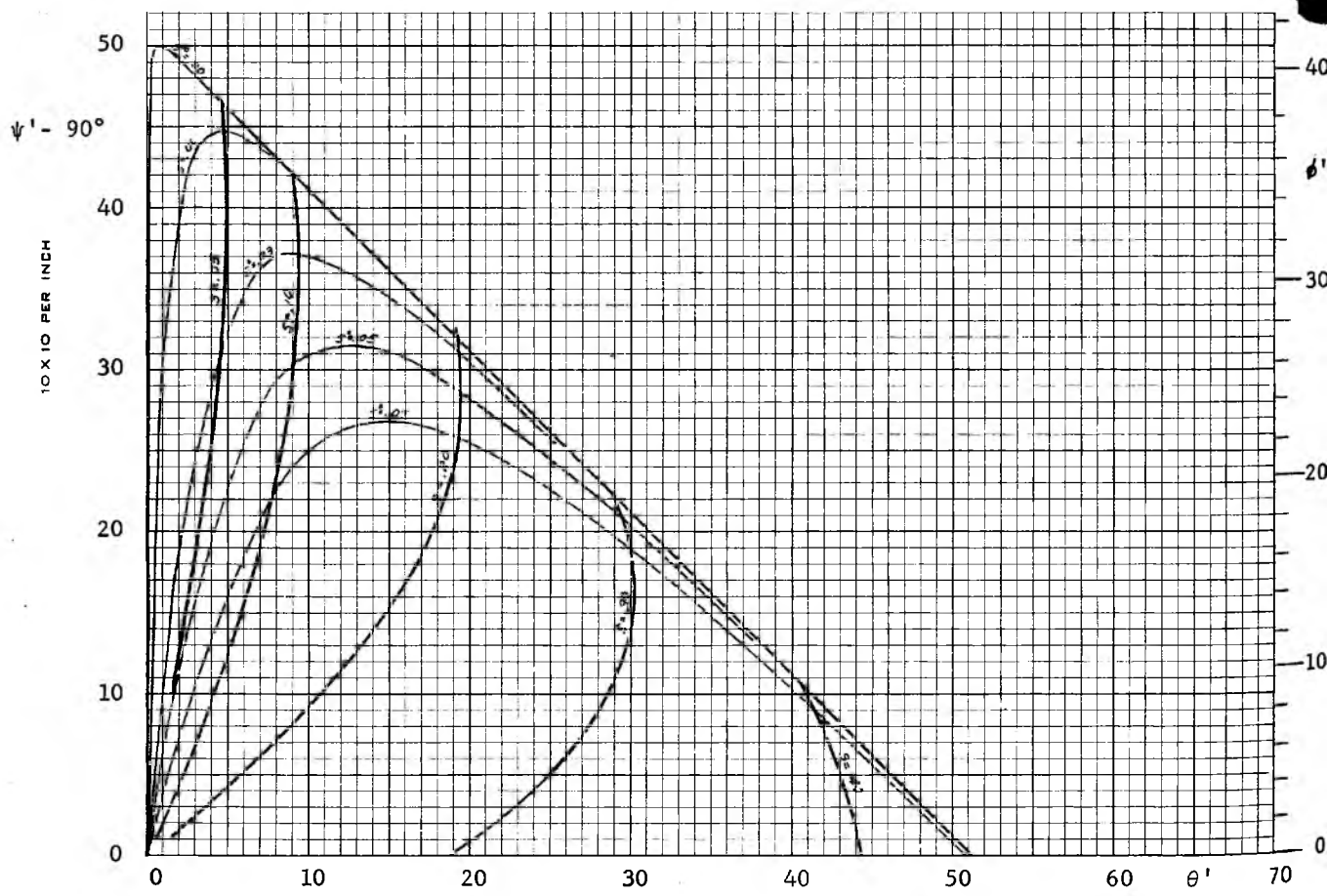

Fig. 63

Function s, $\beta = 0.10$, $\delta = 50°$

Axial symmetry (conical flow)

The above equations are equivalent to the integral equations

$$\psi(\theta) = \psi(\theta^\circ) + \int_{\theta^\circ}^{\theta} \Phi[t,\psi(t),s(t)]dt, \qquad (113)$$

$$s(\theta) = s(\theta^\circ) + \int_{\theta^\circ}^{\theta} [t,\psi(t),s(t)]dt, \qquad (114)$$

from which the functions ψ and s are computed in the same way as for incompressible solids.

In order to estimate the quantitative effect of compressibility, several numerical calculations were carried out for $\beta = .10$, which is a rather extreme value. Function $s(\theta)$ is plotted in Figures 62 and 63 for symmetric plane strain and for axial symmetry with $\delta = 50°$. A comparison with the corresponding values for an incompressible solid, Figures 31 and 36, shows that the influence of compressibility is small.

It should be noted that these equations apply at some distance from the vertex where σ[lb per sq ft] $\gg$ 1. For $\beta = 0$, these equations reduce to the form obtained for incompressible solids.

General stress field

Proof of convergence to a radial stress field at the vertex. The significance of the radial stress field is greatly enhanced by the fact that all useful stress fields converge to radial stress fields at the vertex. This statement will now be proved under the assumption that ψ, γ and their first derivatives are continuous in a sufficiently small neighborhood of the vertex. This assures the continuity of f, g, h, and j, equations (87) - (90).

Eq. (85) is integrated to yield

$$s(r,\theta) = s(r,\theta^\circ)e^{-\int_{\theta^\circ}^{\theta} f(r,t)dt} - e^{-\int_{\theta^\circ}^{\theta} f(r,t)dt} \int_{\theta^\circ}^{\theta} g(r,t)e^{\int_{\theta^\circ}^{t} f(r,u)du} dt. \quad (115)$$

These integrals are bounded over a field satisfying the above conditions of continuity. Therefore,

$$|s(r,\theta)| < |s(r,\theta^\circ)| M_1 + M_2$$

for some constants M_1 and M_2. Hence, if there is one angle θ° for which

$$|s(r,\theta^\circ)| < \infty,$$

then

$$|s(r,\theta)| < \infty$$

for all values of θ within that field.

Eq. (86) is now integrated, yielding

$$s(r,\theta) = s(r_o,\theta)e^{-\int_{r_o}^{r} \frac{h(t,\theta)}{t}dt} - e^{-\int_{r_o}^{r} \frac{h(t,\theta)}{t}dt} \int_{r_o}^{r} \frac{j(t,\theta)}{t} e^{\int_{r_o}^{t} \frac{h(u,\theta)}{t}du} dt. \quad (116)$$

where $r_o > r$.

The value of this function will now be analyzed in the limit as $r \to o$. It will be observed that the signs of $\lim_{r \to o} h$ and $\lim_{r \to o} j$ play an important role in the analysis, and the following two cases are distinguished:

1. $\lim_{r \to o} h < 0$, $\lim_{r \to o} j \neq 0$. In this case $\lim_{r \to o} e^{-\int_{r_o}^{r} \frac{h(t,\theta)}{t}} = 0$, the first term of eq. (116) vanishes, while in the second term $\lim_{r \to o} \int_{r_o}^{r} \frac{j(t,\theta)}{t} e^{\int_{r_o}^{t} \frac{h(u,\theta)}{u}du} dt = \infty$. The second term is evaluated by using L'Hospital's rule, yielding

$$\lim_{r\to o} s(r,\theta) = \lim_{r\to o} - \frac{\int_{r_o}^{r} \frac{j(t,\theta)}{t} e^{\int_{r_o}^{r} \frac{h(u,\theta)}{u} du} dt}{\int_{e}^{r_o} \frac{h(t,\theta)}{u} dt} = \lim_{r\to o} - \frac{j(r,\theta)}{h(r,\theta)}. \qquad (117)$$

It will be noted that the boundary value $s(r_o,\theta)$ does not affect $\lim_{r\to o} s(r,\theta)$, and that, in this case, no condition is imposed on the value at the boundary.

2. $\lim_{r\to o} h > 0$, $\lim_{r\to o} j \neq 0$. Now $\lim_{r\to o} e^{-\int_{r_o}^{r} \frac{h(t,\theta)}{t} dt} = \infty$ and, for a useful solution to exist, it is necessary that the boundary value satisfy the condition

$$s(r_o,\theta) = \lim_{r\to o} \int_{r_o}^{r} \frac{j(t,\theta)}{t} e^{\int_{r_o}^{t} \frac{h(u,\theta)}{u} du} dt, \qquad (118)$$

then, as in the case 1, the application of L'Hospital's rule yields

$$\lim_{r\to o} s(r,\theta) = \lim_{r\to o} - \frac{j(r,\theta)}{h(r,\theta)}.$$

The satisfaction of the condition (118) implies $s(r_o,\theta) \neq 0$, i. e. no traction-free boundary, within the region of θ in which $\lim_{r\to o} h > 0$.

If the condition (118) is not satisfied, then $\lim s(r,\theta) = \infty$. While a mathematical solution may exist in the neightborhood of the vertex, the large values of s and, in turn, the relatively large values of pressure σ in the region of the outlet of the channel would consolidate a real solid to a degree likely to cause the development of a stable dome,

and flow would fail to develop. Hence, it is expected that in physical channels condition (118) is satisfied.

The physically acceptable solutions are further restricted by the condition that the solid does not transfer tensions, hence, $s(r,\theta) > 0$. This implies $\lim_{r\to o} -\frac{j(r,\theta)}{h(r,\theta)} > 0$ and requires: in case 1, $\lim_{r\to o} h < 0$, $\lim_{r\to o} j > 0$; in case 2, $\lim_{r\to o} h > 0$, $\lim_{r\to o} j < 0$. To conform with this condition, the change of sign of $\lim_{r\to o} h$ and $\lim_{r\to o} j$ must occur along the same ray θ. It is easy to show that the latter is also necessary for a bounded solution to exist along that ray,

because for $\lim_{r\to o} h = 0$, $\lim_{r\to o} e^{\int_{r_o}^{t} \frac{h(t,\theta)}{t} dt}$ is finite and non-zero, while

$$\lim_{r\to o} \int_{r_o}^{r} \frac{i(t,\theta)}{t} e^{\int_{r_o}^{t} \frac{h(u,\theta)}{u} du} dt = \infty$$

and, hence, $\lim_{r\to o} s(r,\theta) = \infty$, unless $\lim_{r\to o} j = 0$.

The significance of the direction established by $\lim_{r\to o} j = 0$ will be further discussed in the next section on Boundaries.

It has thus been shown that the useful solutions of the equations (85) and (86) approach the form (117) in the neighborhood of the vertex. It will now be shown that $\lim_{r\to o} s(r,\theta)$ of eq.(117), is the same as $s(\theta)$, eq.(97), obtained for the radial stress field.

In view of the relation (117), eq.(86) may be written

$$s\, h(r,\theta) + j(r,\theta) = \epsilon_1,$$

where

$$\lim_{r\to o} \epsilon_1 = 0.$$

Equations (85) and (86) are now solved for $\partial\psi/\partial\theta$ and $\partial s/\partial\theta$:

$$\frac{\partial\psi}{\partial\theta} = F(\theta,\psi,s) + \frac{\epsilon_1 \cos^2\delta - \frac{s}{\gamma}\frac{\partial\gamma}{\partial\theta}\cos^2\delta - 2rs\frac{\partial\psi}{\partial r}(\sin\delta + \cos 2\psi)\sin\delta}{2\,s\sin\delta\,(\cos 2\psi - \sin\delta)}, \qquad (o)$$

$$\frac{\partial s}{\partial\theta} = G(\theta,\psi,s) - \frac{s}{\gamma}\frac{\partial\gamma}{\partial\theta} - \frac{2rs\frac{\partial\psi}{\partial\theta}\sin\delta + \epsilon_1 \sin 2\psi - s\sin 2\psi\,\frac{r}{\gamma}\frac{\partial\gamma}{\partial r}}{\cos 2\psi - \sin\delta}, \qquad (p)$$

where $F(\theta,\psi,s)$ and $G(\theta,\psi,s)$ are given by equations (h) and (i). It will now be shown that the remainders of the right hand sides of equations (o) and (p) approach zero as $r \to 0$. Since the walls of a channel at most follow a slipline and $\phi < \delta$, nowhere within the field does $\cos 2\psi - \sin\delta \to 0$. Therefore, all the terms of the remainders approach zero for $r \to 0$, including $\frac{1}{\gamma}\frac{\partial\gamma}{\partial\theta}$. The latter is shown as follows: eq. (25), with the substitution (84) for σ, is differentiated with respect to θ, yielding

$$\frac{\partial\gamma}{\partial\theta} = \gamma'(\sigma)\frac{\partial\sigma}{\partial\theta} = \gamma'(\sigma)\left[r\frac{\partial\gamma}{\partial\theta}\,s + r\,\gamma\frac{\partial s}{\partial\theta}\right],$$

and from it

$$\frac{1}{\gamma}\frac{\partial\gamma}{\partial\theta} = \frac{r\frac{\partial s}{\partial\theta}}{\frac{1}{\gamma'(\sigma)} - r\,s}.$$

since $\partial s/\partial\theta$ is bounded, $\lim_{r\to 0}\frac{1}{\gamma}\frac{\partial\gamma}{\partial\theta} = 0$.

Equations (o) and (p) can now be written:

$$\frac{\partial\psi}{\partial\theta} = F(\theta,\psi,s) + \epsilon_2 \qquad (q)$$

$$\frac{\partial s}{\partial\theta} = G(\theta,\psi,s) + \epsilon_3. \qquad (r)$$

where $\lim_{r\to 0}\epsilon_2 = \lim_{r\to 0}\epsilon_3 = 0$.

The equivelant integral equations are:

$$\psi(r,\theta) = \psi(r,\theta^\circ) + \int_{\theta^\circ}^{\theta} F[t,\psi(r,t),\ s(r,t)]dt + \int_{\theta^\circ}^{\theta} \epsilon_2(r,t)dt, \qquad (s)$$

$$s(r,\theta) = s(r,\theta^\circ) + \int_{\theta^\circ}^{\theta} G[t,\psi(r,t),s(r,t)]dt + \int_{\theta^\circ}^{\theta} \epsilon_3(r,t)dt. \qquad (t)$$

now as $r \to o$, $\psi(r,\theta^\circ)$ and $s(r,\theta^\circ)$ approach limits $\psi(\theta^\circ)$ and $s(\theta^\circ)$. Equations (100) and (101) give the radial flow solution corresponding to these boundary conditions. Equations (100) and (101) are now subtracted from eq.(s) and (t) yielding:

$$\psi(r,\theta) - \psi(\theta) = \psi(r,\theta^\circ) - \psi(\theta^\circ) +$$

$$+ \int_{\theta^\circ}^{\theta} \left\{F[t,\psi,(r,t),s(r,t)] - F[t,\psi(t),\ s(t)]\right\}dt + \int_{\theta^\circ}^{\theta} \epsilon_2(r,t)dt,$$

$$s(r,\theta) - s(\theta) = s(r,\theta^\circ) - s(\theta^\circ) +$$

$$+ \int_{\theta^\circ}^{\theta} \left\{G[\,t,\psi\,(r,t),\ s(r,t)] - G[t,\psi(t),s(t)]\right\}dt + \int_{\theta^\circ}^{\theta} \epsilon_3(r,t)dt.$$

In axial symmetry, $f(\theta,\psi,s)$ is not Lipschitz in ψ in any region about the axis of symmetry. This is due to the term containing $\cot\theta$. However, in plane strain or in axial symmetry, if the axis of symmetry is avoided, F and G are Lipschitz in both ψ and s. Then:

$$|F[t,\psi(r,t),s(r,t)] - F[t,\psi(t),s(t)]| \leqslant L_1|\psi(r,t) - \psi(t)| +$$

$$+ L_2|s(r,t) - s(t)|,$$

$$|G[t,\psi\ (r,t),s(r,t)] - G[t,\psi(t),s(t)]| \leqslant L_3|\psi(r,t) - \psi(t)| +$$

$$+ L_4|s(r,t) - s(t)|,$$

and therefore

$$|\psi(r,\theta) - \psi(\theta)| \leqslant |\psi(r,\theta^\circ) - \psi(\theta^\circ)| +$$

$$+ \int_{\theta^\circ}^{\theta} [L_1|\psi(r,t) - \psi(t)| + L_2|s(r,t) - s(t)|]|dt| + \int_{\theta^\circ}^{\theta} |\epsilon_2(r,t)||dt|,$$

$$|s(r,\theta) - s(\theta)| \leqslant |s(r,\theta^\circ) - s(\theta^\circ)| +$$

$$+ \int_{\theta^\circ}^{\theta} [L_3|\psi(r,t) - \psi(t)| + L_4|s(r,t) - s(t)|]|dt| + \int_{\theta^\circ}^{\theta} |\epsilon_3(r,t)||dt|.$$

These inequalities are now added, yielding:

$$\alpha(r,\theta) \leqslant L \int_{\theta^\circ}^{\theta} \alpha(r,t)|dt| + \beta(r,\theta,\theta^\circ), \tag{u}$$

where:

$$\alpha(r,\theta) = |\psi(r,\theta) - \psi(\theta)| + |s(r,\theta) - s(\theta)|,$$

$$\beta(r,\theta,\theta^\circ) = |\psi(r,\theta^\circ) - \psi(\theta^\circ)| + |s(r,\theta^\circ) - s(\theta^\circ)| +$$

$$+ \int_{\theta^\circ}^{\theta} [|\epsilon_2(r,t)| + |\epsilon_3(r,t)|]|dt|$$

and $L = \max\{L_1, L_2, L_3, L_4\}$.

The method of successive approximations, used on (u) yields:

$$\alpha(r,\theta) \leqslant \beta(r,\theta,\theta^\circ)\ e^{L|\theta + \theta'|}. \tag{v}$$

But $\lim_{r\to o} \beta(r,\theta,\theta^\circ) = 0$ and, therefore, $\lim_{r\to o} \alpha(r,\theta) = 0$, or

$$\lim_{r\to o} \psi(r,\theta) = \psi(\theta), \tag{w}$$

$$\lim_{r\to o} s(r,\theta) = s(\theta). \tag{x}$$

The significance is this:

Given a converging stress field satisfying the conditions stated in this proof, and a ray $\theta = \theta^\circ$ along which $\psi(r,\theta^\circ)$ and $s(r,\theta^\circ)$ approach limits $\psi(\theta^\circ)$ and $s(\theta^\circ)$ as $r \to o$, there is a radial stress field given by

$\psi(\theta)$ and $s(\theta)$ from eqs.(100) and (101), with boundary conditions $\psi(\theta^\circ)$ and $s(\theta$ such that throughout the field $\psi(r,\theta) \to \psi(\theta)$ and $s(r,\theta) \to s(\theta)$ as $r \to o$. Althou the proof, as given, does not hold if θ and θ° are separated by $\theta = 0$ in axial symmetry, the axi-symmetric field is completely determined if it is known on only one side of $\theta = 0$. Hence the axis, $\theta = 0$, need not be crossed.

Boundaries. A general problem satisfying equations (85) and (86) is defined by the specification of adequate boundary conditions. Such conditions are $\psi_o = \psi_o(\theta)$ and $s_o = s_o(\theta)$, at the top boundary, and $\psi' = \psi'(\theta)$, $\psi'' = \psi''(\theta)$, at the walls, Fig. 64. The stress field is then defined down to the stress characteristics passing through the end points of the walls. Hence, the stresses at these two points are independent of the bottom boundary conditions, and, as has been shown in the previous section, approach the magnitude of the appropriate radial stress field. This is important, because these two stresses are used in the derivation of the flow criteria which are, therefore, independent of the top boundary. This justifies the development of the design criteria on the basis of the radial stress fields and eliminates the need for a large number of particular solutions of general fields. Several general fields are discussed in a separate publication [15].

In gravity flow, the slopes of the walls in the neighborhood of the vertex seem to satisfy the condition $\lim_{r \to o} j > 0$. There is a physical meaning to this bound, namely the horizontal component σ_h of the stress vector acting on the solid from a wall, Fig. 65, is given by

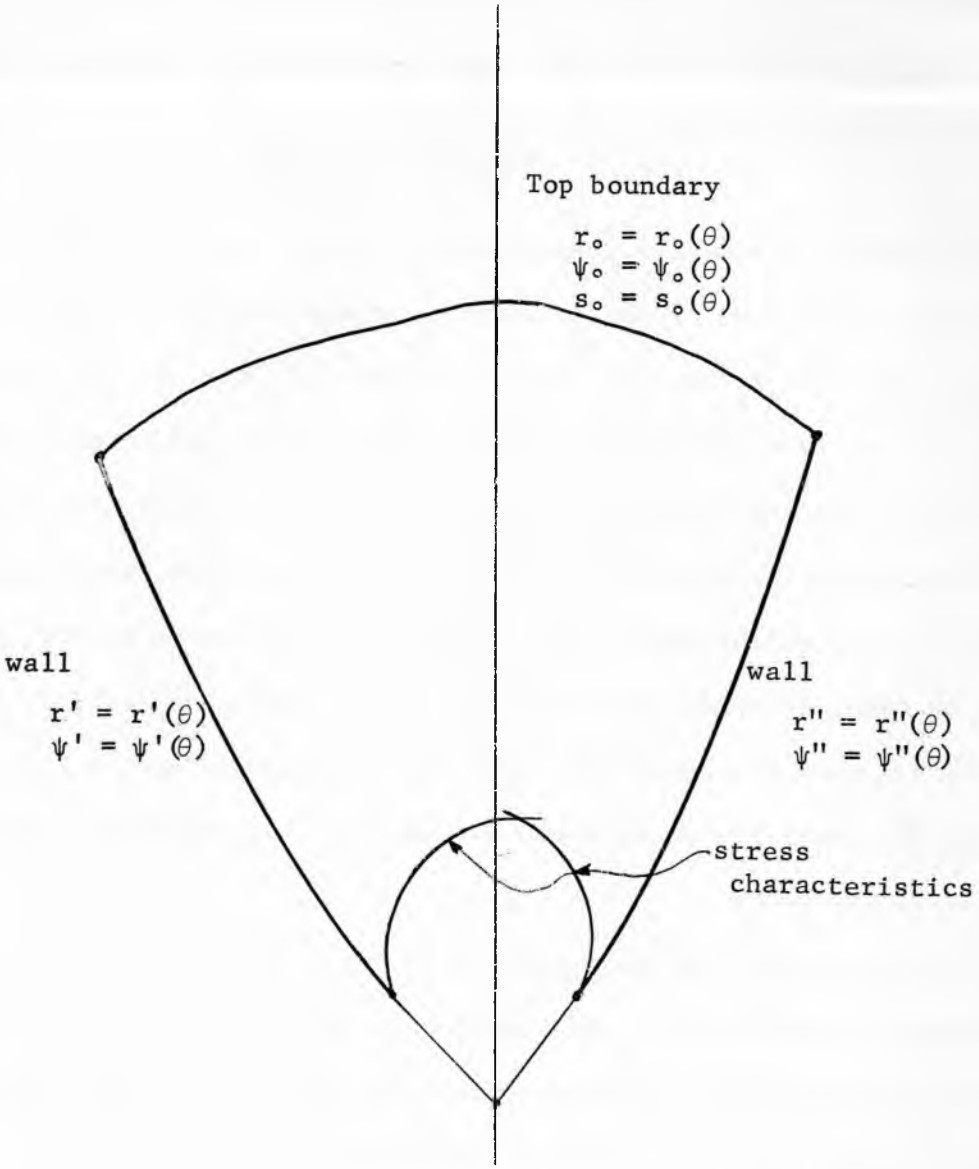

Fig. 64

Boundary conditions of a general stress field

$$\sigma_h = \sigma_\theta \cos\theta + \tau_{r\theta} \sin\theta.$$

With sibstitutions (18) and (19), the inequality $\sigma_h > 0$ yields

$$\tan\theta' < \frac{1 - \sin\delta \cos 2\psi'}{-\sin\delta \sin 2\psi'}, \qquad (119)$$

and is identical with the condition $\lim j > 0$. The latter then implies a positive direction of the horizontal component of the stress vector at the wall. In a channel with a straight wall, Fig. 66, it is apparent that, if the above condition is not satisfied, the top boundary cannot be traction-free, but requires stresses which have a resultant force containing a positive horizontal component. This follows from the consideration of the equilibrium of the horizontal forces acting on the flowing mass between the wall and a vertical plane through the vertex. The pressure across the vertical wall cannot be balanced by $H = \int_0^{r_o} \sigma_h \cos\theta' dr$ if $\sigma_h \leqslant 0$, hence the requirement for the positive horizontal component at the top boundary.

While such top boundary conditions are possible, they are unlikely to occur in gravity flow, and cannot occur with a traction-free boundary. Observations of flow in physical channels confirm this conclusion: they indicate that inequality (119) is satisfied.

The above argument tallies with the results of the analysis of the previous section which indicated that for case 1, $\lim_{r\to o} h < 0$, $\lim_{r\to o} j > 0$, a bounded solution $\lim_{r\to o} s(r,\theta) = \lim_{r\to o} -(j/h)$ is obtained for all top boundary values $s(r_o,\theta)$; but for Case 2, $\lim_{r\to o} h > 0$, $\lim_{r\to o} j < 0$, a bounded

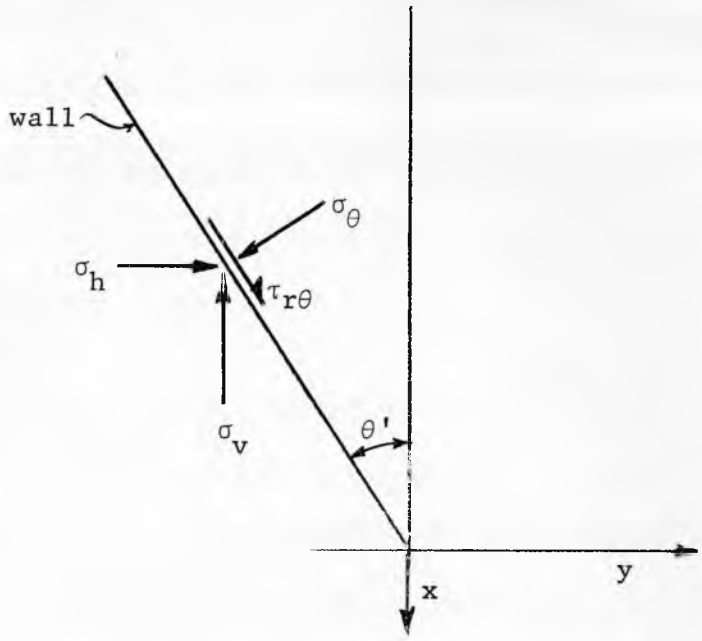

Fig. 65

Stress vector at a wall

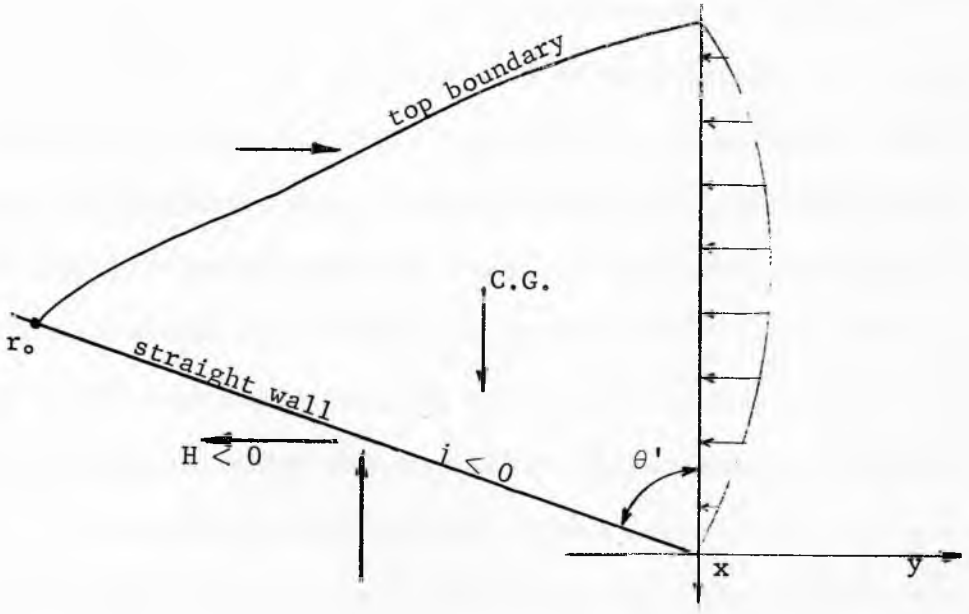

Fig. 66

Equilibrium of a flowing mass

solution requires the satisfaction of the condition (118) for the top boundary stress.

There thus seems to be sufficient reason to limit the consideration of the radial stress fields (which occur in the neighborhood of $r \to o$) to regions in which $j > 0$.

The substitution of expression (44) with $\Theta' = \theta'$ in inequality (119) yields

$$\theta' < \frac{\pi}{2} - \phi'. \tag{120}$$

For a rough wall, similarly,

$$\theta' < \frac{\pi}{2} - \phi .$$

These bounds for θ' apply only in plane strain. In axial symmetry, the acceptable solutions of the radial stress fields occur within regions of (θ,ψ) which are more restricted than the bound $j = 0$, $\cos 2\psi - \sin \delta = 0$.

The shape of the walls, $r' = r'(\theta)$ and $r'' = r''(\theta)$, away from the vertex, is a function of the shape of the top boundary, $r_o = r_o(\theta)$, and the functions $\psi_o = \psi_o(\theta)$, $s_o = s_o(\theta)$ along the top boundary. In gravity flow, the top boundary usually varies within wide limits and, therefore, the shape of the walls should vary accordingly. However, this is possible only when a solid flows within itself and forms its own rough walls. Even then, the free adjustment of the shape of the walls is inhibited by the fact that a solid develops cohesion at different rates in the plastic and in the rigid regions. In the rigid regions, the time effect comes into play and, after a while the rigid regions may, in effect, behave as if they were made of a different solid and a plane which is weak with respect to the

rigid solid may develop along the walls.

When the channel is built of weak walls, the solid will flow along the walls, provided the walls are sufficiently steep and do not contain sharp corners. Typical shapes of channels are discussed in Chapter VI.

Radial velocity field.

As was shown in the previous section, radial stress fields are approached in all channels in the vicinity of the vertex. A radial velocity field is compatible with a radial stress field. It should be emphasized that there is no unique velocity field which corresponds to a given stress field and that there are other velocity solutions compatible with a radial stress field. Indeed, radial velocity fields, which include the lines $\psi = \pi/4$ and $\psi = 3\pi/4$, are physically unacceptable because these fields require velocity to be zero along these lines and, in some cases, also require a velocity discontinuity along these lines, which is impossible since they are not sliplines. However, for wall conditions $\psi' < 3\pi/4$ and $\psi'' > \pi/4$, the radial velocity fields closely represent the fields observed in physical channels. Since velocity fields are subject to superposition, the radial field provides one readily obtainable solution which can be combined with other fields to satisfy the required boundary conditions.

It will again be convenient to use polar/spherical coordinates. The equation of continuity in steady state flow is

$$\frac{\partial}{\partial r}\left[\gamma u_r r(r \sin\theta)^m\right] + \frac{\partial}{\partial\theta}\left[\gamma u_\theta (r \sin\theta)^m\right] = 0, \qquad (121)$$

where u_r and u_θ are the two components of the velocity vector, Fig. 67.

The equation of isotropy is

$$\tan 2\psi(r,\theta) = \frac{\frac{\partial u_r}{r\partial\theta} + \frac{\partial u_\theta}{\partial r} - \frac{u_\theta}{r}}{\frac{\partial u_r}{\partial r} - \frac{u_r}{r} - \frac{\partial u_\theta}{r\partial\theta}} \tag{122}$$

In radial flow

$$u_r = V, \qquad u_\theta = 0, \tag{123}$$

and the above two equations reduce to

$$r\frac{\partial V}{\partial r} + (1 + m + \frac{r}{\gamma}\frac{\partial \gamma}{\partial r})V = 0, \tag{y}$$

$$\frac{\partial V}{\partial \theta} + (-r\frac{\partial V}{\partial r} + V)\tan 2\psi = 0.$$

Elimination of $\partial V/\partial r$ in the last equation leads to

$$\frac{\partial V}{\partial \theta} + (2 + m + \frac{r}{\gamma}\frac{\partial \gamma}{\partial r})\, V \tan 2\psi = 0. \tag{z}$$

$\frac{r}{\gamma}\frac{\partial \gamma}{\partial r}$ is now eliminated in equations (y) and (z) by means of the second expression (108) yielding

$$r\frac{\partial V}{\partial r} + (1 + m + \frac{\beta}{1-\beta})\, V = 0,$$

$$\frac{\partial V}{\partial \theta} + (2 + m + \frac{\beta}{1-\beta})\, V \tan 2\psi = 0.$$

Integration of these equations produces

$$V = f(\theta)\, r^{-(1 + m + \frac{\beta}{1-\beta})},$$

$$V = g(r)\, e^{-(2 + m + \frac{\beta}{1-\beta})\int \tan 2\psi\, d\theta}$$

To satisfy the differential equations it is necessary that

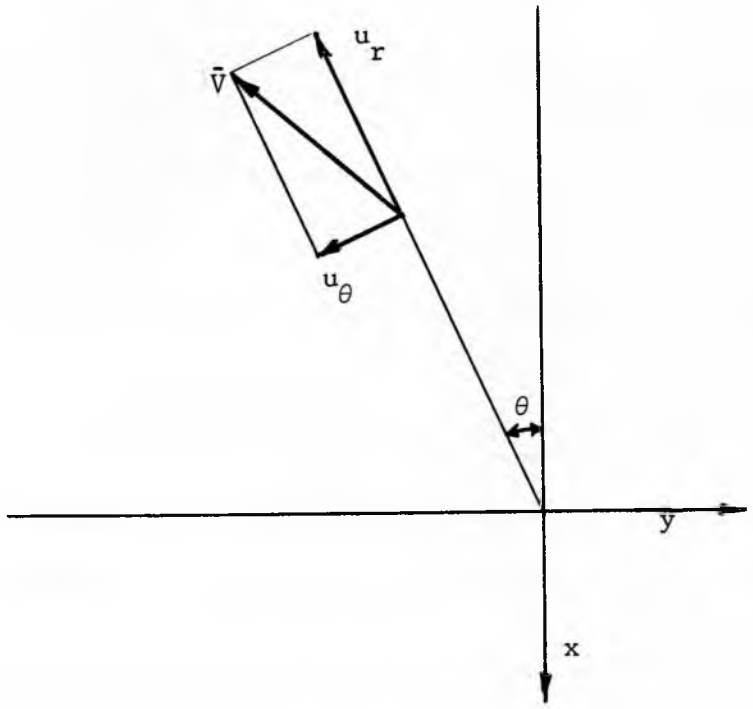

Fig. 67

Velocity components in polar-spherical coordinates

$$f(\theta) = e^{-(2 + m + \frac{\beta}{1-\beta})\int \tan 2\psi \, d\theta} \quad \text{and}$$

$$g(r) = r^{-(1 + m + \frac{\beta}{1-\beta})},$$

which enforce

$$\psi = \psi(\theta),$$

as was assumed by the eq.(91) in the radial stress field.

The expression for the velocity is

$$V = V^{\circ}(\frac{r^{\circ}}{r})^{1 + m + \frac{\beta}{1-\beta}} e^{-(2 + m + \frac{\beta}{1-\beta})\int_{\theta^{\circ}}^{\theta} \tan 2\psi \, d\theta}. \qquad (124)$$

It will be noticed that along the rays $\psi = 3\pi/4$ and $\psi = \pi/4$, $\tan 2\psi = \infty$, and $V = 0$. The derivative $\partial V/\partial\theta$ along one of these rays, e. g. $\psi = \pi/4$, will now be determined. Eliminate V in eq. (z) to obtain

$$\frac{\partial V}{\partial \theta} = F(r) \tan 2\psi \; e^{-(2 + m + \frac{\beta}{1-\beta})\int_{\theta^{\circ}}^{\theta} \tan 2\psi \, d\theta}.$$

It is necessary to find the limit of $\partial V/\partial\theta$ as θ approaches the value at which $\psi(\theta) = \pi/4$. The function is rewritten as follows

$$\frac{\partial V}{\partial \theta} = F(r) \tan 2\psi \; e^{-(2 + m + \frac{\beta}{1-\beta})\int_{\theta^{\circ}}^{\theta_1} \tan 2\psi \, d\theta} \; e^{-(2 + m + \frac{\beta}{1-\beta})\int_{\theta_1}^{\theta} \tan 2\psi \, d\theta},$$

where θ_1 is a constant, while $\theta - \theta_1$ is arbitrarily small. The first exponential is constant and the function can further be transformed into

$$\frac{\partial V}{\partial \theta} = c \, F(r) \tan 2\psi \; e^{-(2 + m + \frac{\beta}{1-\beta})[\frac{d\theta}{d(2\psi)}]' \int_{\psi_1}^{\psi} \tan 2\psi \, d(2\psi)},$$

where $d\theta/d(2\psi)'$ is evaluated in the interval $\psi_1 - \psi$. Then, through integration,

$$\frac{\partial V}{\partial \theta} = c \, F(r) \tan 2\psi \, (\frac{\cos 2\psi}{\cos 2\psi'})^{[1 + \frac{m}{2} + \frac{\beta}{2(1-\beta)}](\frac{d\theta}{d\psi})' - 1} =$$

$$= c'F(r)\sin 2\psi(\cos 2\psi)^{\left[1 + \frac{m}{2} + \frac{\beta}{2(1-\beta)}\right]}\left(\frac{d\theta}{d\psi}\right)' - 1.$$

In the limit

$$\lim_{\psi \to \frac{\pi}{4}} \frac{\partial V}{\partial \theta} \to \infty, \quad \text{for } \left[1 + \frac{m}{2} + \frac{\beta}{2(\beta-1)}\right]\frac{d\theta}{d\psi} - 1 < 0,$$

$$\lim_{\psi \to \frac{\pi}{4}} \frac{\partial V}{\partial \theta} \to 0, \quad \text{for } \left[1 + \frac{m}{2} + \frac{\beta}{2(\beta-1)}\right]\frac{d\theta}{d\psi} - 1 > 0.$$

For incompressible solids, $\beta = 0$, and the limits are tabulated below:

Table 3

Limit	Plane strain	Axial symmetry
$\frac{\partial V}{\partial \theta} \to \infty$	$\frac{d\psi}{d\theta} > 1$	$\frac{d\psi}{d\theta} > \frac{3}{2}$
$\frac{\partial V}{\partial \theta} = 0$	$\frac{d\psi}{d\theta} < 1$	$\frac{d\psi}{d\theta} < \frac{3}{2}$

It should be noted that the above expressions for $\beta > 0$ apply only at some distance from the vertex of the channel where σ[lb. per sq.ft.] $\gg 1$.

Typical radial flow profiles are shown in Fig. 68 for the two $\partial V/\partial\theta$ limits. In both cases velocity is zero along the two rays $\psi = 3\pi/4$ and $\psi = \pi/4$. These two rays coincide with velocity characteristics and, of course, are streamlines. The profiles shown in the figure are physically acceptable only within the internal region, that is for channels with weak walls whose wall yield loci intersect the Mohr stress circle within the arc T'MT".

Lines of constant velocity in the internal regions for $\beta = 0$ are shown in Figures 69 and 70 for plane strain and axial symmetry for $\delta = 50°$. These lines show ratios $V/V°$ along an arc $r = r°$ and, therefore, in accordance with eq. (124) present the function

$$\frac{V}{V°} = e^{-(2 + m) \int_0^{\theta} \tan 2\psi \, d\theta}. \qquad (125)$$

Vertical channels

Vertical channels are a limiting condition of converging channels. However, the relations derived for flow in converging channels are not suitable for application to vertical channels, hence the latter will now be considered separately.

The radial stress and velocity fields of the converging channels go over to fields independent of the vertical coordinate x in vertical channels. The solutions to such fields in vertical channels are obtained in closed form. There is one major difference between converging and vertical channels. In the former there is no doubt as to the value of the circumferential pressure: that pressure is major. In the latter, assuming complete independence of the vertical coordinate, there is no basis for the selection of either the major or the minor value for the circumferential pressure. The physical consequence of this uncertainty appears in the erratic and unsteady flow pattern which is observed in tall vertical channels.

Some conclusions can be drawn, however, on the basis of compressibility if even a slight gradient of pressure exists in the vertical

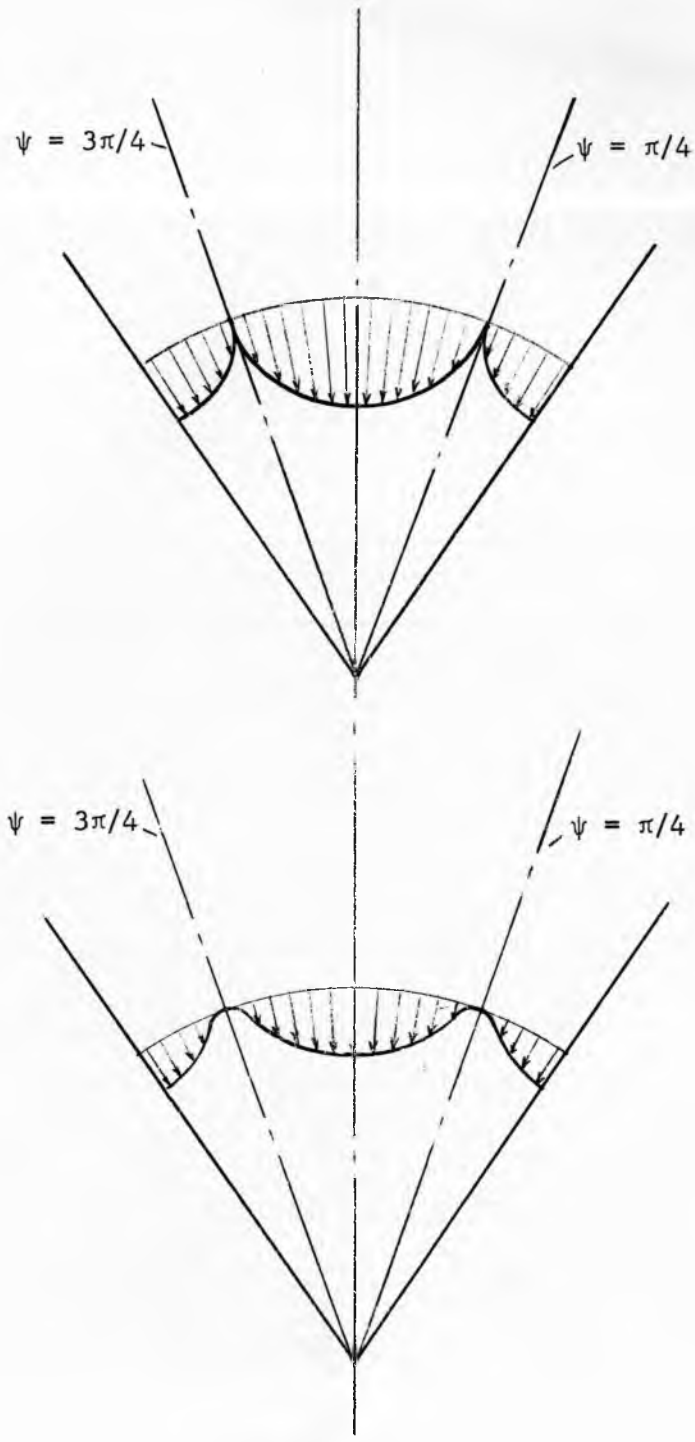

Fig. 68

Radial velocity profiles

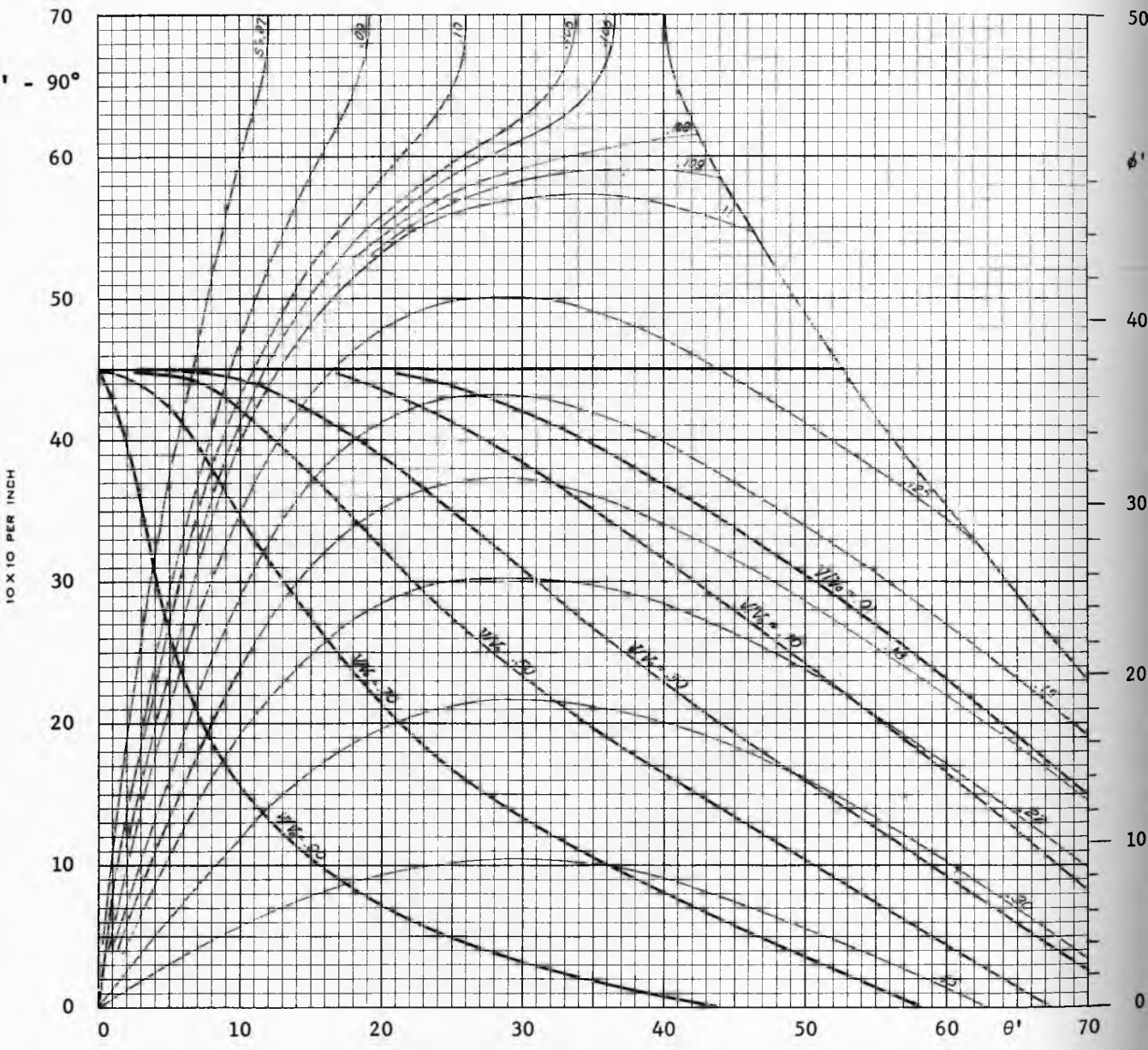

Fig. 69

Function V/V^{o}, $\delta = 50°$

Plane symmetry (symmetric plane flow)

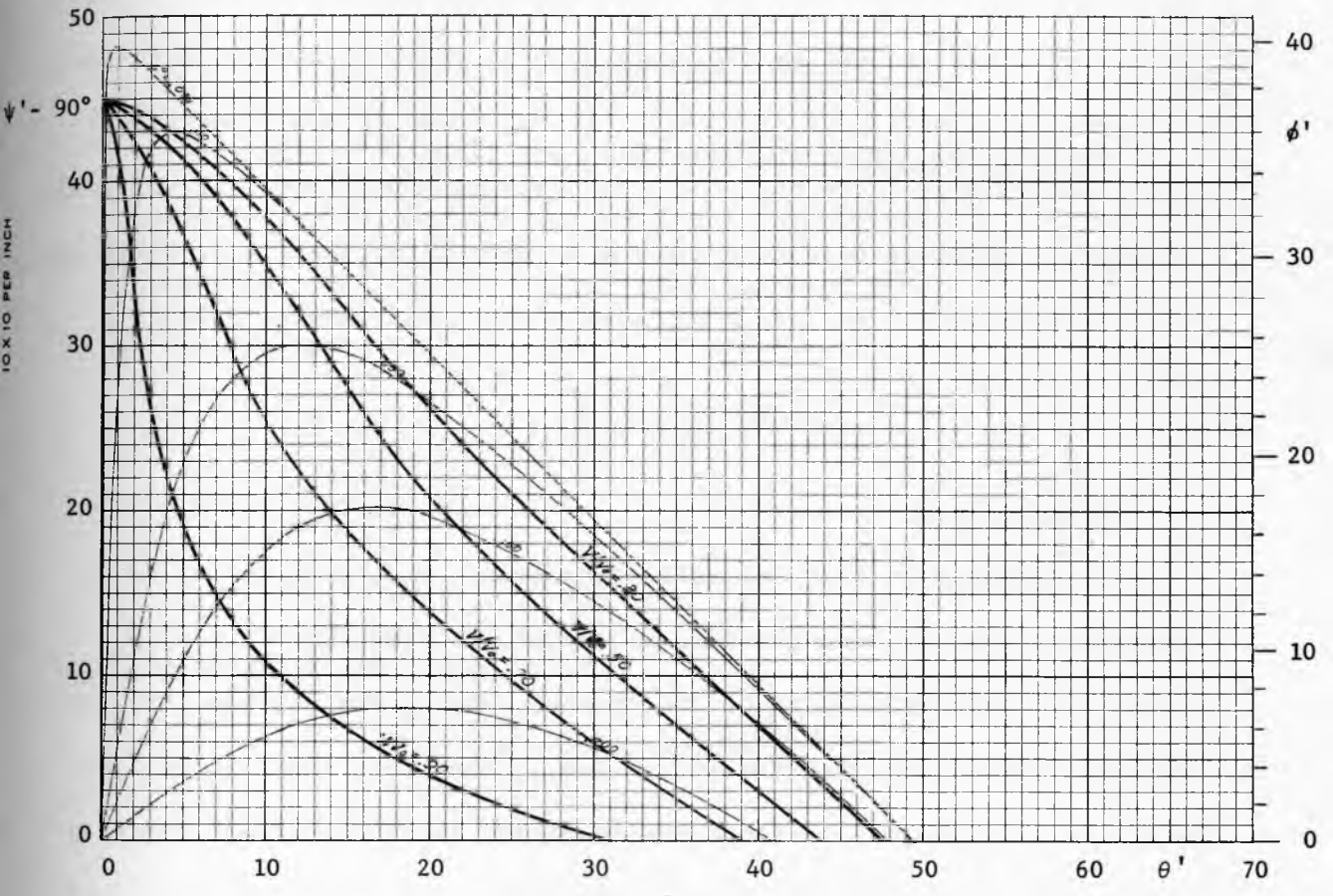

Fig. 70

Function V/V^{O}, $\delta = 50°$

Axial symmetry (conical flow)

direction. If pressure increases downward then the solid consolidates as it flows and flow has to be divergent ($k = -1$) to keep each horizontal cross-section filled out. This condition is expected to exist in the upper part of a channel from a stress-free top surface down. In fact, this condition seems to prevail in most channels.

It was shown in the analysis of the radial stress fields in axial symmetry that fields with a velocity discontinuity at the walls can be generated only within walls of a sufficient degree of weakness. This limitation carries over to the vertical axi-symmetric channel with the assumption of convergence ($k = +1$). Hence, it would seem that divergence more likely represents the actual stress conditions in a vertical channel of moderate height, while the erratic flow, when it is observed, may be explained by shifts of the circumferential pressure between minor and major.

Stress field.

The purpose of this analysis is twofold: first, to derive an expression for the mean pressure σ, second, to find the ratio y''/y_e, where y'' is the half width of the channel, and y_e the distance from the axis of symmetry to the line of $\omega = \pi/4$. Along this line, as will be shown in the analysis of the velocity field, rapid non-steady velocity changes may occur and are, indeed, observed in full size channels. In models with transparent walls this ratio can be observed, measured, and compared with the computed values.

Plane-Cartesian/cylindrical-polar coordinates will be used. Pressure

is found from eq.(48) which in this case reduces to

$$\frac{d\tau_{xy}}{dy} + m\frac{\tau_{xy}}{y} = \gamma$$

and, with the constant of integration evaluated at the axis y = 0, $\tau_{xy} = 0$, integrates to

$$\tau_{xy} = \frac{\gamma y}{1+m}.$$

τ_{xy} is now eliminated by means of eq. (16), yielding

$$\sigma = \frac{\gamma y}{(1+m)\sin\delta \sin 2\omega}. \tag{126}$$

The ratio y''/y_e will now be determined. Plane strain flow is considered first. Eq.(49) now applies in the form $d\sigma_y/dy = 0$, hence σ_y is constant. The elimination of σ between eq.(126), with m = 0, and eq. (15) yields

$$y = \frac{\sigma_y}{\gamma}\frac{\sin\delta \sin 2\omega}{1 - \sin\delta \cos 2\omega}. \tag{127}$$

For $\omega = \pi/4$, this becomes

$$y_e = \frac{\sigma_y}{\gamma}\sin\delta,$$

while for $\omega'' = \pi/4 - \phi/2$, it is

$$y'' = \frac{\sigma_y}{\gamma}\frac{\sin\delta \cos\phi}{1 - \sin\delta \sin\phi}.$$

Hence, in plane strain, the ratio is

$$\frac{y''}{ye} = \frac{\cos\phi}{1 - \sin\delta \sin\phi}. \tag{128}$$

In axially symmetric flow, m = 1, and the equation of equilibrium (49) is of the form

$$\frac{d\sigma_y}{dy} + \frac{\sigma_y - \sigma_\alpha}{y} = 0.$$

The substitution of expression (126) for σ (with $m = 1$) in equations (15) and (22) yields

$$\sigma_y = \gamma\, y\, \frac{1 - \sin\delta\cos 2\omega}{2\sin\delta\sin 2\omega},$$

$$\sigma_y = \gamma\, y\, \frac{1 + k\sin\delta}{2\sin\delta\sin 2\omega}.$$

These expressions and the appropriate derivative are now substituted in the equation of equilibrium yielding, after transformations,

$$\frac{dy}{y} = -\frac{(\cos 2\omega - \sin\delta)\, d(2\omega)}{(1 - k\sin\delta - 2\sin\delta\cos 2\omega)\sin 2\omega},$$

which integrates into

$$y = c(1 + \cos 2\omega)^A\,(1 - \cos 2\omega)^B\,\left(\frac{1 - k\sin\delta}{2\sin\delta} - \cos 2\omega\right)^C, \qquad (129)$$

where the exponents A, B, C are as presented below in Table 4.

Table 4

	Converging	Diverging
A	$\frac{1 - \sin\delta}{2(3\sin\delta - 1)}$	$-1/2$
B	$1/2$	$\frac{1 + \sin\delta}{2(3\sin\delta + 1)}$
C	$-\frac{2\sin\delta - 1}{3\sin\delta - 1}$	$-\frac{2\sin\delta + 1}{3\sin\delta + 1}$

Within the field, including the boundary $\omega = \omega''$, the observed fields are of the type $d\omega/dy \leqslant 0$. Since, at the axis of symmetry for $y = 0$,

there is $\omega = \pi/2$, this implies

$$1 - k \sin \delta - 2 \sin \delta \cos 2\omega \geqslant 0,$$

or

$$\cos 2\omega \leqslant \frac{1 - k \sin \delta}{2 \sin \delta}.$$

For diverging flow this condition is always satisfied, but for converging flow

$$\frac{1}{2} \text{Arc cos} \frac{1 - \sin \delta}{2 \sin \delta} \leqslant \omega \leqslant \pi - \frac{1}{2} \text{Arc cos} \frac{1 - \sin \delta}{2 \sin \delta}.$$

The bounds for ω are

Table 5

δ	30°	40°	50°	60°	70°
ω''	30.00°	36.94°	40.61°	42.75°	44.09°
ω'	150.00°	143.06°	139.39°	137.25°	135.51°

It will be observed that these bounds match the values of ψ' for $\theta \to 0$ plotted for the radial fields in converging channels, Figures 34 to 38. At the wall, $y = y''$, for a solid flowing on a rough wall, $2\omega'' = \pi/2 - \phi$. From this relation it is possible to determine the maximum values of ϕ which will allow the formation of a vertical, converging field within rough walls

$$\phi \leqslant \pi/2 - 2\omega''$$

This is given in Table 6

Table 6

δ	30°	40°	50°	60°	70°
ϕ	30.00°	16.12°	8.78°	4.50°	1.82°

These values of ϕ are small for $\delta > 40°$, hence it would appear that this field is unlikely to develop in most solids.

The ratio y''/y_e is now computed for axially symmetric flow, as follows: for $\omega = \pi/4$

$$y_e = c\left(\frac{1 - k \sin \delta}{2 \sin \delta}\right)^C,$$

while for $\omega'' = \pi/4 - \phi/2$

$$y'' = c(1 + \sin \phi)^A \, (1 - \sin \phi)^B \, \left(\frac{1 - k \sin \delta}{2 \sin \delta} - \sin \phi\right)^C,$$

and the ratio becomes

$$\frac{y''}{y_e} = (1 + \sin \phi)^A \, (1 - \sin \phi)^B \, \left(1 - \frac{2 \sin \delta \sin \phi}{1 - k \sin \delta}\right)^C. \qquad (130)$$

Velocity field

The velocity field is also computed with the assumption of independence of the vertical coordinate. The equations of continuity and isotropy (57) and (61) reduce to

$$\gamma \, v \, y^m = c,$$

and

$$du + dv \tan 2\omega = 0.$$

Since the constant of integration c evaluates at zero for $y = y''$, at the wall, $v = 0$ throughout the field. From the second equation it now follows that $u = V$ is constant, except possibly for $\omega = \pi/4$ and $\omega = 3\pi/4$, where the velocity field allows velocity discontinuities in V. However, these lines are not sliplines and, therefore, steady state velocity discontinuities do not occur along these lines. Unsteady slips are observed.

This flow pattern is shown on the photograph, Fig. 71. Since unsteady effects cannot be reproduced on a still photograph the steady velocity discontinuities at the walls, where $\omega' = 3\pi/4 + \phi/2$ and $\omega'' = \pi/4 - \phi/2$, and the unsteady slips along the lines $\omega = \pi/4$ and $\omega = 3\pi/4$ appear identical. The measured ratio $y''/y_e = 1.6$. While the flow pattern of this model was almost perfectly of the plane strain type, the front and back glass walls obviously prevent a plane strain stress field from developing. The actual stress field deviates somewhat from plane strain toward the axi-symmetric.

Ratio y''/y_e is now computed for the plane strain stress field from eq.(128), and for the axially symmetric, diverging stress field from eq.(130). Tests of flowability of the solid indicate that $\delta = 55°$, $\phi = 50°$.

For plane strain

$$\frac{y''}{y_e} = 1.73$$

For axial symmetry

$$\frac{y''}{y_e} = 1.766^{-.5} \times .234^{.263} \times .310^{-.762} = 1.25$$

The observed value of 1.6 falls between these two bounds.

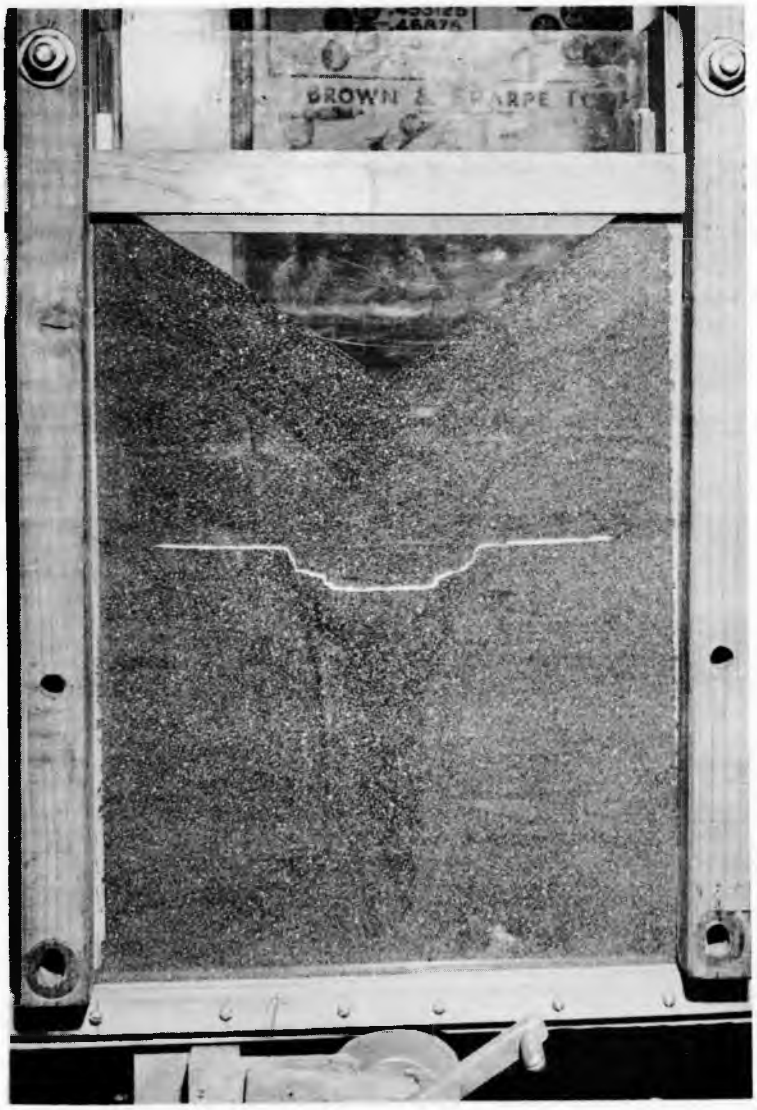

Fig. 71

Observed flow pattern in a vertical channel

PART III

INCIPIENT FAILURE

General equations

The derivation of the differential equations for incipient failure follows the pattern described for steady state flow with the following differences: First, during steady flow the stresses are governed by the effective yield pyramid, and are located at the edge of the base of the pyramid. The latter implies that normality provides only a cone within which the direction of the strain rate vector has to lie. During incipient failure the stresses are govered by the yield pyramid, and are located either on a face or on a side edge of the pyramid, away from its base. Here, normality imposes either a unique direction of the strain rate vector or a plane sector within which the vector has to lie.

Second, in steady state flow, the solid is flowing and a velocity field is computed. In incipient failure, velocities are zero, and an initial acceleration field is calculated.

In earlier work [e.g. 8, 19, 20, 21] attempts have been made to compute the velocity fields which follow incipient failure. In these computations it has been assumed that the yield surface remains constant as failure progresses, and that the stress field also remains essentially constant. With the concurrent assumption of normality this enforced continuous expansion of the solid. Since continuous expansion could never be verified experimentally, a serious doubt was cast on the validity of the principle of normality. This doubt appears unjustified,

the error seems to lie not in normality but in the assumption of a constant yield surface. The size of the yield surface certainly is a function of density, and changes as the solid expands. In fact, as will be shown presently, these computations produced not velocity fields but initial acceleration fields.

The process of failure is complicated: failure seldom takes place simultaneously throughout a stress field, usually failure occurs along some active sliplines while regions of material bounded by those sliplines remain rigid (or elastic). The mass becomes non-homogeneous and unisotropic, the yield function varies across the mass with discontinuities along the active sliplines. The moment the first active slipline has developed, the incipient stress field does not apply any more and neither does the initial acceleration field. The value of the acceleration field associated with a stress field lies in showing that failure can start under the prescribed boundary condition. No attempt will be made in this work to determine how failure proceeds and how steady state flow is ultimately approached.

The adopted yield function allows the stress equations to be solved independently of acceleration. The solution produces the function $\omega(x,y)$ throughout the field and the acceleration field can then be computed. It is shown that, at zero velocity, the direction of the strain rate vector coincides with the direction of the time derivative of that vector, so that normality and isotropy provide the necessary relations for the solution of the acceleration field.

Stress field

The equations are derived in plane-Cartesian/cylindrical- polar coordinates. The two equations of equilibrium (48) and (49), together with the equations (29) - (31), which contain the condition of plasticity, provide a solution for the three variables $(\bar{\sigma}_x, \bar{\sigma}_y, \bar{\tau}_{xy})$ in plane strain. In axial symmetry, the fourth variable $\bar{\sigma}_\alpha$ is taken care of by the additional equation (37). In these considerations, the yield locus given by ϕ and f_c, is assumed constant throughout the plastic field. The equations of equilibrium are expressed in terms of $\bar{\sigma}$ and ω as follows

$$(1 + \sin\phi \cos 2\omega)\frac{\partial\bar{\sigma}}{\partial x} + \sin\phi \sin 2\omega \frac{\partial\bar{\sigma}}{\partial y} - 2\bar{\sigma} \sin\phi \sin 2\omega \frac{\partial\omega}{\partial x} + $$

$$+ 2\bar{\sigma} \sin\phi \cos 2\omega \frac{\partial\omega}{\partial y} = \gamma - m\frac{\bar{\sigma}}{y} \sin\phi \sin 2\omega, \qquad (131)$$

$$\sin\phi \sin 2\omega \frac{\partial\bar{\sigma}}{\partial x} + (1 - \sin\phi \cos 2\omega)\frac{\partial\bar{\sigma}}{\partial y} + 2\bar{\sigma} \sin\phi \cos 2\omega \frac{\partial\omega}{\partial x} +$$

$$+ 2\bar{\sigma} \sin\phi \sin 2\omega \frac{\partial\omega}{\partial y} = m\frac{\bar{\sigma}}{y} \sin\phi (k + \cos 2\omega). \qquad (132)$$

Now the following abbrevation is introduced

$$S = \frac{\cot\phi}{2} \ln\frac{\bar{\sigma}}{\bar{\sigma}_o}, \qquad (133)$$

where $\bar{\sigma}_o$ is an arbitrary constant. The differential equations then reduce to the form

$$\frac{\partial(S + \omega)}{\partial x} + \frac{\partial(S + \omega)}{\partial y} \tan(\omega + \frac{\pi}{4} - \frac{\phi}{2}) = A, \qquad (a)$$

$$\frac{\partial(S - \omega)}{\partial x} + \frac{\partial(S - \omega)}{\partial y} \tan(\omega - \frac{\pi}{4} + \frac{\phi}{2}) = B, \qquad (b)$$

where

$$A = -\frac{\gamma \sin\left(\omega - \frac{\pi}{4} + \frac{\phi}{2}\right)}{2\bar{\sigma} \sin\phi \cos\left(\omega + \frac{\pi}{4} - \frac{\phi}{2}\right)} + m\frac{\cos\left(\omega + \frac{\pi}{4} - \frac{\phi}{2}\right) + k\cos\left(\omega - \frac{\pi}{4} + \frac{\phi}{2}\right)}{2y\cos\left(\omega + \frac{\pi}{4} - \frac{\phi}{2}\right)}, \quad (134)$$

$$B = \frac{\gamma \sin\left(\omega + \frac{\pi}{4} - \frac{\phi}{2}\right)}{2\bar{\sigma} \sin\phi \cos\left(\omega - \frac{\pi}{4} + \frac{\phi}{2}\right)} - m\frac{\cos\left(\omega - \frac{\pi}{4} + \frac{\phi}{2}\right) + k\cos\left(\omega + \frac{\pi}{4} - \frac{\phi}{2}\right)}{2y\cos\left(\omega - \frac{\pi}{4} + \frac{\phi}{2}\right)}. \quad (135)$$

In the first characteristic direction,

$$\frac{dy}{dx} = \tan\left(\omega + \frac{\pi}{4} - \frac{\phi}{2}\right), \quad (136)$$

the left hand side of eq.(a) is a total derivative

$$\frac{d(S + \omega)}{dx} = A. \quad (137)$$

Similarly, in the second characteristic direction,

$$\frac{dy}{dx} = \tan\left(\omega - \frac{\pi}{4} + \frac{\phi}{2}\right), \quad (138)$$

the left hand side of eq. (b) is a total derivative,

$$\frac{d(S - \omega)}{dx} = B. \quad (139)$$

The two stress characteristics intersect at an angle $\pi/2 - \phi$, and form angles $\pm (\pi/4 - \phi/2)$ with the direction of the major pressure. In incipient failure the stress characteristics coincide with the sliplines.

Initital acceleration field

The equations of the acceleration field are derived on the basis of isotropy, eq.(61), and the conditions imposed by normality on the direction of the strain rate vector. The three principal strain rates are ordered $\epsilon_1 > 0$, $\epsilon_2 < 0$, $m\, k\, \epsilon_\alpha > 0$.

Following Shield's reasoning [10], normality requires

$\epsilon_1 = \lambda(1 - \sin\phi)$, $\epsilon_2 = -(\lambda + \mu)(1 + \sin\phi)$, $m\,\epsilon_\alpha = \mu(1 + k \sin\phi)$,

where λ and μ are positive scalars, whose elimination yields

$$\epsilon_1 - \epsilon_2 + (\epsilon_1 - \epsilon_2)\sin\phi + m\,\epsilon_\alpha(1 + k \sin\phi) = 0.$$

The principal strain rates are now replaced by

$$\epsilon_1 + \epsilon_2 = \epsilon_x + \epsilon_y = -\frac{\partial u}{\partial x} - \frac{\partial v}{\partial y},$$

$$\epsilon_1 - \epsilon_2 = [(\epsilon_x - \epsilon_y)^2 + \gamma_{xy}^2]^{\frac{1}{2}} = [(\frac{\partial u}{\partial x} - \frac{\partial v}{\partial y})^2 + (\frac{\partial u}{\partial y} + \frac{\partial v}{\partial x})^2]^{\frac{1}{2}},$$

which, with the use of the equation of isotropy (61), reduces to

$$\epsilon_1 - \epsilon_2 = -\frac{\frac{\partial u}{\partial x} - \frac{\partial v}{\partial y}}{\cos 2\omega},$$

and

$$\epsilon_\alpha = -\frac{v}{y},$$

leading to

$$\frac{\partial u}{\partial x}(\cos 2\omega + \sin\phi) + \frac{\partial v}{\partial y}(\cos 2\omega - \sin\phi) + m\,\frac{v}{y}(1 + k \sin\phi)\cos 2\omega = 0. \quad (c)$$

It is now easy to show that the velocities u and v are proportional to the initial accelerations $\dot{u}$ and $\dot{v}$ and, since the equation (c) as well as the equation of isotropy are homogeneous, the velocities can be replaced by the accelerations. The total derivative of the velocity component u,

$$\frac{du}{dt} = \dot{u} + \frac{\partial u}{\partial x}\,u + \frac{\partial u}{\partial y}\,v,$$

is integrated and, upon application of the mean value theorem, becomes

$$u = (\dot{u})'t + (\frac{\partial u}{\partial x}\,u + \frac{\partial u}{\partial y}\,v)'t.$$

evidently $u = a\,t$ and, similarly, $v = b\,t$, where a and b are bounded functions, therefore, the second term on the right hand side contains t^2 and becomes insignificant as $t \to 0$, hence

$$\lim_{t\to o} u = \dot{u}\,t, \quad \text{similarly,} \quad \lim_{t\to o} v = \dot{v}\,t.$$

Since t is independent of the coordinates (x,y), the expressions for the strain rates become

$$\lim_{t\to o} \frac{\partial u}{\partial x} = \frac{\partial \dot{u}}{\partial x}\,t, \qquad \lim_{t\to o} \frac{\partial u}{\partial y} = \frac{\partial \dot{u}}{\partial y}\,t,$$

$$\lim_{t\to o} \frac{\partial v}{\partial x} = \frac{\partial \dot{v}}{\partial x}\,t, \qquad \lim_{t\to o} \frac{\partial v}{\partial y} = \frac{\partial \dot{v}}{\partial y}\,t.$$

Substitution of these expressions for the strain rates in equations (c) and (61) produces

$$\frac{\partial \dot{u}}{\partial x}(\cos 2\omega + \sin \phi) + \frac{d\dot{v}}{\partial y}(\cos 2\omega - \sin \phi) + m\,\frac{\dot{v}}{y}(1 + k \sin \phi)\cos 2\omega = 0, \quad \text{(d)}$$

$$\frac{\partial \dot{u}}{\partial x}\tan 2\omega - \frac{\partial \dot{u}}{\partial y} - \frac{\partial \dot{v}}{\partial x} - \frac{\partial \dot{v}}{\partial y}\tan 2\omega = 0. \quad \text{(e)}$$

The above two equations, together with the equations of the total derivatives,

$$d\dot{u} = \frac{\partial \dot{u}}{\partial x}\,dx + \frac{\partial \dot{u}}{\partial y}\,dy, \qquad d\dot{v} = \frac{\partial \dot{v}}{\partial x}\,dx + \frac{\partial \dot{v}}{\partial y}\,dy,$$

are solved for $\partial\dot{u}/\partial x$, yielding

$$\frac{\partial \dot{u}}{\partial x} = \frac{dy}{dx}\left\{\left(\frac{d\dot{u}}{dx} + \frac{d\dot{v}}{dx}\right)(\sin \phi - \cos 2\omega) - m\,\frac{\dot{v}}{y}(1 + k \sin \phi)\left(\frac{dy}{dx}\cos 2\omega - \sin 2\omega\right)\right\}$$

$$/\left[\frac{dy}{dx} - \tan\left(\omega + \frac{\pi}{4} - \frac{\phi}{2}\right)\right]\left[\frac{dy}{dx} - \tan\left(\omega - \frac{\pi}{4} + \frac{\phi}{2}\right)\right]. \quad \text{(f)}$$

The directions of the characteristics are

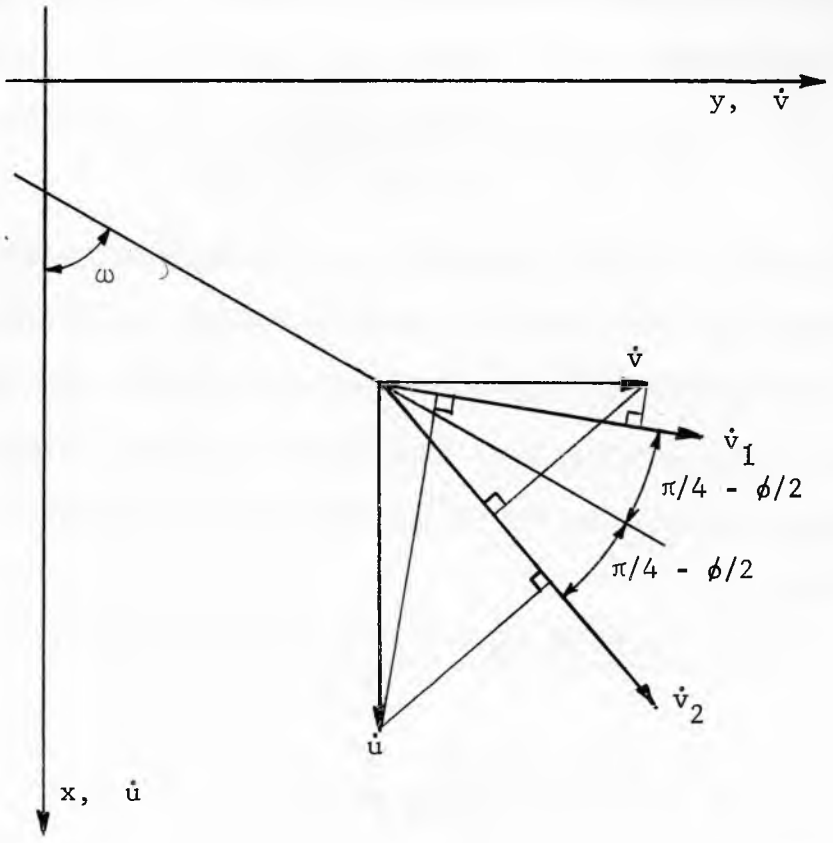

Fig. 72

Projections of the acceleration components

on the characteristic directions

$$\frac{dy}{dx} = \tan[\omega \pm (\frac{\pi}{4} - \frac{\phi}{2})]. \tag{140}$$

Along the characteristics, the numerator of eq.(f) is zero. With the substitution of the above expressions for dy/dx in the numerator of (f) that equation becomes

$$\frac{d\dot{u}}{dy} + \frac{d\dot{v}}{dx} + m\frac{\dot{v}}{y}\frac{1 + k \sin\phi}{\sin 2[\omega \pm (\frac{\pi}{4} - \frac{\phi}{2})]} = 0. \tag{141}$$

In both equations (140) and (141) the top sign applies along the first characteristic and the bottom sign along the second characteristic.

For the purpose of numerical calculation, it is often more convenient to express these equations not by the $\dot{u}$ and $\dot{v}$ components but by their projections $\dot{v}_1$ and $\dot{v}_2$ on the characteristic directions, Fig. 72. The relations are

$$\dot{u} = \frac{-\dot{v}_1 \sin(\omega - \frac{\pi}{4} + \frac{\phi}{2}) + \dot{v}_2 \sin(\omega + \frac{\pi}{4} - \frac{\phi}{2})}{\cos\phi},$$

$$\dot{v} = \frac{\dot{v}_1 \cos(\omega - \frac{\pi}{4} + \frac{\phi}{2}) - \dot{v}_2 \cos(\omega + \frac{\pi}{4} - \frac{\phi}{2})}{\cos\phi}.$$

The transformation leads to:

along the first characteristic: $\frac{dy}{dx} = \tan(\omega + \frac{\pi}{4} - \frac{\phi}{2})$, (142)

$$\frac{d\dot{v}_1}{dy} - (\dot{v}_1 \tan\phi - \frac{\dot{v}_2}{\cos\phi})\frac{d\omega}{dy} + m\frac{\dot{v}(1 + k \sin\phi)}{2y \sin(\omega + \frac{\pi}{4} - \frac{\phi}{2})} = 0. \tag{143}$$

along the second characteristic: $\frac{dy}{dx} = \tan(\omega - \frac{\pi}{4} + \frac{\phi}{2})$, (144)

$$\frac{d\dot{v}_2}{dy} - (\frac{\dot{v}_1}{\cos\phi} - \dot{v}_2 \tan\phi)\frac{d\omega}{dy} + m\frac{\dot{v}(1 + k \sin\phi)}{2y \sin(\omega - \frac{\pi}{4} + \frac{\phi}{2})} = 0 \tag{145}$$

It will be noted that the acceleration characteristics, as well as the stress characteristics, coincide with the sliplines.

Superposition. Since both, the equation of continuity (d) and isotropy (e), are linear and homogeneous, a linear combination of two (or more) solutions of an initial acceleration field is also a solution.

Physical conditions.

The physical conditions which need to be applied to incipient failure are less restrictive than they were for steady state flow.

A. Some, small, tensile (negative) stresses are permissible.

B. A line of infinite shear strain rate may occur along a slipline or a weak wall.

C. The velocity $\bar{V}$ of an element of a solid is zero.

D. The acceleration of an element,

$$\frac{d\bar{V}}{dt} = \frac{dV}{dt}\,\bar{s} + \frac{V^2}{\rho_s}\,\bar{n},$$

along the path of its travel, Fig. 18, is bounded. This implies that dV/dt is bounded but $1/\rho_s$ need not be bounded since $\bar{V} = 0$.

E. Singularities in density are inadmissible.

Grids and special lines.

There is a great deal of similarity between the grids and special lines of steady state flow and incipient failure. The differences will be particularly emphasized here. As before, the solution of the stress

field contains the direction of the major pressure $\bar{\sigma}_1$ in the differential form $\omega = \omega(x,y)$.

1. Sliplines, stress and acceleration characteristics. These three grids coincide in incipient failure. They form lines inclined at angles

$$\omega \pm (\pi/4 - \phi/2).$$

2. Lines of maximum shear strain rate. These lines are, of course, inclined at $\omega \pm \pi/4$ but they are of little significance in incipient failure since they are not observed.

3. Trajectories. Failure is a time dependent process and, therefore, paths of travel of the elements will be referred to as trajectories. The trajectories may have cusps at the initial points, since velocity starts from zero at those points. This is important, because the stress field may be bounded by a stress envelope and incipient failure may occur along a slipline merging into the envelope. This slipline may have a cusp at the envelope yet become a trajectory.

4. Acceleration discontinuities. A line of acceleration discontinuity develops into a line of velocity discontinuity. Such a line has to be a trajectory (or a streamline) and has to follow a slipline or a weak wall. It separates two regions which may be both plastic, both rigid (or elastic), or one plastic and the other rigid (or elastic).

5. A straight acceleration characteristic in plane strain enforces a constant projection of the acceleration vector on that characteristic. This is evident from, say, eq. (143).

6. Walls. A wall separates a plastic region from a stationary rigid (or elastic) region. Usually, there is a velocity discontinuity

along a wall: the wall then is a streamline and stresses along it are defined either by the yield locus, for a rough wall, or by the wall yield locus, for a weak wall. When the solid fails along a rough wall, the wall is a slipline and a stress and acceleration characteristic. The coincidence of an acceleration characteristic with a streamline leads to the relation

$$\dot{V}^2 \; {}_y m(1 + k \sin \phi) = c, \tag{146}$$

along the wall. This relation is readily obtained from, say, eq. (143) with $\dot{v}_1 = \dot{V}$, $\dot{v}_2 = \dot{V} \sin \phi$. Evidently $\dot{V}$ can be zero along such a wall, which means that a field can develop without an acceleration discontinuity along the rough wall.

When the solid fails along a weak wall, equations (79) and (80) apply along the wall with ϕ substituted for δ, and an acceleration discontinuity is mandatory since a zero acceleration along the wall would enforce a zero acceleration within a region of the plastic field.

7. A stress discontinuity may occur only along a trajectory for the reason given in steady state flow, point 11.

8. Stress singularities are inadmissible for the reason given in steady state flow, point 12.

Doming

Consider the pressures acting in a dome which has formed across a channel of width B, Fig. 73. It is assumed that the dome will fail if the bottom layer of the dome fails. The bottom layer is taken of a

unit thickness, measured in the vertical direction. Evidently, the pressures in the layer are at a minimum when the surface of the dome is smooth and regular and, barring the possibility of tensions, when the mass above does not bear down on the layer. The latter implies zero stress between the layer and the mass above. Under these conditions the layer can be thought of as a self-supporting dome, geometrically and stress-wise independent of the vertical coordinate. The major pressure $\bar{\sigma}_1$ acts in the plane of the dome.

If the vertical axis of the dome is drawn through its highest point, then at a distance y from the axis

$$\bar{\sigma}_1 \sin 2\omega = \frac{2\gamma y}{1 + m}.$$

For failure to occur $\bar{\sigma}_1 \geqslant f_c$, or

$$2y \geqslant (1 + m)\frac{f_c}{\gamma} \sin 2\omega. \qquad (g)$$

For <u>symmetric channels</u>, $2y = B$ and the largest dome occurs for $\omega' = 3\pi/4$ and $\omega'' = \pi/4$. For such a dome to fail, it is necessary that

$$B \geqslant (1 + m)\frac{f_c}{\gamma}. \qquad (147)$$

For <u>asymmetric plane strain</u> with one wall vertical, $\theta'' = 0$, eq.(g) gives different relations for each abutment. The conditions on the sloping wall, $\theta = \theta'$, will be denoted by a prime, while the conditions at the vertical wall will be denoted by the superscript v. The relations for failure at the two abutments are

$$B - a > -\frac{f_c' \sin 2\omega'}{2\gamma} \quad \text{and} \quad a > \frac{f_c^v \sin 2\omega^v}{2\gamma} \qquad (148)$$

The above formulas (147) and (148) assume that the wall is sufficiently

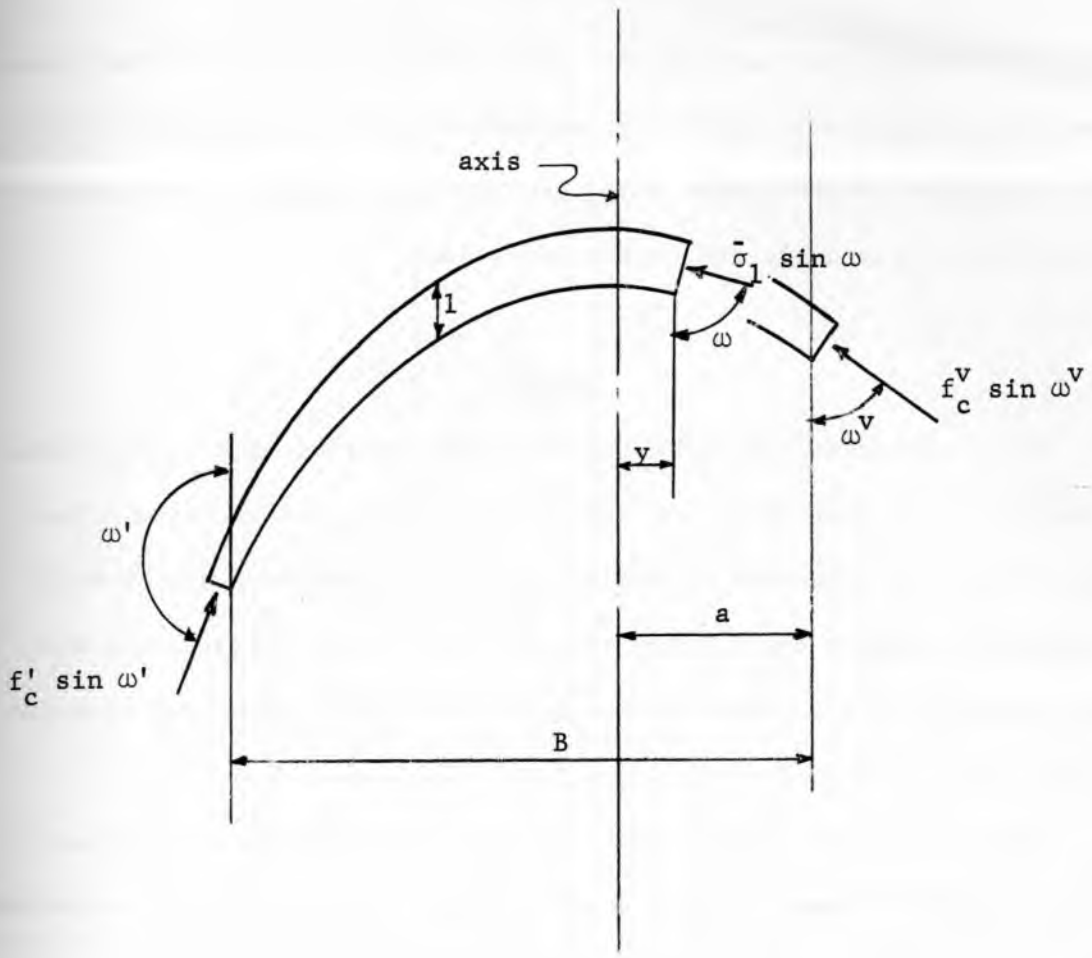

Fig. 73

Doming

strong to support the major stress at an angle $\omega'' = \pi/4$, for the symmetric dome, and at angles ω' and ω'' for asymmetric plane strain. In view of the uncertainty of the value of ϕ' in incipient failure, these assumptions appear reasonable and on the safe side.

Piping

The conditions leading to the incipient failure of a solid around a vertical, circular hole, or pipe is analysed in this section. The unconfined yield pressure f_c and the angle of friction ϕ are assumed constant throughout the failing region. The stress field is assumed axi-symmetric with a traction-free inner boundary of constant diameter D, Fig. 74.

These assumptions imply independence of the vertical coordinate x as well as the circumferential coordinate α. A relation will be derived between the yield properties of the solid (f_c, ϕ) and the smallest diameter D at which a bounded plastic field can develop.

The equations of equilibrium (48) and (49) now reduce to

$$\frac{d\bar{\tau}_{xy}}{dy} + \frac{\bar{\tau}_{xy}}{y} = \gamma, \qquad \frac{d\bar{\sigma}_y}{dy} + \frac{\bar{\sigma}_y - \bar{\sigma}_\alpha}{y} = 0.$$

Ratio

$$\left(\frac{2y}{D}\right)^2 = n \tag{149}$$

is introduced and the equations of equilibrium transform to

$$\frac{d\bar{\tau}_{xy}}{dn} + \frac{\bar{\tau}_{xy}}{2n} = \frac{\gamma D}{4n^{\frac{1}{2}}}, \tag{h}$$

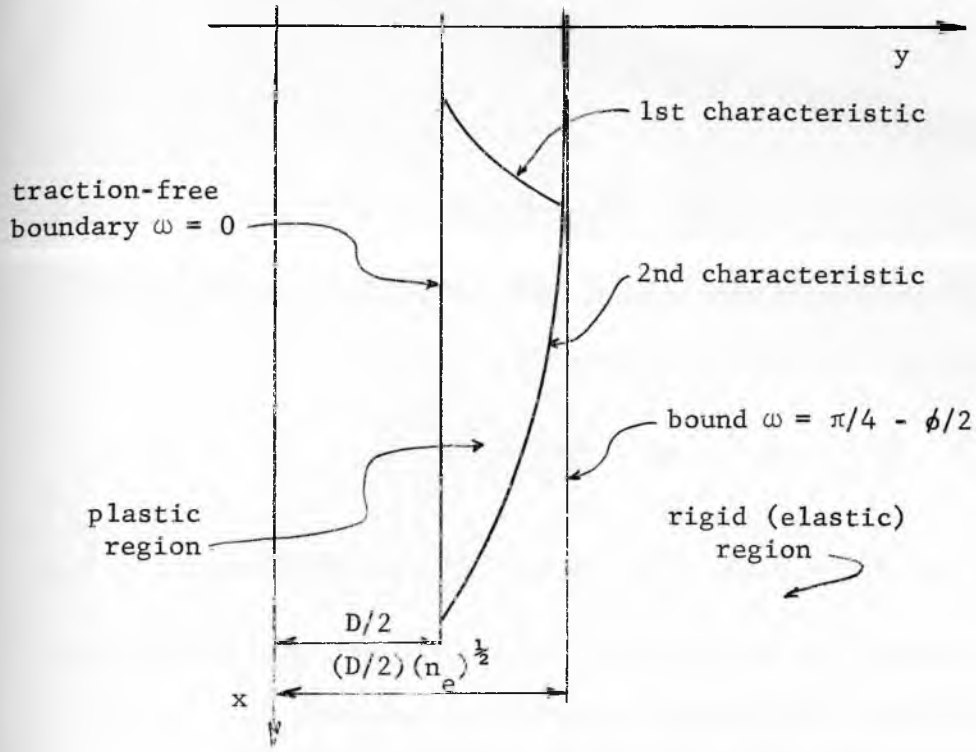

(a) Bounded field

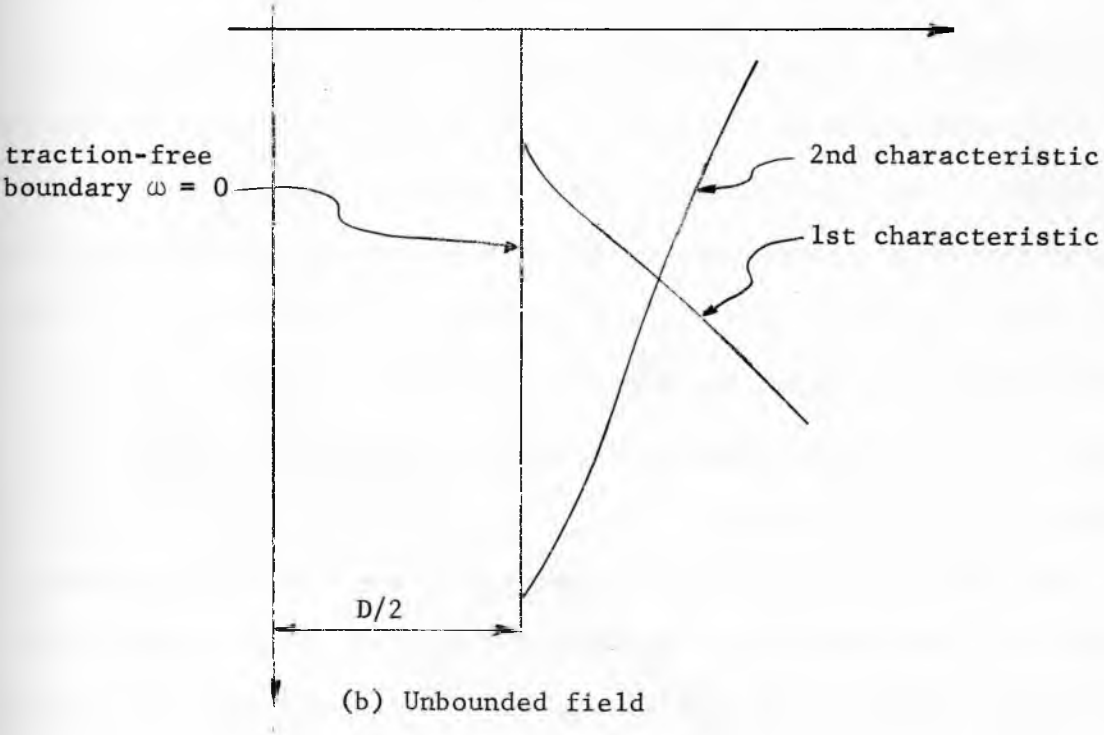

(b) Unbounded field

Fig. 74

Piping

$$\frac{d\bar{\sigma}_y}{dn} + \frac{\bar{\sigma}_y - \bar{\sigma}_\alpha}{2n} = 0.$$

The substitution of expressions (30), (31), (37) (with k = +1), and their appropriate derivatives yields

$$\frac{d\bar{\sigma}}{\bar{\sigma}} + 2 \cot 2\omega \, d\omega - \frac{n+1}{2n(n-1)} \, dn = 0,$$

$$\frac{d\bar{\sigma}}{\bar{\sigma}}(1 - \sin \delta \cos 2\omega) + 2 \sin \phi \sin 2\omega \, d\omega - \frac{dn}{2n} \sin \phi (1 + \cos 2\omega) = 0.$$

$\bar{\sigma}$ is now eliminated between these two equations and, after transformation, the following differential equation is obtained.

$$\frac{d\omega}{dn} = \frac{1}{2} \frac{\sin 2\omega}{\cos 2\omega - \sin \phi} \left(\frac{1 - \sin \phi \cos 2\omega}{n - 1} - \frac{1 + \sin \phi}{2n} \right). \qquad (150)$$

The solution of this equation produces a family of curves $\omega = \omega(n)$ Fig. 75, passing through the point $(n - 1, \omega = 0)$. Two types of solutions are distinguished: (a) bounded fields. The bound of the plastic field is provided by an envelope of the second family of characteristics. The envelope occurs for $\omega = \pi/4 - \phi/2$, and along it $d\omega/dn \to \infty$. (b) Unbounded fields, for which the term within brackets, and with it $d\omega/dn$, change sign for ω less than $\pi/4 - \phi/2$. The physical field extends without bound as n increases.

Since the plastic field is independent of the vertical coordinate, a field (b), unbounded in the horizontal direction, is unbounded in all directions. Such a field does not represent a real situation and, hence, only the bounded fields (a) are accepted as solution to piping. The question is now posed: What is the smallest diameter D at which incipient

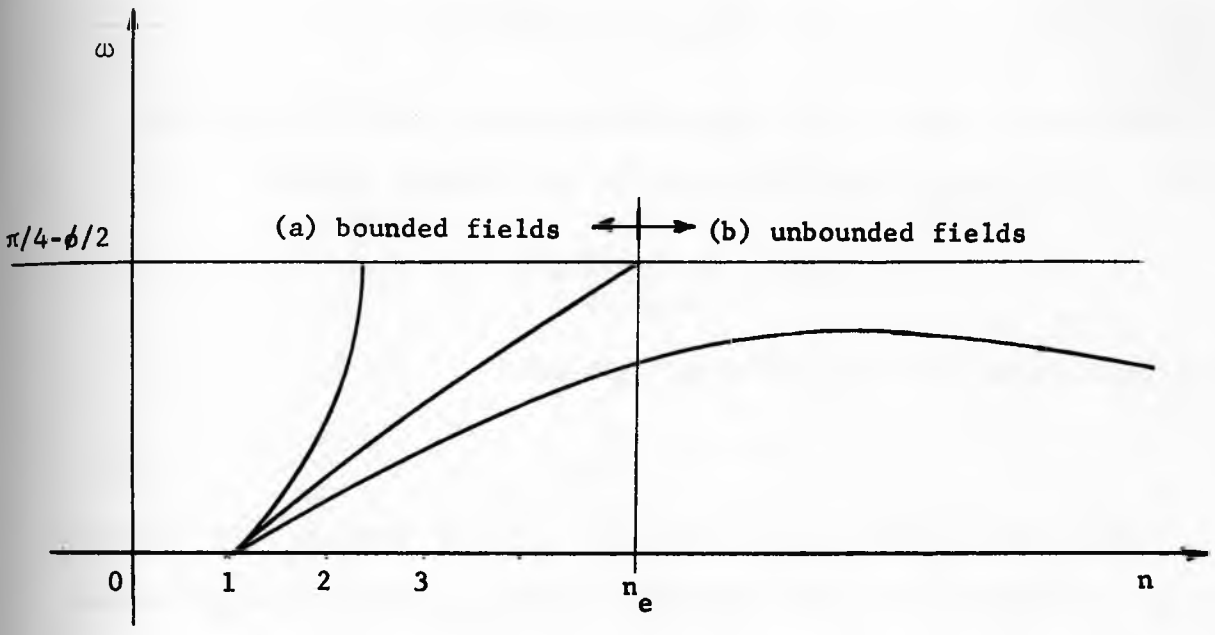

Fig. 75

Function $\omega = \omega(n)$

failure will occur in a bounded field? To answer this question $(d\omega/dn)_{n=1}$ is taken as the parameter of the family $\omega = \omega(n)$, and a relation is found between this parameter and the diameter D. Eq.(h) is integrated

$$\tau_{xy} = \gamma D \frac{n - 1}{4n^{\frac{1}{2}}}.$$

Expression (31) is substituted for τ_{xy}, leading to

$$D = \frac{4n^{\frac{1}{2}} \bar{\sigma} \sin \phi \sin 2\omega}{\gamma(n - 1)},$$

In the limit as $n \to 1$, $\omega \to 0$, $\bar{\sigma}_2 \to 0$, $\bar{\sigma}_1 \to f_c$ and, in accordance with eq. (38), $2\bar{\sigma} \sin \phi \to f_c$. The expression for the diameter becomes

$$D = 2 \frac{f_c}{\gamma} \lim_{n \to 1} \frac{\sin 2\omega}{n - 1}.$$

The application of 1'Hospital's rule yields

$$D = 4 \frac{f_c}{\gamma} \left(\frac{d\omega}{dn}\right)_{n=1}. \tag{151}$$

It is now evident that the required smallest diameter D is determined by the smallest value of the parameter $(d\omega/dn)_{n=1}$ which causes a bounded field. The corresponding curve $\omega = \omega(n)$ is shown in Fig. 75. The curve intersects the line $\omega = \pi/4 - \phi/2$ for a value of $n = n_e$, hence, the outer diameter of the plastic field is $Dn_e^{\frac{1}{2}}$.

The ratio n_e is obtained directly by placing $\omega = \pi/4 - \phi/2$ in the expression within brackets of eq. (150), and equating the expression to zero,

$$n_e^{\frac{1}{2}} = (2 \sin \phi - 1)^{-\frac{1}{2}}. \tag{152}$$

This relation is plotted in Fig. 76; n_e increases rapidly as ϕ decreases

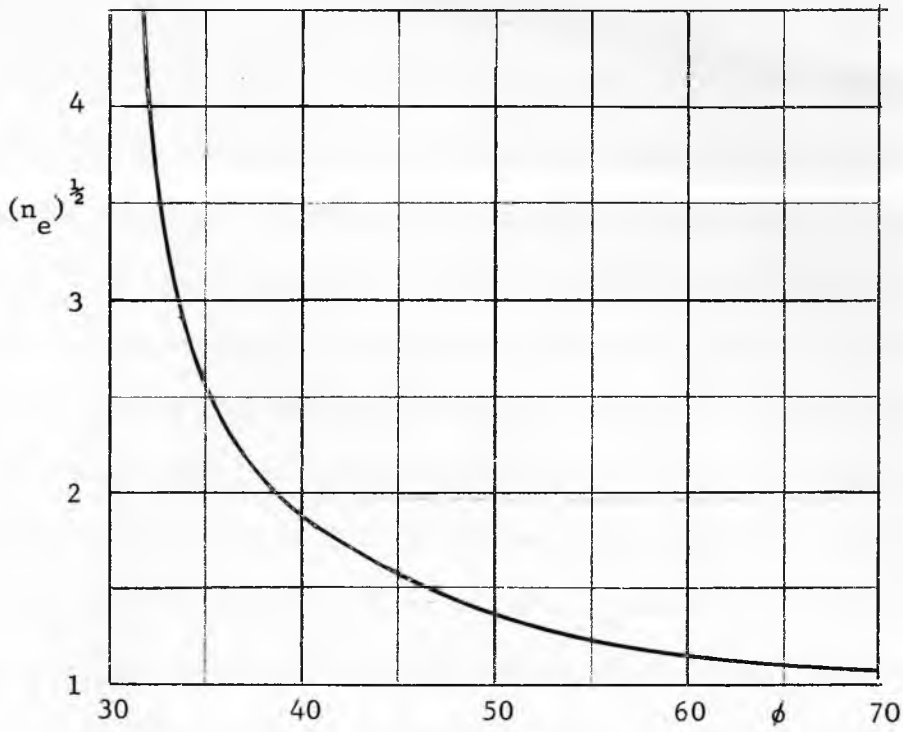

Fig. 76

Function $n_e^{\frac{1}{2}} = f(\delta)$

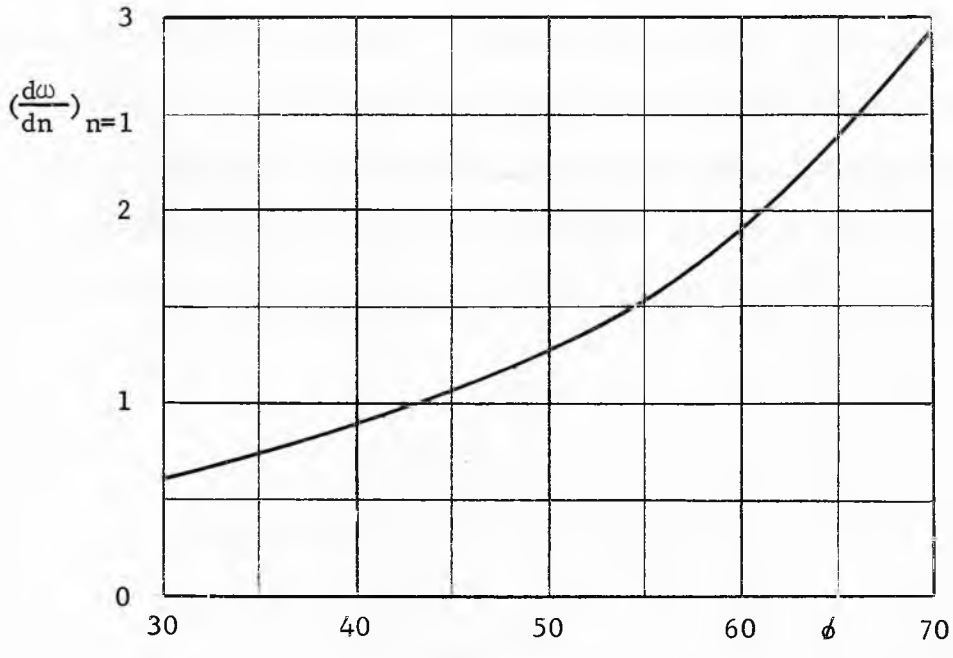

Fig. 77

Function $(d\omega\ dn)_{n=1} = g(\delta)$

toward 30°. For $\phi = 30°$, $n_e = \infty$.

Solids whose angle ϕ approaches the low value of 30° also have low values of f_c and stable piping is not observed in these solids. Hence, the analysis loses its practical value as that value of ϕ is approached. However, it is of interest to note that, for values of $\phi > 19.5°$ ($\sin \phi = 1/3$), both types of fields, (a) and (b), exist. For $\phi < 19.5°$, only type (a) remains, because the expression within brackets of eq. (150) does not change sign and $d\omega/dn$ is positive for all values of $n > 1$.

Values of $(d\omega/dn)_{n=1}$ for the smallest diameter D at which incipient failure must occur in a bounded field have been computed numerically and are plotted in Fig. 77. The diameter D is then obtained for any material of known ratio f_c/γ from eq.(151).

It is interesting to note that investigations of slope stability in axial symmetry [22] lead to profiles which all converge to a vertical hole, Fig. 78. Within the accuracy of numerical calculations, the diameter of that hole seems to be independent of the starting diameter at the surface and seems to equal D, the diameter computed above for the smallest bounded field independent of the vertical coordinate.

An acceleration field for piping is given in reference [22].

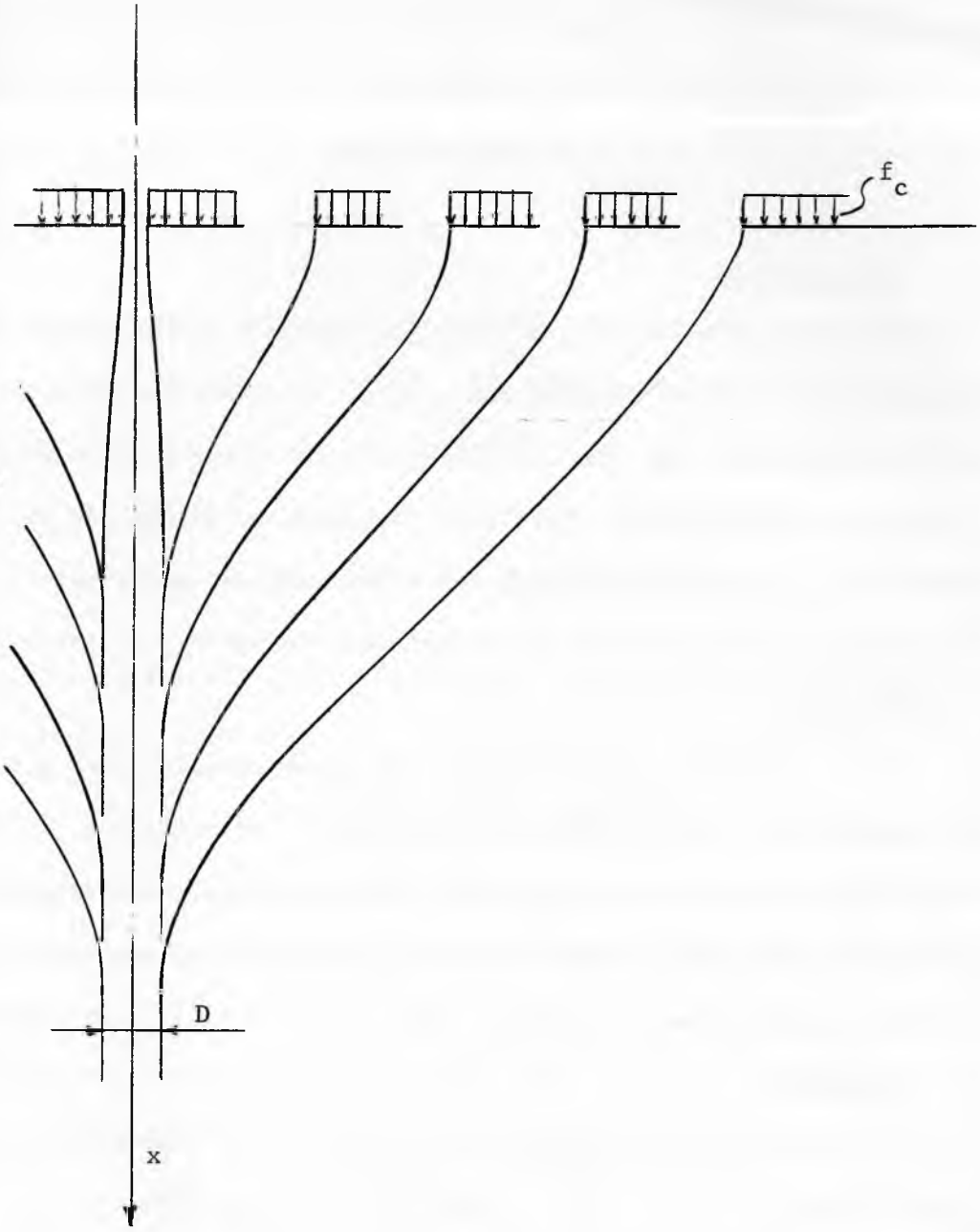

Fig. 78

Slope stability in axial symmetry

PART IV

FLOW CRITERIA

Introduction

The flow of a solid in a converging channel is subject to two typical obstructions: doming and piping. The flow criteria are based on the assumption that the solid consolidates under the pressures prevailing during steady state flow, develops an unconfined yield pressure f_c, in accordance with its flow-function, and flows if the unconfined yield pressure is insufficient to support a stable dome or a stable pipe.

Thus, the flow criteria relate the major consolidating pressure of steady state flow σ_1 with the pressures f_c of incipient failure, defining minimum ratios $\sigma_1/f_c = ff$, called critical flow-factors, which the solid must exceed for flow to start and to continue.

No-doming

Doming usually originates at the outlet of a channel where a radial stress field is closely approached during flow, and that field is assumed in the derivation of the flow criteria. The dome formulas (147) and (148) contain the unconfined yield pressure f_c at the abutments of the dome, i.e. at the end points of the walls. The major consolidating pressure σ_1 is given by eq.(20). With substitution (102) for σ in radial flow, the major pressure at a wall is

$$\sigma_1' = r\,\gamma\,s(\theta')(1 + \sin\delta).$$

σ_1' is eliminated by means of the flowfactor ff, eq.(41) thus

$$ff = r\,\frac{\gamma}{f_c}\,s(\theta')(1 + \sin\delta). \qquad (a)$$

Plane and axial symmetry. A channel, Fig. 79 (a), is symmetric for the purpose of this analysis if its walls are symmetric with respect to the vertical axis in the neighborhood of the vertex, hence, $-\theta'' = \theta'$, Then, from the figure, $r = B/2 \sin\theta'$ and eq.(a) becomes

$$ff = \frac{B\,\gamma}{f_c}\,\frac{s(\theta')(1 + \sin\delta)}{2\sin\theta'}.$$

Substitution for $B\,\gamma/f_c$ from the eq.(147) produces the following value of the critical flowfactor

$$ff = \frac{1 + m}{2}\,\frac{s(\theta')(1 + \sin\delta)}{\sin\theta'} \qquad (153)$$

This is the no-doming formula for symmetric channels.

For the particular case of vertical chanels, $\theta' = \theta'' = 0$, an expression for the flowfactor is obtained in a closed form by substituting expression (126) for σ in eq.(20), thus

$$\sigma_1 = \frac{\gamma\,y\,(1 + \sin\delta)}{(1 + m)\,\sin\delta\,\sin 2\omega}. \qquad (b)$$

σ_1 is eliminated by means of eq.(41) and, since at a wall $y = y' = -B/2$, the expression for the flowfactor becomes

$$ff = \frac{B\,\gamma}{f_c}\,\frac{1 + \sin\delta}{2(1 + m)\,\sin\delta\,\sin(2\omega' - \pi)}.$$

Substitution for $B\gamma/f_c$ from the eq.(147) yields

$$ff = \frac{1 + \sin \delta}{2 \sin \delta \sin (2\omega' - \pi)}. \qquad (154)$$

Plane asymmetry. This channel, Fig. 79(b), has one wall sloping at an angle θ' and the other wall vertical, $\theta'' = 0$. Here the conditions at each wall are different, and are considered separately. At the sloping wall $r' = B \sin \theta'$ and eq.(a) becomes

$$ff' = \frac{B \gamma s(\theta')(1 + \sin \delta)}{f_c' \sin \theta'}.$$

Substitution for $\gamma f_c'$ from the first of equations (148) yields

$$ff' = - \frac{B}{B-a} \frac{\sin 2\omega'}{2} \frac{s(\theta')(1 + \sin \delta)}{\sin \theta'}. \qquad (c)$$

At the vertical wall $r^v = B \cot \theta' + b - c$, eq.(a) becomes

$$ff^v = \frac{(B \cot \theta' + b - c) \gamma s(\theta^v)(1 + \sin \delta)}{f_c^v},$$

and substitution for γf_c^v from the second of equations (148) produces

$$ff^v = \frac{B \cot \theta' + b - c}{a} \frac{\sin 2\omega^v}{2} s(\theta^v)(1 + \sin \delta). \qquad (d)$$

From equilibrium it follows that the assumed dome has the shape of the parabola

$$x = \frac{b(a + y)^2}{(B - a)^2}. \qquad (e)$$

The parameters a, b, c and the functions $\sin 2\omega'$ and $\sin 2\omega^v$ in equation (c) and (d) are now replaced by $\tan \omega'$ and $\tan \omega^v$, leading to

$$ff' = \frac{\tan \omega^v - \tan \omega'}{\tan \omega^v} \frac{- \tan \omega'}{1 + \tan^2 \omega'} \frac{s(\theta')(1 + \sin \delta)}{\sin \theta'}, \qquad (155)$$

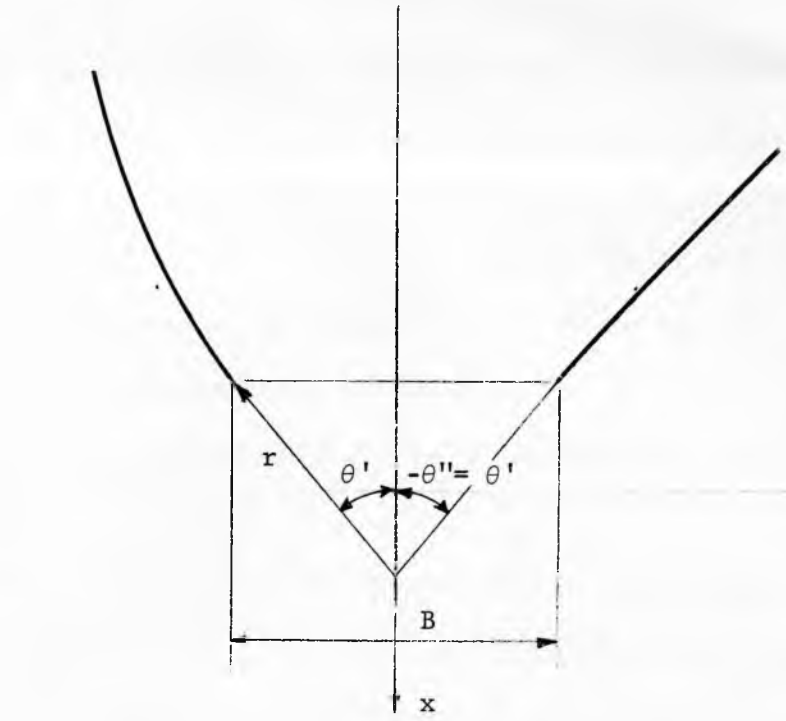

(a)

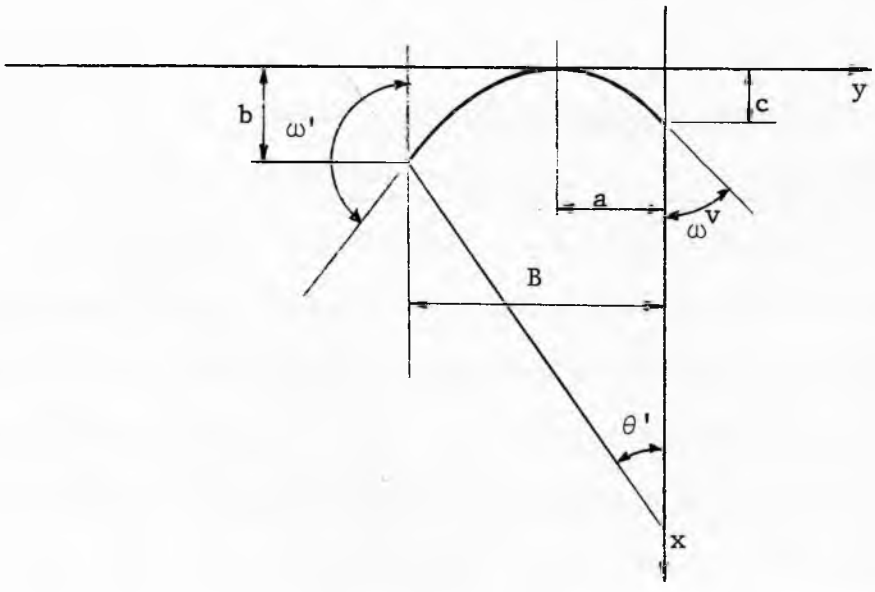

(b)

Fig. 79

Outlet conditions for no doming

$$ff^v = \frac{(\tan \omega' - \tan \omega^v)(2 \cot \theta' \tan \omega' \tan \omega^v - \tan \omega^v - \tan \omega')}{2 \tan^2 \omega'(1 + \tan^2 \omega^v)} x$$

$$x\, s(\theta^v)(1 + \sin \delta). \qquad (156)$$

The acceptable range for angle ω' is $3\pi/4 < \omega' < \pi$. Within this range $\partial ff^v/\partial \omega' > 0$, while $\partial ff'/\partial \omega' < 0$, and there is one value of ω' for which $ff^v = ff' = ff$. This value of the flowfactor is maximized with respect to ω^v, yielding the critical flowfactor.

Flowfactor plots. Contours of constant values of the critical flowfactors are plotted for $\delta = 30°$, $40°$, $50°$, $60°$ and $70°$ for plane symmetry in Figures 80 to 84, and for axial symmetry in Figures 85 to 89. For plane asymmetry, the flowfactor is plotted in Figures 90 to 92 for $\delta = 50°$ and for an angle of friction at the vertical wall $\phi^v = 20°$, $30°$, and $40°$.

Influence of compressibility. Figures 93 and 94 show a comparison of the flowfactors for a compressible solid with $\beta = 0.10$, with those of an incompressible solid. The plots are for $\delta = 50°$. Figure 93 shows symmetric plane strain, and Figure 94 axial symmetry. The continuous lines are for the compressible solid, and the dashed lines for the incompressible solid. The latter are copied from Figures 82 and 87.

It is evident that even the large degree of compressibility corresponding to $\beta = 0.10$ does not appreciably affect the no-doming criterium. Hence, the compressibility of the solids may be neglected.

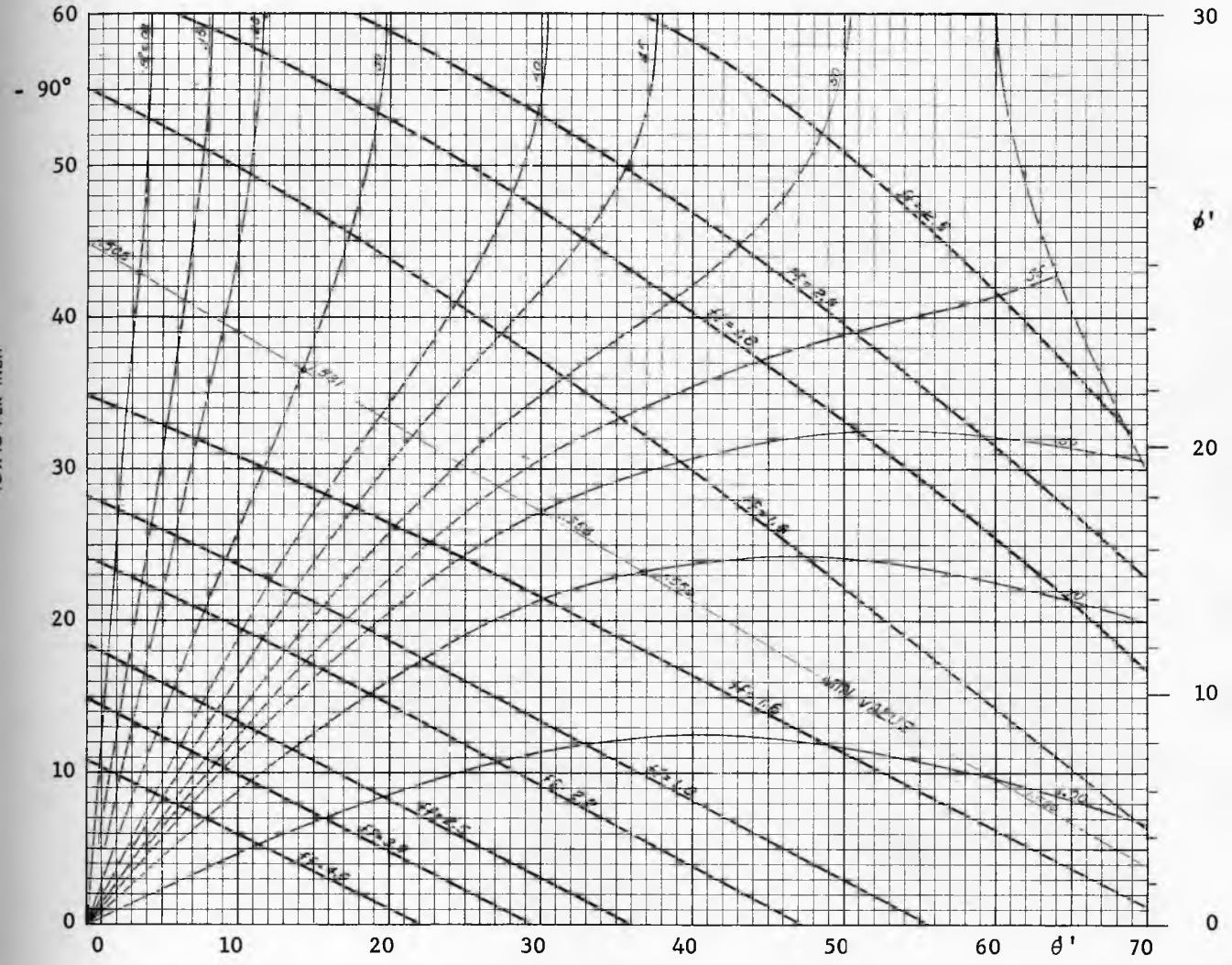

Fig. 80

Critical flowfactor ff, $\delta = 30°$

Plane symmetry (symmetric plane flow)

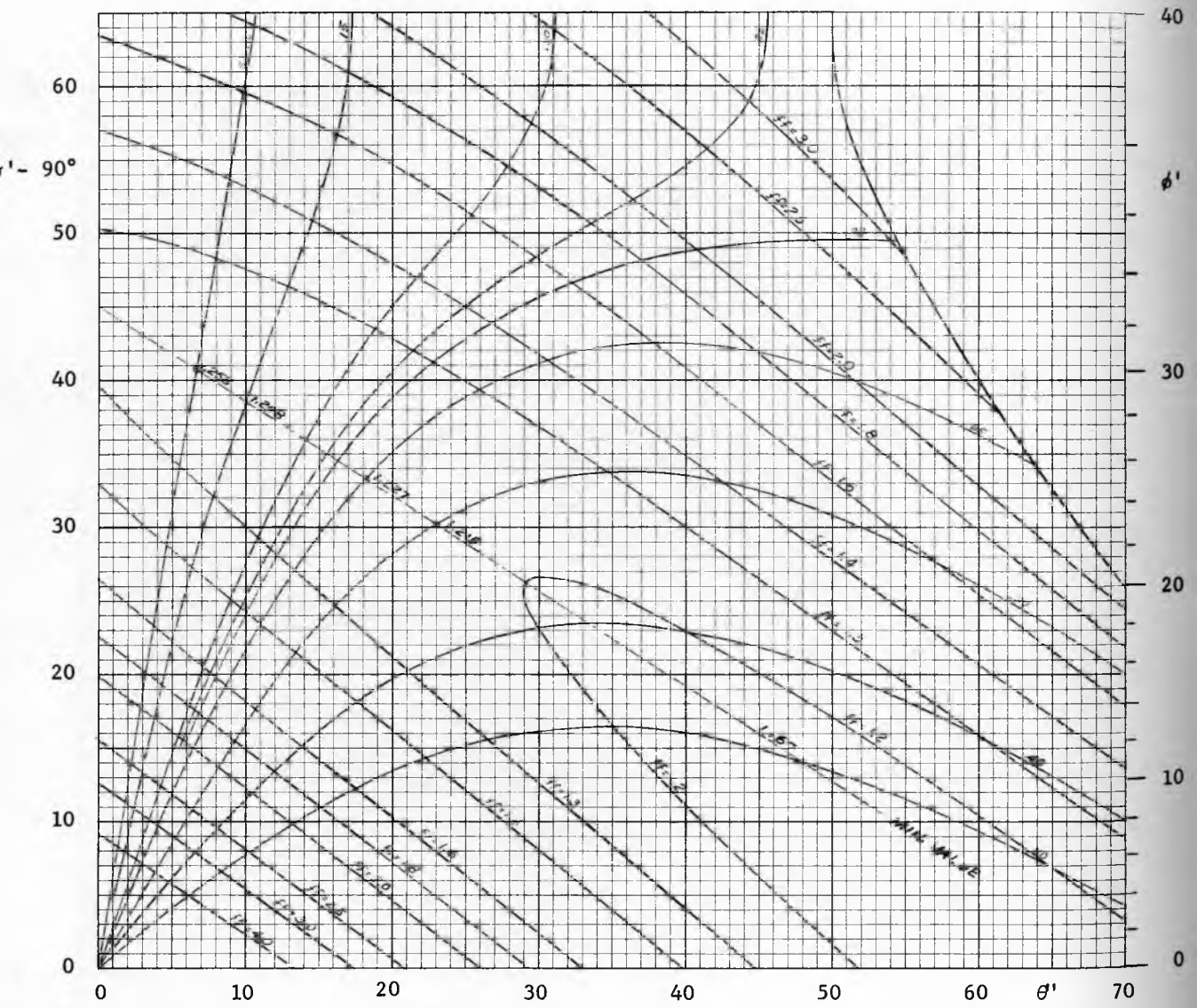

Fig. 81

Critical flowfactor ff, $\delta = 40°$

Plane symmetry (symmetric plane flow)

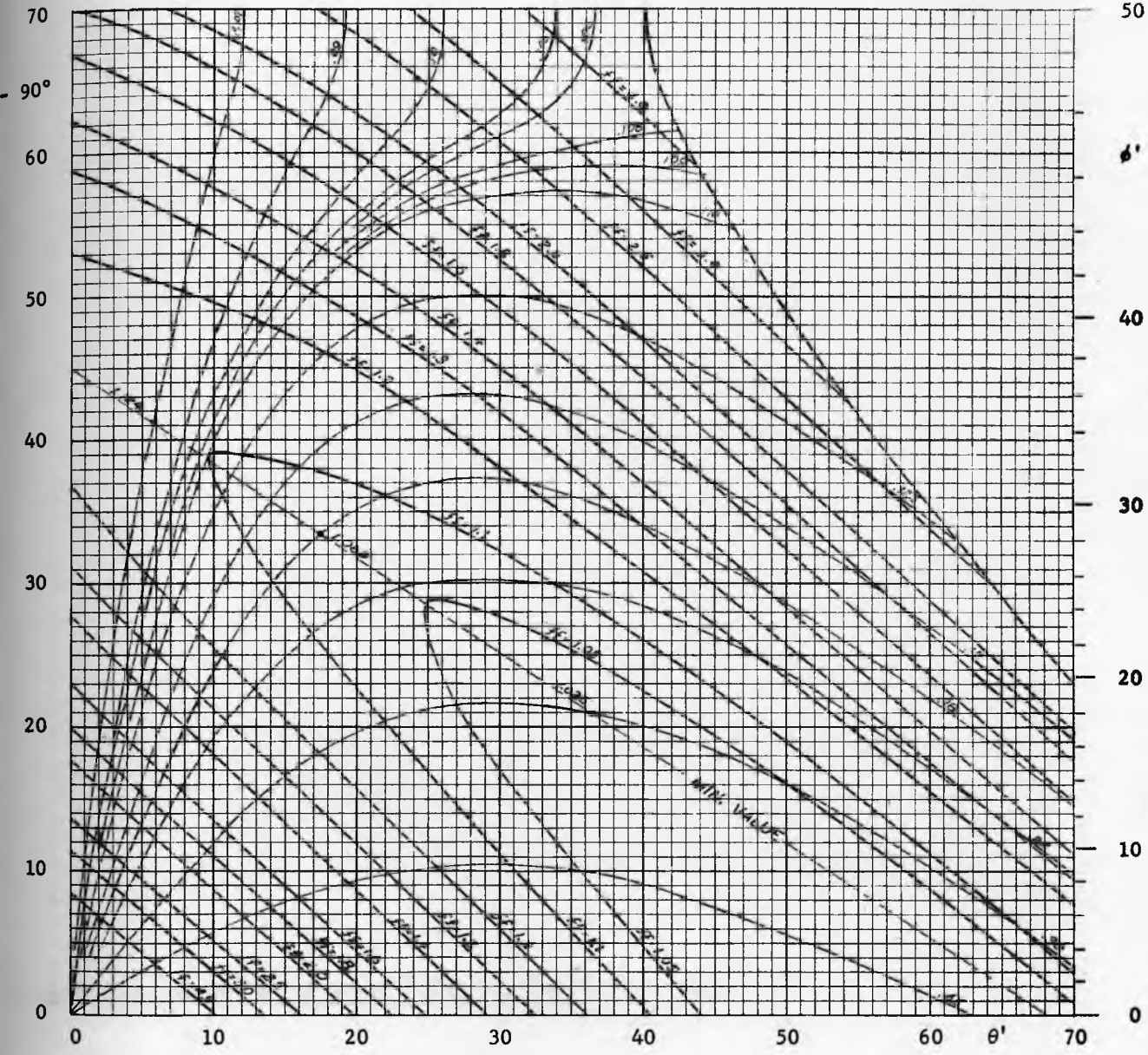

Fig. 82

Critical flowfactor ff, $\delta = 50°$

Plane symmetry (symmetric plane flow)

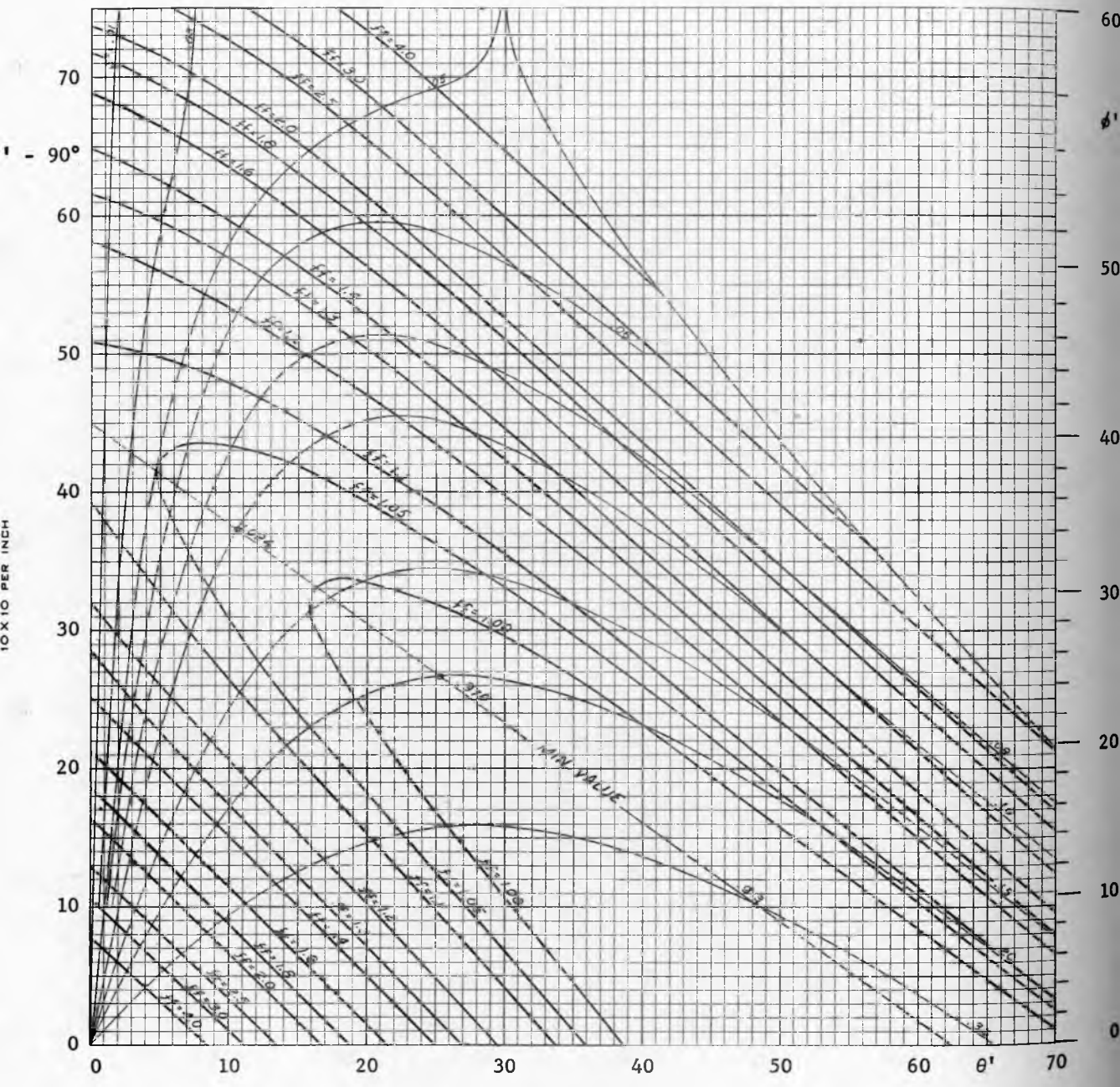

Fig. 83

Critical flowfactor ff, $\delta = 60°$

Plane symmetry (symmetric plane flow)

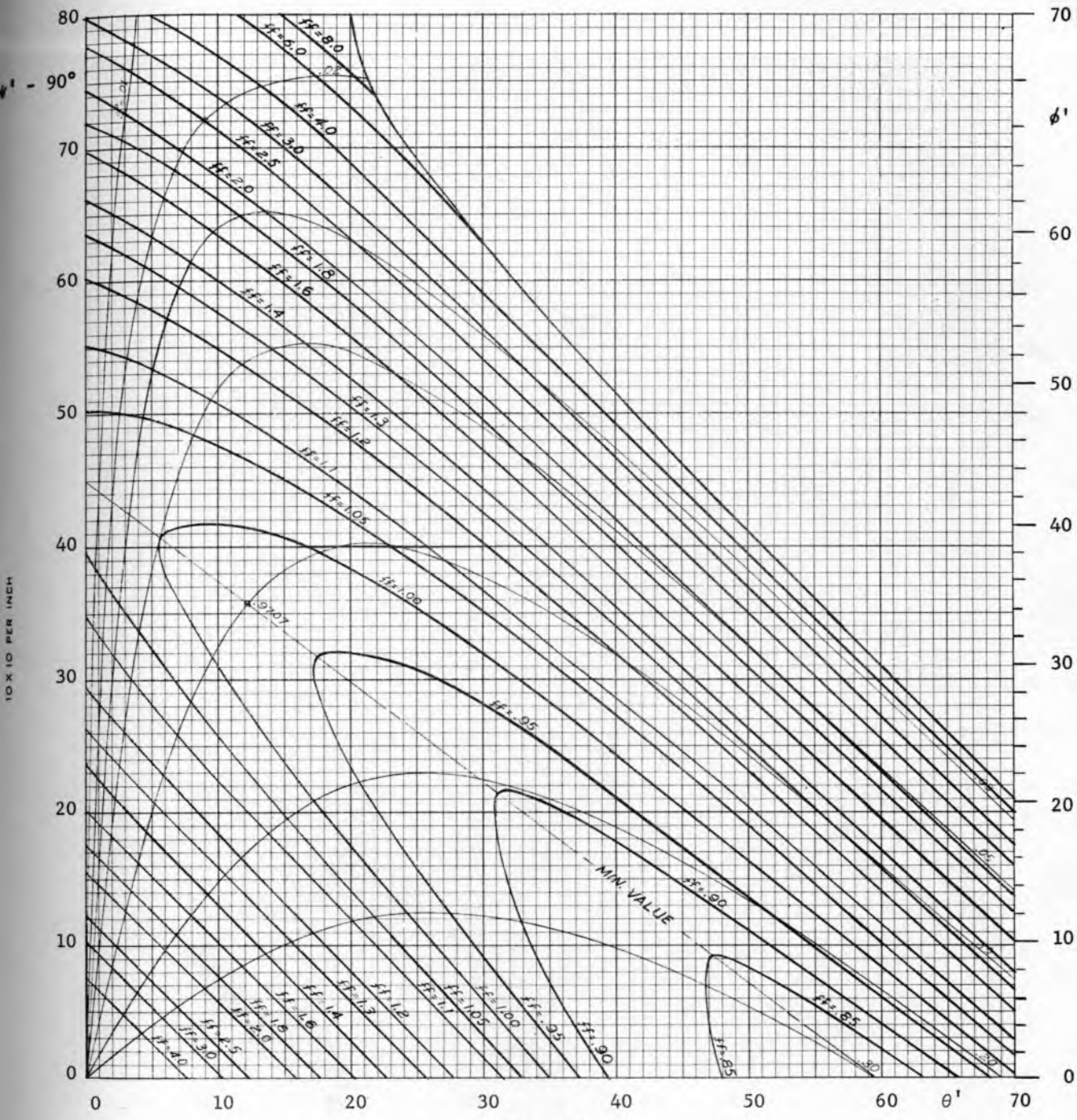

Fig. 84

Critical flowfactor ff, $\delta = 70°$

Plane symmetry (symmetric plane flow)

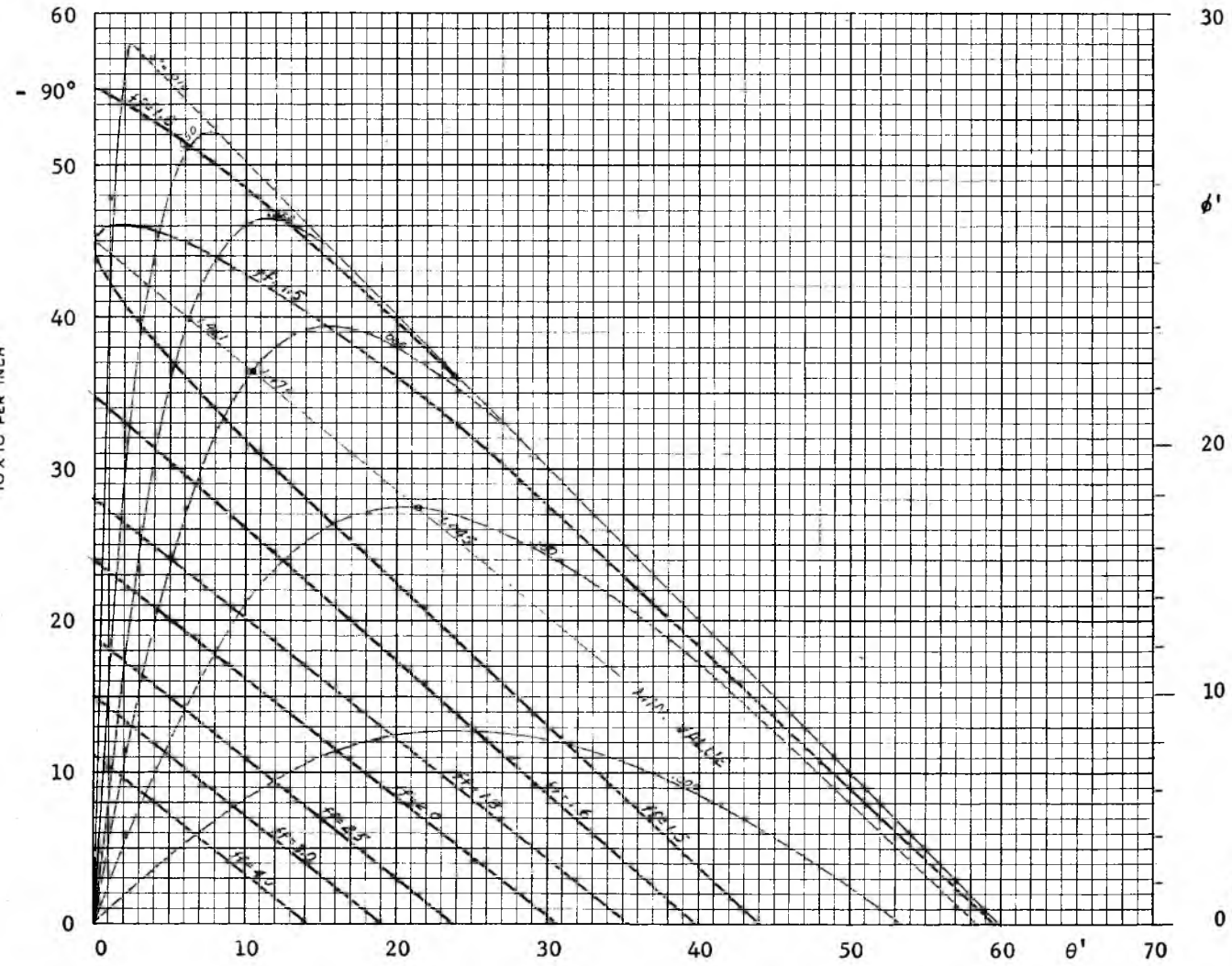

Fig. 85

Critical flowfactor ff, $\delta = 30°$

Axial symmetry (conical flow)

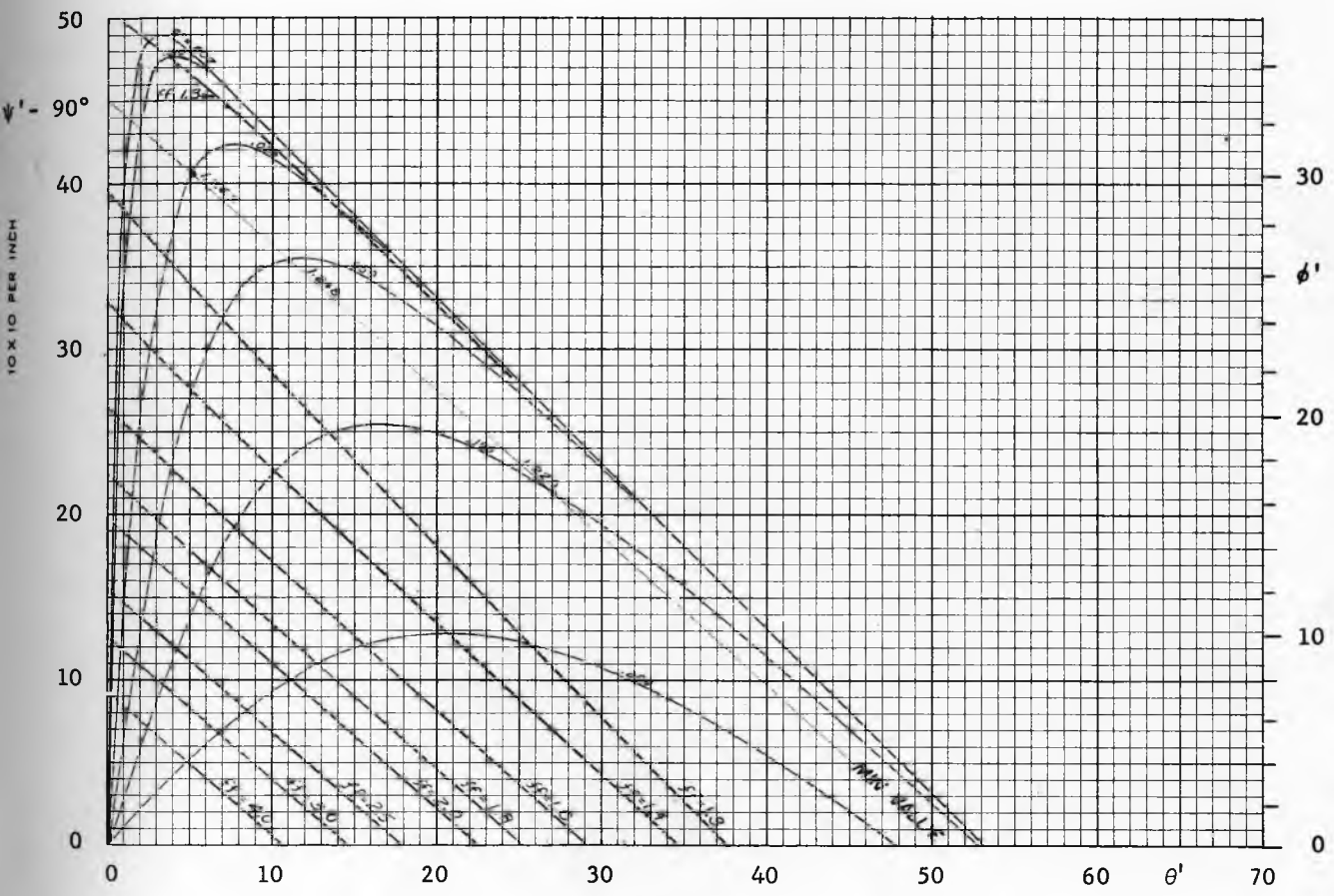

Fig. 86

Critical flowfactor ff, $\delta = 40°$

Axial symmetry (conical flow)

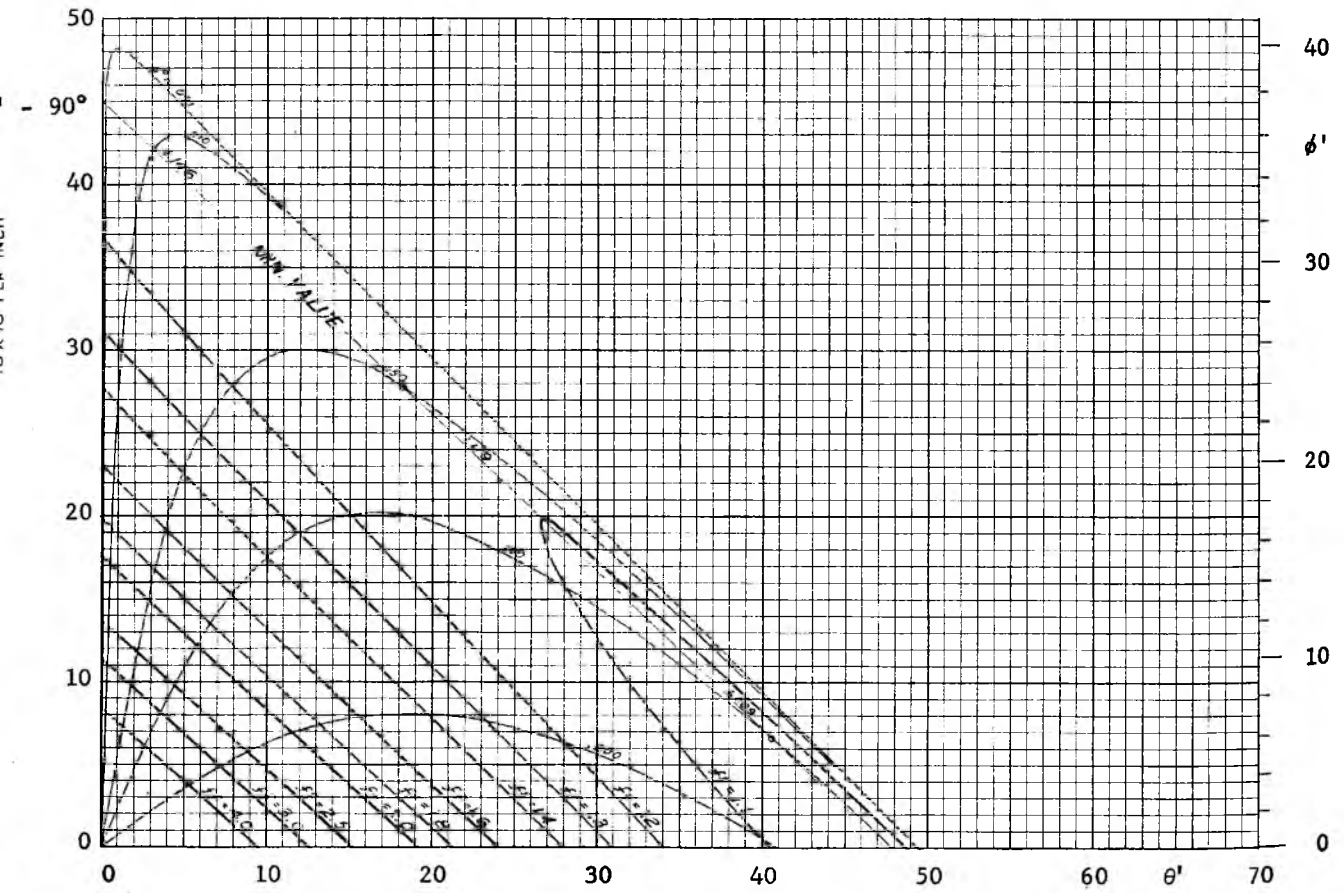

Fig. 87

Critical flowfactor ff, $\delta = 50°$

Axial symmetry (conical flow)

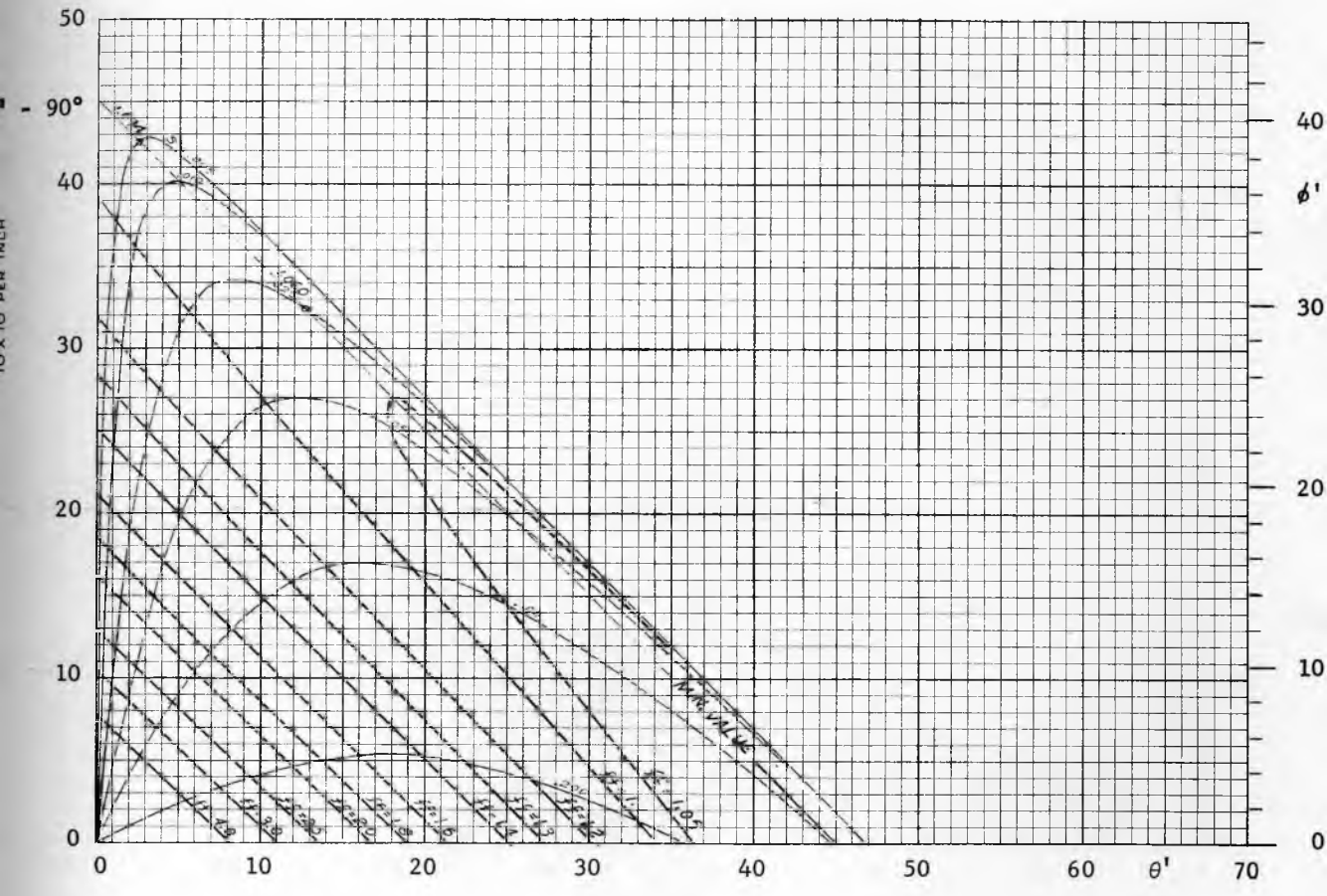

Fig. 88

Critical flowfactor ff, $\delta = 60°$

Axial symmetry (conical flow)

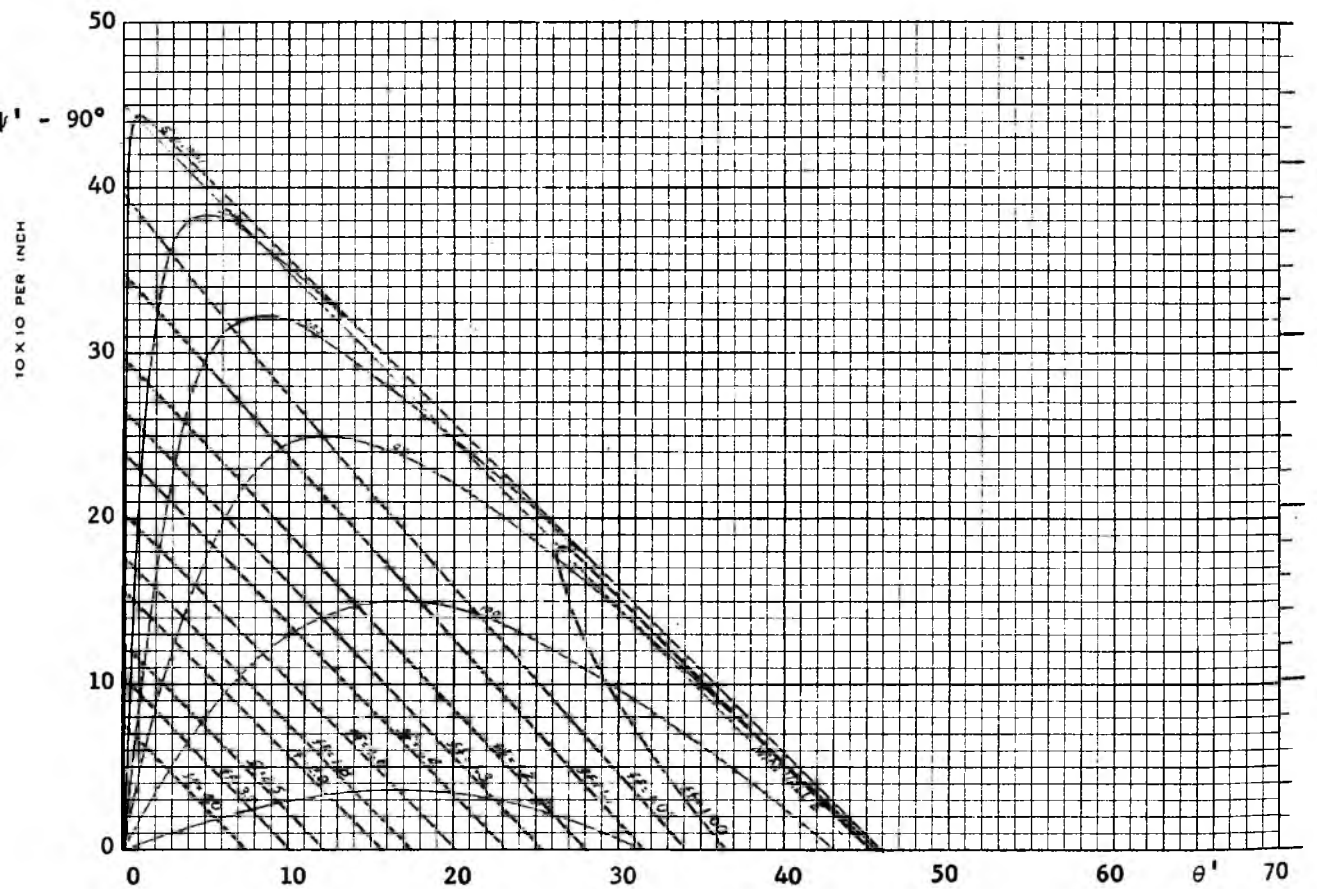

Fig. 89

Critical flowfactor ff, $\delta = 70°$

Axial symmetry (conical flow)

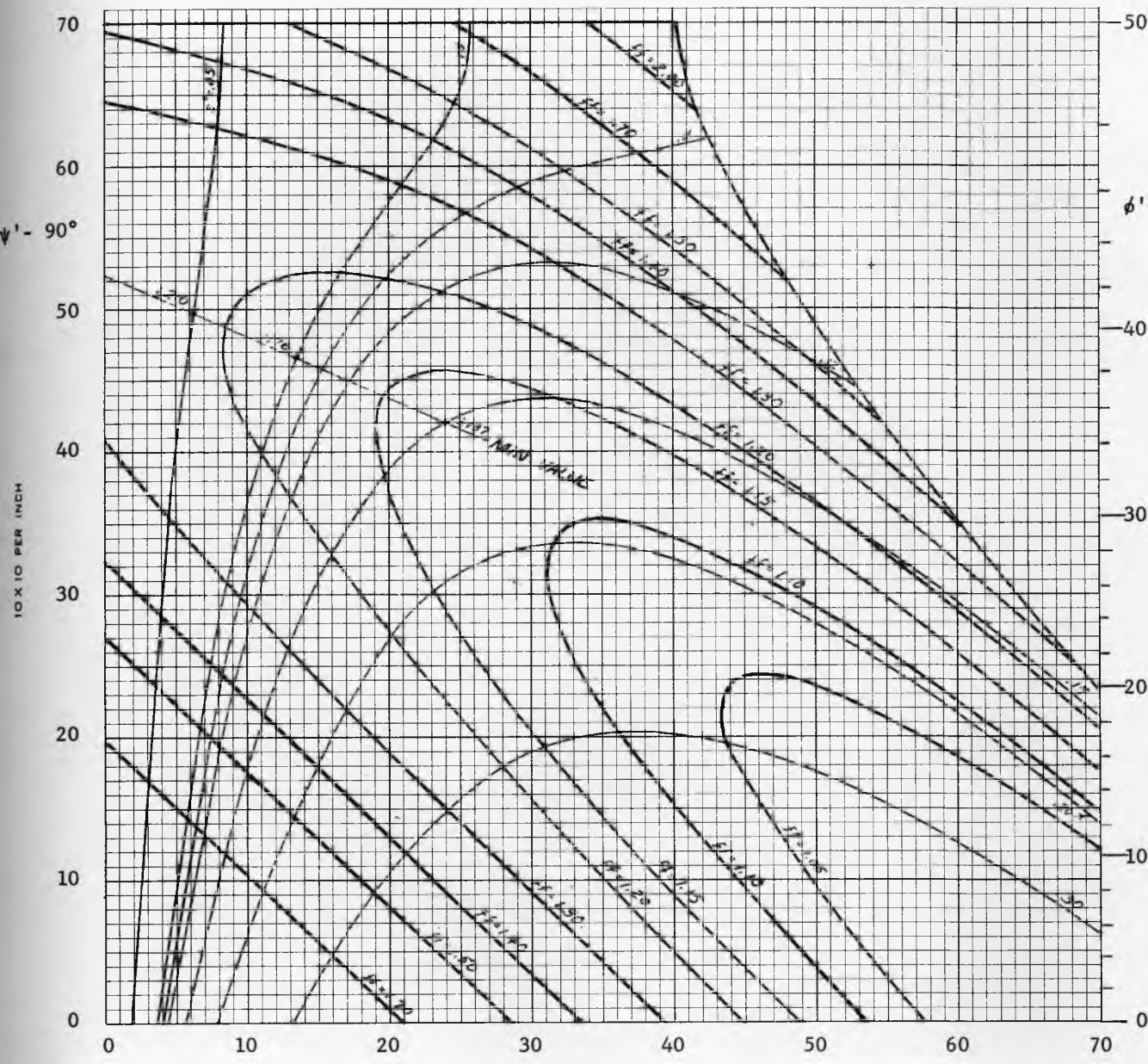

Fig. 90

Critical flowfactor ff, $\delta = 50°$, $\phi^V = 20°$

Plane asymmetry (plane flow-one vertical wall)

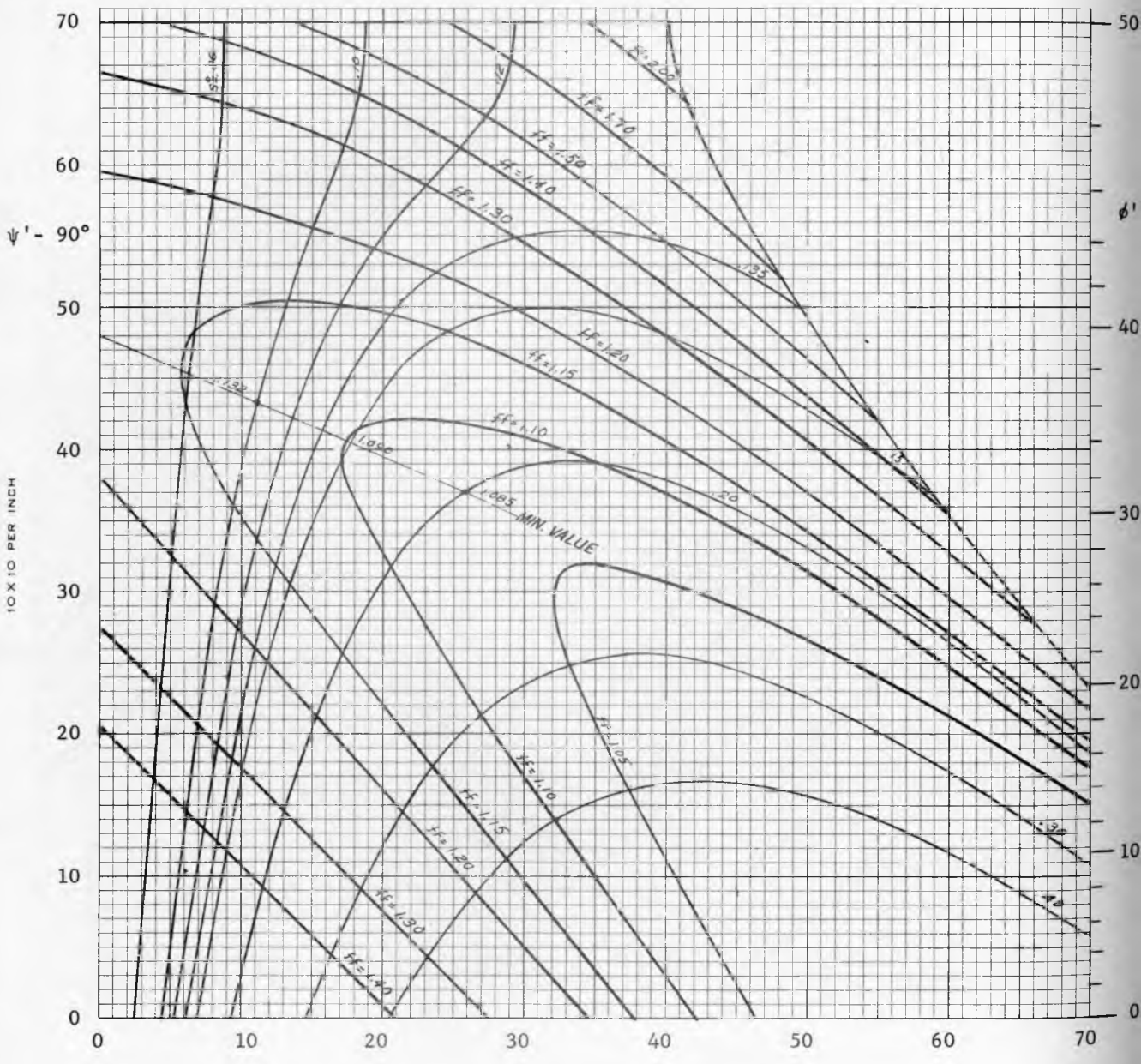

Fig. 91

Critical flowfactor ff, $\delta = 50°$, $\phi^V = 30°$

Plane asymmetry (plane flow-one vertical wall)

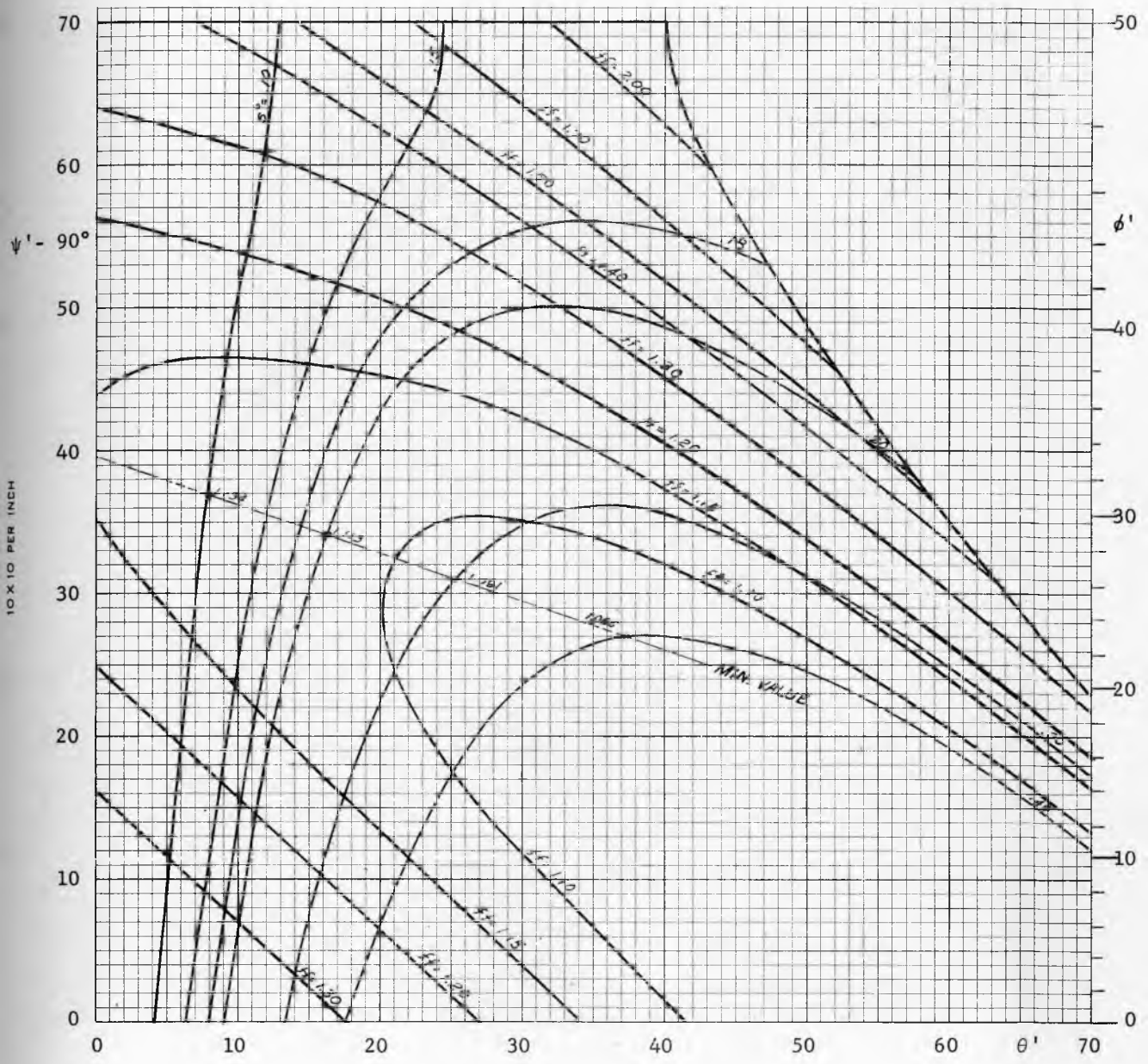

Fig. 92

Critical flowfactor ff, $\delta = 50°$, $\phi^v = 40°$

Plane asymmetry (plane flow-one vertical wall)

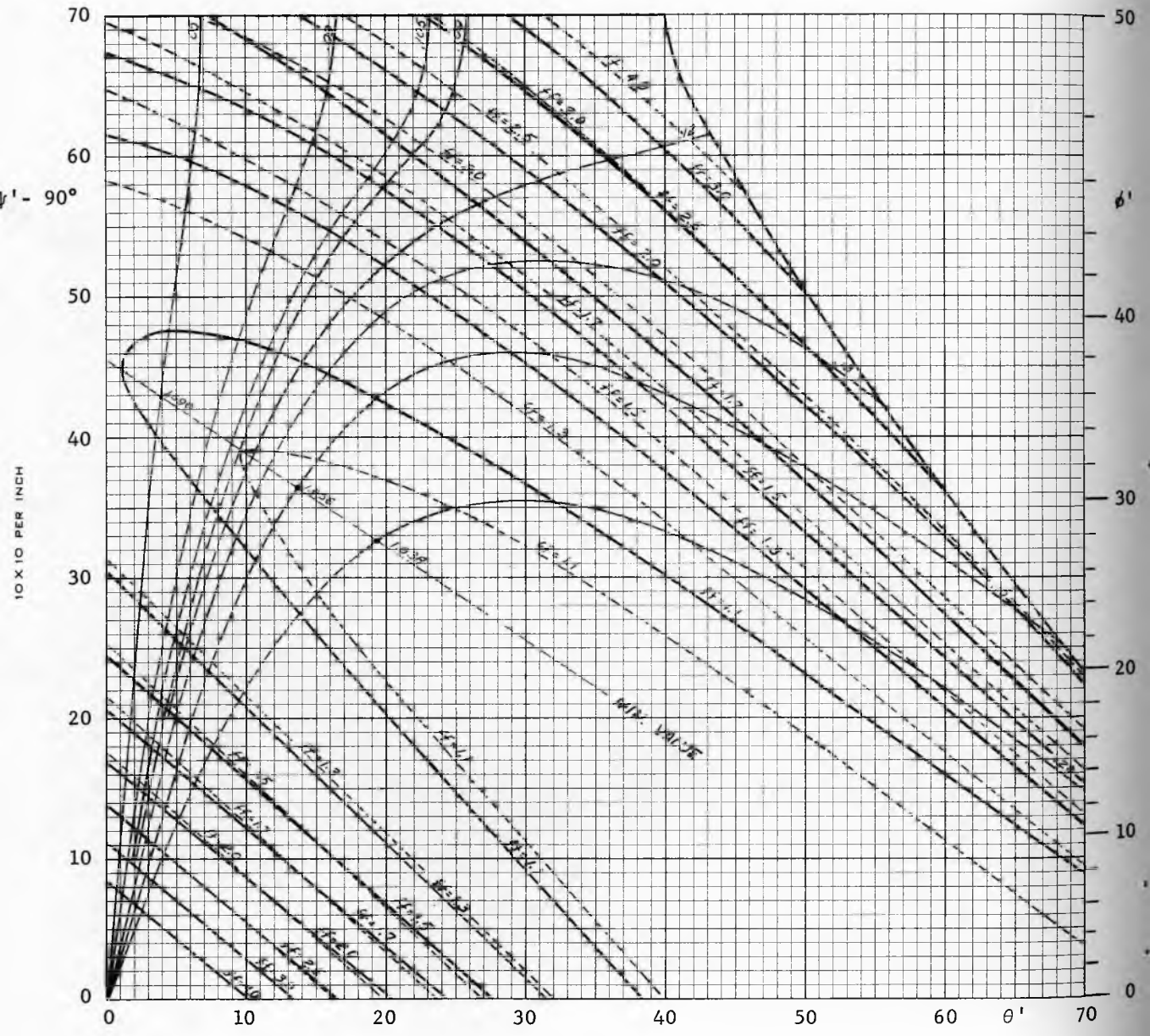

Fig. 93

Critical flowfactor ff, $\delta = 50°$, $\beta = 0.10$

Plane symmetry (symmetric plane flow)

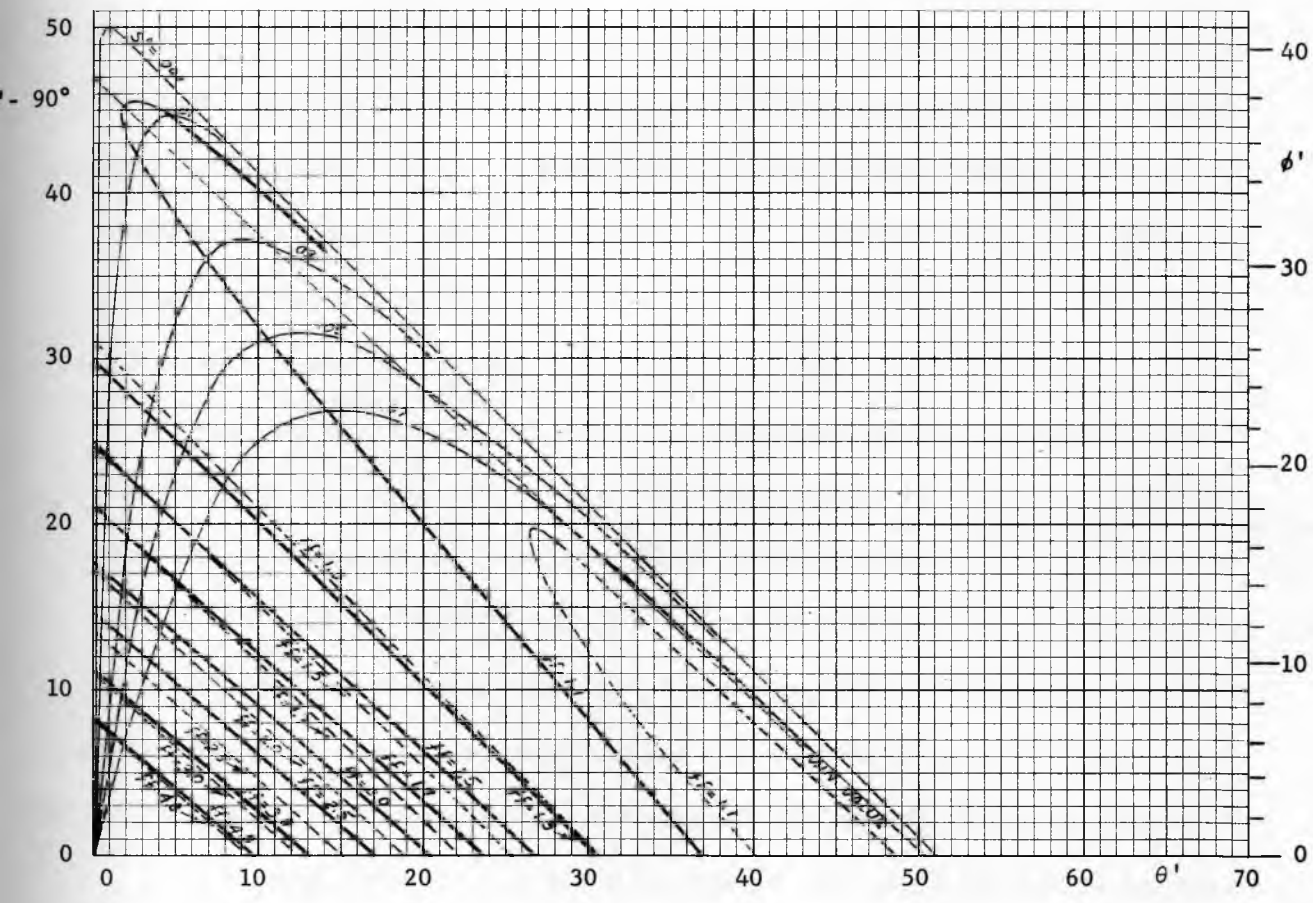

Fig. 94

Critical flowfactor ff, $\delta = 50°$, $\beta = 0.10$

Axial symmetry (conical flow)

No-piping

A tendency for piping exists in all channels in which the solid flows within rough walls. It was shown in the analysis of axi-symmetric radial stress fields that such channels are very steep or, indeed, vertical. It is observed in experiments that these channels circumscribe the outlet and, hence, that the largest dimension of the outlet defines the diameter of the channel.

In the derivation of the formula for no-piping it is assumed that the values of the unconfined yield pressure f_c, and of the angle of friction ϕ are constant throughout the plastic region, Fig. 74 (a). The values developed at the inner surface of the pipe are assumed to prevail throughout the region. These assumptions are reasonable, because the plastic region is quite thin (see ratio $n_e^{\frac{1}{2}}$, Fig. 76) for the solids with large angles of friction, i.e. for the solids which have the greatest tendency to pipe. In selecting the value of f_c it is necessary to use the time flow-function because, while the solid is flowing within the pipe, outside the pipe the solid is consolidating at rest. The angle of friction $\phi = \Phi_t$, which exists at a traction-free, inner surface, is measured at the point of tangency of the time yield locus with the f_c circle, Fig. 95.

The unconfined yield pressure f_c at the inner surface of the pipe is assumed to be generated by the major pressure σ''_1 due to steady state flow in a vertical channel of diameter D. This pressure is given by eq.(20) with substitution (126) for σ, and with $y = D/2$, $\omega = \omega''$, thus

$$\sigma''_1 = \frac{D\,\gamma(1 + \sin\delta)}{4 \sin\delta \sin 2\omega''}. \qquad (f)$$

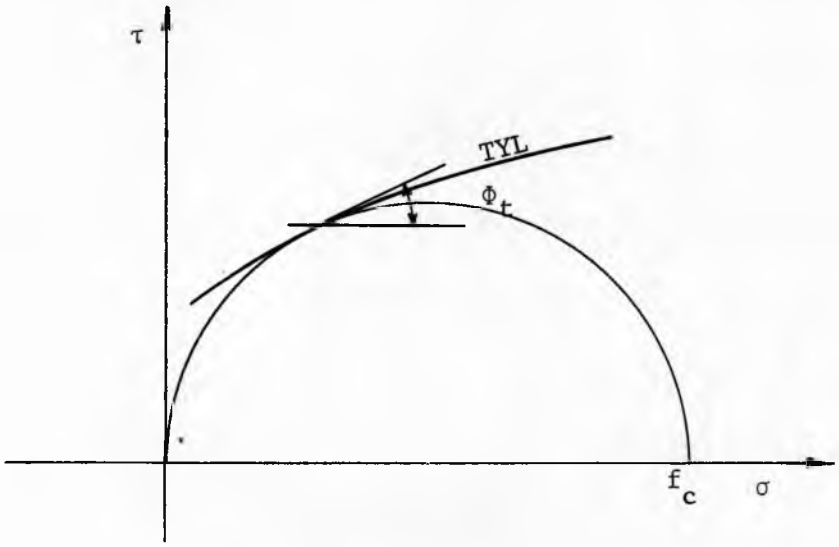

Fig. 95

Angle of friction Φ_t for no-piping

The value of ω'' in the above formula likely varies between $\pi/4$ and $\pi/4 - \phi/2$ If the axi-symmetric analysis for converging channels is adopted, then flow within rough walls requires $\psi'' = \pi/4$. Since θ'' is small, or zero, $\omega'' \approx \psi'' = \pi/4$. Further, it is likely that as the solid flows within the rough walls, the surface of the walls soon becomes smoother and a degree of weakness develops along them. This also would tend to shift ω'' toward the value of $\pi/4$. Hence, the latter value is assumed in the analysis, and the consolidating pressure, eq. (f), becomes

$$\sigma_1'' = \frac{D\,\gamma(1 + \sin\delta)}{4 \sin\delta} .$$

σ_1'' is now eliminated by means of the flowfactor ff, eq.(41) thus

$$ff = \frac{D\gamma}{4f_c} \frac{1 + \sin\delta}{\sin\delta} .$$

Elimination of $D\,\gamma/4f_c$ by means of eq. (151) yields the critical flowfactor for no-piping

$$ff = \frac{1 + \sin\delta}{\sin\delta} \left(\frac{d\omega}{dn}\right)_{n=1} . \qquad (157)$$

It will be noted that $(d\omega/dn)_{n=1}$, Fig. 77, is a function of the angle of friction $\phi = \Phi_t$. Hence ff in eq.(157) is a function of both angles, δ and Φ_t. Contours of constant values of ff are plotted in Fig. 96.

When the effect of time of consolidation is negligible, i.e. when the time flow-function is about the same as the instantaneous flow-function, then a relation between δ and ϕ exists in accordance with the linearized yield locus, Fig. 13, and the critical flowfactor can be

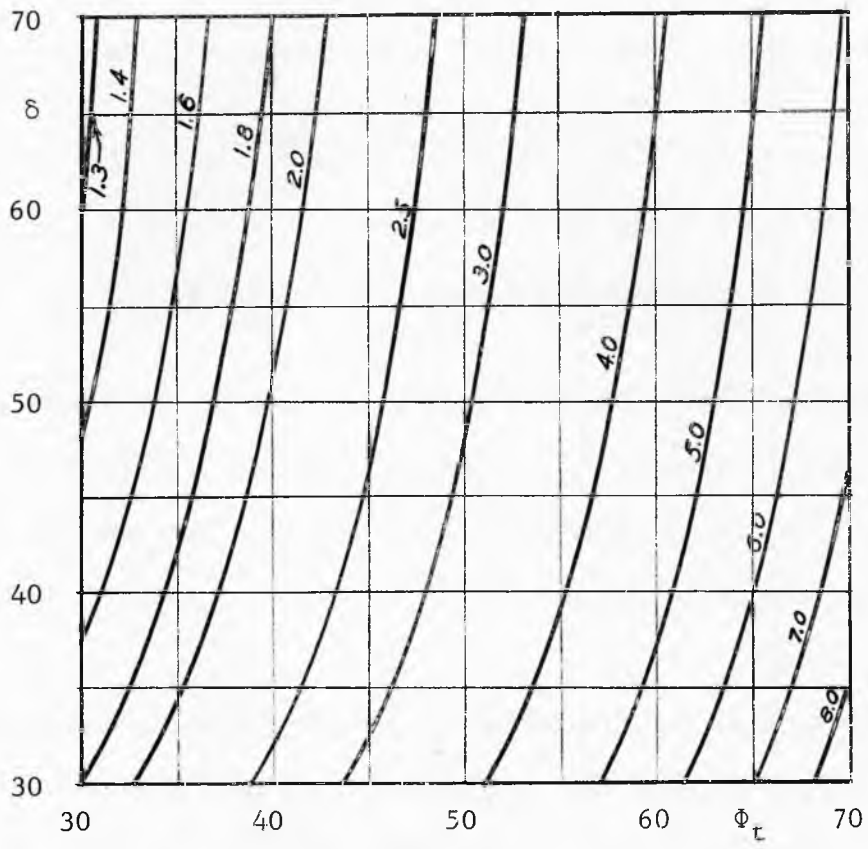

Fig. 96

Critical flowfactor for no-piping

computed as a function of angle δ only. In this case

$$\bar{\sigma}_1 = \sigma_1 \text{ and } \bar{\sigma} = \sigma + f_c(1 - \sin \phi)/2 \sin \phi.$$

From equation (20) and (35)

$$\sigma = \frac{\sigma_1}{1 + \sin \delta} \text{ and } \bar{\sigma} = \frac{\bar{\sigma}_1 + f_c(1 - \sin \phi)/2 \sin \phi}{1 + \sin \phi},$$

Elimination of σ and $\bar{\sigma}$ by means of the above equations, and of the ratio σ_1/f_c by means of the flowfactor ff, in accordance with eq.(41), yields

$$\sin \delta = \frac{2 \text{ ff } \sin \phi + 1 - \sin \phi}{2 \text{ ff} - 1 + \sin \phi}. \qquad (g)$$

Elimination of sin δ in eq.(157) produces

$$\text{ff} = \frac{1 + \sin \phi}{\sin \phi} \left(\frac{d\omega}{dn}\right)_{n=1} - \frac{1 - \sin \phi}{2 \sin \phi}.$$

ff is computed as a function of ϕ from this equation, then δ is computed as a function of ϕ from eq.(g). Angle ϕ is eliminated, yielding the function ff(δ) which is plotted in Fig. 97. It is noticed that piping does not occur in solids which are not affected by consolidation at rest, and whose $\delta < 54.5°$.

A comparison of the flowfactor values for no-doming and no-piping shows that piping is much more apt to occur and more difficult to avoid than doming. In fact, solids which gain a significant amount of strength with consolidation at rest invariably tend to pipe.

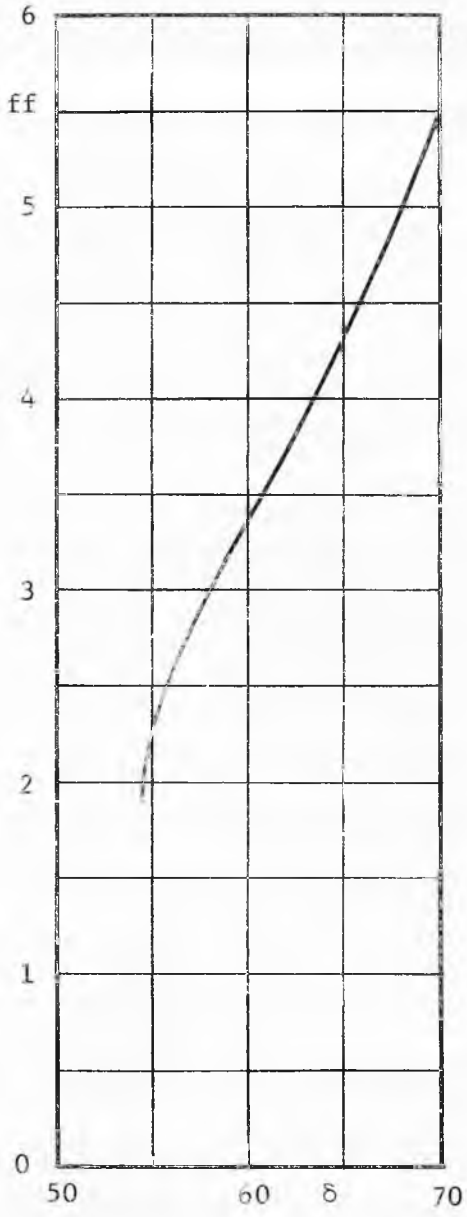

Fig. 97

Critical flowfactor for no-piping for

solids not affected by consolidation at rest

PART V

TESTING THE FLOW PROPERTIES OF BULK SOLIDS

Apparatus

The solids considered in this work include soils. Since the field of soil mechanics was well developed at the time when this study originated (1952), it was natural first to investigate the applicability of the soil mechanics testing apparatus to the measurement of the flow properties of bulk solids.

Standard direct shear apparatus and unconfined compression apparatus were tried. The results obtained with shear apparatus were not satisfactory, primarily, because the range of values of cohesion for which the soil test machines were designed was outside the useful range for bulk solids. By the terminology of soil mechanics, bulk solids can be considered cohesionless, and cohesive soils under their usual degree of consolidation would not flow by gravity in any storage system. Unconfined compression apparatus was found unsuitable because of the impossibility of applying a known, uniform consolidation, and because the stresses due to the weight of the sample were in the range of the measured yield stresses. These samples often disintegrated during handling. The application of a triaxial compression apparatus was considered and rejected as impractical because of the considerable time required to obtain results by this method. It was decided to develop a machine especially for testing bulk solids.

A direct shear test machine was designed and built in 1953. It has

since undergone many refinements; the type now in use in the USA and in England is shown in Fig. 98. It is equipped with a shear cell, a gravity vertical loading system, and an electric-pneumatic shearing force device. The shearing force device has a constant strain-rate of 0.036 in. per min. The shearing force necessary to maintain the strain-rate is continuously recorded on a pneumatic recorder. This arrangement produces a permanent record of the stress-strain relations for each test. A test cell is shown in Fig. 99. It is composed of a base located on the frame of the machine, a ring resting on top of the base, and a cover. The bottom of the cover and the inside of the base are roughened to increase adhesion of the tested solid. The base and the ring are filled with the tested solid. The vertical compressive force V is applied to the cover. The horizontal shearing force S is applied by means of a stem which acts on a bracket attached to the cover. The stem acts in the plane of contact between the ring and the base. A part of the shearing force is tranferred from the bracket to the ring through a loading pin. The difference between the inside diameter of the ring and the outside diameter of the cover is 0.04 in.

Shear cells are used in two sizes: 2.5 and 3.75 inches inside diameter. The smaller cell is used for heavy solids like ores, while the larger cell is preferred for light solids. The machine is capable of applying a vertical force up to 100 lb and a shearing force up to 60 lb.

The shear test machine is used in conjunction with a six cell consolidating bench in which the whole cells are placed for the time of consolidation at rest, Fig. 100.

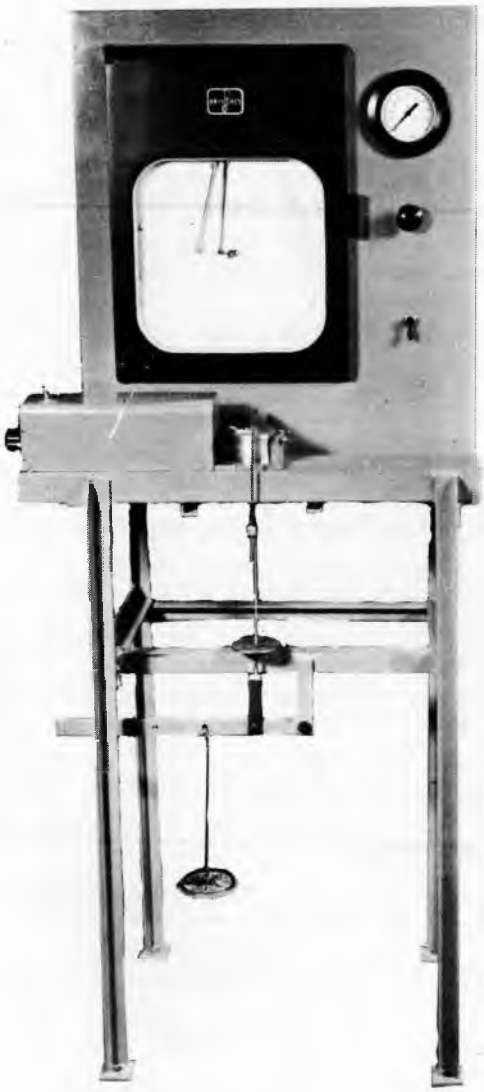

Fig. 98

Direct shear apparatus

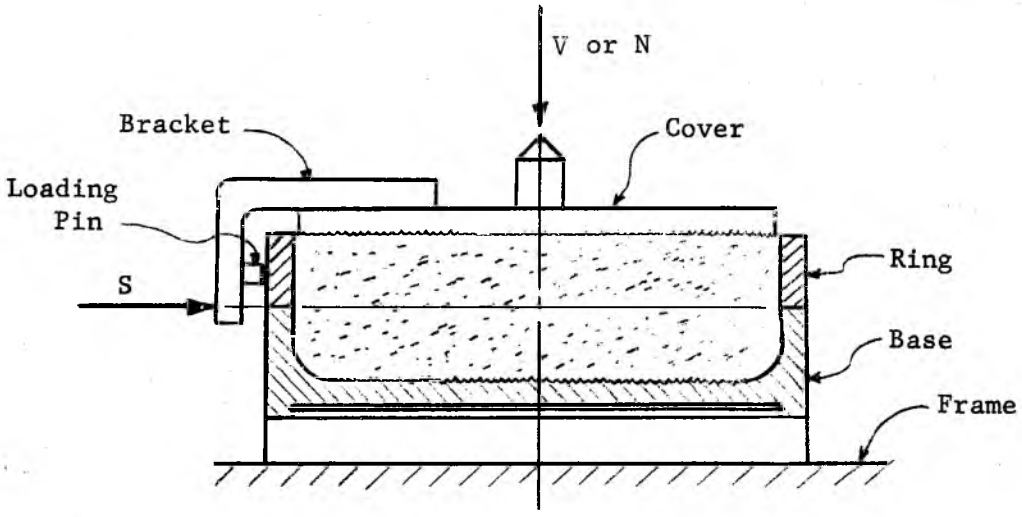

Fig. 99

Shear test cell

Testing

The purpose of the tests is to measure the flow properties of a solid (δ and flow-function), its density, and the angle of friction ϕ' between the solid and a sample of the wall. The flow properties are measured for two consolidating conditions: the condition of continuous flow, and the time effect of consolidation at rest after flow has stopped and material is left under pressure. Density and the angle of friction ϕ' are measured for continuous flow only.

The tests give significant results provided the procedure is such as to assure: (a) a representative specimen, (b) a uniform specimen, and provided that the stresses occurring during (c) flow, and (d) shear are known with sufficient accuracy. While these requirements sound commonplace, they are by no means easy to satisfy. Both the apparatus and the procedure described herein are the result of extensive experimentation. It is believed that the described method has brought the errors of tests within the range of scatter inherent in bulk solids flowing in a channel.

Continuous flow

(a) Representative specimen. In general, the yield locus of a solid for a given consolidating pressure and given strain-rate is affected by the water content, temperature, and particle size distribution of the specimen. The tests are conducted on solids containing water below the point of saturation. In view of the considerable influence which water content has on the yield loci of many materials it is

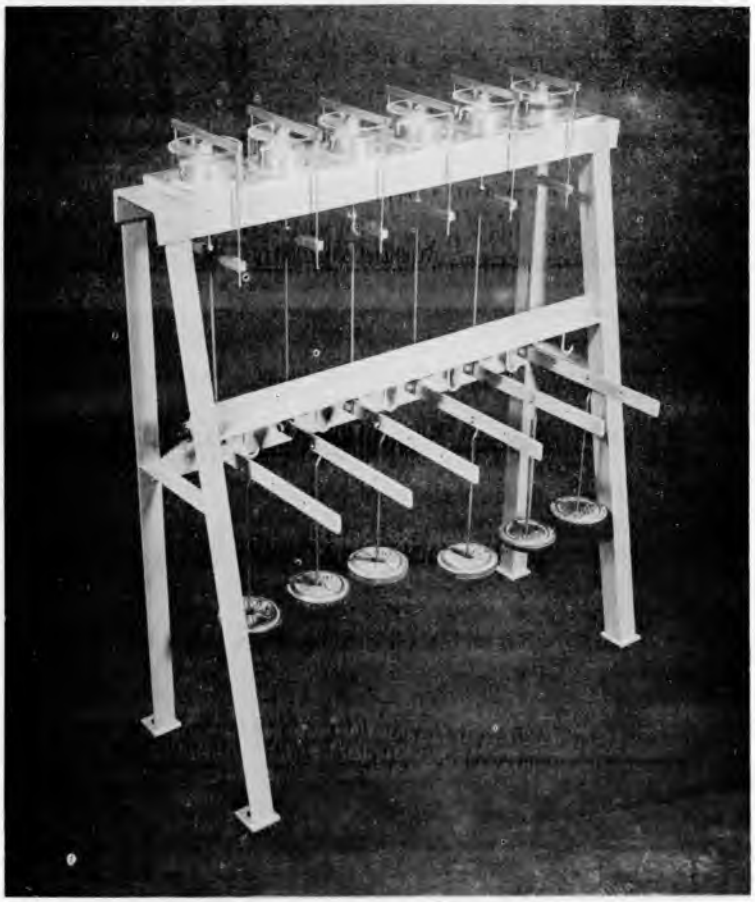

Fig. 100

Consolidating bench

necessary to reproduce the required content in the specimen accurately and to handle the specimen rapidly so as to minimize errors through evaporation.

When temperature is a significant factor, the solid and the consolidating bench are placed in a heated chamber, Fig. 101. The tests are carried out when the solid has reached the required temperature.

The particle size distribution is not as perplexing as it might appear at first sight. In the flow of bulk solids, the interest lies in the conditions that lead to stoppages of flow, which it is necessary to avoid. Stoppages occur when the solid reaches a sufficiently high yield strength. Thus, the critical conditions to be considered are those of highest strength. During the flow of a mass of mixed particle sizes, the large particles move bodily while the material shears across the fines. Therefore, the yield strength of the mass depends on the properties of the fines. The coarse particles are a passive agent and like aggregate in concrete they do not develop yield strength without fines to bind them. Experience shows that screened out coarse ores in bulk are invariably free flowing; they do not develop any cohesion. To determine the yield loci of a mixed material, the fines are screened out through an arbitrarily chosen No. 20 mesh (0.033 in. aperture) sieve and tested.

(b) Uniform specimen. The consolidation of the sample is carried out in two stages. The purpose of the first stage is the preconsolidation of a uniform specimen. With the cover off the test cell, a packing mold is placed on top of the ring and both the mold and the ring are

Fig. 101

Heated chamber

placed in an offset position on the base, as shown in Fig. 102. A specimen of the tested solid is then placed in the cell. One layer after another is slightly packed with the fingers, up to the top of the mold. The excess material is scraped off level with the top of the mold. A twisting top is placed over the specimen. The top is essentially like the cover of Fig. 99 but with a smooth bottom surface and without the bracket. A vertical force V is applied to the top by means of the system of lever and weight shown in Fig. 98. Force V causes a vertical pressure σ_v in the material. By means of a special wrench, an oscillating twist is now applied to the cover. This preconsolidates the solid and assures a uniform specimen.

(c) Flow. Consolidation is completed by causing the specimen to flow under given stresses until a steady state is closely approached. This is attained in the following way: Load V is released, the twisting top and the mold are removed, the excess material is scraped off level with the top of the ring, and the test cover is placed on the material. Load V is now replaced and a shearing force S is applied to the bracket, Fig. 103, by means of the electric-pneumatic shearing device. The shearing force is distributed between the cover and the ring.

This method of applying the shearing force seems to assure a fairly uniform distribution of the stresses across the specimen. Prior to the adoption of this method, the shearing force used to be applied directly to the ring. This would cause distinct stress concentration at the loaded edges of the ring and of the base. Material in the ring would

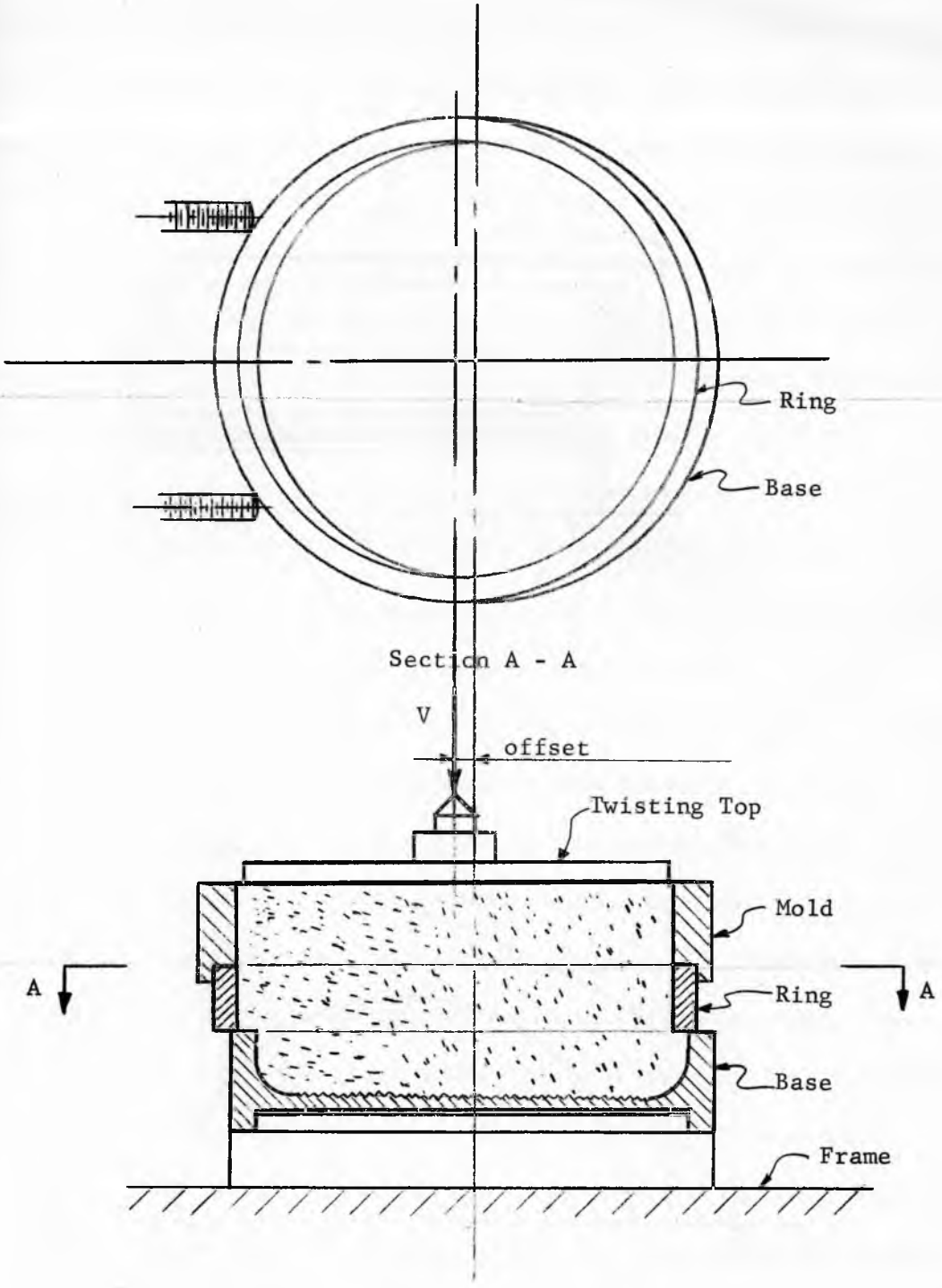

Fig. 102

Preconsolidation of a specimen

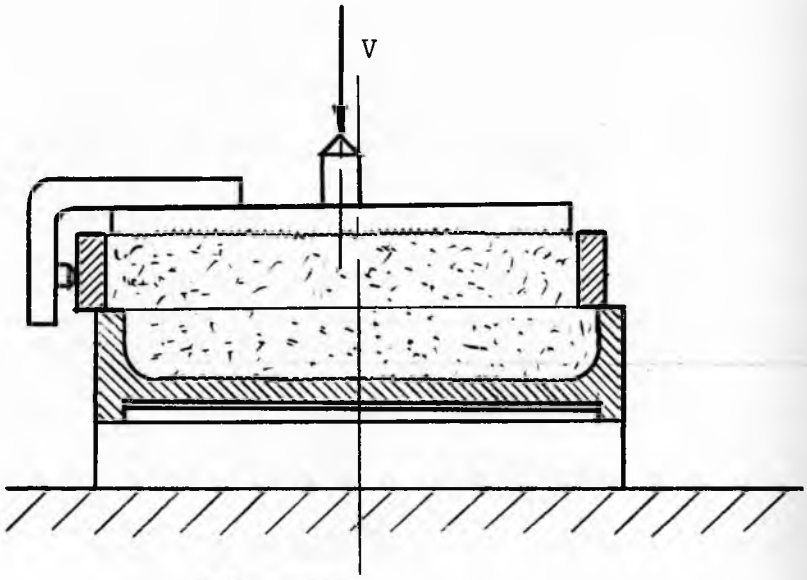

(a) Loading

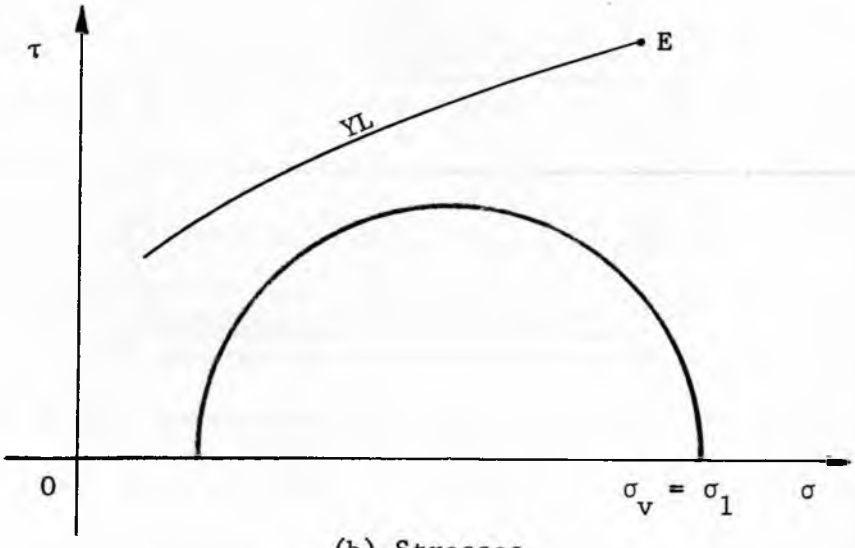

(b) Stresses

Fig. 103

Beginning of flow

pack against the loaded half of the ring, causing an empty gap to appear along the unloaded half of the ring. Furthermore, the unloaded side of the ring would often rise off the base, exposing the sheared specimen and weakening it significantly. It will be noted from Fig. 99 that the loading pin bears against the ring at its mid-height point; this reduces the tendency of the ring to rise off the base. As an additional safeguard against the rising of the ring, it is sometimes pressed down with the fingers, at intervals, during the process of flow.

As the strain proceeds, a condition is reached when a layer of material across the whole specimen is caused to flow plastically; the recorded shearing force reaches a steady value. The stresses which occur in the specimen during this stage of consolidation can be visualized as follows: the process starts with only the vertical pressure $\sigma_v = V/A$, where A is the area of the horizontal cross-section of the specimen, Fig. 103(a), σ_v is then the major stress and the corresponding Mohr semicircle is shown in Fig. 103(b) together with some yield locus which was developed during the twists of preconsolidation. The Mohr semicircle is below the yield locus and no flow occurs at this stage. Now the shearing stress $\tau_v = S/A$ is applied. As τ_v increases, the direction of the major stress σ_1 rotates away from the vertical until a steady state is reached for which the direction of σ_1 is shown in Fig. 104(a). For a steady state, there is no change of density, the strain rate vector $\dot{\epsilon}$ acts in the direction of axis $\gamma/2$, and the center of the Mohr semicircle of strain rates, Fig. 104(b), is located at the origin of the system of coordinates $(\epsilon, \gamma/2)$. For this state the compressive strain

rate, normal to the plane of greatest shear (plane γ_{max}), is equal to zero.

If the specimen were perfectly restricted in the cell, the height of the specimen would remain constant and the plane of greatest shear (γ_{max}) would be forced to coincide with the plane of shear of the cell. The principal strain rates ϵ_1 and ϵ_2, which are inclined at 45° to the plane of greatest shear, would be inclined at the same angle to the plane of shear of the cell. Assuming isotropy, the directions of the principal pressures σ_1 and σ_2 coincide with the directions of the principal strain rates ϵ_1 and ϵ_2 and would also be inclined at 45° to the plane of shear of the cell. The vertical pressure σ_v would then be inclined at 45° to the principal pressures. The measured stresses (σ_v,τ_v) would determine point T at the top of the Mohr semicircle, Fig. 104(c), [See ref. 3, pages 294-297].

On the other hand, if the specimen were quite unrestricted, one can speculate that one of the slip planes of the specimen would coincide with the plane of shear of the cell. The major pressure σ_1 is inclined at an angle 45° - $\phi/2$ to the slip planes. This would locate the direction of the major pressure σ_1 at 45° + $\phi/2$ from the vertical pressure σ_v and the recorded shearing stress τ_v would now lie at point E, the terminus of the yield locus, Fig. 104(d).

In fact, the specimen is partially restricted and the recorded point R falls on the Mohr semicircle between E and T, Fig. 104(e). The degree of restriction varies within certain limits between one test and another;

therefore, the position of point R on the Mohr semicircle also varies somewhat. The determination of the yield locus requires the measurement of at least two and usually more points (σ_n,τ_n) on the locus. For each point, the specimen is first consolidated and then sheared. It is necessary to reproduce the same degree of consolidation each time. To attain this goal, the shearing strain during consolidation is not continued to the steady state but is interrupted when the shearing force reaches a given value chosen at about 95 per cent of the expected steady value. (A preliminary test is run first to determine the approximate steady value of the shearing force.) This assures an acceptable scatter of the (σ_n,τ_n) points. The amount of the offset of the ring over the base is so adjusted that by the time this desired degree of consolidation is reached, the ring is in a central position.

(d) Shear. When consolidation is completed, the stem of the shearing force device is retracted. The vertical compacting load V is replaced by a smaller load N, such that pressure $\sigma_n = N/A$, Fig. 104(e), will locate a useful point of the yield locus. The shearing force is now applied until a failure plane has developed. That fact is indicated on the recorder by the force passing a maximum value. After shearing, the plane of failure of the specimen is checked. It should coincide with the plane of shear of the cell as shown in Fig. 105. If the planes do not coincide it means that the measured point (σ_n,τ_n) does not lie on the yield locus and the test is repeated. Tests are begun with the lowest required normal pressure σ_n. After each successful test, pressure σ_n is stepped up until a sufficient number of points is obtained to

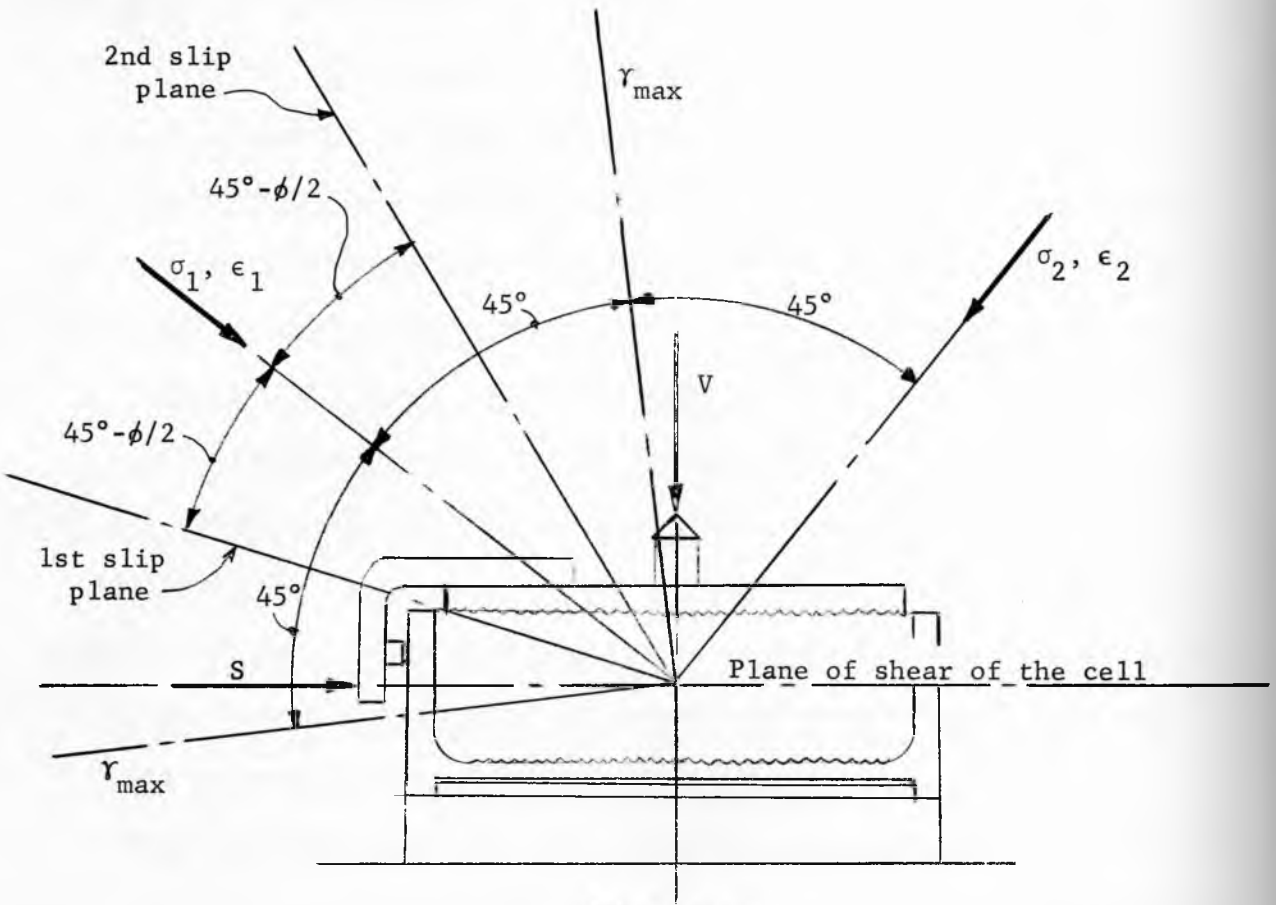

(a) Loading

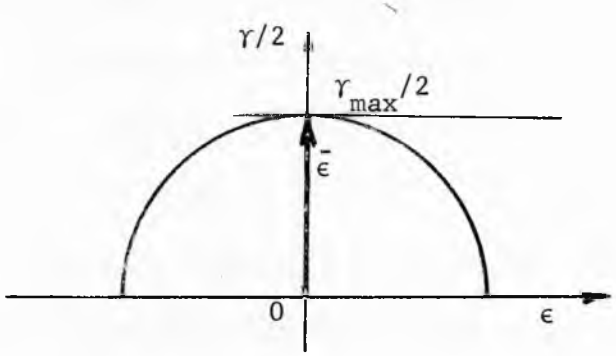

(b) Strain rate Mohr circle

Fig. 104

Steady state flow

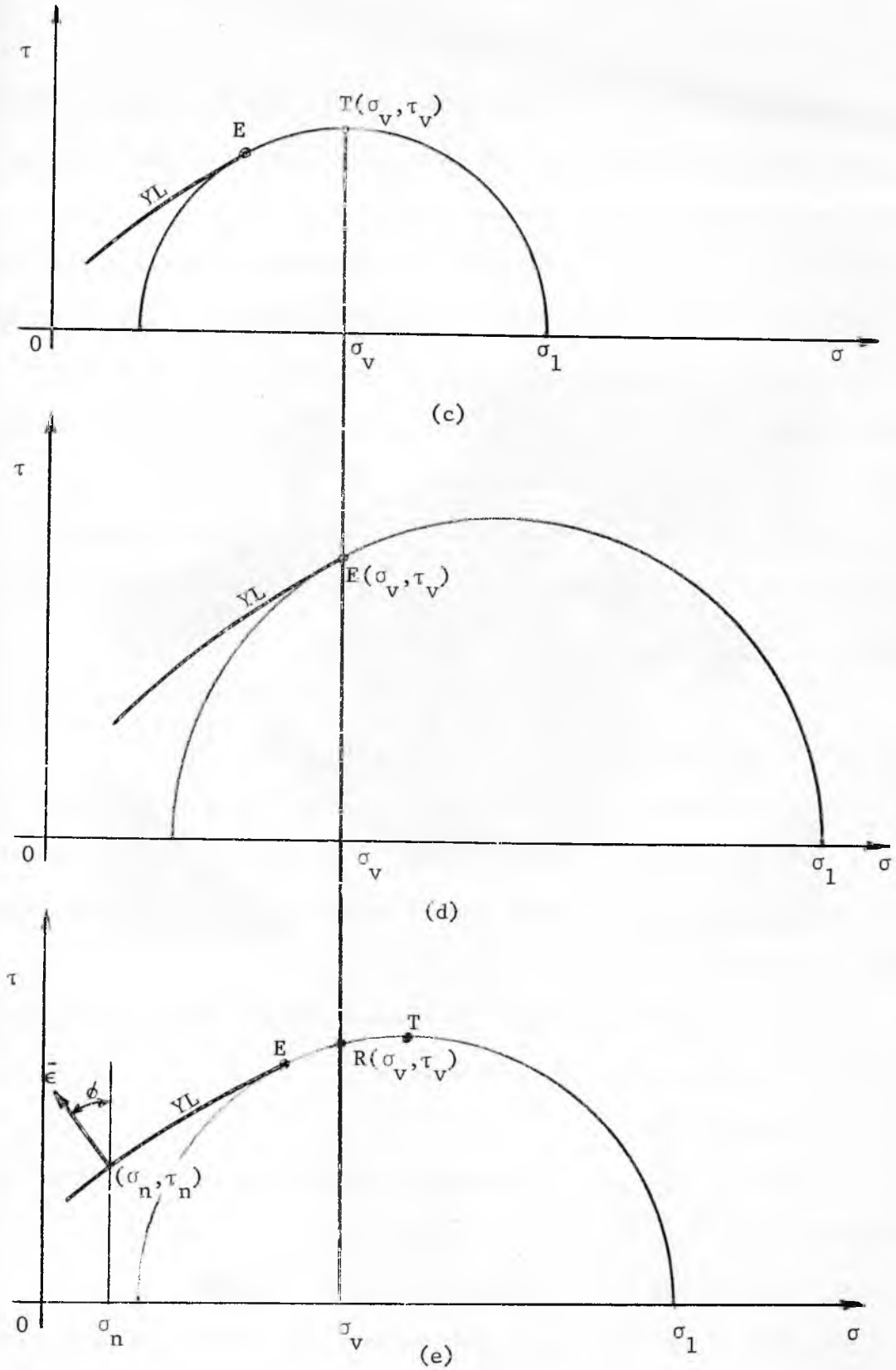

Fig. 104

Steady state flow

determine the yield locus. Experience shows that the largest value of σ_n for which a coincidence of the plane of failure with the plane of shear of the cell can be expected equals about 3/4 of σ_v. When the yield locus has been determined, the major consolidating pressure σ_1 is found by extrapolating the locus toward the higher values of σ and by drawing a Mohr semicircle through point (σ_v,τ_v) tangentially to the yield locus. The point of intersection of the semicircle with the σ-axis determines the value of the major pressure σ_1.

Example. A recorder chart of the tests of a lead concentrate is shown in Fig. 106. The curves are numbered and represent the following steps:

1. Preliminary test to determine the value of the steady flow shearing stress corresponding to a vertical pressure σ_v.

2. Consolidation of a test specimen under the same pressure σ_v and a shearing stress τ_v equal to about 95 per cent of the steady value. The jogs in the recorded lines occurred when the ring was pressed down with the fingers.

3. The consolidated sample is sheared under a normal pressure σ_n, giving a shearing stress τ_n at failure.

4. Same as (2).

5. Same as (3) but σ_n is stepped up and a higher value of τ_n is obtained.

6. Same as (2).

7. Same as (5) but σ_n is again stepped up and a still higher value of τ_n is obtained.

Fig. 105

Plane of failure of a specimen

The results of the tests are tabulated below.

TABLE 7

Test No.	1	2	3	4	5	6	7
V, lb	11.1	11.1	....	11.1	....	11.1	....
σ_v, lb per sq ft.	326	326	....	326	....	326	....
N, lb	....	....	1.1	....	3.1	....	6.1
σ_n, lb per sq. ft.	....	....	32	....	91	....	179
Chart reading	18.1	17.0	5.1	17.0	9.3	17.0	13.4
S, lb.	9.1	8.6	2.7	8.6	4.7	8.6	6.8
τ_v, lb per sq. ft.	267	252	....	252	....	252	....
τ_n, lb per sq. ft.	....	....	79	....	138	....	199

Points (σ,τ) obtained in tests 2,3,5, and 7 are plotted in Fig. 107. A smooth curve is drawn through points 3, 5, and 7, and extended toward point 2. A Mohr semicircle is drawn through point 2 tangentially to the curve. The point of tangency determines the terminus E of the yield locus and the point of intersection of the circle with axis σ (outside the figure) defines the major consolidating pressure σ_1 = 590 lb per sq. ft. Another Mohr semicircle is drawn through the origin and tangentially to the yield locus. The point of intersection of this circle with axis σ determines the value of the unconfined yield pressure f_c = 210 lb per sq ft. The first approximation of the effective yield

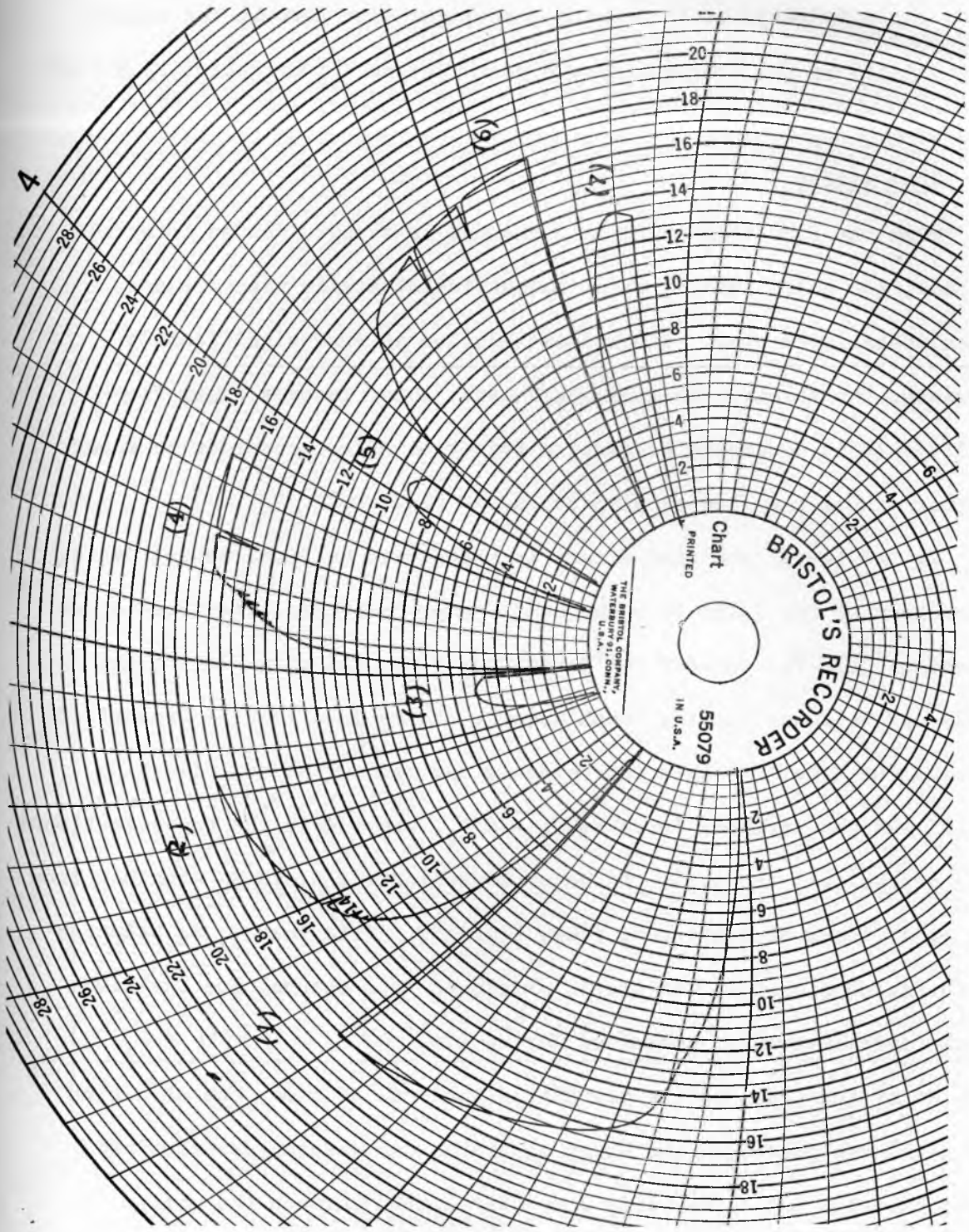

Fig. 106

Typical recorder chart

locus angle is obtained by drawing a straight line through the origin tangentially to the Mohr semicircle which passes through point E; $\delta = 49°$.

Time effect

When the flow of a solid in a channel is stopped for an interval of time, the solid remains under the action of static pressure and consolidates with time. Since consolidation at rest significantly increases the strength of some solids and, thus, reduces their flowability, it is necessary to measure this time effect in order to know whether or not the flow of a solid can be resumed.

In the tests, the time effect is reproduced by first consolidating a specimen of the solid in shear cells under conditions described above in stages (a), (b) and (c) for continuous flow, and then placing the cells on the consolidating bench under a static load for the prescribed interval of time. No shearing force is applied on the consolidating bench and the vertical force is $V_1 = A\ \sigma_1$, where A is the cross-sectional area of the cell and σ_1 is the major consolidating pressure obtained from the yield locus of continuous flow, Fig. 107. This load V_1 is selected on the assumption that the static pressures in a channel are the same as the pressures which prevailed during flow.

After the lapse of the prescribed interval of time, one at a time, the cells are placed on the shear apparatus and sheared as described above in stage (d). The yield locus is plotted through the points (σ_n, τ_n) and the value of the unconfined yield pressure f_c is obtained in the usual way.

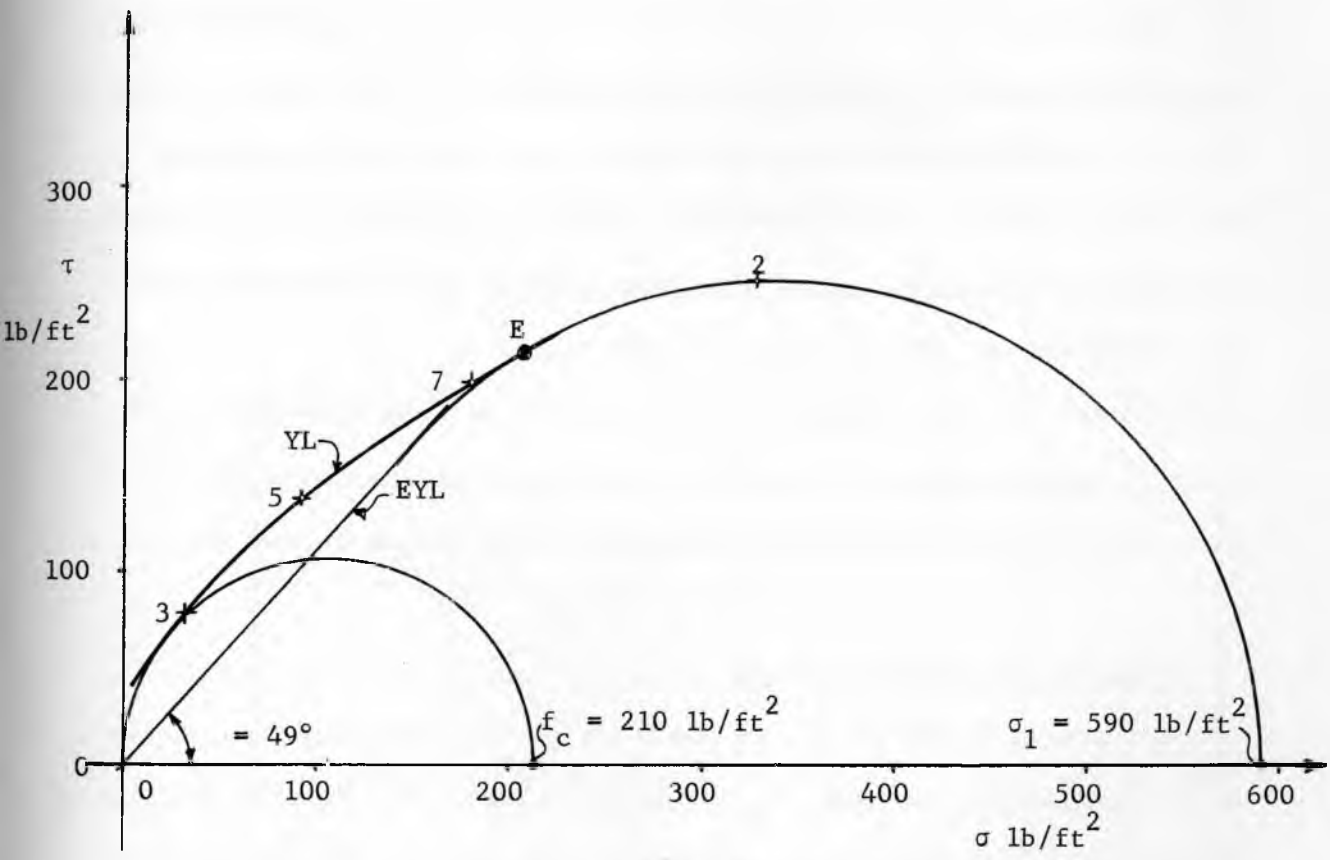

Fig. 107

Construction of a yield locus

During the static compaction it is necessary to preserve the moisture content of the specimen. This is down by covering the shear cells with plastic cups shown in Fig. 100; the bases of the cups are sealed by baths of a sealing liquid. When the tests are to be carried out at an elevated temperature, the consolidating bench is placed in a heated, thermostatically controlled chamber, Fig. 101.

Density

Since the analysis shows that the influence of the compressibility of a solid (change of density with consolidating pressure) on the process of flow is negligible, it is not necessary to obtain a very accurate function of density versus pressure. However, the density of a solid at the outlet of a channel, or at the inner surface of a pipe enters the flow formulas and, hence, needs to be obtained.

The easiest way to measure the density is to weigh the whole cell after it has been sheared (section (d) above), subtract the weight of the cell itself and divide the net weight by the volume of the cell.

Plots of the flow properties

For design purposes, f_c, γ, and δ are plotted as a function of the major consolidating pressure σ_1, as shown in Fig. 108. As will be shown in Part VI, these plots are very convenient in determining the actual value of angle δ and density γ which occur at the outlet of a channel or the inner surface of a pipe.

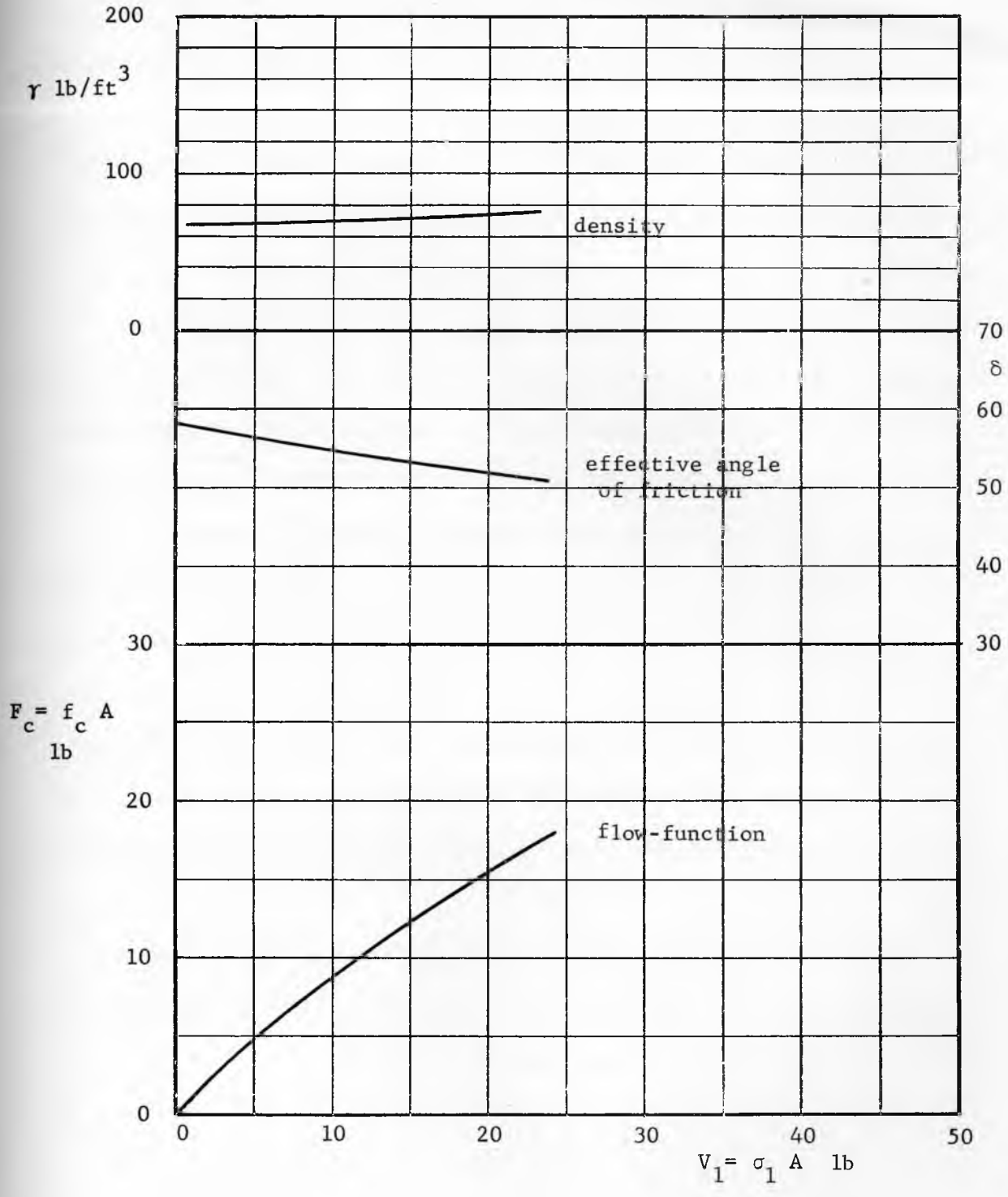

Fig. 108

Plots of flow properties

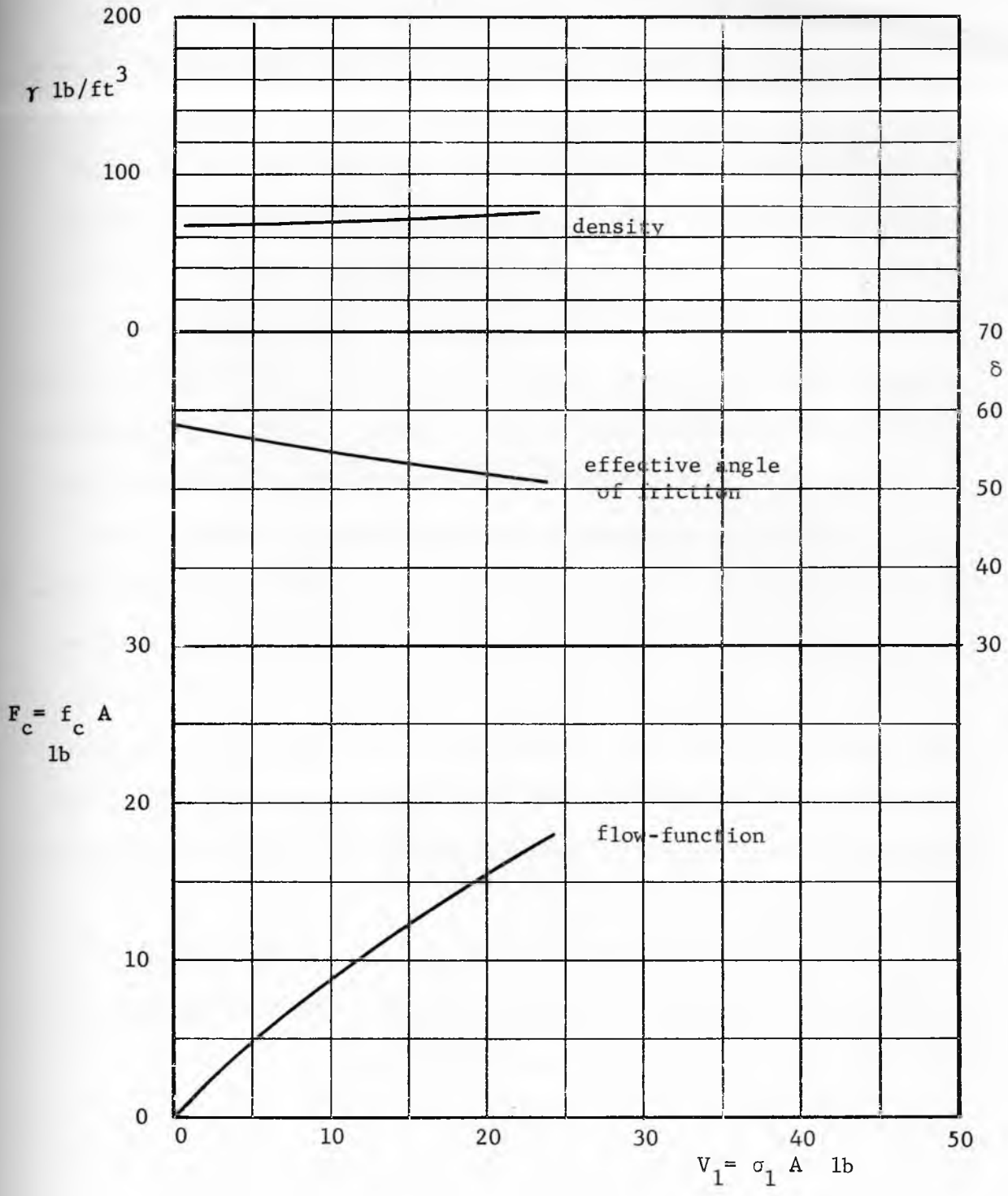

Fig. 108

Plots of flow properties

Angle of friction ϕ'

The angle of friction ϕ' between a solid and a material of the wall is measured on the direct shear apparatus, Fig. 98. The arrangement of the cell is shown in Fig. 109. In this case, the base is replaced by a filler covered with a specimen of the material of the wall, the ring is placed over it, filled with the solid, and enclosed with the cover. All the tests necessary to determine angle ϕ' are now run without replacing the solid. The procedure is as follows: the smallest vertical load V is placed and the shear foce S is applied until a steady reading is obtained. The stem is then retracted, the load V is increased and the force S is again applied until a steady value is reached. This precess is repeated for the required range of loads V. After the highest load V has been run, some solid is added to the cell so that the level of the solid in the ring is flush with the top of the ring. This is done without disturbing the consolidated solid in the ring. The tests are now repeated by decreasing the steps of the vertical force V. The unloading (return) branch of the relation S(V) is used in the determination of the angle ϕ'.

It should be noted that angle ϕ' may be very much affected by contamination of the wall material with other solids. It is better to use a fresh wall material specimen for each solid.

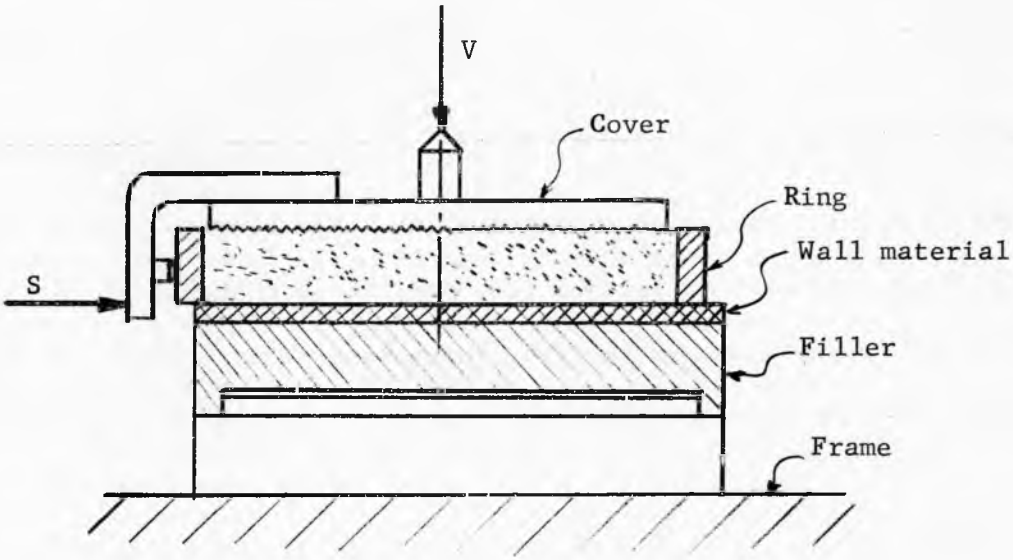

Fig. 109

Measurement of the angle ϕ'

PART VI

DESIGN

Introduction

The first significant studies of problems related to the handling and storage of bulk solids were reported at the end of the nineteenth century. That work originated from the necessity to store large quantities of grain and was concerned mainly with pressures affecting the structural design of silos and bins. The Janssen formula (about 1898) and the work of Ketchum [24] form the highlights of that period. In more recent years, automation, increasing plant capacities, and rising costs of labor have focused the attention of engineers on the problem of gravity flow of solids. A great deal of work has been done with models, and flow patterns obtained in small scale bins have been described in several publications [for example, 25, 26].

The problem of gravity flow of a bulk solid is the reverse of the usual structural problem. In a structural problem, design is directed toward assuring the stability and permanence of a structure under the action of loads. In solids flow, design is aimed at the failure of a consolidated mass of a solid under the action of its own weight and of applied external forces.

This part of the work reports the development of a quantitative method of design for flow of bulk solids in storage plants and flow channels. In order to make this part as self-contained as possible, some of the basic concepts will be restated.

Flow properties of bulk solids

In the technical language, the word 'flow' is more often associated with fluids than with solids, and when the 'flow of solids' is mentioned, it is often assumed by association that the solid will behave much like a fluid. Such an assumption is incorrect and has lead to serious errors of design which have impaired plant efficiency and disrupted production schedules. The major mechanical difference between a fluid and a solid is that, under static conditions, a fluid cannot transfer any shear stresses, while a solid can. An illustration is provided by the water in a lake which, at rest, assumes a smooth, horizontal surface, while the solids around the lake form dunes and mountains. The ability to transfer shear stresses at rest is a characteristic of all solids, even the quite free flowing ones, like dry sand.

The magnitude of the shear stress τ, at which a material shears (yields) along a certain plane, depends on the normal pressure σ acting in that plane, and is represented graphically in the (σ,τ) coordinates by a line called the yield locus (YL). They yield locus of a perfectly free flowing bulk solid is a straight line, Fig. 110, inclined at an angle ϕ to the σ-axis and passing through the origin. ϕ is the angle of internal friction of the material. Since fluids do not transfer any shear (under static loading), the angle of internal friction for fluids is zero. For bulk solids, ϕ is greater than zero and, if a stress (σ_e,τ_e) lying below the yield locus is applied in some plane of a solid, the solid does not shear but only undergoes an elastic deformation; this reflects the fact that a solid can transfer

a shear stress without yielding.

The bulk solids of real life deviate more or less from the perfectly free flowing solid. In the (σ,τ) coordinates, Fig. 111, this deviation shows up in four ways: (1) the yield locus is not a straight line but is convex upward [7]; (2) the position of the yield locus is a function of the degree of consolidation of the solid, hence, one solid has an infinite number of yield loci; (3) each yield locus terminates at some point E; (4) each yield locus intercepts the τ-axis at some value c greater than zero, c is called cohesion. All the flow properties of a solid are based on the concept of the yield locus.

The purpose of the analysis is to relate the flow properties of solids with the shape and frictional properties of channels with a view to determining the conditions which assure flow.

It is first assumed that the solid is flowing in the channel. During flow, the stresses in the deforming (plastic) regions of a solid are continuously located at the points E. This defines a line called the effective yield locus (EYL), and angle δ, Fig. 111. Angle δ enters the analysis of flow under the name of effective angle of friction. In general, angle δ differs from the angle of friction ϕ. The two are equal only in perfectly free flowing solids. In real solids, during flow, $\delta > \phi$. The analysis of flow provides a field of the major consolidating pressure σ_1 within the channel. This pressure causes a consolidation of the solid and generates a yield locus. Since the pressure varies from point to point within the channel, so does the yield locus.

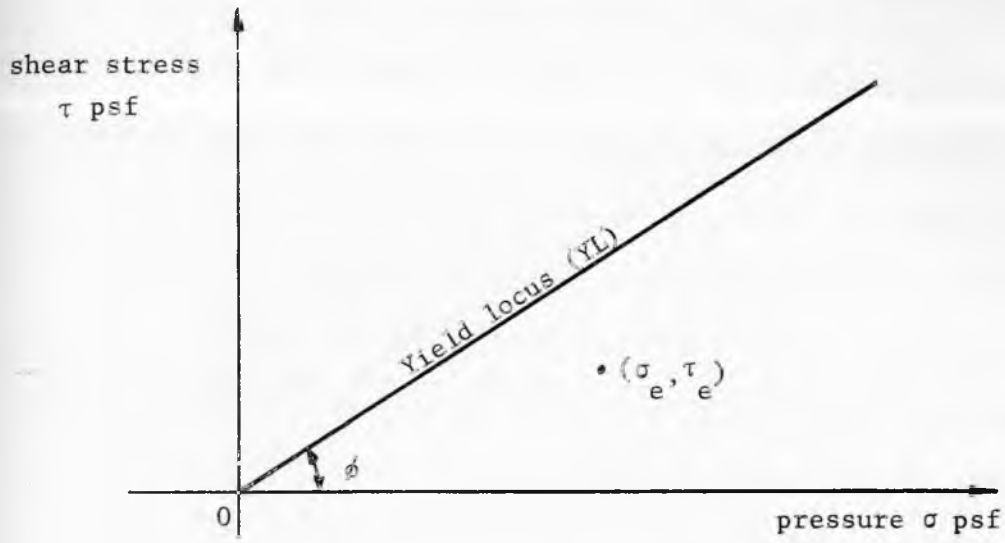

Fig. 110

The yield locus of a perfectly free-flowing solid

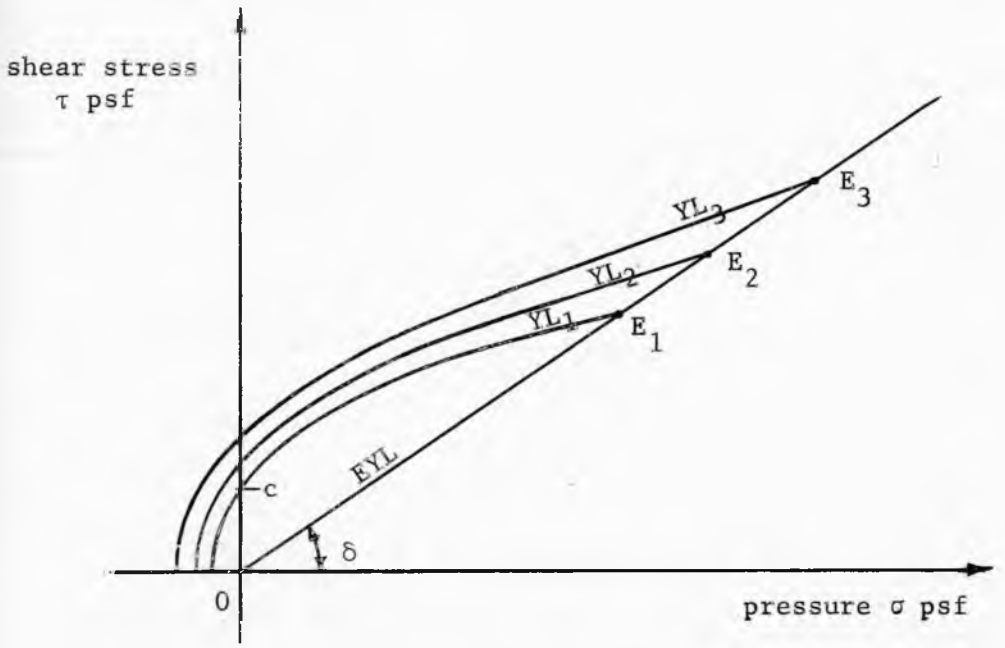

Fig. 111

The family of yield loci of a real solid

Now obstructions to flow are considered. It is postulated that, if the flowing solid develops enough strength to support its own weight in some stable structure over or about the outlet of the channel, then that structure will form and flow will not occur. The two typical structures which form obstructions to flow are: a dome across the channel, and a vertical (or almost vertical), circular, empty pipe circumscribing the outlet. For flow to prevail, the stresses in these structures must exceed the strength of the solid so that the structures fail. Since failure usually originates in a thin layer at the surface of an obstruction, the stresses which act at some point of the surface and the yield strength which the solid develops at that point of the surface are critical.

The stresses which act at the surface of a dome, $(\bar{\sigma}_1)_{\text{dome}}$, and of a pipe, $(\bar{\sigma}_1)_{\text{pipe}}$ have been determined in the analysis of incipient failure. The yield strength which a solid develops at an exposed (traction-free) surface is called the unconfined yield pressure, f_c, and is assumed to have been generated by the major consolidating pressure of flow, σ_1; hence

$$f_c = f_c(\sigma_1). \qquad \text{(a)}$$

In the calculations it is more convenient to operate with forces

$$(\bar{V}_1)_{\text{dome}} = A(\bar{\sigma}_1)_{\text{dome}}, \qquad (\bar{V}_1)_{\text{pipe}} = A(\bar{\sigma}_1)_{\text{pipe}},$$

$$V_1 = A\,\sigma_1 \qquad \text{and} \qquad F_c = A\,f_c,$$

where A is the area of the cross-section of the shear cell used to measure the flow properties (Part V). Relation (a) then transforms into

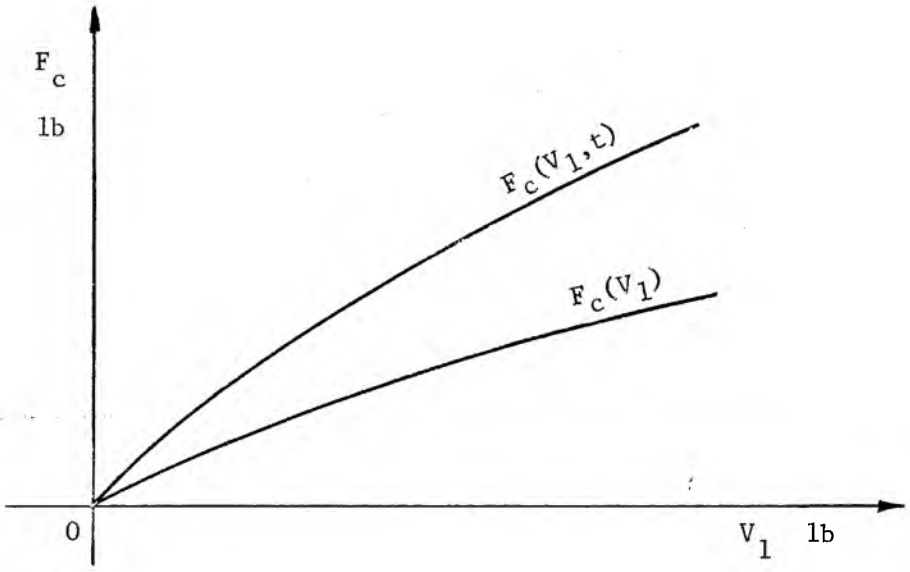

Fig. 112

Flow-functions

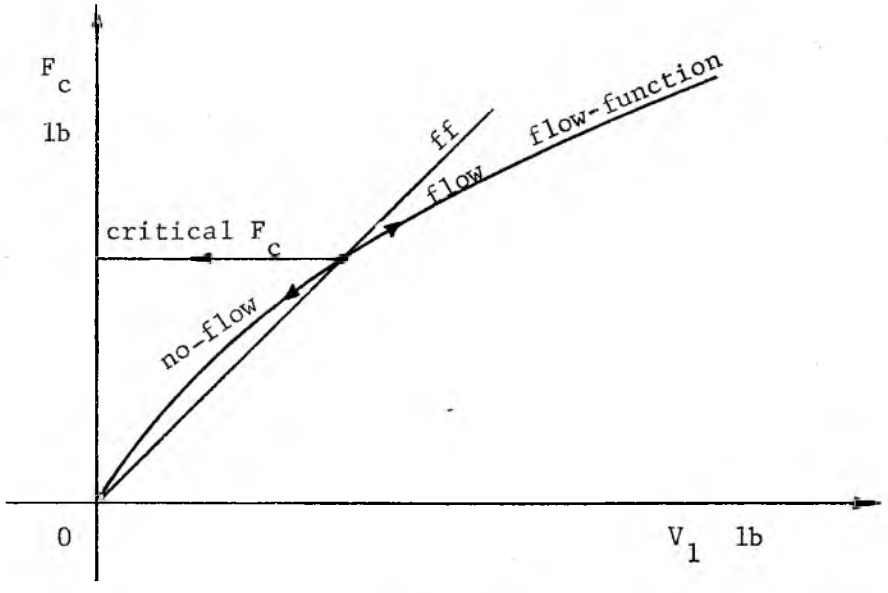

Fig. 113

The flow, no-flow condition

$$F_c = F_c(V_1) \qquad (b)$$

and is plotted in Fig. 112. For a dome to be unstable

$$(\bar{V}_1)_{dome} > F_c(V_1),$$

or, dividing both sides of the inequality by V_1,

$$\frac{(\bar{V}_1)_{dome}}{V_1} > \frac{F_c(V_1)}{V_1}. \qquad (c)$$

Ratio

$$\frac{V_1}{(\bar{V}_1)_{dome}} = ff$$

is called the critical flowfactor for no-doming, and inequality (c) is rewritten

$$\frac{V_1}{F_c(V_1)} < ff. \qquad (d)$$

The relation (d) is shown graphically in Fig. 113, in which the critical flowfactor ff and the flow-function of the solid are plotted. The inequality is satisfied in those regions of the channel in which the force $V_1 = A\ \sigma_1$ exceeds the value at the point of intersection.

It was shown in the analysis of steady state flow, eq.(102), that pressures in a solid increase with the distance from the vertex of the channel. Hence the point of intersection in Fig. 113 defines a minimum dimension of the outlet of the channel necessary to assure flow.

The analysis of the condition for no-piping also leads to a condition (d), but the values of the critical flowfactor for no-piping are, of course, different. In oblong outlets, which have two principal dimensions, the minor dimension is determined from the condition of

no-doming and the major dimension from the condition of no-piping. In view of the fact that a pipe circumscribes the outlet, the major dimension of an outlet is its largest dimension, e.g., the diagonal of a rectangle.

It is useful to introduce a rough guide to the flowability of solids by classifying them in accordance with the value of the ratio V_1/F_c of the flow-function. Namely,

$10 < V_1/F_c$ - free-flowing,

$4 < V_1/F_c < 10$ - easy-flowing,

$1.6 < V_1/F_c < 4$ - cohesive,

$V_1/F_c < 1.6$ - very cohesive and non-flowing.

When a solid is flowing, the yield locus of an element of the solid and the value of F_c which the locus defines are functions of the moisture content of the solid H, its temperature T, and the major consolidating pressure $\sigma_1 = V_1/A$ acting on the element. For given H and T, the relation $F_c = F_c(V_1)$, plotted in Fig. 112, is called the instantaneous flow-function of the solid and, together with angle δ, determines the flowability of the solid under conditions of continuous flow.

If flow in a channel is stopped and the solid is left at rest for an interval of time t, say hours or days, it is assumed that the pressures within the solid remain essentially unchanged, the solid keeps consolidating with time, and may gain strength. The relation $F_c = F_c(V_1,t)$ obtained under these conditions is referred to as the time flow-function.

In Fig. 112, the latter usually lies above the instantaneous flow-function, indicating a gain in strength with the time interval of consolidation at rest. This gain may be caused by any one or a combination of the following factors:

1. Eascape of entrained air with corresonding increase of density and strength of the solid.
2. External vibrations due to operating machinery, railroads, or wind which cause a rearrangement of particles and an increase in the consolidation of the solid.
3. Evaporation of free water with concurrent precipitation of dissolved salts which cement the particles.
4. Break-up or softening of particles or crystals under pressure, causing an increase in cohesion.
5. Chemical changes in the surface of particles, e.g., fermentation.

Particle Size. As a general rule, solids which do not contain particles smaller than, say, 0.01 inch are free-flowing. There are exceptions to this rule. For instance, grain ferments under adverse moisture and atmospheric conditions and can develop sufficient strength to cease being free-flowing. Soybean meal contains oil which under conditions of high moisture and temperature binds the particles into a non-flowing mass. Flaky or stringy materials, like wood shavings, mica, asbestos, interlock and also form obstructions to flow. Most ores, however, come under the general rule.

The flowability of a solid containing a range of sieve sizes, which

includes both, fine and coarse particles, is invariably governed by the flow properties of the fine fraction. This is explained by the fact that during flow the shearing takes place across the fines. The coarse particles are a passive agent in this process. However, the size of the coarse particles will affect the tendency to interlock at the outlet, and the impact of the heavy, coarse particles charged into a container may cause compaction of the solid along the trajectory of the falling stream.

Limitations of the analysis

In the discussion of the yield stresses, the solid has been assumed at rest, that means, the influence of the velocities and accelerations on the stresses has been neglected. To understand the implications of these simplifications it is necessary to consider the effect of velocity and acceleration. An element of a solid flowing down a channel undergoes a change of pressure which changes the bulk volume of the element and, hence, the volume of voids within the element. Unless the solid is in a vacuum, changes in the volume of voids set up gas pressure gradients in the mass. Since these gradients are not included in the analysis, they must be negligible, hence, the velocities of flow must be low.

In the analysis of the stress fields, the equations of equilibrium have been used. For these equations to be applicable, the dynamic forces must be negligible, compared to the gravitational forces. Hence, the accelerations of the particles must also be low.

These restrictions on the velocity and acceleration are not too serious. The analysis applies to most cases of flow controlled by means of feeders. However, the work may not apply to cases of free fall out of a hopper, and does not apply to free fall through any channel of constant cross-section, like a straight spout. Some of these problems are now under study. The present work does not give any absolute values of velocities. Where velocities are mentioned, the values are only relative to some asigned value; e.g., the velocity profiles, Figures 68, 69 and 70, have a unit velocity at the axis of the channels and give the relative values at other points of a cross-section of the channel.

For controlled flow, this work prescribes the dimensions, shapes, and wall properties of channels necessary to assure a given type of flow to a solid of given flow properties.

Types of flow

A solid may flow in a channel made of an extraneous material, like steel, concrete, wood, or it may form a channel within itself. In both cases, the boundaries between the flowing mass and the stationary, confining material will be called walls. Walls made of an extraneous material will be referred to as weak walls, and walls formed within the solid itself will be referred to as rough walls. The frictional and cohesive strength of a rough wall is usually the same as that of the flowing solid and, hence, is described by the flow properties of the solid (angle δ and flow-function). A weak wall introduces

a degree of weakness, compared to a rough wall; the strength of a weak wall depends on both, the flowing solid and the material of the wall, and is measured by the angle of friction ϕ' under conditions of sliding.

Mass flow is said to occur within a channel made of an extraneous material when the solid flows everywhere along the weak walls of the channel. For complete mass flow to occur, the walls must be sufficiently steep and smooth (weak), and the channel must not have any sharp corners, abrupt transitions, or discontinuities in the frictional properties of the walls. Any one of the last three conditions will enforce a dead region in its vicinity, though mass flow may prevail in the remainder of the channel.

Mass flow is characterized by uniform and comparatively low velocities, because the flow pattern is steady and flow takes place across the whole section of the channel. This type of flow is particularly advantageous when an even rate of draw is required or when the solid is to provide a seal against gas counter-flow. Mass flow is well suited to fine solids which have a tendency to flood upon aeration. Mass flow can assure a first-in, first-out flow sequence which is vital when the flowing solid is subject to deterioration with time, or when the solid segregates while charged into the container. While this flow pattern does not prevent segregation during charging it can cause remixing during flow.

The containers which lead to mass flow have also disadvantages: they are tall for a given capacity, they require extensive forming to provide a smooth channel, the walls wear out as the solid continuously

slides on them. These things add to the expense. Mass flow containers for coarse solids should not have steep walls, because large rocks carry a great deal of momentum when charged into a container and when they hit the mass deposited in a steep hopper they tend to wedge the solid within the walls and cause it to dome across the channel.

Typical mass flow containers are shown in Figures 114. Containers (a), (c) and (d) have no sharp corners and give perfect mass flow. The other containers will have dead regions as shown by dashed lines. A dead region at a transition contains a core (area ABC in Fig. 25) within which the solid is not flowing at all, and approaches, above and below the core, in which flow is very slow. If the solid develops strength with the time of consolidation at rest, the dead regions gain strength and may provide substantial abutments which constrict the channel and may lead to doming at the transition. This phenomenon is frequently observed and can be corrected by filling in the sharp corners to provide the effect of the smooth transition shown in Fig. 114 (c). The filling material should be the same as the material of the walls, and the radius of curvature of the smooth transition should be sufficiently large. The work on what constitutes a 'sufficiently large' radius is now in progress. At this stage, it is recommended that the radius of the transition be equal to one half the width of the vertical portion of the channel.

The selection of the hopper slopes for mass flow is done on the basis of the effective angle of friction of the solid δ, and the angle of friction between the solid and the wall ϕ'. The values of these

two angles are obtained from the tests described in Part V.

For conical, circular hoppers, Fig. 114 (a) and for conical hoppers with a smooth transition, Fig. 114 (c) the selection is based on the charts given in Figures 85 to 89. These charts have been computed for axially symmetric radial flow and represent quite closely the conditions which occur in conical hoppers. The abscissa in the charts is θ', the slope of the hopper walls measured from the vertical; the ordinate, which is of interest in this part of the work, is the angle ϕ'. It will be noticed that the regions within which solutions are available are bounded. If a wall described by same pair (θ', ϕ') is selected outside of such a region, flow along the wall will not occur, though flow may occur across the solid in a vertical, or almost vertical, pipe circumscribing the outlet. There is no in-between stage, if flow occurs, it occurs either along the weak walls or in a pipe. This means that, for a given angle of friction ϕ', a maximum slope angle θ' is prescribed by the charts.

In measuring angle ϕ', there is usually some scatter and a range of values is obtained. For the purpose of design it is safe to use an upper value of the range. The charts are plotted for five values of δ: 30°, 40°, 50°, 60°, 70°. Since the actual value of δ will usually lie in between two of these values, the maximum value of θ' is obtained by interpolation between the values obtained from the appropriate charts. For design, the interpolated value of θ' is reduced by 3° to 5°. It can then be said with a high degree of certainty that mass flow will occur in the channel for practically all levels of the solid in the

channel.

Containers with conical hoppers have advantages: the shells are light and require no lateral reinforcement, because they do not transfer any bending stresses; their shape is regular, hence they are easy to design and to fabricate; the hoppers can often be brought to quite small outlets which require but small feeders or valves. However, conical hoppers have a serious disadvantage in the comparatively high headroom which they need for a given capacity. High headroom is expensive since it requires a high structure, a high elevation of the solid, often a high building.

The height of a container can frequently be reduced by providing a hopper with an oblong outlet rather than a circular one. In such a hopper, Figures 114 (e), (f), (g), the slope of the end walls is either vertical or as described above for the circular hoppers, but the slope of the side walls can be considerably less. A mathematical determination of the flow criteria in hoppers of these shapes is not feasible at this time. From observation, it appears, however, that in the central part of an oblong cross-section flow closely approaches a pattern of plane flow (referred to as plane strain in the previous parts of this work). Plane flow is the type which would occur in the container, Fig. 114 (g), if the dimension L were infinite and flow were uniform along the whole length L. Plane flow has been analyzed mathematically. In particular, plane radial flow, which is approached in straight hoppers, has been analyzed and the selection charts are presented in Figures 80 to 84 for symmetric channels, for $\delta = 30°$,

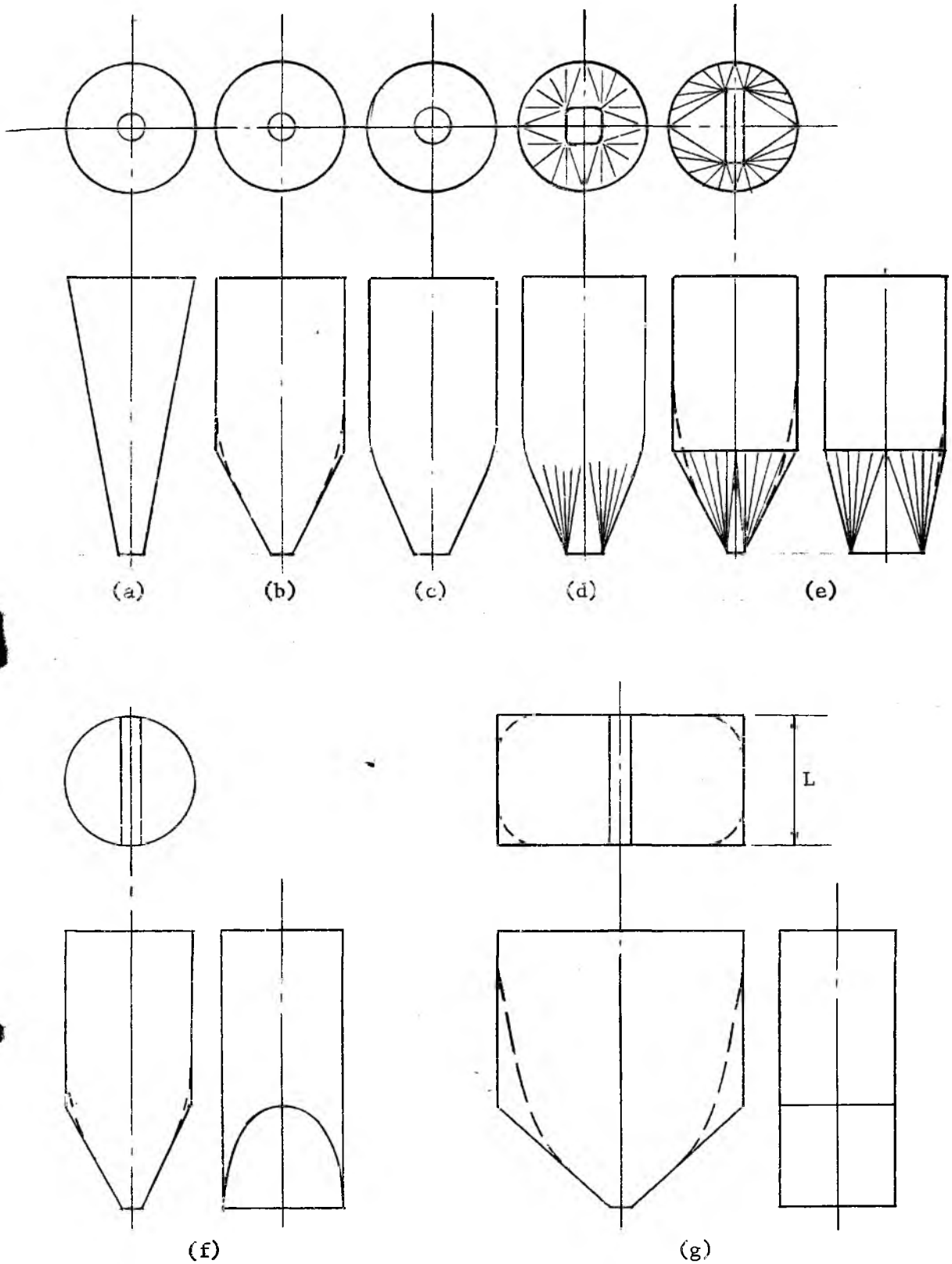

Fig. 114

Mass-flow containers

40°, 50°, 60°, and 70°. In addition, selection charts for asymmetric channels with one vertical weak wall and the other wall sloping at an angle θ' are given in Figures 90 to 92 for $\delta = 50°$, and for three frictional values of the vertical walls $\phi^v = 20°$, 30°, and 40°.

As is seen from these charts, the regions of θ', ϕ' for which solutions are available in plane radial flow are much larger than the corresponding regions in conical flow. This means that plane radial flow can occur within less steep and rougher walls. Indeed, in plane flow, $\theta' = 90° - \phi'$ at the bounds. However, these very high values of θ' are practically unattainable not only because plane radial flow is never actually reached in channels of oblong cross-section but also because plane radial flow is not approached from the top of the channel until a sufficiently high pressure has been developed in the solid. Consider a case of plane flow in a wedge-shaped channel, Fig. 115. The magnitude of the major pressure σ_1 which acts within the solid along the wall of the channel is plotted in the figure with a continuous line. The pressure required for plane radial flow is given by eq.(102), and is plotted with a dashed line. At some height h above the outlet the two lines separate and this causes the flow channel to break away from the walls and approach the vertical. The shaded regions of the solid may remain stationary for some time and then slide down like rigid bodies. Having gained strength during the consolidation at rest, the shaded regions may cause an obstruction to flow as they descend bodily toward the narrower section of the hopper.

Thus, to ensure plane mass flow, the channel should either be very

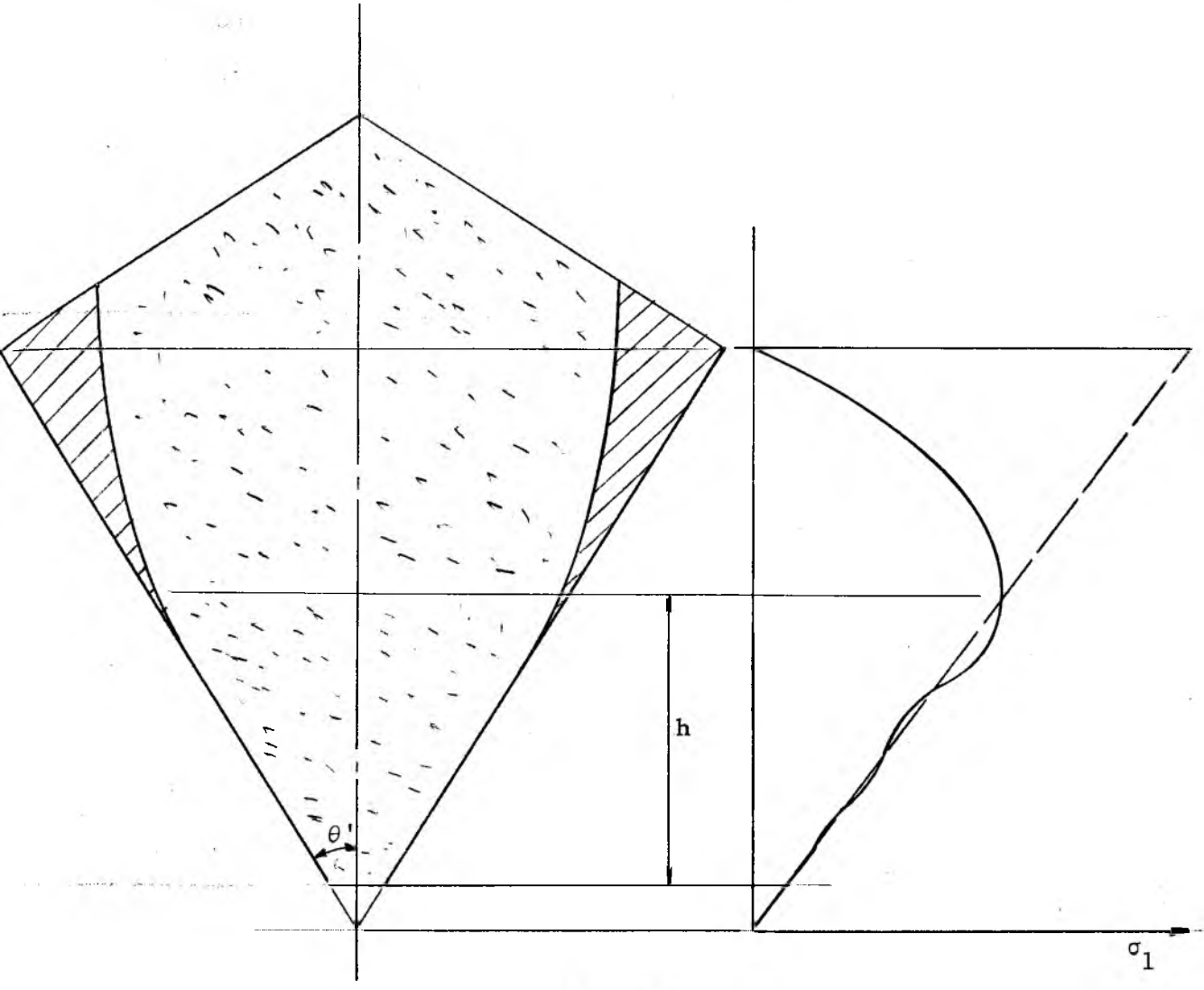

Fig. 115

Plane flow in a wedge-shaped channel

steep, for instance, as prescribed by conical flow, or should have a vertical portion, which is normally operated with a sufficient head of material, and a smooth transition of a sufficiently large radius. If the transition is sharp, it will generate a dead region in its vicinity. The size of that region is a function of the angles δ and ϕ' but, primarily, of the angle θ' of the hopper at the transition. As that angle is increased, Fig. 116, the size of the dead regions increases. For a sufficiently large angle θ', flow along the walls ceases completely and only flow in a vertical pipe through the solid may take place (see Plug flow). The study of these relations is now in progress. In the meantime, it is recommended that θ'_{max} does not exceed the values plotted in Fig. 117 as a function of the angle δ.

Since a sufficient head of the solid and a smooth transition are required to induce perfect mass flow in a channel, it is of interest to consider an example of the flow pattern which may develop as the level of the solid drops in a bin with a sharp transition, Fig. 118. From stage 1 to stage 2, the solid within the vertical portion of the channel flows bodily, like a rigid mass. Approaching stage 3, flow at the sides slows down and stops, as shown in the figure, the channel breaks away from the walls, stage 4, and the width of the channel narrows down to about 2/3 of the height of the vertical portion. The solid flows into the channel from the top, as in plug flow (see below). As the level of the solid keeps dropping, the channel keeps narrowing, stage 5.

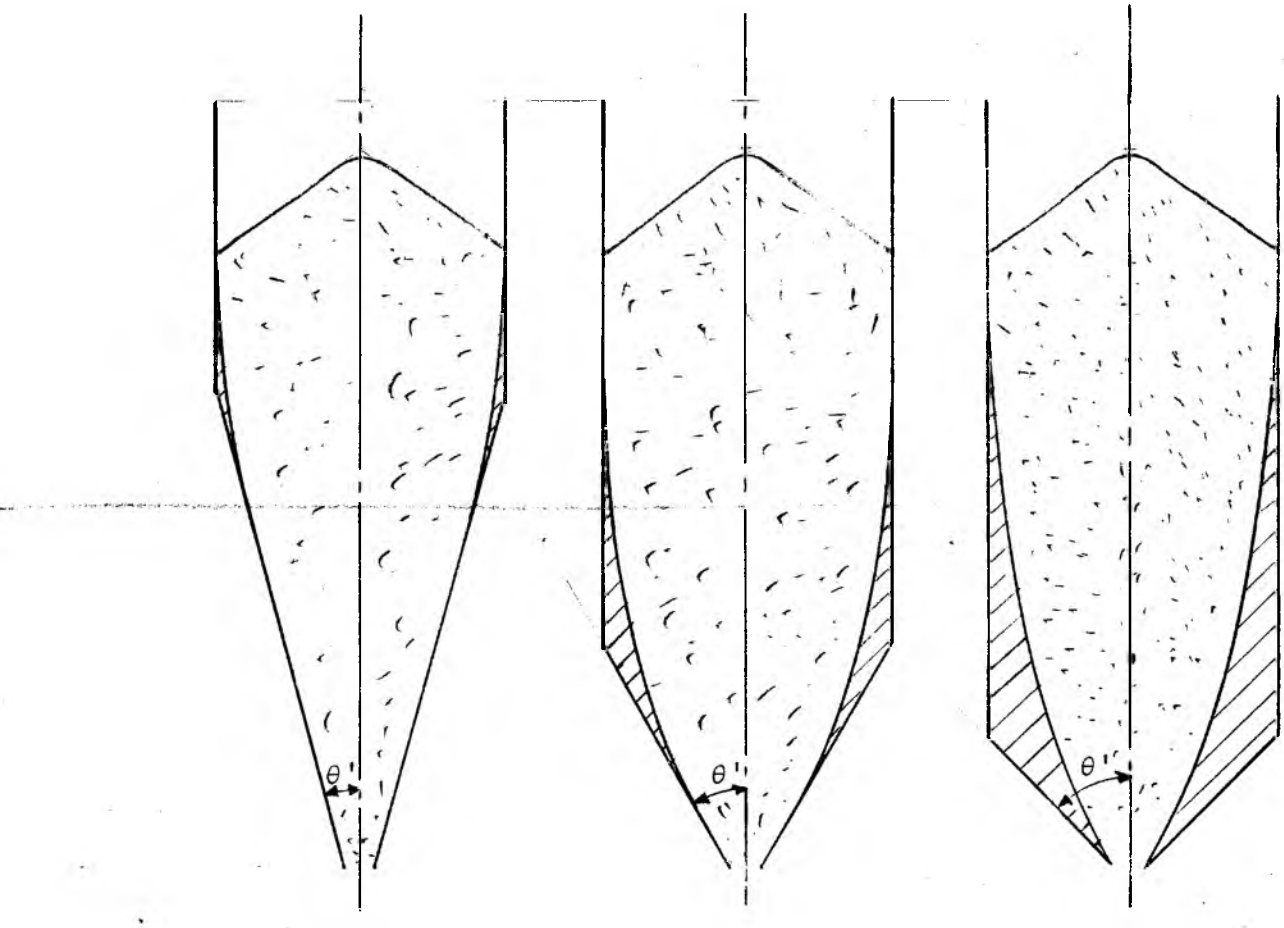

Fig. 116

Dead regions generated by a sharp transition

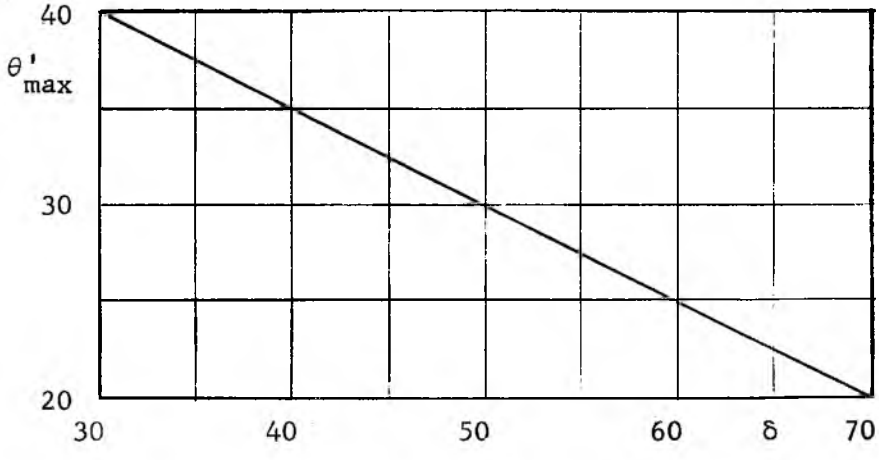

Fig. 117

Recommended maximum values of the hopper slope angle θ' in plane flow

It should be stressed that square and rectangular bins, shown in Fig. 119 (a) and (b), do not produce mass flow. The sharp corners fill out with packed solid and flow along the walls cannot occur. Mass flow may be approached if the corners are sufficiently rounded off, Fig. 119 (c), but no specific design recommendations can be made at this time without experimentation.

Hoppers with one vertical wall. The influence of the asymmetry of a hopper on the critical flowfactor has been analyzed for plane flow for the angle $\delta = 50°$, and for three angles of friction ϕ^V between the solid and the vertical wall, Figures 90 to 92. A comparison of these values of the flowfactors with those plotted in Fig. 82 for the corresponding symmetrical channel shows that the minimum values are not affected by asymmetry, but the trough of minimum values is shifted by asymmetry toward the larger values θ', ϕ'. For walls of a given frictional value and a given critical flow-factor the allowable included angle is, in general, greater in symmetry than in asymmetry. For instance, for $\phi' = \phi^V = 40°$, ff = 1.3, in symmetry $2\theta' = 40°$, in asymmetry $\theta' = 35°$. A channel with one vertical wall may have an advantage if mass flow fails to develop, because a break along a rough wall ($\theta' = 0$) occurs at lower values of the flowfactor in the asymmetric channel. For instance, for $\theta' = 0$, $\phi^V = 40°$, $\phi' \approx \delta = 50°$ (rough vertical wall), ff = 1.8 in symmetry, but only 1.36 in asymmetry. Further, a symmetric hopper with a vertical partition, Fig. 120, permits a somewhat larger included angle than a similar hopper without the partition. However, it should be observed that to obtain a controlled

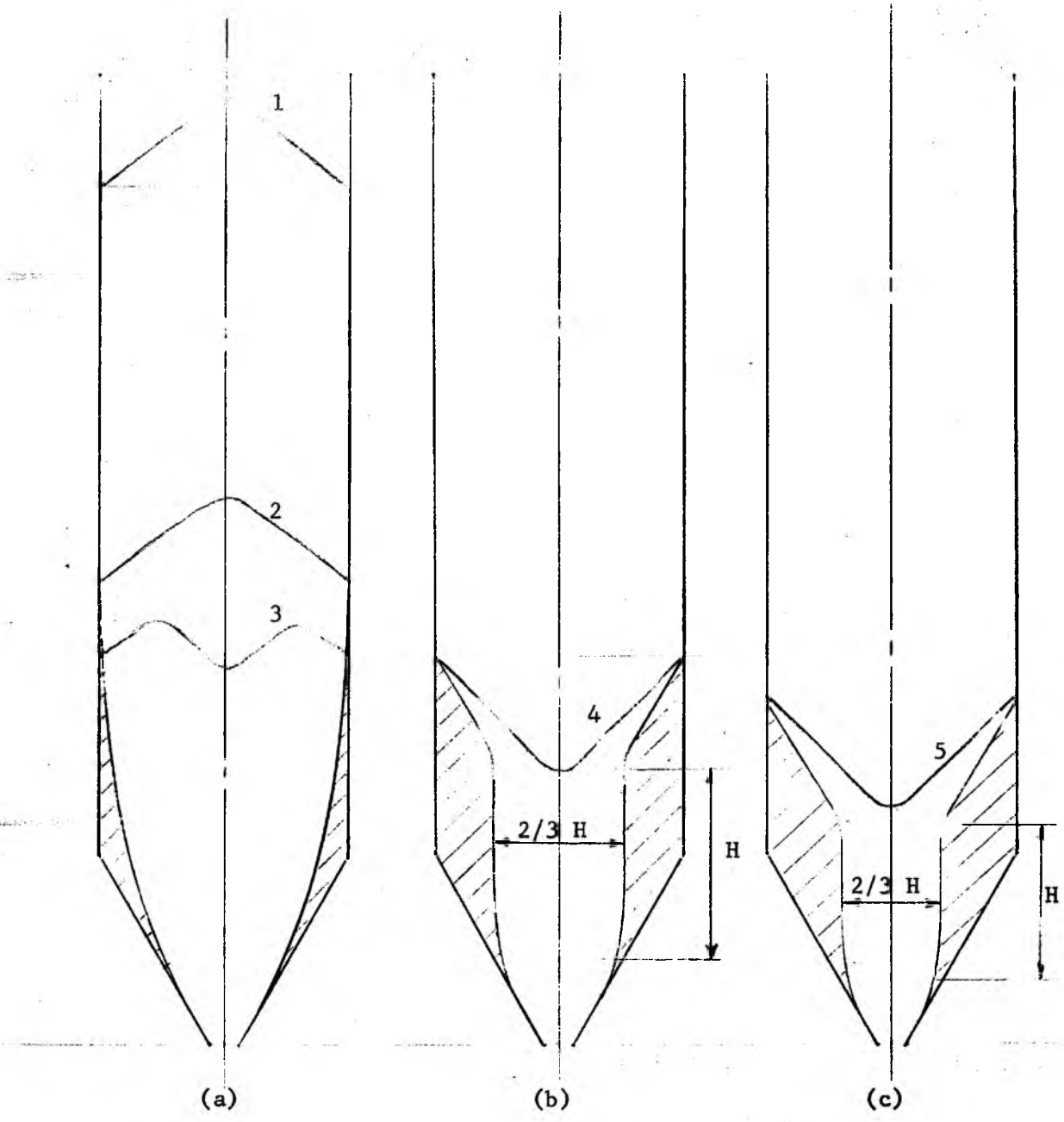

Fig. 118

Usual sequence in plane flow

effect the partition must be sufficiently strong to stand up to the difference between the pressures on each side. Should one side dome and the other empty out, the resultant pressure may be substantial.

Plug flow occurs when a channel either has no weak walls (storage pile, flat bottom bin) or the walls are not sufficiently steep and smooth for mass flow to develop. The solid then forms a channel within itself and flows within rough walls.

Conical flow within rough walls narrows down to values of θ' which are at most as given in Table 2, page 68. More often, θ' is zero and the channel is vertical: flow takes place in a vertical pipe. The diameter of such a channel approaches the largest dimension D of the outlet. That dimension is the diameter of a circular outlet, the diagonal of a square or rectangular outlet, etc. The transition from the shape of the outlet to the circular pipe occurs within a height of one to two diameters of the pipe. The transition is explained by the fact that, at the sides of an oblong outlet or of a square outlet, the condition of plane radial flow is approached and, hence, the angle θ' Fig. 121, is larger at the sides than at the ends or corners of the outlet where conical flow is approached.

As the solid flows along a rough wall, a degree of weakness develops along it. It is not practical to try to measure that weakness, nor does the effort seem to be justified. It is sufficient to estimate the value of the angle ϕ' by taking an average value# between

That value of ϕ' is probably approached from an original ϕ' corresponding to $\psi' - 90° = 45°$, at which flow starts without a velocity discontinuity along the wall. As flow continues, a weakness develops. If ratio V_1/F_c of the solid permits, flow may start along a slipline

δ and the value of ϕ' corresponding to $\psi' - 90° = 45°$. E. g. for $= 50°$, Fig. 82°, $\phi' = \frac{1}{2}(50 + 38) = 44°$.

Calculation of the dimensions of the outlet

The dimensions of the outlet of a channel should be sufficient to prevent: (a) doming, (b) piping, (c) particle interlocking, and to provide the required rate of draw.

(a) Doming. The critical value of the flowfactor ff is read from the appropriate chart, Figures 80 to 92, for the selected wall conditions (θ', ϕ'). In order that a solid does not dome at the outlet, the ratio V_1/F_c at the outlet must exceed the value of the critical flowfactor ff. The flowfactor is plotted together with the appropriate flow-function and the critical value of F_c is read at the point of intersection, Fig. 113. For circular outlets the diameter is then computed from the relation

$$B \geqslant 2F_c/A\,\gamma, \tag{158}$$

for square outlets, the side of the square is found from

$$B \geqslant 1.8\,F_c/A\,\gamma, \tag{159}$$

and for oblong outlets of ratio length to width in excess of 2.5 the width is found from

$$B \geqslant F_c/A\,\gamma. \tag{160}$$

The flow-function to be used in this analysis depends on the operation. For continuous operation, the instantaneous flow-function should be used; for intermittent operation, the time flow-function measured for the time interval of the stoppages should be used.

with a velocity discontinuity occurring from the beginning.

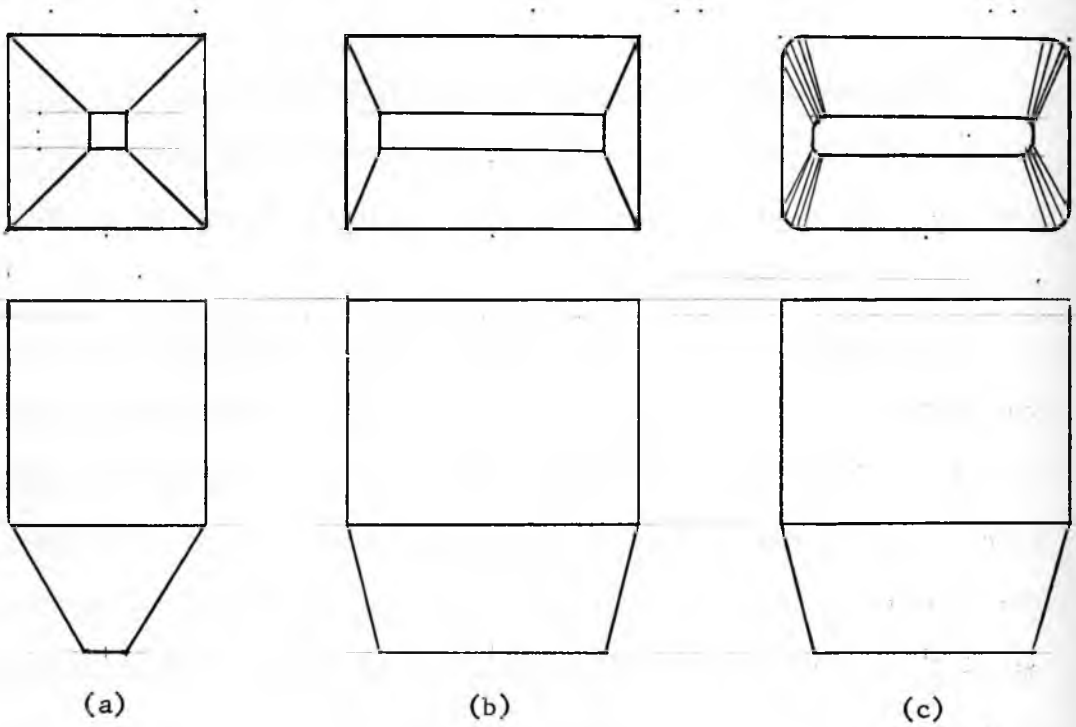

Fig. 119

Square and rectangular bins

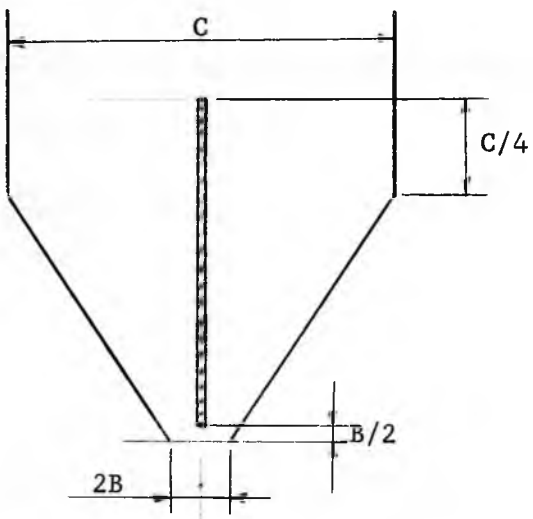

Fig. 120

Plane-flow hopper with a vertical partition

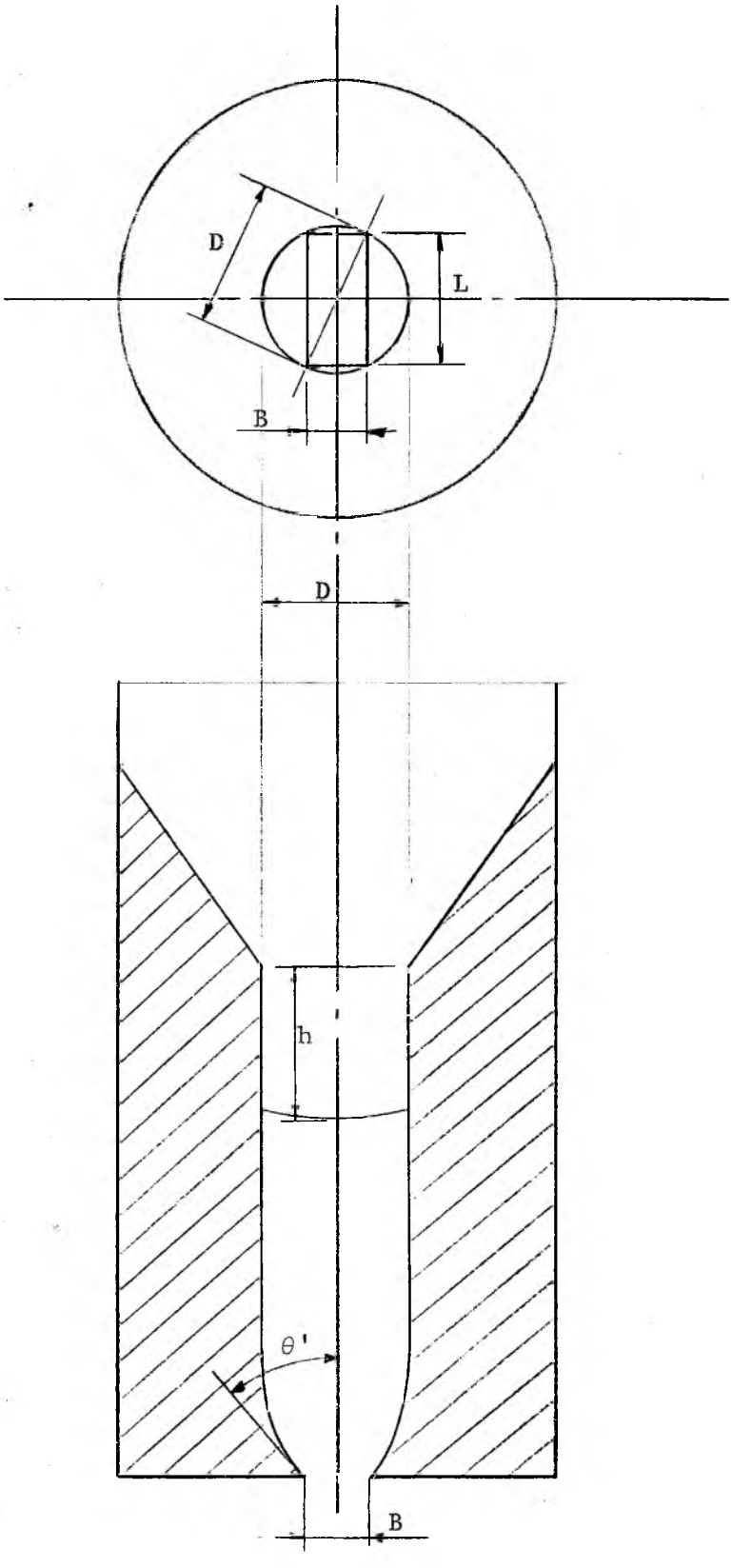

Fig. 121

Plug flow

The latter will sometimes call for an impractically large dimension. If, concurrently, the instantaneous flow-function gives a reasonable dimension, then the latter should be selected and a flow promoting device should be applied. Flow promoting devices are very effective in starting the flow of solids which pack when at rest but flow well under continuous operation.

For many solids, this analysis does not produce any minimum dimension of B, because the flow-function curve lies completely below the critical flowfactor line. On the other hand, the flow-function curve may be completely above the critical flowfactor line; this would indicate that the solid will not flow by gravity.

(b) Piping. This analysis applies to channels in which plug flow is expected. In plug flow, Fig. 121, as the solid is drawn out of the bin and the channel empties out, some height h of the vertical pipe may become exposed before a layer of the solid outside the pipe fails and slides into the channel. The height h at which the pipe fails depends on the diameter of the channel. For a given value of strength of the solid, the channel becomes less stable with an increase in diameter D. The channel is least stable when the diameter is infinite, which occurs in plane flow. The height of an exposed pipe should not be excessive because the failure and the drop of a deep layer of the solid creates considerable impact and may pack the solid within the pipe and cause doming. On the other hand, if the solid contains fines and is prone to aeration, such a drop may cause a flooding of the feeder. A large value of h may also lead to a significant

reduction in the live storage capacity. In an extreme case the empty pipe may extend through the full height of the bin, silo or pile.

Since the pipe circumscribes the outlet, the largest dimension of the outlet determines the diameter of the pipe. The largest dimension D is the diagonal of a square or rectangular outlet, or the diameter of a circular outlet. While the solid flows within the pipe, the solid outside the pipe is at rest and undergoes consolidation with time. Hence, the effect of time is of considerable importance in this analysis, and the time flow-function should be used in this part of the analysis.

Contours of critical flowfactor values are plotted in Fig. 96 as a function of the effective angle of friction δ and the angle of internal friction Φ_t, obtained from the time yield locus in the manner shown in Fig. 95. The applicable value of the flowfactor ff is now superposed over the appropriate time flow-function, Fig. 113, and the critical value of F_c is obtained at the point of intersection of the two lines. The required dimension D is found from the formula

$$D \geq \frac{F_c}{A\gamma} 4\left(\frac{d\omega}{dn}\right)_{n=1}. \qquad (161)$$

The factor $4(d\omega/dn)_{n=1}$ is plotted as a function of Φ_t in Fig. 122, line a.

For solids which are not affected by consolidation at rest, i.e. for solids whose time flow-function differs little (say, by less than 10%) from the instantaneous flow-function, a simpler analysis is offered. The value of the flowfactor is read off Fig. 97 for the appropriate value of the angle δ. Then the critical value of F_c is

obtained, as above, and the dimension D is found from eq. (161) with the factor $4(d\omega/dn)_{n=1}$ taken from Fig. 122, line b for the given value of the angle δ. It will be noticed that in these solids piping is unlikely to occur for $\delta < 54.5°$.

If the flow-function lies completely below the critical flowfactor, the solid will not pipe; on the other hand, if the flow-function lies completely above the critical flowfactor, or the point of intersection indicates an impractically large dimension D, piping will occur about the outlet unless the container is designed for mass flow.

(c) Particle interlocking. Solids which do not contain fines are usually free flowing and the size of the outlet needs to be only large enough to assure the required rate of flow without interlocking of the particles. It is not possible to specify outlet dimensions which will apply to all solids under all circumstances. The guide shown in Fig. 123 applies to particles of uniform shape, but not to chips, flakes and fibres. d is the intermediate dimension of the largest particles; the area A and the dimension B of the outlet should exceed the plotted values.

Influence of dynamic over-pressures

So far, the developed flow criteria have neglected all pressures due the acceleration or deceleration of the flowing particles. It is of course inherent in the theory of plasticity, which is the basis for this work, to neglect the velocity terms and to apply the equations of equilibrium instead of the equation of momentum in the development of

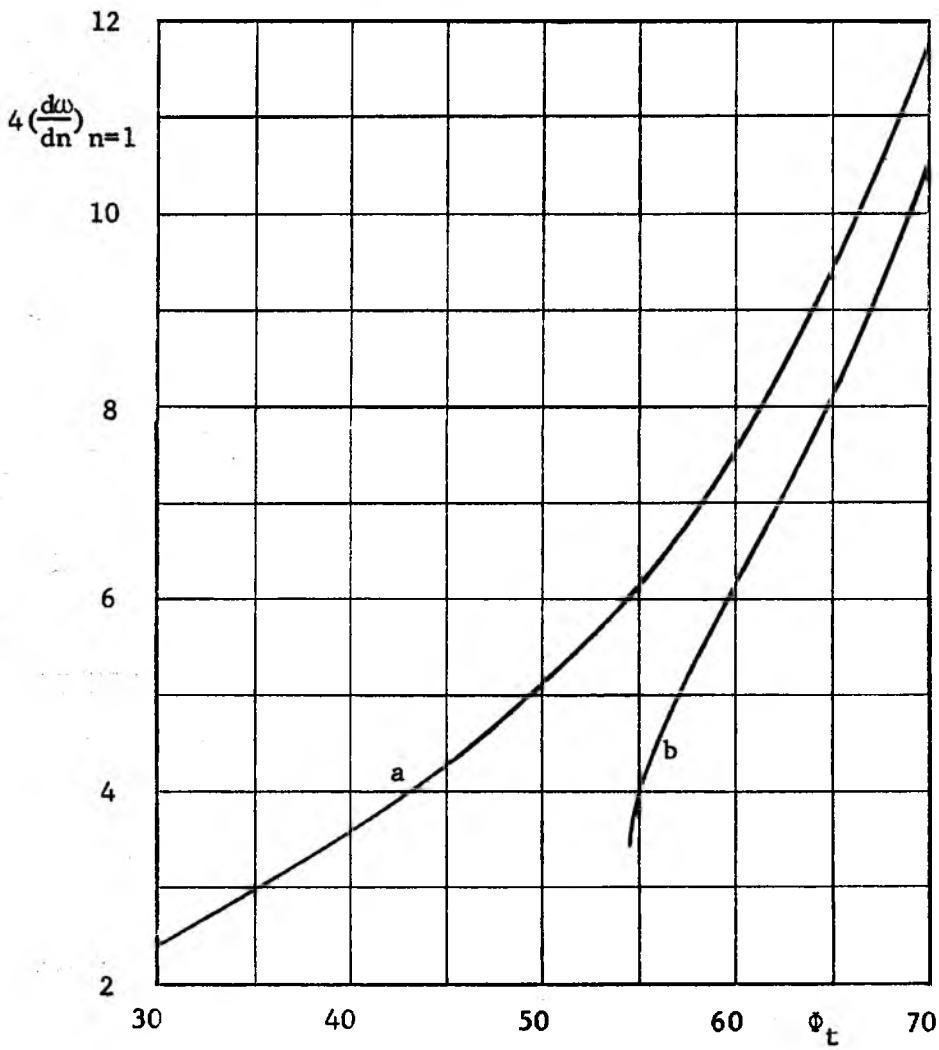

Fig. 122

Factor $4(d\omega/dn)_{n=1}$

of the stress field. This implies that the velocities throughout the mass are low so that the accelerations which exist in steady state flow be negligible. Steady state flow is an ideal which is approached by a suitable design of the channel and of the feeder but which is never achieved completely. For one thing, flow has to be started and stopped, and that involves acceleration and deceleration.

Non-steady flow is also prevalent in vertical channels. Hence, it is prevalent under most conditions of plug flow. Another condition leading to non-steady mass flow can be inferred from the plots of the conical fields. These fields extend only within well defined regions in the (θ', ϕ') coordinates. Outside of these regions steady state flow cannot occur. If the slope of the wall θ' and the frictional conditions at the wall ϕ' are such that point (θ', ϕ') lies close to the bound of the field, then it can be expected that a slight momentary change in ϕ' may move the point over the bound, thus momentarily stopping flow. Many solids exhibit a slip-stick effect: their angles of friction vary over wide limits. These solids have a strong tendency for non-steady pulsating flow.

The accelerations and decelerations superimpose dynamic pressures over the consolidating pressures of steady state flow, causing an additional consolidation of the solid and developing additional strength in it. These dynamic pressures become more pronounced as the velocities of the particles increase. For a given rate of flow of a solid through a channel, the velocities increase with the reduction of the cross-sectional area of the channel. Hence, as the area decreases toward

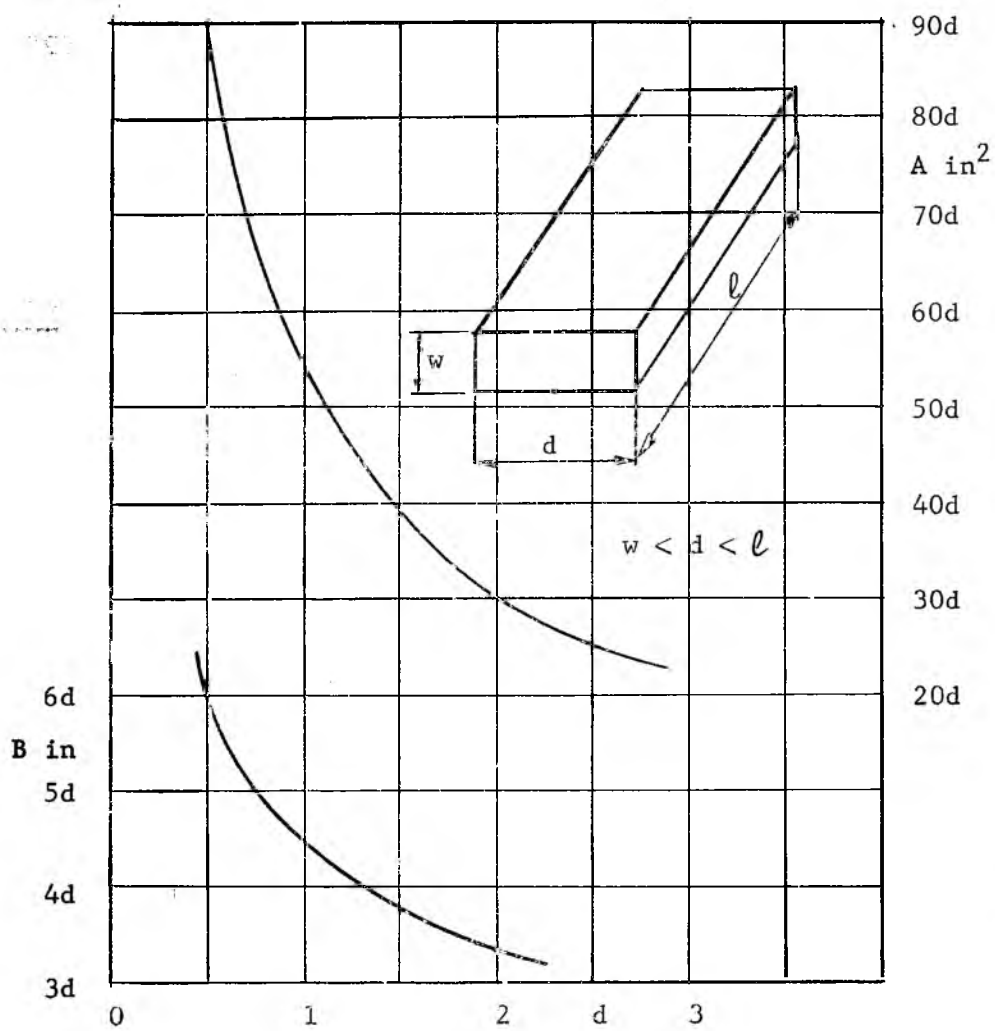

Fig. 123

Dimensions of outlets to avoid particle interlocking

the outlet, the dynamic pressures increase while, simultaneously, the pressures due to steady flow decrease (see eq.102). The relative influence of the dynamic effect thus mounts rapidly with the approach to the outlet of the channel.

This explains why flow through small, square or round orifices is often erratic and unreliable. These conditions often lead to free fall and the development of excessive velocities. It also explains why the scaling down of a channel exaggerates the disturbances of flow and why the flow criteria cannot be determined by small scale models. On the other hand, if a channel is equipped with an adequate feeder and the velocities are low, non-steady flow will produce but negligible dynamic over-pressures.

A quantitative estimate of the influence of the velocity of flow is provided by assuming that a solid flowing at the outlet with an average velocity u is stopped in a time interval t, at a uniform rate of deceleration. Assuming that the vertical component of the velocity closely approaches u, the total vertical body force is

$$\gamma(1 + u/gt)$$

The consolidating pressure σ_1 is increased by a factor of

$$1 + u/gt \qquad (162)$$

and the critical flowfactors should also be increased in that ratio. Since the duration of these effects is brief, these increased flowfactors should be used in conjunction with the instantaneous flowfunction.

Impact and vibration. Beside the pressures of steady flow, a solid

may undergo consolidation as a result of impact pressures which occur during the charging of the solid into a container. This can be particularly critical when charging the solid into an empty bin, and when the falling solid hits the outlet area directly. In cohesive solids, these conditions should not be allowed to occur. Even in easy-flowing solids it is advisable to design the trajectory so that direct hits in the outlet area do not take place and to provide a shelf in the stream of the falling solid to distribute the impact over a wide area of the container. This consolidation can be especially severe if the solid contains coarse particles which carry high momentum and exert severe localized consolidating pressures at the point of impact. Since the duration of impact pressures is brief, the instantaneous flow-function should be used in estimating their effect.

Continuous vibration of a container will often lead to flow difficulties because vibration tends to rearrange the particles of the solid and increase its density and its strength. So far as possible, containers should not be supported from structures which also carry heavy vibrating equipment. The use of vibrators to provide flow is discussed in the next section.

Flow promoting devices

Since this work is on the subject of gravity flow of solids, devices such as extruders, used to cause the flow of solids which are inherently unsuited for gravity flow, will not be discussed. A solid is not suitable for gravity flow if its instantaneous flow-function lies above the minimum critical flowfactor applicable to the solid. For instance, a solid of $\delta = 50°$ has a minimum flow-factor of about 1.035 in plane flow for $\phi' = 20°$, Fig. 82. If the ratio V_1/F_c of the instantaneous flow-function of the solid is less than this value for the practical range of pressure $\sigma_1 = V_1/A$, then the given solid is not suitable for gravity flow. If the instantaneous flow-function lies below the minimum critical flowfactor then the solid is suitable for gravity flow even though its time flow-function may lie above the flowfactor. In the latter case, the application of a flow promoting device is in order.

It is not proposed to discuss the respective merits of all the available devices but to describe those combinations of hoppers and flow promoting devices which seem particularly well suited to handle certain classes of solids. Mass flow and plug flow will be considered separately.

In a mass-flow bin, the solid slides along the walls and the introduction into the hopper of any device, like an air pad, pulsating panel, planetary arch breaker, would destroy the flow pattern and is not acceptable. Flow in such a bin can be effectively promoted by the application of either a vibrator or an air (or other gas) pressure

gradient. Since, by assumption, the discussed solids need promotion only at the start of flow, these devices are not used as flow is proceeding. A vibrator is particularly effective in plane-flow, asymmetric hoppers when applied to the vertical wall. It readily causes the failure of the dome along a vertical plane through the solid, Fig. 124, after which the solid slides down along the inclined wall. In a symmetric, plane-flow hopper with a vertical partition, Fig. 120, vibrators can be mounted within the partition. The effect will be the same as described above for the asymmetric hopper.

If the top of the bin can be made air-tight for the starting of flow, then air under pressure can be applied at the top of the bin. Air will flow down through the solid causing an air pressure gradient which adds to the forces of gravity and promotes the failure and flow of the doming mass. Since the required pressure is usually comparatively low (a few pounds per square inch), the air density can be considered constant and the following simple analysis indicates the effectiveness of this method and provides a way to calculate the required pressure and consumption of air.

Consider the conical bin shown in Fig. 125. The gradient of pressure in the hopper is

$$\frac{dp}{dx} = \frac{k}{x^2} \qquad (e)$$

where k is a constant. At the bottom of the dome, $x = h$, the pressure is atomospheric, $p = p_o$. The pressure at the transition, $x = h_1$, is obtained by integration

$$p_1 = p_o + k(\frac{1}{h} - \frac{1}{h_1}).$$

In the vertical portion, the gradient of pressure is

$$\frac{p_2 - p_1}{h_2} = \frac{k}{h_1^2}, \tag{f}$$

and the gage pressure applied at the top of the bin is obtained by the elimination of p_1

$$p_2 - p_o = k(\frac{1}{h} + \frac{h_2 - h_1}{h_1^2}). \tag{g}$$

The pressure gradient, eq.(e), at the bottom of the dome, x = h, is now expressed as a multiple, α, of the bulk weight γ of the solid, thus

$$\alpha\ \gamma = \frac{k}{h^2}, \tag{h}$$

and k is eliminated in the expression (g), yielding

$$p_2 - p_o = \alpha\ \gamma\ h(1 + \frac{h_2 - h_1}{h_1^2}\ h). \tag{163}$$

In the design of the hopper, the critical flowfactor ff is divided by a factor of $1 + \alpha$. α must be sufficiently large so that

$$\frac{ff}{1 + \alpha} \leq \frac{V_1}{F_c} \tag{164}$$

for all values of h within the hopper. The air pressure gradient is very effective. For instance, for $h_1 = h_2$, h = 6 ft., γ = 50 pcf, the gage pressure at the top of the bin necessary to obtain $\alpha = 1$ is computed from eq.(163) at $p_2 - p_o$ = 300 psf = 2.08 psi. This small gage pressure justifies the assumption of a constant air density and

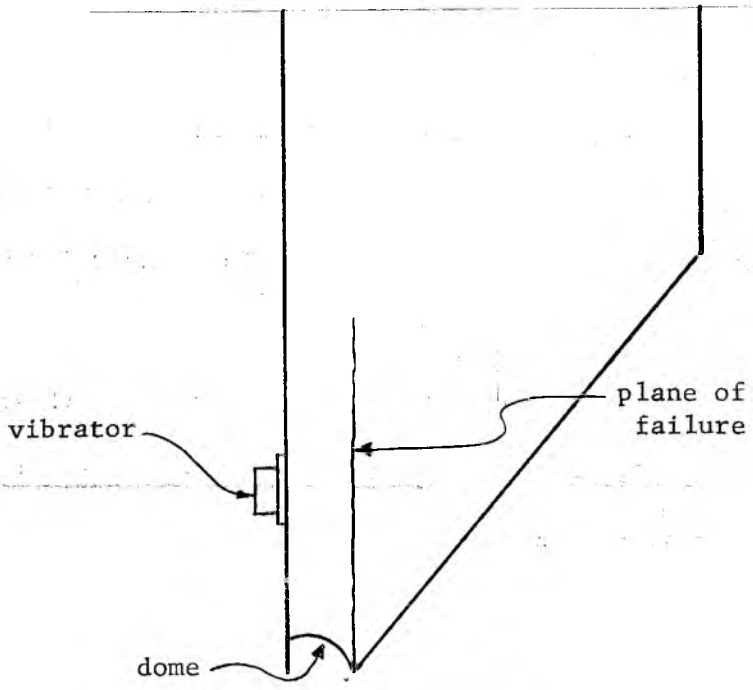

Fig. 124

Vibrator at a vertical wall of a plane flow hopper

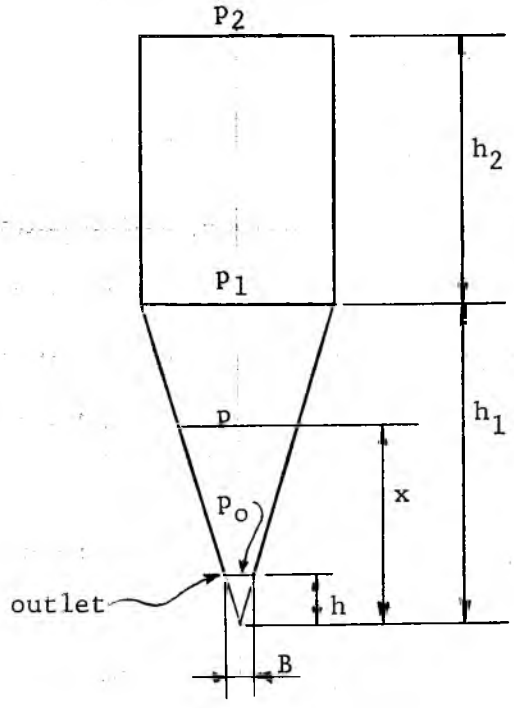

Fig. 125

Air pressure gradient applied to promote flow

the resultant relation (e).

The rate of flow of air V[cfm], necessary to sustain the required pressure p_2 at the top of the bin, depends on the resistance ρ[lb min ft^{-4}] of the solid to the flow of air [27, 28, 29]. The relation is

$$V = \frac{A}{\rho} \frac{dp}{dx}, \qquad (i)$$

where A is the cross-section of the channel at which there is a pressure gradient dp/dx. Consider the vertical portion of the bin. From eq.(f), the pressure gradient is

$$\frac{dp}{dx} = \frac{k}{h_1^2}.$$

Eliminate k by means of eq.(h) to obtain

$$\frac{dp}{dx} = \alpha \gamma \left(\frac{h}{h_1}\right)^2,$$

and the rate of flow, eq.(i) becomes

$$V = \frac{A}{\rho} \alpha \gamma \left(\frac{h}{h_1}\right)^2. \qquad (165)$$

In this equation A[ft^2] is the area of the horizontal cross-section of the vertical portion of the bin. The resistance to flow ρ varies within wide limits from solid to solid. For powders, the resistance is high, the rate of flow is small, and the method of the air gradient is quite attractive.

An ingenious method of increasing the effective width B of a screw feeder is to place the screw in a trough which is independent of the hopper and connected to the hopper by means of short flexible walls, and to vibrate the trough with the screw. The vibrations promote

the flow of the solid at the outlet without consolidating the solid in the bin.

In plug-flow bins, any means that will break up a doming or piping solid and start flow are acceptable [30]. The usual methods are: air pads, air jets, pulsating panels, knockers, vibrators, arch breakers in the shape of stars, paddles, or planetary arms. In view of the irregularity of plug flow, the selection and application of these devices is likely to remain an art. Vibrators are effective in these bins when used for final clearance. They are also effective in starting flow, if installed in a vertical partition, but they should only be used briefly, especially, if the instantaneous flow-function of the solid is close to the critical flowfactor; otherwise, vibration will tend to pack the solid.

Examples of design for flow

1. A fine solid whose flow properties are given in Fig. 126 is to be stored in a quantity of 100,000 lb. The instantaneous flow-function curve, $F_c(V_1)$, lies below a flowfactor of 2.5; the time curve, $F_c(V_1,t)$, lies higher. A mass flow bin with a conical hopper is selected. From both, Figures 86 and 87, $\theta'_{max} = 20°$ for $\phi' = 25°$. Select $\theta' = 15°$, then the flowfactors at point $\theta' = 15°$, $\phi' = 25°$ are respectively, 1.26 and 1.13 for $\delta = 40°$ and $50°$. For $\delta = 48°$, interpolation gives ff = 1.16. In eq.(158) A = 1/13 sq ft and the diameter of the outlet $B \geqslant 2 \times 1.25 \times 13/19.2 = 1.7$ ft.

The point of intersection of the flow-function with the critical flowfactor lies at some distance from the lower test point of the flow-function, hence, there is some uncertainty about the shape of the curve at the point of intersection and about the exact value of F_c. It is, therefore, advisable to increase the opening to, say, B = 2.0 ft.

The selected bin is shown in Fig. 127.

2. Another fine solid with flow properties given in Fig. 128 is to be stored in a quantity of 100,000 lb. Here $\delta \approx 40°$. The time flow-function is a straight line and coincides with a critical flow-factor of 1.4. A mass flow bin with a conical hopper is selected. For $\delta = 40°$, Fig. 86 applies. Since $\phi' = 19°$, the solid will flow within a range of hopper slopes θ' from 8° to 28°. For $\theta' = 0$, ff = 1.65, hence, the solid is likely to dome across a vertical channel. The bin should have either no vertical portion, or only a short vertical portion, as shown in Fig. 129, otherwise doming will occur from the transition up.

Angle θ' is selected at 23°. This analysis does not determine any minimum for the diameter of the outlet: if the solid flows at all, it flows through any orifice, but, of course, the orifice has to be sufficient to provide the required rate of flow, prevent interlocking and allow for dynamic effects. Hence it, probably, should not be less than 6 inches.

3. A micron size, fine solid of flow properties given in Fig. 130 is to be stored in a quantity of 30,000 lb. In view of the high value of the angle ϕ', the maximum θ' in a conical hopper would be only about 5°, hence a slot outlet is selected with side slopes $\theta' = 15°$. The critical flowfactors then are: 1.14 for $\delta = 50°$ and 1.04 for $\delta = 60°$, Figures 82 and 83 respectively. At the origin of the flow-function, δ is estimated at 54° and the value of the flowfactor for that δ is interpolated at ff = 1.10. The analysis does not define a width B. A bin of the type presented in Fig. 114 (e) is selected and the dimensions are shown in Fig. 131. The volume of the bin is computed on the assumption that, at the time of charging into the bin, the density of the solid is 10 pcf, i.e. one half of what it is in a consolidated state. This allows for a rapid charging of the fully aerated solid. The dimensions of the outlet are determined by the required rate of flow.

4. A minus 1/2 inch ore to be stored with a minimum of size segregation. The flow properties are given in Fig. 132 and the capacity of the bin is to be 200 tons = 400,000 lb. The angle of friction between the solid and the wall, ϕ' is taken with an allowance of 5° for

possible rusting, so that $\phi' = 35° + 5° = 40°$. A mass flow bin with an oblong outlet is selected. The side walls are taken from Fig. 117 at $\theta' = 25°$. For the point $\theta' = 25°$, $\phi' = 40°$, the values of the flow-factor are, respectively, 1.40 and 1.24 for $\delta = 50°$ and 60°. For $\delta = 56.5°$, the interpolated value is ff = 1.34. Since the ore will be subject to impact, a safety factor of 15% is added to the flowfactor, thus, ff = 1.34 x 1.15 = 1.54. The minimum width of the slot is obtained from eq. (156): B = 10.8 x 13/141 = 1.0 ft. The ends of the hopper are taken vertical, because at $\phi' = 40°$, $\theta'_{max} \approx 0$ in Figures 87 and 88. The bin is of the chisel type, Fig. 114 (f).

In order to minimize segregation, the level of the ore in the bin is allowed to fluctuate only within the top 16 feet shown in Fig. 133, and only that part of the mass is used in the calculation of the storage capacity.

5. A metal concentrate is to be stored in a large quantity. Segregation is not a problem. The flow properties are given in Fig. 134. A storage pile with a short hopper and a rectangular outlet is selected, Fig. 135. The end walls are vertical, the side walls are chosen at $\theta' = 25°$. Allowing 5° over the measured angle of friction, $\phi' = 43°$. From Fig. 83, the flowfactor is ff = 1.35 and the width of the outlet is computed at B = 6.0 x 13/137 = .57 ft. The hopper is extended a height of 5 ft, so that the width at the top is B = 5.23 ft. For that width, the value of F_c is 5.23 x 140/13 = 56.3. The point of intersection of this value of F_c with the flow-function is outside the figure, but it is estimated that, at the point of intersection, ff > 4. Above the hopper the solid flows

within rough walls. The angle of friction ϕ' along the rough walls is not known accurately but it is certain that, as the solid flows along the walls, the walls become somewhat smoother. Angle ϕ' is estimated by taking the average value between δ and the value of ϕ' for $\psi' - 90° = 45°$. This yields $\phi' = 44°$ and $50°$ for $\delta = 50°$ and $60°$, respectively. For these values of ϕ' a flow-factor in excess of 4 allows a maximum value of θ', which is between $40°$ and $46°$ depending on the exact value of δ.

The analysis for no-piping gives a maximum dimension for the channel. This dimension determines the diagonal of the channel at the top of the hopper since mass flow is assumed within the hopper. The critical flowfactor is read from Fig. 96 for $\delta = 60°$, $\Phi_t = 45°$ at ff = 2.3. This determines $F_c = 27.8$ and the diagonal is computed from eq. (161) in which $4(d\omega/dn)_{n=1} = 4.3$ from Fig. 122, line a, thus: $D = 27.8 \times 4.3 \times 13/142 = 11.0$ ft. Hence the length of the hopper and of the slot is: $L = \sqrt{11.0^2 - 5.23^2} = 9.7$ ft. The stable slope of the dead solid is estimated, at some height above the hopper, at $50° - \delta/2 = 50° - 20° = 30°$.

6. Storage of minus 8 inch unscreened coarse ore. The flow properties are given in Fig. 136. The selected design is shown in Fig. 137. The ore is stored in a flat bottom pile with continuous slot outlets and short hoppers. The angle of friction of the hoppers is increased by $5°$ to allow for rusting, hence, $\phi' = 35° + 5° = 40°$. The slope of the hoppers is taken at $\theta' = 30°$, therefore, ff = 1.6, from Fig. 82. The width of the slot at the outlet is $B = 30 \times 13/137 = 2.85$ ft

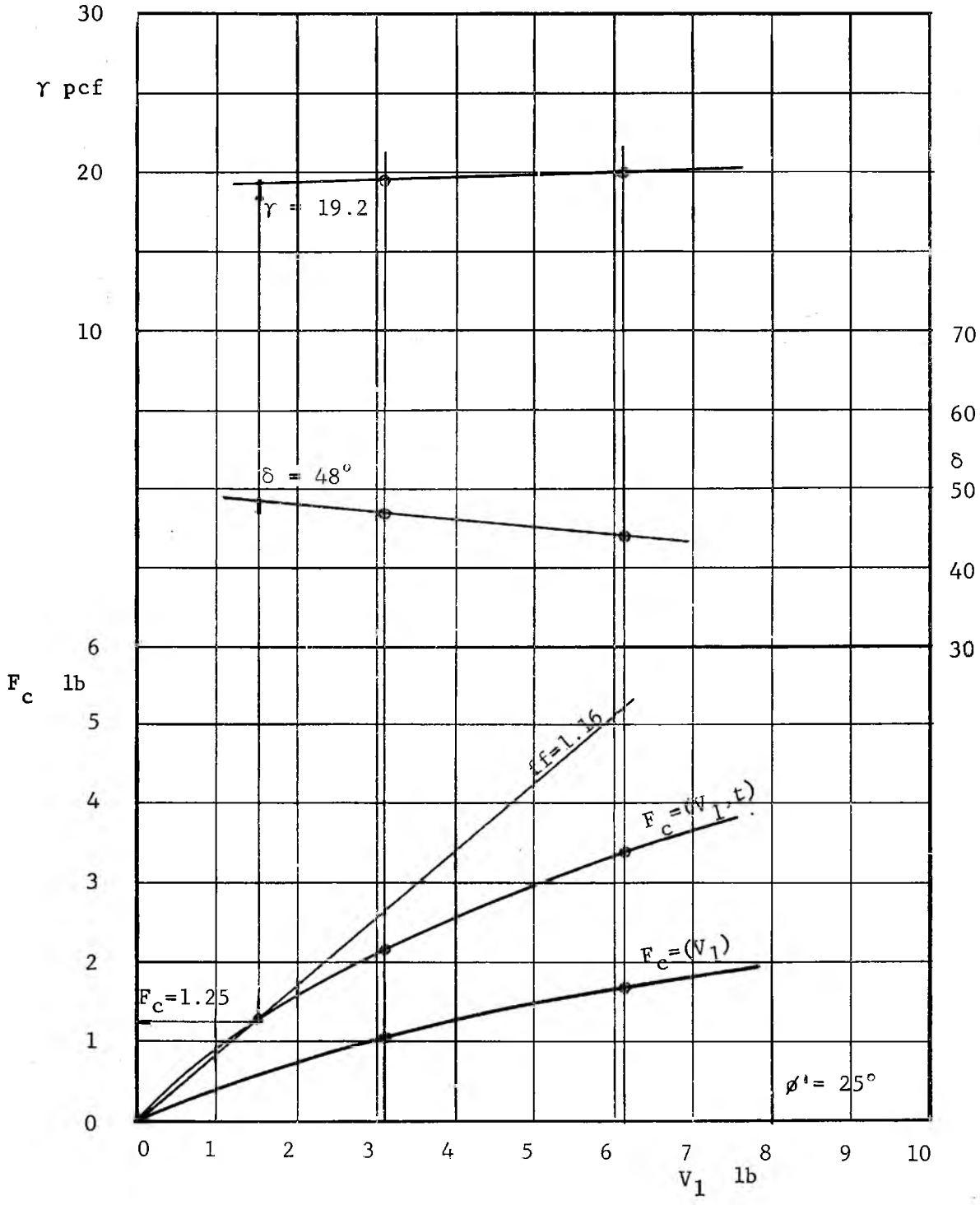

Fig. 126

Example 1, Flow properties

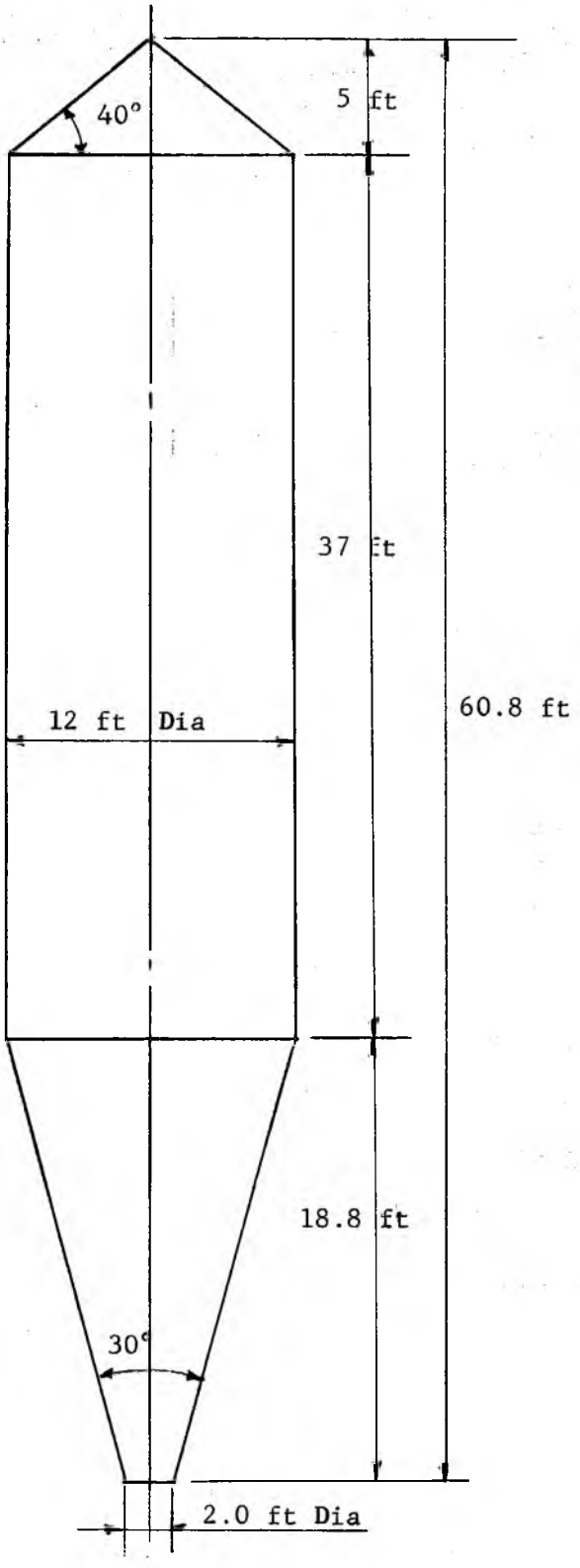

Fig. 127

Example 1, Selected bin

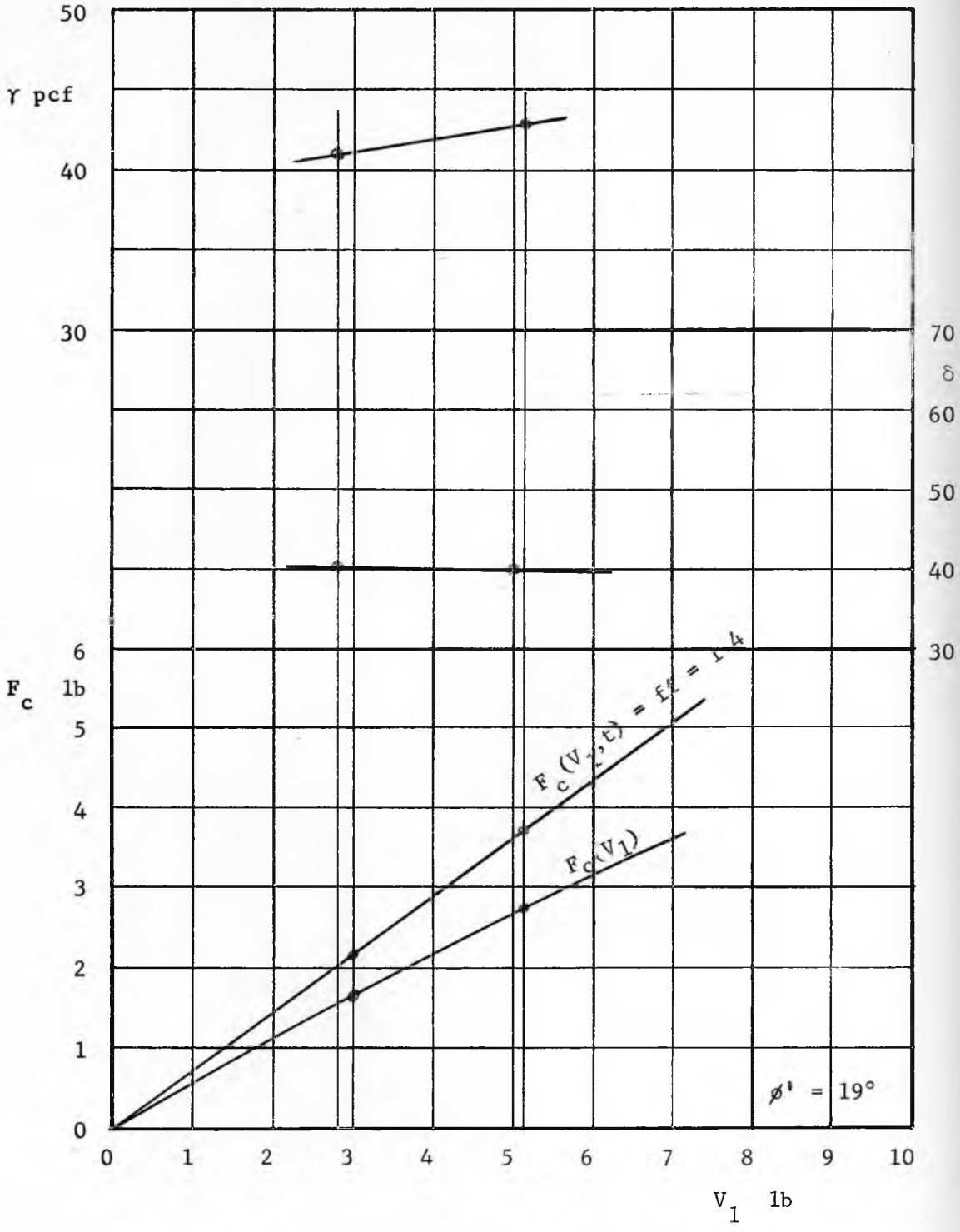

Fig. 128

Example 2, Flow properties

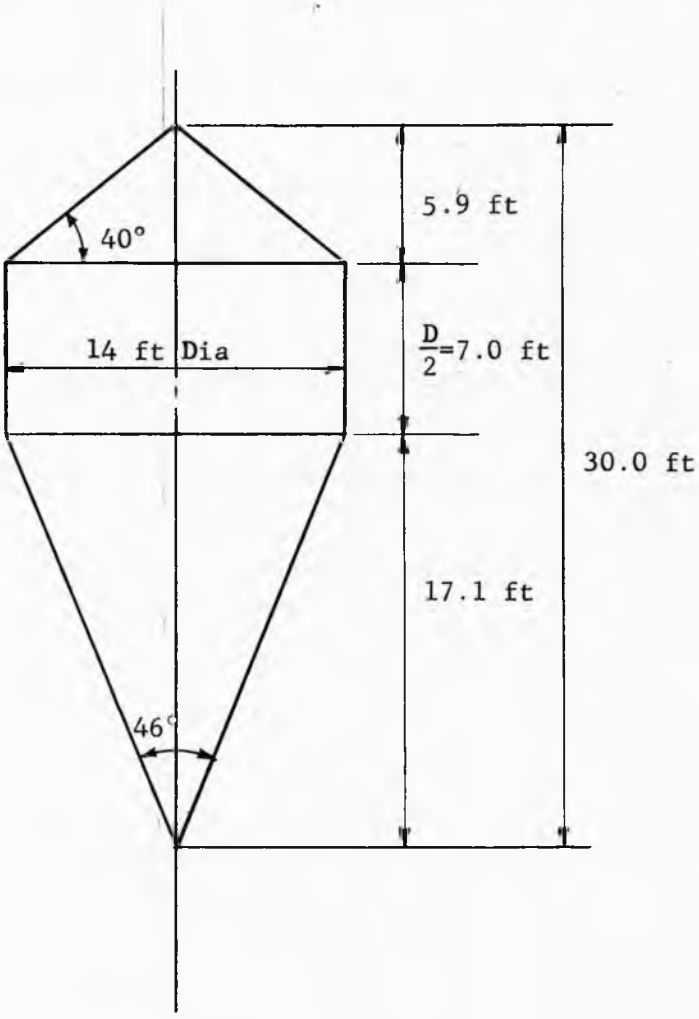

Fig. 129

Example 2, Selected bin

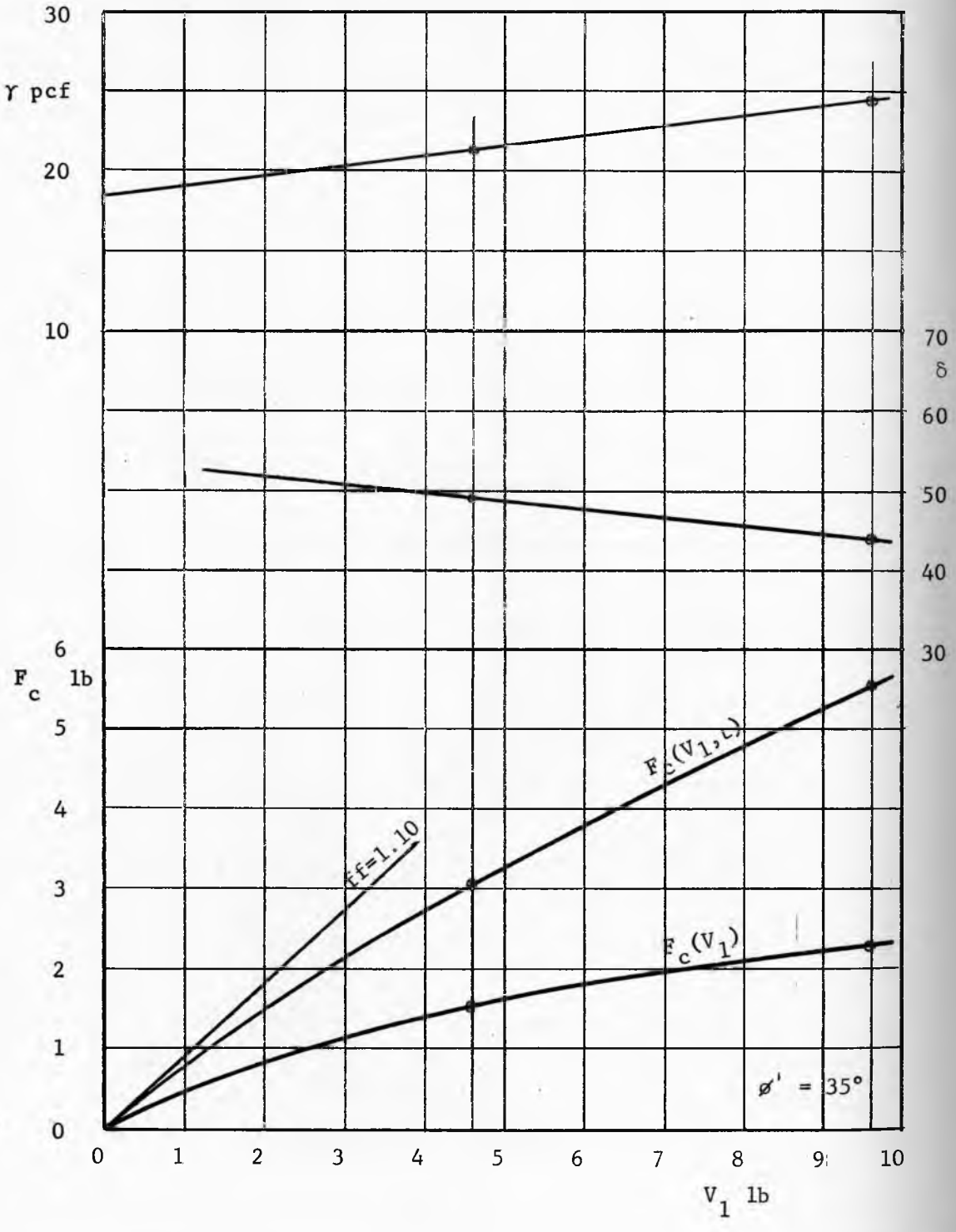

Fig. 130

Example 3, Flow properties

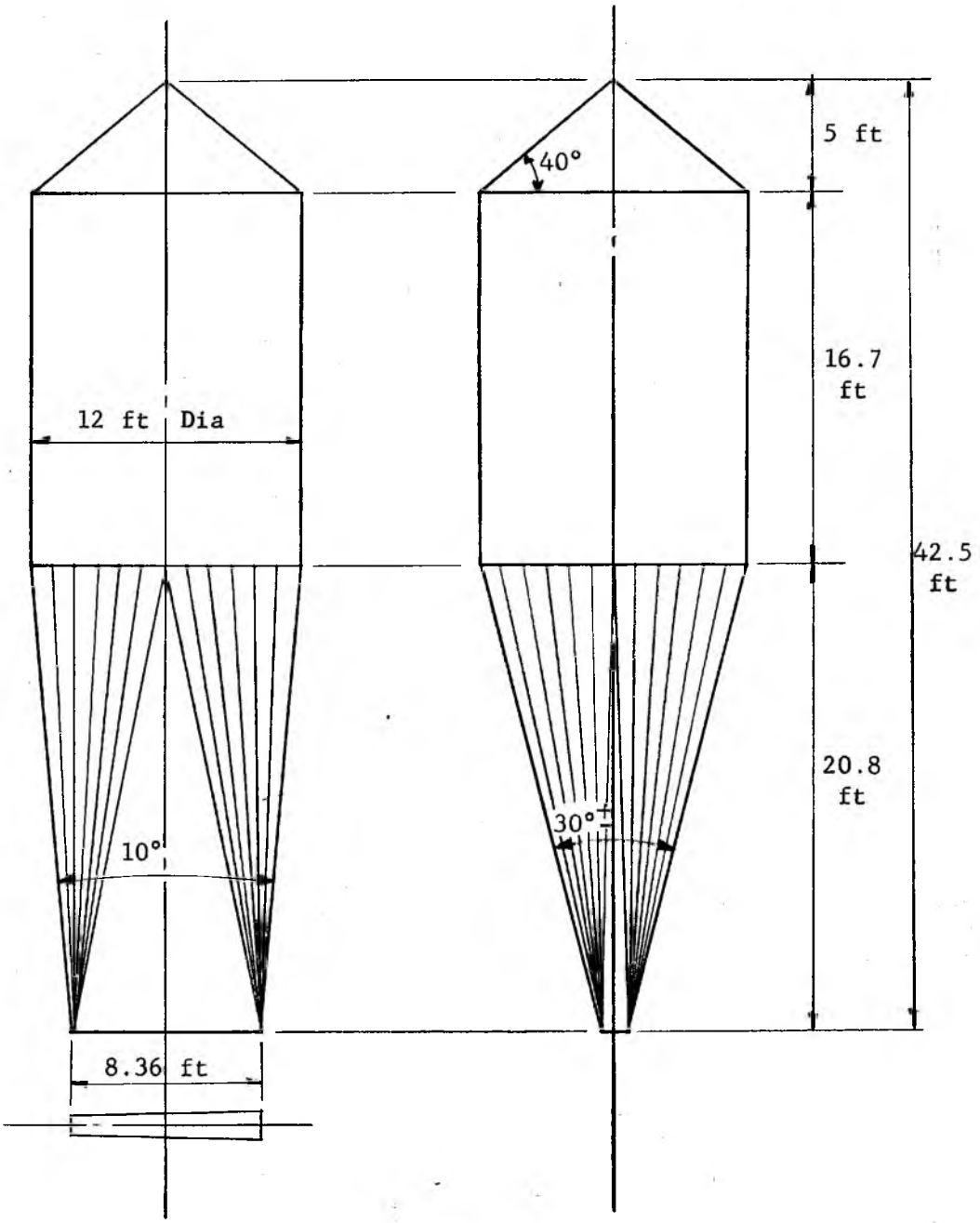

Fig. 131

Example 3, Selected bin

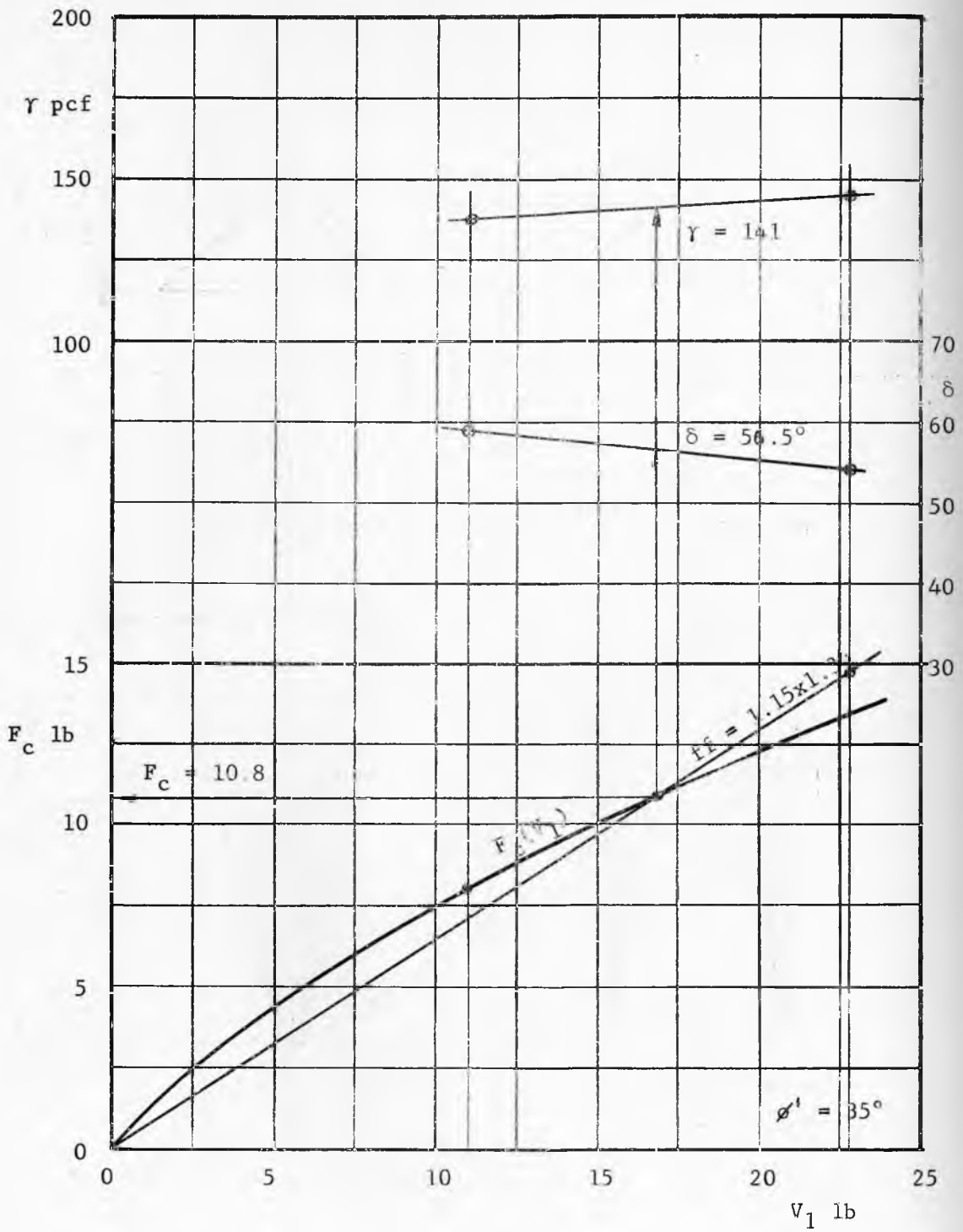

Fig. 132

Example 4, Flow properties

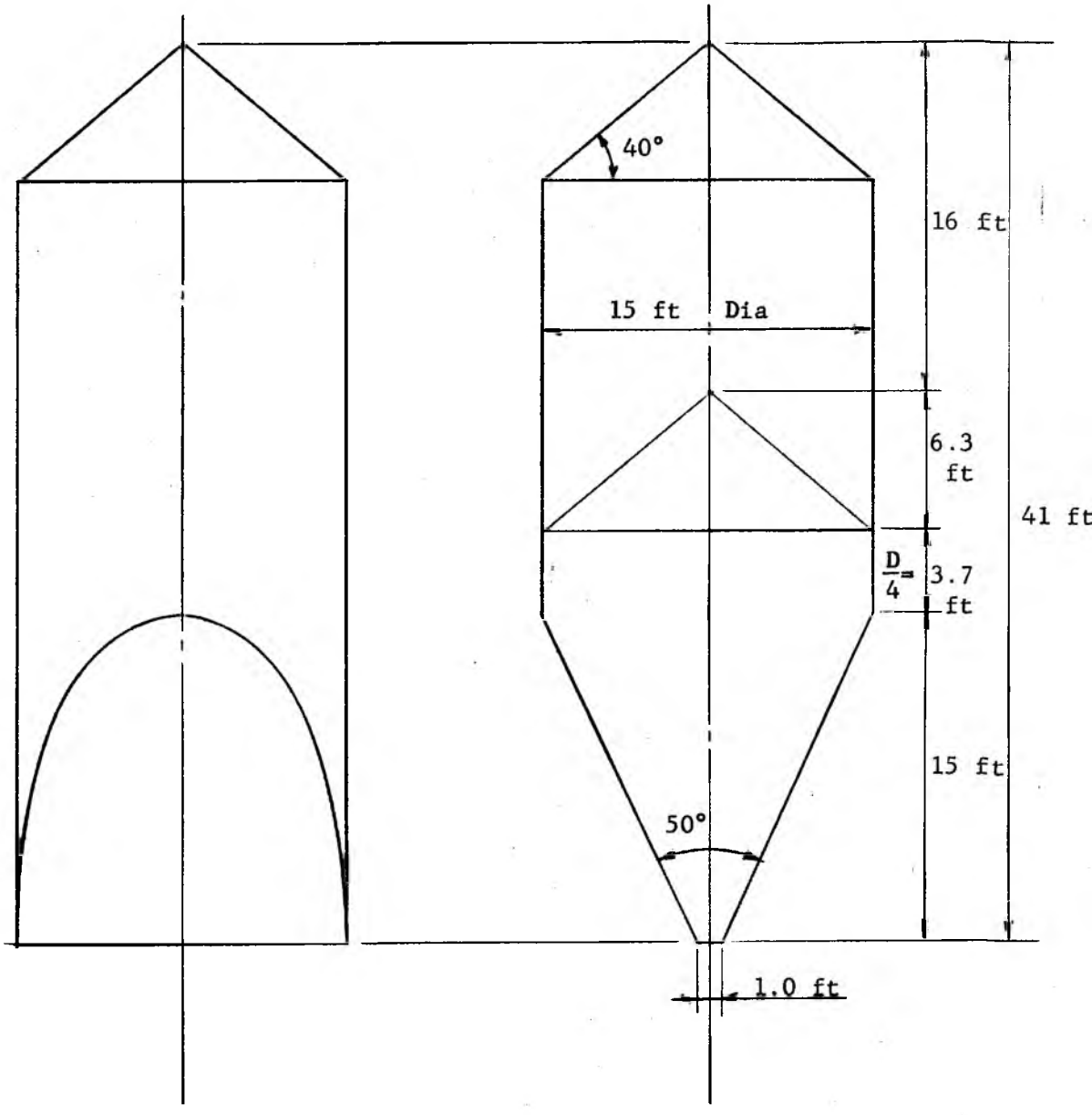

Fig. 133

Example 4, Selected bin

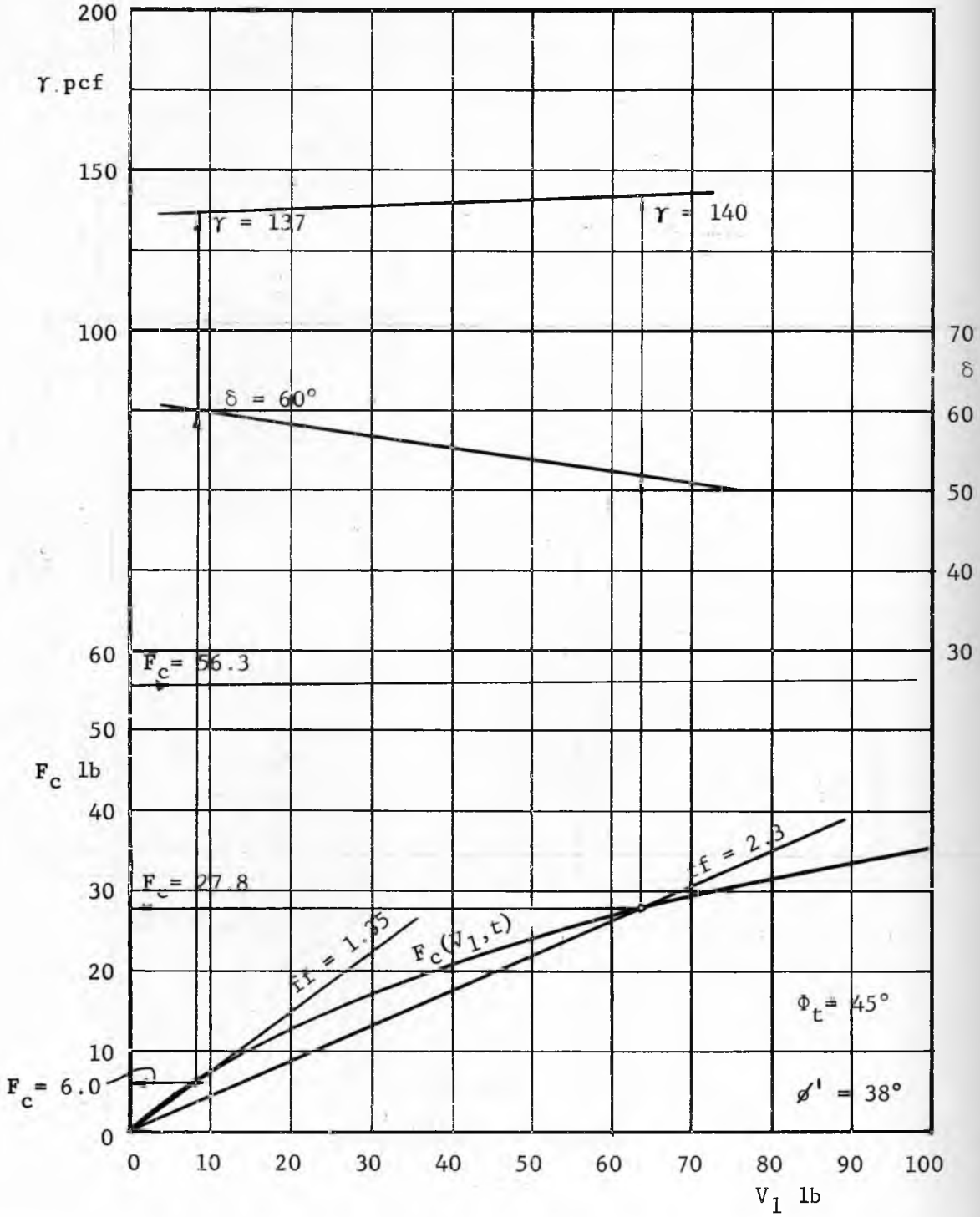

Fig. 134

Example 5, Flow properties

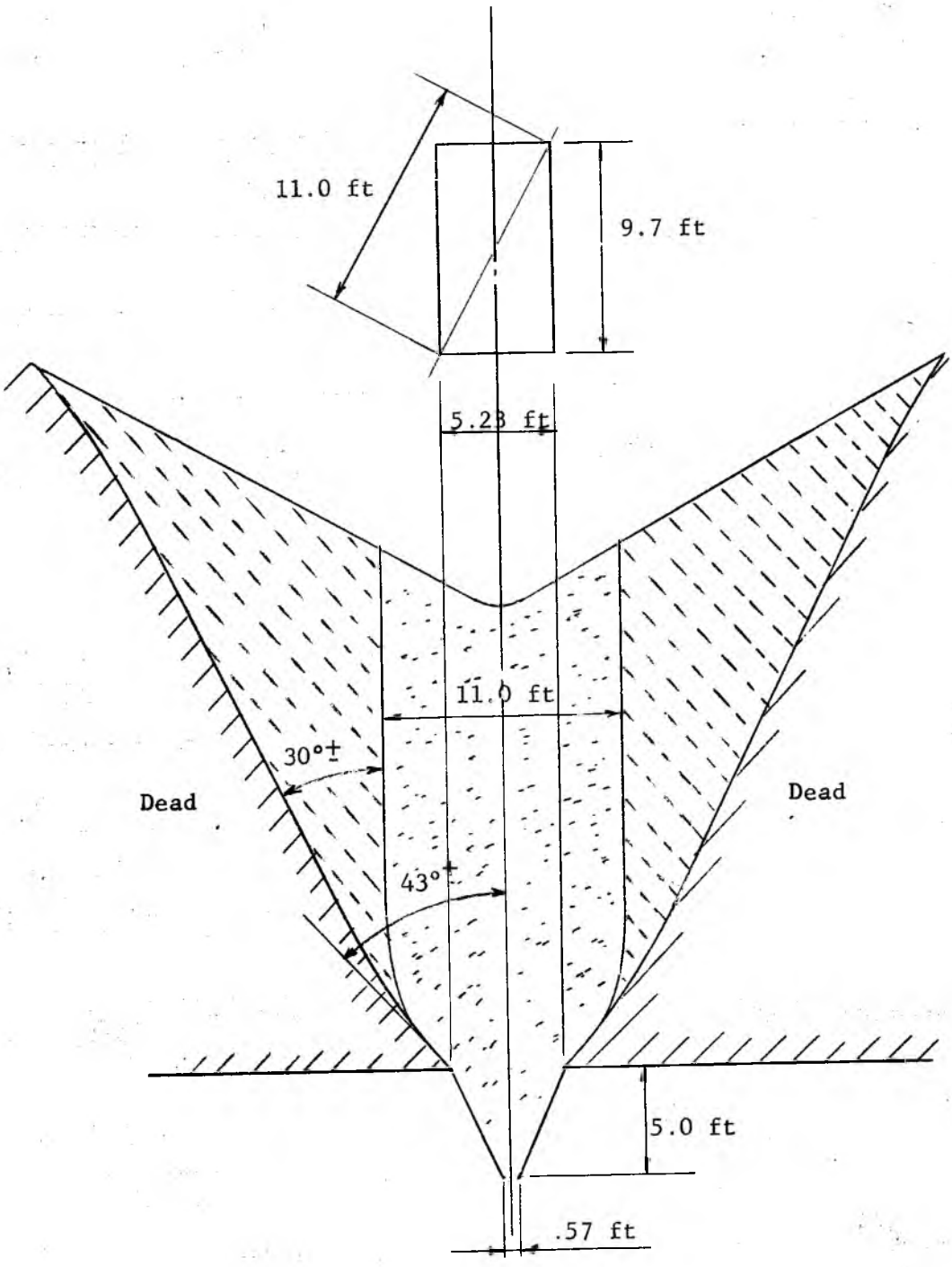

Fig. 135

Example 5, Selected hopper

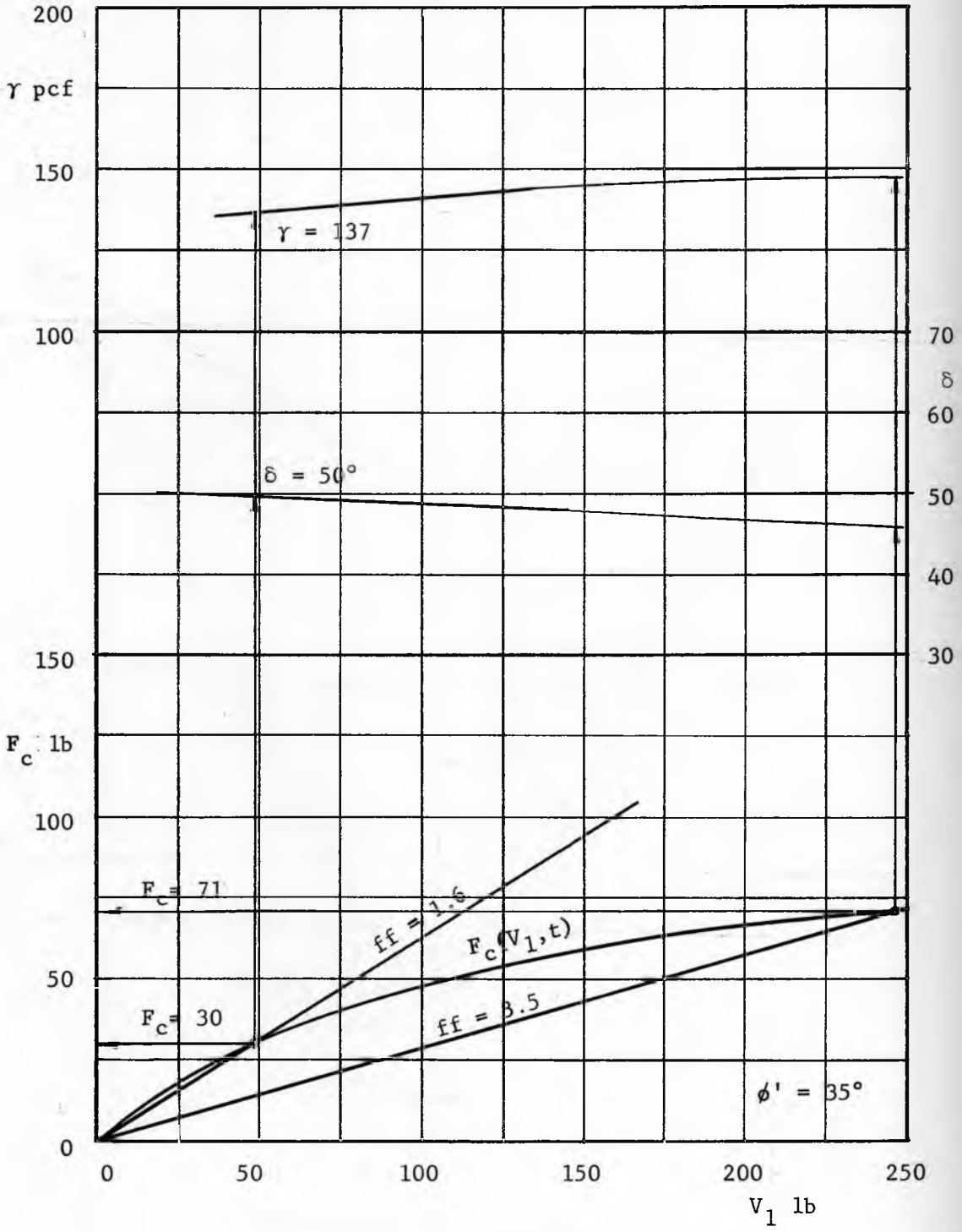

Fig. 136

Example 6, Flow properties

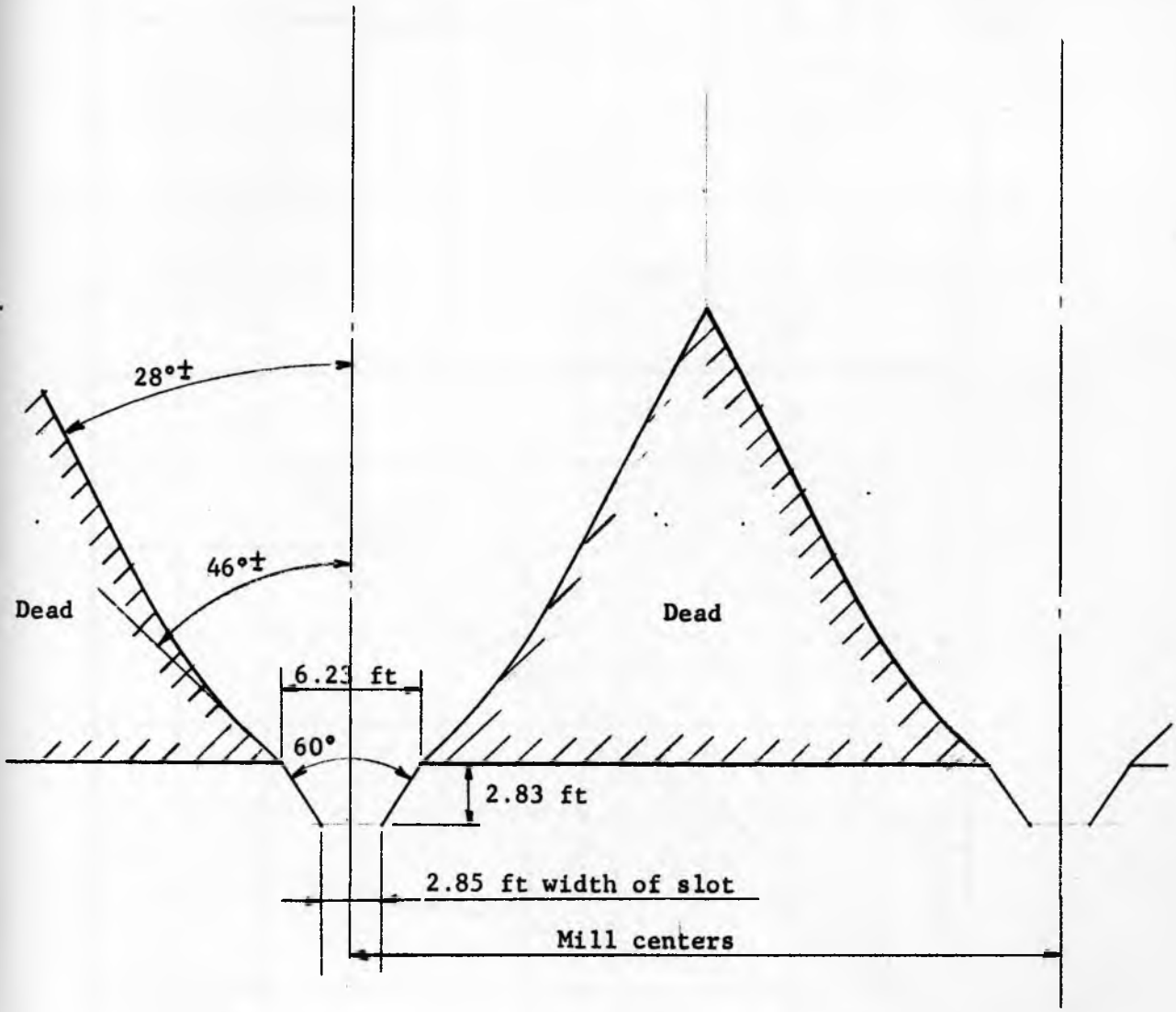

Fig. 137

Example 6, Selected hopper

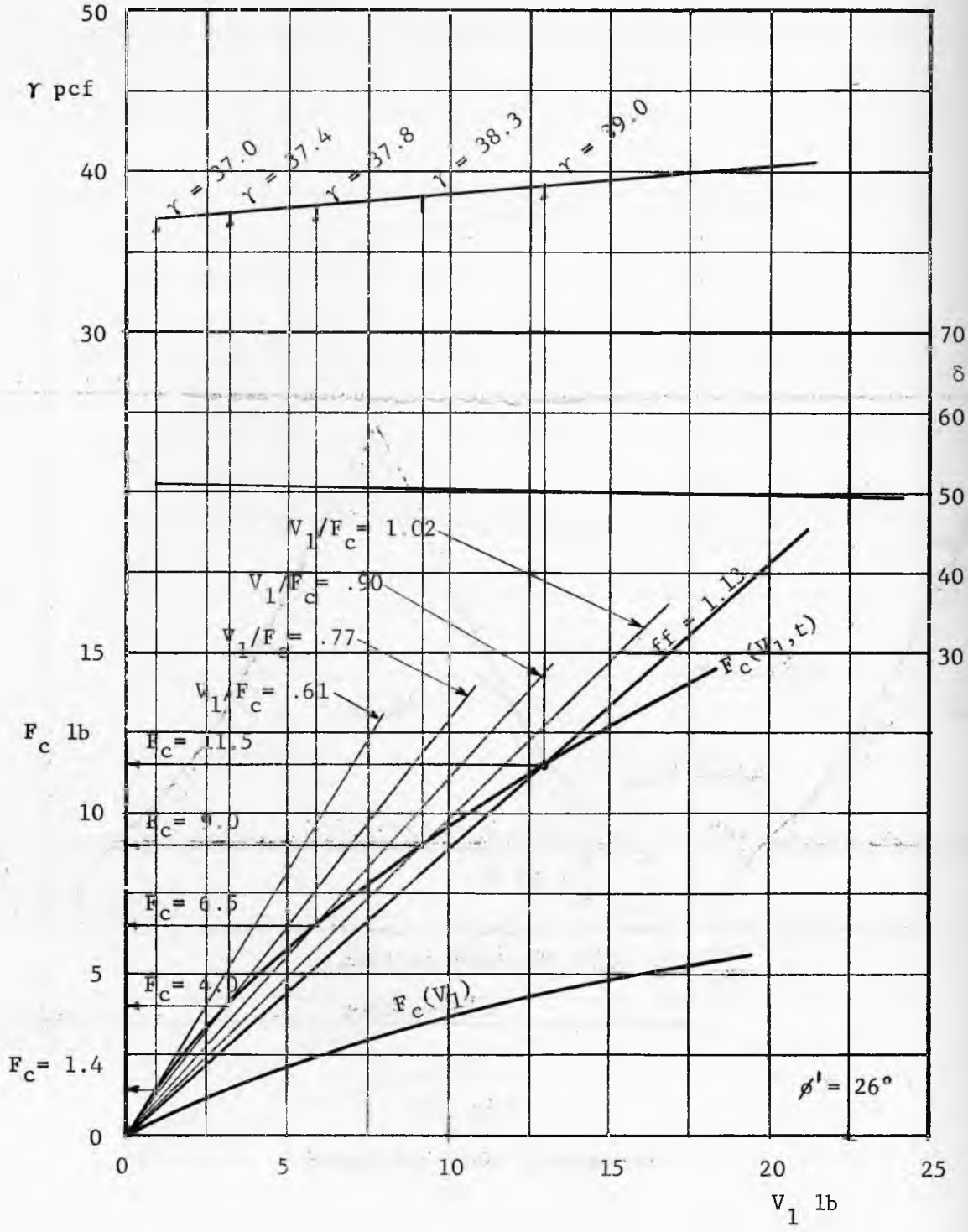

Fig. 138

Example 7, Flow properties

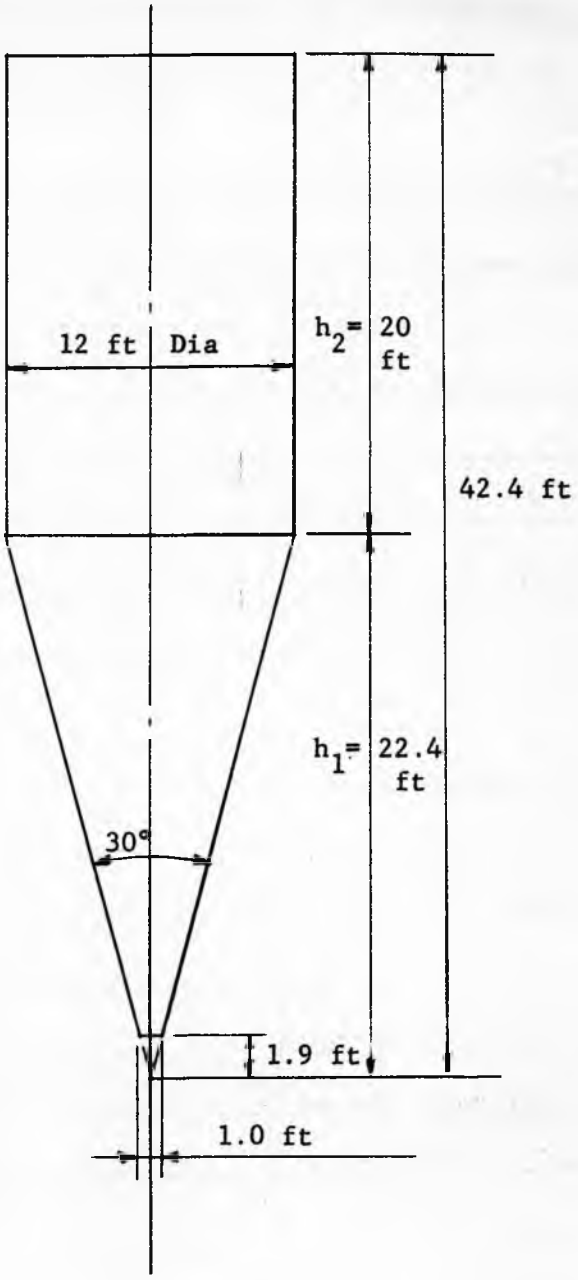

Fig. 139

Example 7, Selected bin

F_c	1.4	4.0	6.5	9.0	11.5
V_1/F_c	.61	.77	.90	1.02	1.13
$1 + \alpha$	1.85	1.47	1.25	1.11	1.00
α	.85	.47	.25	.11	.00
γ	37.0	37.4	37.8	38.3	39.0
B	.98	2.78	4.47	6.11	7.67
h	1.83	5.19	8.34	11.40	14.30
1 - .0048h	.991	.975	.960	.945	
$p_2 - p_o$	.40	.62	.53	.31	.00

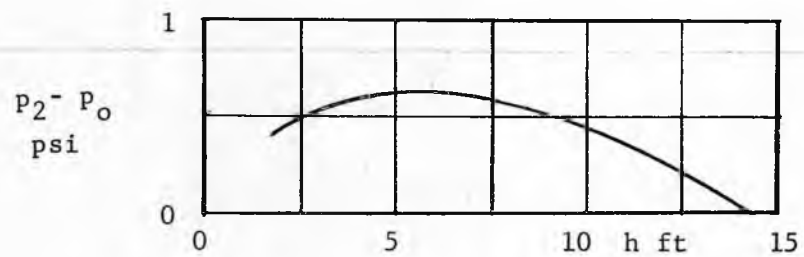

Fig. 140

Example 7, Calculation of air pressure at top of bin

Above the hopper the ore flows on itself, i.e. within rough walls. At the rough walls the angle ϕ' is again computed by taking the average value between $\delta = 50°$ and the value of ϕ' corresponding to $\psi' - 90° = 45°$. This yields $\phi' = 44°$. The hopper walls are extended upwards until a width B is reached at which ff = 3.5. This permits a maximum value of $\theta' \approx 46°$ at the base of the rough walls. That width is B = 71 x x 13/148 = 6.23 ft. Above the base, the stable slope of the pile is likely to be about $50° - \delta/2$, or assuming $\delta = 44°$ in that region, 50 - 22 = 28°. With the exception of the angle ϕ' within the hopper, no safety allowance has been made in these calculations, because the use of the long, continuous slot makes it unlikely that a complete obstruction will occur.

7. A feed product has flow properties shown in Fig. 138. For $\delta = 50°$, $\phi' = 26°$, the minimum critical flowfactor is ff = 1.13 in conical flow. The time flow-function lies above that flowfactor up to a value $F_c = 11.5$. Thus, the minimum hopper outlet for unassisted flow is B = 2 x 11.5 x 13/39 = 7.67 ft. A bin with a conical hopper, $\theta' = 15°$, and an outlet B = 1.0 ft, shown in Fig. 139, is selected. Since the instantaneous flow-function lies well below the flowfactor, Fig. 138, the one-foot outlet is ample, once flow has started. To start flow, air pressure will be applied at the top of the bin. The values of V_1/F_c are read off Fig. 138 for four values of F_c. In the table of Fig. 140, the values of α are computed from eq. (164) for these four points; B is then computed at these points, and then $h = B/2 \tan \theta'$. Then, in accordance with eq. (163), $p_2 - p_o = \alpha\gamma h(1-0.0048h$ /144 psi. The gage pressure is plotted in the figure and shows a maximum

of 0.62 psi in the vicinity of h = 5.19 ft.

The resistance to the flow of air of this solid, ρ = 1.2 lb min ft^{-4}. The rate of flow is found from eq. (165) for h = 5.19 ft, thus

$V = A \alpha \gamma(h/h_1)^2/\rho = \pi \times 36 \times .47 \times 37.4(5.19/22.4)^2/1.2 = 89$ cfm.

Feeders

In this section it is not proposed to discuss the merits of the various designs of feeders but to point out those features of design which particularly affect flow, to describe the loads acting on the feeders, and to report on two feeders which seem especially well suited for certain materials and applications but have not received the attention of industry which they deserve.

In a previous section, the method of calculating the dimensions B and D of an outlet was described. It is now necessary to select a feeder which will draw the solid through the whole specified cross-section B x D of the outlet. It will be realized that many feeders activate only a part of the area of the outlet, while the rest of the outlet remains inactive (dead). Such is the case, Fig. 141, with screw feeders of constant diameter and pitch, which draw only at the back end of the outlet; with belt feeders, which can draw either at the back or at the front, depending on the friction between the solid and the belt, and switch from front to back as the friction changes with changes of the moisture content in the solid; with rotary table feeders, which tend to draw the solid only over the plow.

A feeder will draw along a length L, or a circumference πD in a rotary table feeder, provided the capacity of the feeder increases at a sufficient rate in the direction of travel. To obtain such an increasing rate the designs shown in Fig. 142 should be used: the screw should be tapered and/or of increasing pitch; the hoppers should be raised above the belt or table feeder to permit sidewise out-flow. In the latter cases, sealing skirts can be provided on the outside of the hoppers as shown in the figure.

These arrangements are necessary if the recommendations of the previous sections are to apply. Beside allowing a quantitative approach to the design for flow, these arrangements will also substantially reduce the feeder loads, and thus allow the installation of lighter feeders as well as produce savings in power and in maintenance. In many cases, most of the power of a feeder goes not on drawing the solid out of the hopper but on overcoming the resistance imposed by the sliding of a hard packed, dead solid and heavily loaded skirts over the moving surface of the feeder. When the whole outlet is live, all the solid is flowing, there is no packing and no sliding. The sealing skirts, placed outside of the main flow channel, are only lightly loaded and cause little resistance to the motion of the feeder.

From the standpoint of feeder economy, the area of the outlet should be as small as possible because the vertical load Q acting on a feeder increases as the 3/2 power of the area of the outlet. The weight, the horsepower and the cost of a feeder increase rapidly with the size of the outlet.

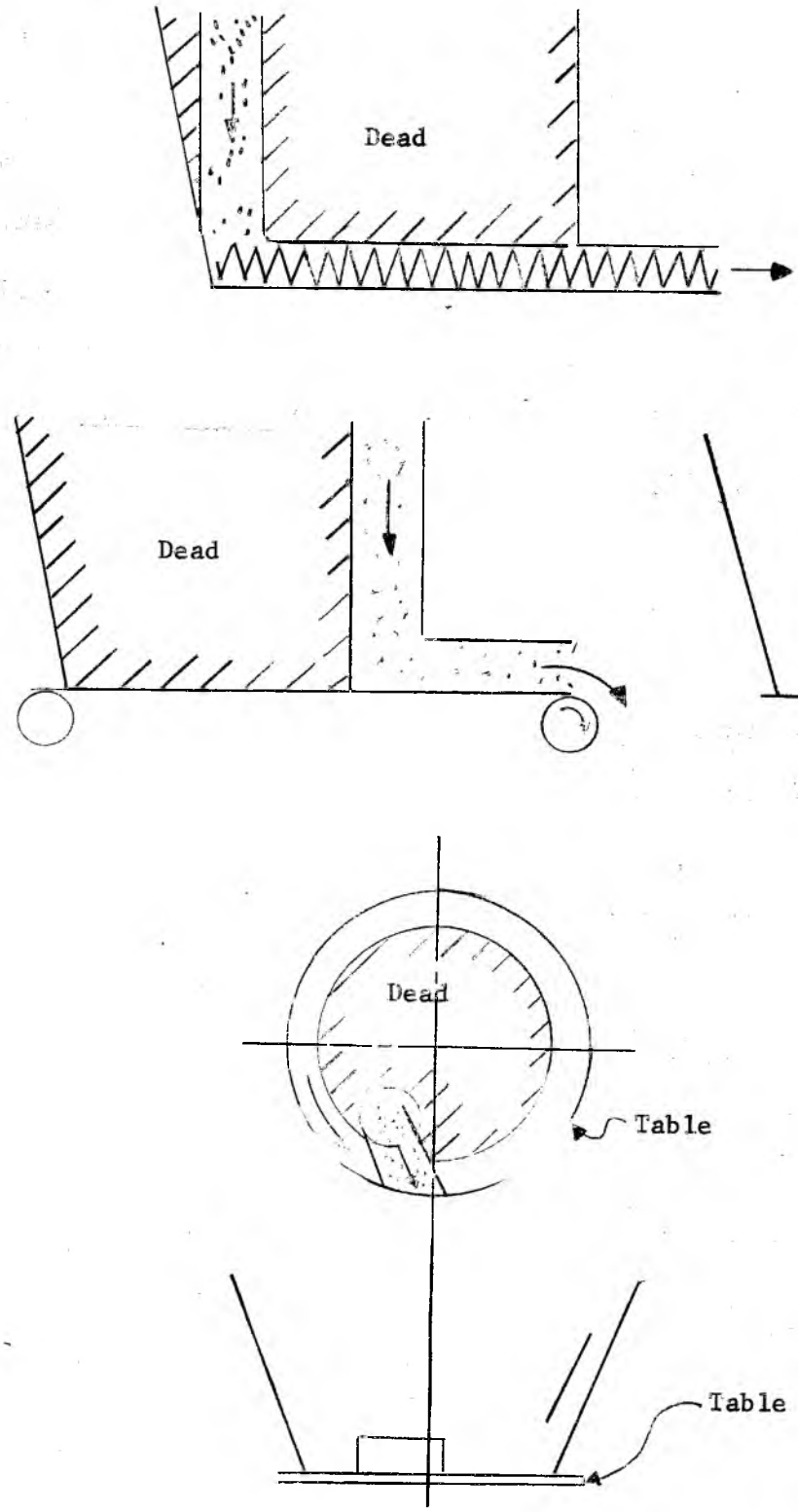

Fig. 141

Unsatisfactory feeders

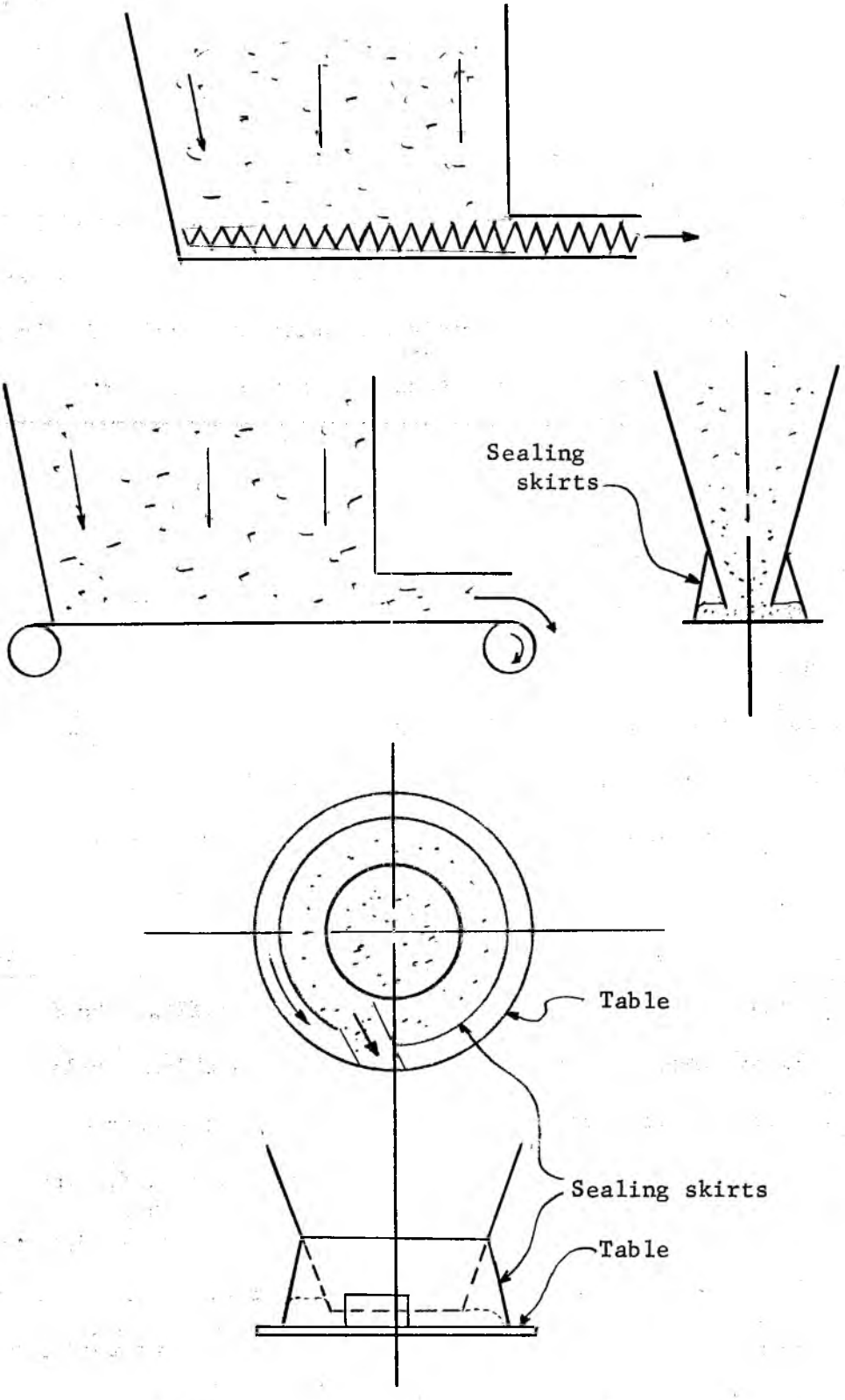

Fig. 142

Satisfactory feeders

The shape of the selected outlet will determine the type of the feeder. In mass flow bins, the conditions of flow specify only the minor dimension of the outlet. In plug flow bins, and in storage piles for solids which do not pipe, because they are not affected by consolidation at rest and their angle δ is less than, say, 50°, also only the minor dimension is specified. In those bins the choice is open between a circular (or square) and an oblong shape of the outlet. The required diameter of a circular outlet will usually be about twice the width of the oblong outlet but other factors, like the cost of the bin, available headroom, plant layout, conformity with other equipment in the plant, will bear decisively on the selection of the type of feeder. Similarly, for solids, whose flowability does not define a minimum dimension and for which the dimensions of the outlet are determined from considerations of particle interlocking or rate of flow, the choice is open between a circular and an oblong outlet.

In plug flow bins and storage piles, for which both dimensions, B and D, are specified by the conditions of flow, the dimension D is always several times greater than B and an oblong outlet, or a slot, is always more economical than a circular or square outlet.

Feeder loads. The vertical force Q which a flowing solid exerts on a feeder can be estimated from eq. (103), in which $m = 0$ for plane flow, $m = 1$ for conical flow, and the parameter q is read off the appropriate chart, Figures 43 to 48. Only the values of $\delta = 30°$, 40° and 50° have been plotted. For solids, whose δ is larger than 50°, the

computed force is quite small and for them it is safer to use $\delta = 50°$. For oblong outlets it is safe to use the plane-flow formula.

As an example: assume a hopper with conical walls inclined at an angle $\theta' = 12°$, angles $\phi' = 28°$, $\delta = 44°$, $\gamma = 80$ pcf, and an outlet of diameter D = 1.5 feet. It is safe to use the chart for the lower value of $\delta = 40°$, Fig. 47; the point (12°, 28°) specifies q = 0.20, and eq.(103), with m = 1, yields $Q = 0.20 \times 80 \times 1.5^3 = 54$ lb.

And another example: a hopper with a rectangular outlet 1 ft x 3 ft., side hopper slopes $\theta' = 25°$, angles $\phi' = 30°$, $\delta = 60°$, and $\gamma = 110$ pcf. From Fig. 45, q = 0.35 and $Q = 0.35 \times 110 \times 3 \times 1^2 = 116$ lb.

One conclusion is immediately apparent: these forces are very small. They have been computed on the assumption that the feeder is perfectly efficient, that no sliding of packed solid occurs. These forces do not allow for the weight of the solid which would collect in the pockets outside the hopper, Fig. 142, for the confining pressures from the skirts, and for starting loads.

The starting loads on a feeder may be several times (a factor of ten has been measured [31]) as much as the running loads. The reasons are as follows: the low pressure which a solid exerts on a feeder during flow is due to the arching effect which develops within the flowing solid and which causes most of its weight to be transferred directly to the hopper walls. This occurs whenever the feeder is in motion and the solid is flowing. When a solid is charged into an empty bin while the feeder is at rest, there is no flow, arching at the outlet of the hopper does not develop, a higher column of the solid

bears down on the feeder, and pressure is much higher. This situation is often aggravated by the fact that, as the solid is charged into a bin, its total weight increases, and the bin structure deflects. If the feeder support is rigid and the feeder does not deflect in unison with the bin, the feeder may take up a considerable part of the weight of the bin and of the stored solid. Of course, as soon as the feeder has started and flow in the bin has caused arching to develop, the vertical force drops, but the initial force on the feeder may be very large. The peak loads are particularly detrimental to belt feeders which rely on pre-tension for traction. In order to assure traction during the peak loads, the pretension must be high, much higher than is required during normal flow. This high tension contributes to the loss of horsepower and to the wear of the feeder. These starting peak loads can be eliminated by running the feeder whenever the bin is being filled or, more positively, by providing a flexible support for the feeder, for instance, a spring support.

Belt feeder. The belt feeder, either flat or troughed, either sliding on a plate (slide-belt feeder) or supported on idlers, provides a simple and economical method of controlling the flow of solids from slot outlets.

The belt feeder is especially well suited to solids which are fine but do not aerate and flood (for instance, when charged into an empty bin), and do not contain particles over 3/4" size. For these solids, the hopper can be raised off the belt, a height of at least two largest particle diameters and not less than 1/12 of the width of the outlet,

to provide a fully live outlet. Such a feeder will work satisfactorily for outlet ratios L/B of 16 or more. A seal can be provided by outside skirts.

The slide-belt feeder, Fig. 143, is low in first cost, reliable and easy to maintain. The even surface of the belt, obtained by the continuous support from the slide plate, tends to minimize the pressures from the flowing solid and allows a tight seal at the skirts. Eq.(103) is adapted to these feeders as follows

$$Q = 2q\ \gamma\ L\ B(B + 0.2) \qquad (166)$$

B and L are measured in feet. The coefficient 2 is an overall safety factor: it allows for the deviations of the actual flow pattern from plane flow, which is used to calculate q (Figures 43 to 45), and for the weight of the solid in the side pockets; whereas 0.2 specifically allows for friction due to increased pressure as the solid flows sidewise under the hopper walls. This formula has been obtained from tests run at the Flow of Bulk Solids Laboratory at the University of Utah. If the outlet is tapered, an average width B provides sufficient accuracy.

The component H of the belt tension necessary to draw the solid is computed from the formula

$$H = .45Q. \qquad (167)$$

The frictional drag on the belt due to the slide plate, or rollers, etc. must be added to H to obtain the net belt tension.

In order to relieve the peak loads on the feeder, the feeder is supported on air or steel springs which are computed as follows.

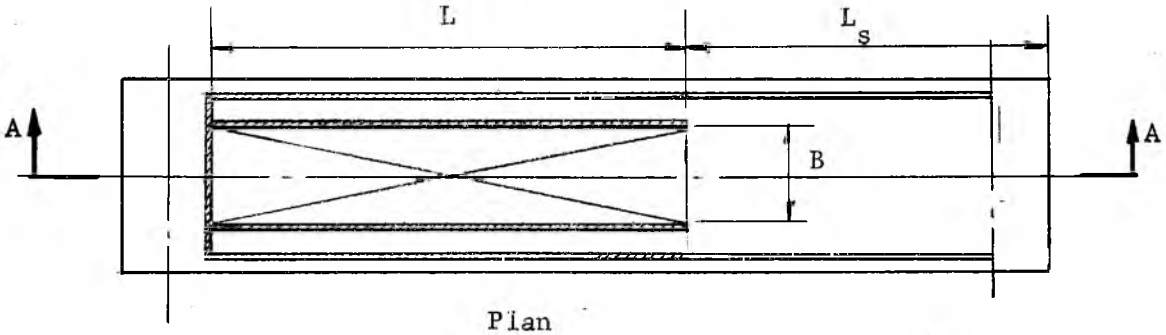

Plan

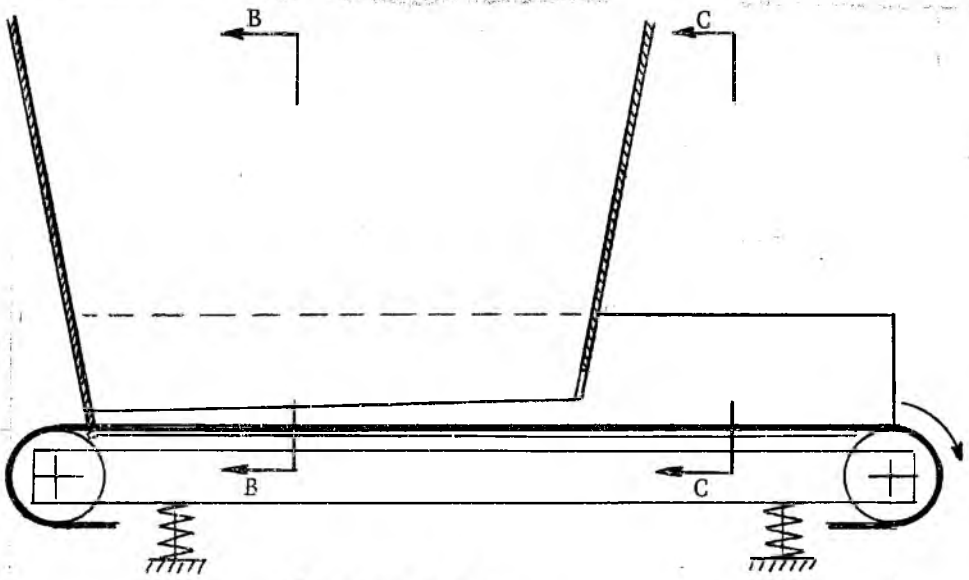

Section A - A

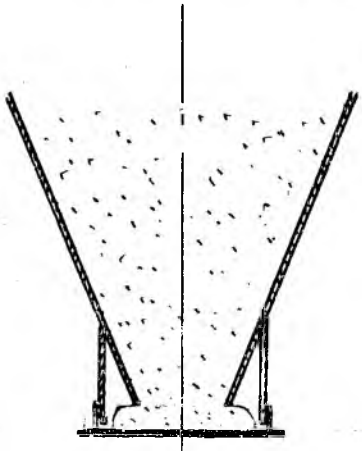

Section B - B

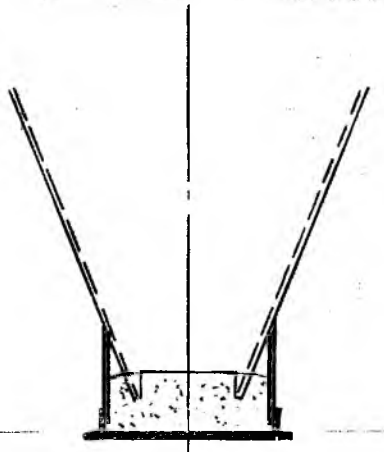

Section C - C

Fig. 143

Slide-belt feeder

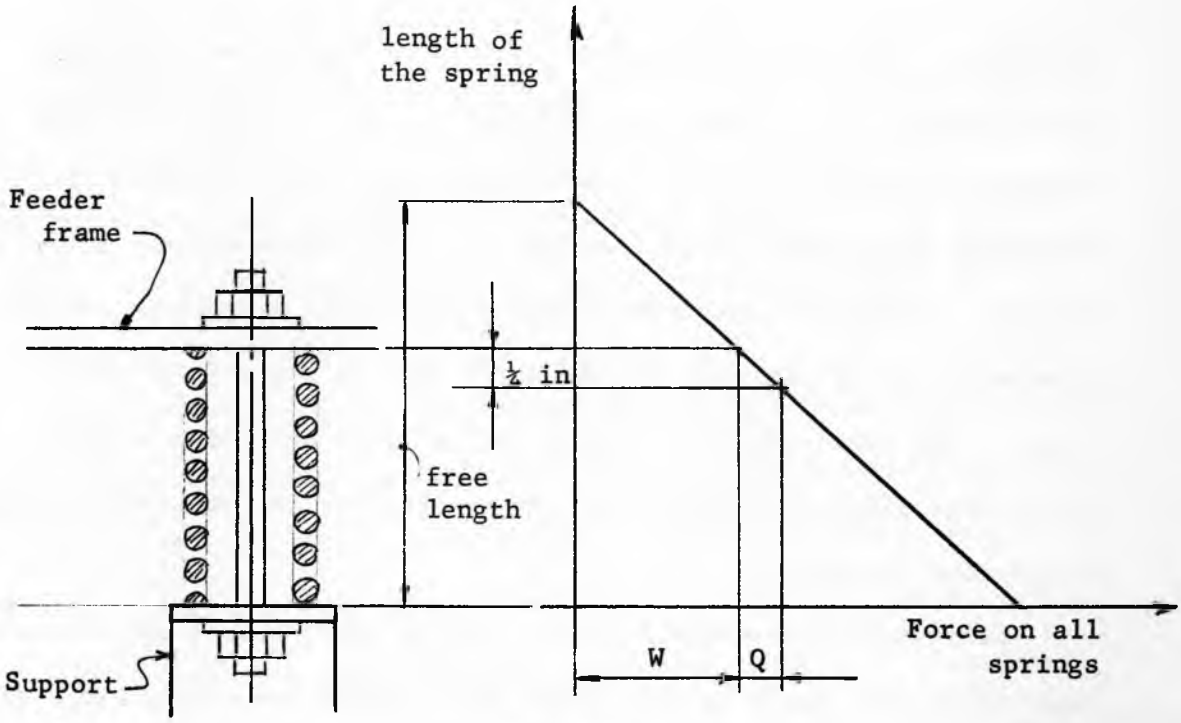

Fig. 144

Springs supporting a feeder

The total vertical load due to the feeder W is

$$W = Q + W_d + W_s, \tag{168}$$

where W_d is the dead weight of the feeder and W_s is the weight of the stream of the solid over the length L_s, outside the outlet. The total spring constant (all springs in parallel) should be

$$C = 4Q \text{ lb/in}, \tag{169}$$

as shown in Fig. 144. The springs should be contracted under the load W and locked so they can contract but cannot expand. In this manner, the feeder will not start deflecting until the load Q is exceeded, and, under a peak load 2Q, the feeder will deflect 1/4 of an inch. Laboratory tests show that a very small deflection, a few hundredths of an inch, is usually sufficient to relieve the peak loads. The feeder should be supported by links or guides in the horizontal plane to prevent sway and to transfer the horizontal driving force into the solid.

Laboratory measurements carried out on sand, gravel and iron ore have shown that the velocity of the belt, within the tested range of up to 80 feet per minute, does not appreciably affect the loads which act on the feeder belt from the flowing solid.

Side-discharge reciprocating feeder. Reciprocating plate feeders are well known and have been used over many years under square and rectangular outlets. The ratio L/B of the outlets has been limited, because the capacity of these feeders does not increase in the direction of travel. An increase of the ratio L/B above 1.5 does not perceptibly widen the flow channel but greatly raises wear and power

requirements.

By changing the design of these feeders, they can be made especially suitable for the feeding of unscreened coarse ore from storage piles. Such ore is cohesive when moist, is often subject to changes of temperature and to freezing. As a result, it pipes around the outlets, gradually packs in the non-flowing regions, and tends to dome. An analysis of the flowability of such an ore usually gives some acceptable value for the width of the outlet B, but the required diagonal of the slot D, necessary to prevent piping, is very large and calls for a continuous slot, running the full width (or length) of the storage pile. The side-discharge reciprocating feeder is the most suitable feeder for such a slot.

To the writer's knowledge there are no such feeders at present in existence, therefore, the description which follows anticipates their application. A possible installation is shown in Figures 145 and 146. The slot runs the full length of the storage pile. A gathering belt conveyor runs in a tunnel alongside the slot. The slot is spanned by cross-beams spaced at a distance ℓ of 8 or 12 feet. Under each length ℓ there is a reciprocating feeder which discharges onto the belt conveyor. The feeders can be suspended from above, as shown in the figures, or supported from below. A flexible suspension is shown to relieve the peak loads and to provide for impact. Vertical walls separate the feeders so that each feeder can run independently of the others.

The motion of the feeders must be coordinated with the speed of

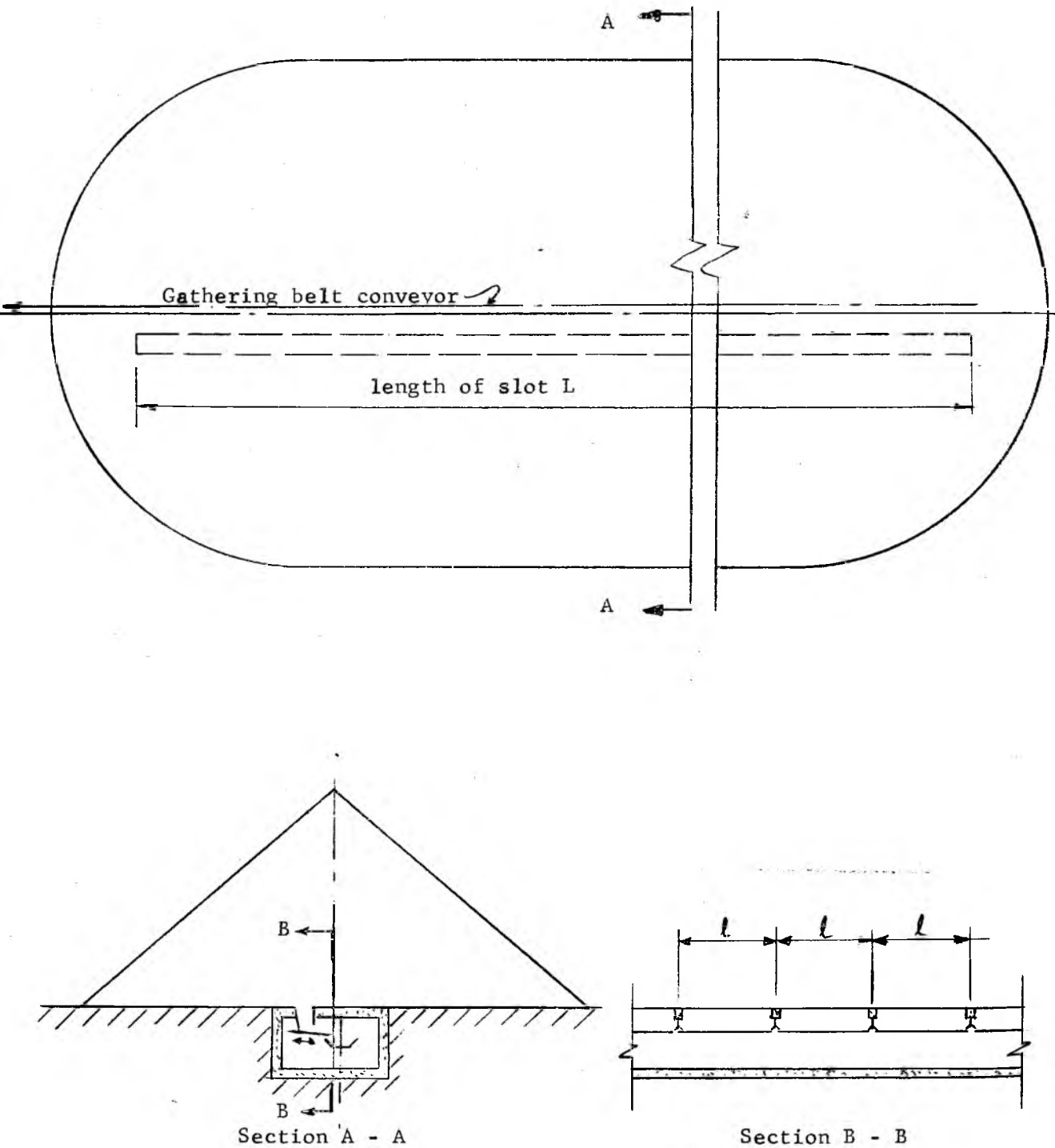

Fig. 145

Layout of a side-discharge reciprocating feeder under a pile

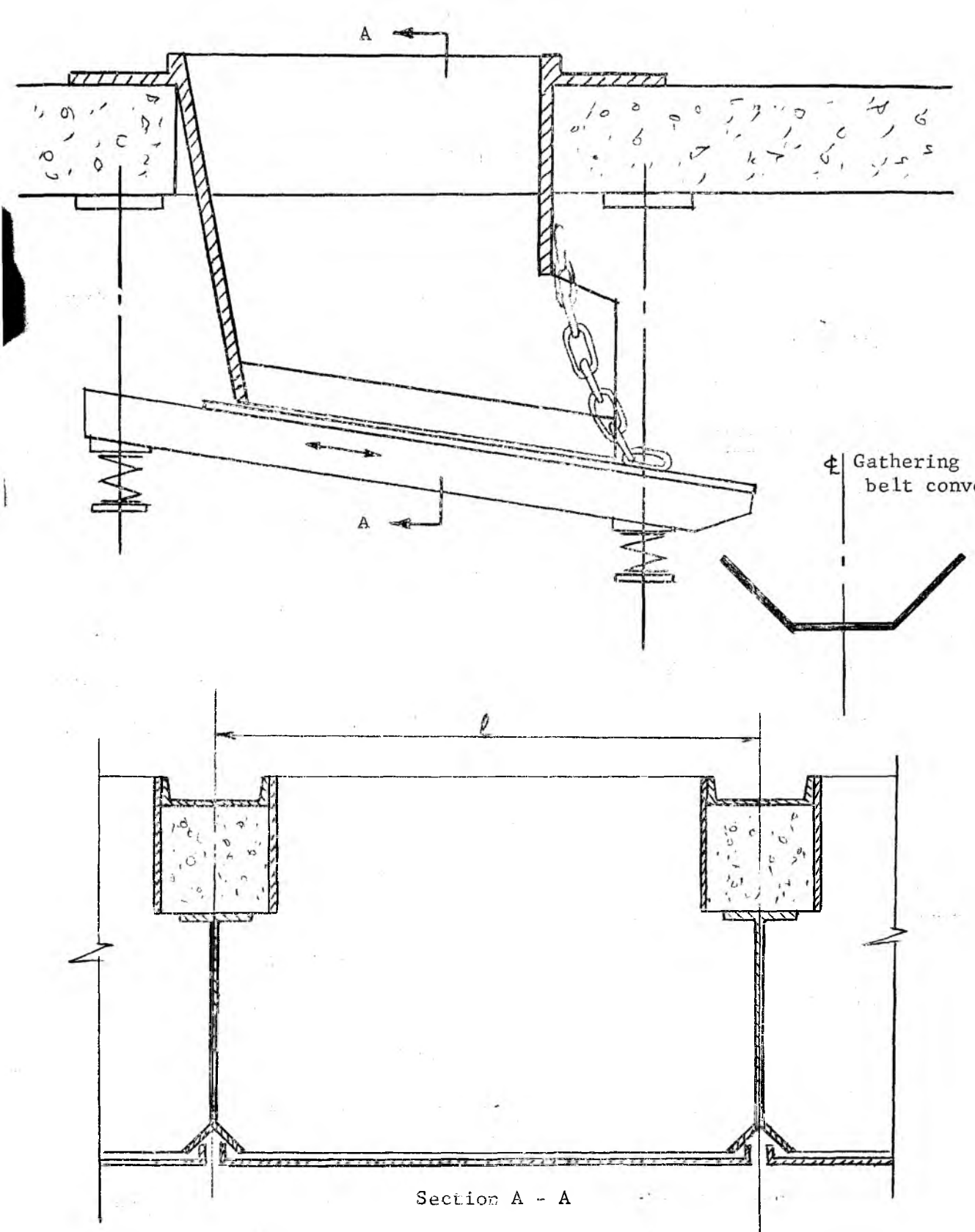

Fig. 146

Details of a side-discharge reciprocating feeder

the gathering belt. If n consecutive feeders spaced at ℓ feet are operating at a cycle of f strokes per minute, then the speed of the belt v should be

$$v = f\ n\ \ell \text{ ft/min}, \tag{170}$$

to obtain a fully loaded belt.

Another layout, which would be used to feed spearate mills, has the slots and the gathering belt conveyors laid out across the pile, as shown in Fig. 147.

Segregation and blending in flow

During the storage and handling operations, a bulk solid tends to segregate (separate) according to the particle size, shape and density. Since segregation is usually detrimental to the further processing and merchandizing of the solid, the conditions leading to segregation, means of minimizing segregation, and methods of remixing during flow will now be described.

Most of the segregation takes place in the following two situations: when a solid flows in a freely falling stream which has a horizontal component of velocity, and when the stream hits an inclined slope of deposited solid. In free fall, each particle is acted upon by two forces: its weight, and air resistance to motion. The former is equal to the product of the size and the density of the particle, and acts vertically down; the latter is a function of the size and shape of the particle and of its velocity, and acts in the direction opposite to the velocity. In vertical free fall, both these forces are vertical

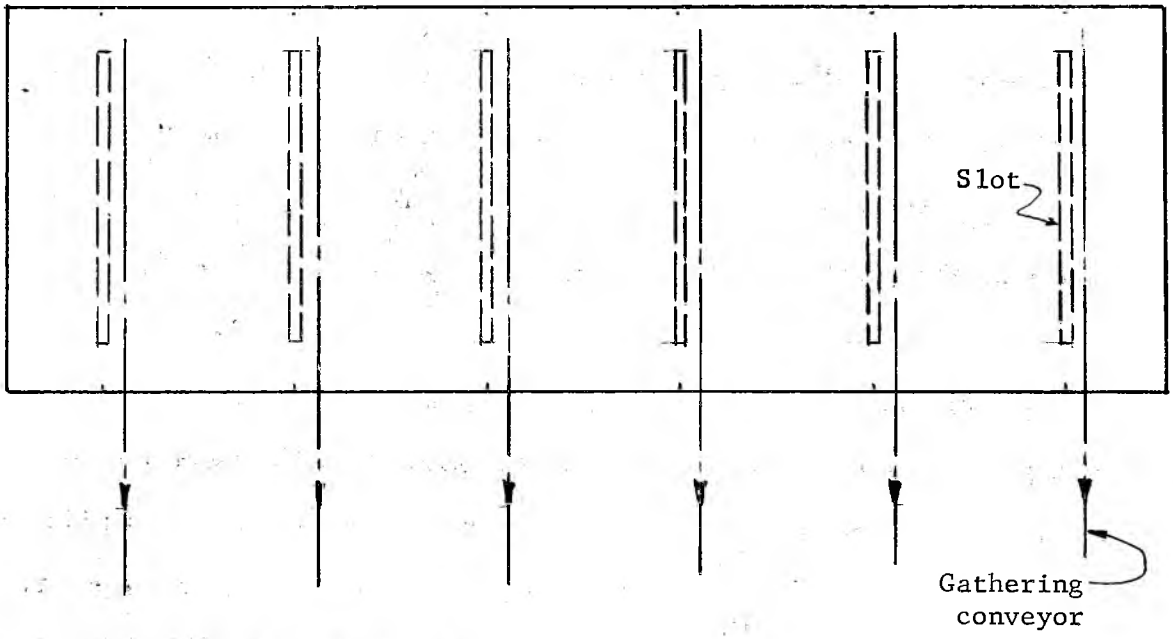

Fig. 147

Mill-feed storage with side-discharge reciprocating feeders

and, while the terminal velocities of the various particles may vary, their trajectories do not, hence there is no significant segregation. When a solid is discharged over a conveyor pulley or spouted through an inclined chute an initital horizontal component of velocity is introduced, the two forces are not aligned any longer and, as their ratios differ for the various particles, so do the trajectories of the particles.

Whenever a stream hits a sloping surface, the particles roll down the slope: the large, heavy, and more nearly spherical particles tend to roll farther than the fine, light, and flaky particles which tend to remain at the point of impact of the stream. As a pile of the solid builds up, the fines congregate in a column which has the shape of the trajectory; the size of the particles gradually increases with the distance from the column, and the lumps collect at the periphery of the pile or at the walls of the container. If the outlet of a pile or of a plug-flow bin is located directly beneath the trajectory, the draw will be heavily segregated: an excess of fines will be drawn every time the feeder is started after charging the solid while the feeder was at rest. When the container has several outlets, the outlet located under the trajectory will consistently draw an excess of fines. This phenomenon can be exploited when some size separation is desired, otherwise the outlets should be located away from the trajectory.

The aforesaid indicates that segregation is a dynamic effect and occurs inevitably when the solid is in free fall. It also indicates methods of minimizing segreation, which are: reducing the velocity of

the particles by shortening the height of free fall, reducing the horizontal component of velocity, and limiting the size of the slopes along which the particles roll. The last method calls either for narrow bins or for means to spread the stream over the top surface of the container. Spreading can be accomplished either by placing a shelf in the stream or by moving the point of discharge and the trajectory of the stream. A combination of the two can be very effective in minimizing segregation.

The degree to which a given solid will segregate under given conditions cannot yet be predicted quantitatively. Jenike [32] made a preliminary study of the problem and suggests that a classification of the solids, possibly, can be developed on the basis of simple tests which would measure a ratio W/K, where W is the weight of a particle and K is its resistance to motion through the air. He suggests that particles of the same ratio W/K will have little tendency to separate from each other, and that the tendency will increase with a spread in the values of the ratio. It would seem that the development of a quantitative approach to the problem of segregation might benefit those who, like the feed processors, handle and produce a variety of complex blends.

When segregation in storage is to be avoided, a mass flow bin should be used and the bin should be operated as explained in the 4th 'Example of design for flow'. Under these conditions first-in, first-out flow obtains; while the solid segregates in charging, it remixes within the hopper and, as a result, the blend of the draw is essentially the same as the blend of the charge.

In slot-outlet bins charged by means of a tripper-conveyor, segregation is much smaller if the slots are perpendicular, Fig. 148(a), than if they are parallel to the conveyor, (b), because in the former case the slot draws a cross-section of the segregated solid which is remixed on the feeder

In a multiple-outlet bin, segregation is reduced by drawing simultaneously through all the outlets and blending the draw.

A bin can be used for the blending of a solid by recirculating the solid in a closed circuit about the bin, provided the following conditions are satisfied: (a) the solid is non-segregating, e.g. it is composed of uniform size, shape and density particles, or of very small size particles; (b) a mass flow bin is used, so that there are no dead regions of the solid within the bin; (c) there is a substantial velocity gradient in every horizontal cross-section of the channel, so that first-in, first-out flow does <u>not</u> occur.

The above points (b) and (c) imply a bin with a short vertical portion, whose height does not exceed one half the diameter of the cylinder, Fig. 129, or no vertical portion at all. A higher vertical portion would induce first-in, first-out flow and may cause dead-regions at the transition.

A series of bins can be used to even out the grade of a run-of-mine ore, Fig. 149, by charging the bins in sequence and drawing them simultaneously.

<u>Flooding</u>

Fine solids which aerate readily should be stored in mass-flow bins

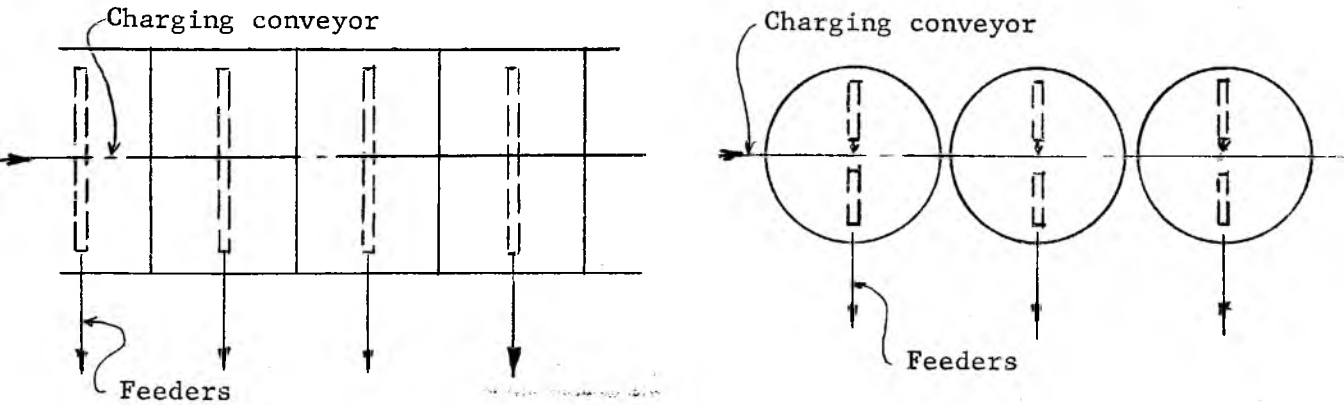

(a) Perpendicular layout

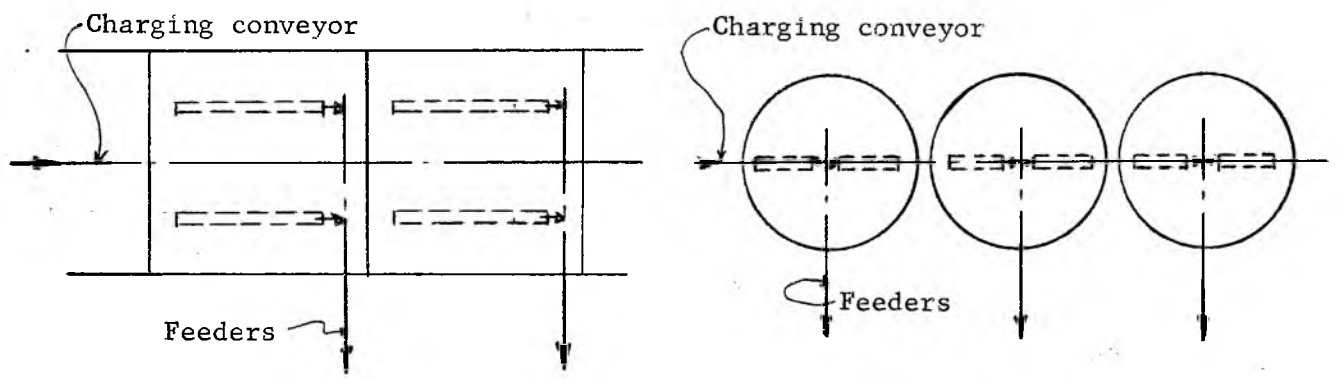

(b) Parallel layout

Fig. 148

Layout of slot-outlet bins

in order to prevent flooding. In a plug-flow bin, flow is non-steady, thick layers of the solid break away all at once, fall down the height of the channel and aerate as they break up. Unless the feeder is completely air-tight, flooding occurs.

Heat transfer

When flow of heat is to occur across the walls of a channel, the channel should be of the mass-flow type, otherwise, the stationary solid at the walls will act as an insulator between the flowing mass and the walls. The channel should also be very steep so that the velocity profile, defined in Fig. 68, and plotted, as an example, in Figures 69 and 70 for $\delta = 50°$, be fairly uniform. If the velocity is much higher at the center of the channel than at the walls, the outer layers of the solid will undergo much more heating or cooling, as the case may be, than the core. To obtain a more uniform transfer of heat, it is advisable to use a conical hopper with a pipe located at the center of the channel and to use the pipe as well as the walls for the transfer of heat. In general, the channels described in this work are not efficient as heat exchanger because of the laminar flow patterns of the solid.

Gas counterflow

In channels which serve as chemical reactors, a gas flows upwards as the solid flows down by gravity. To cause the flow of the gas, a pressure gradient is applied to it. This gradient opposes the forces

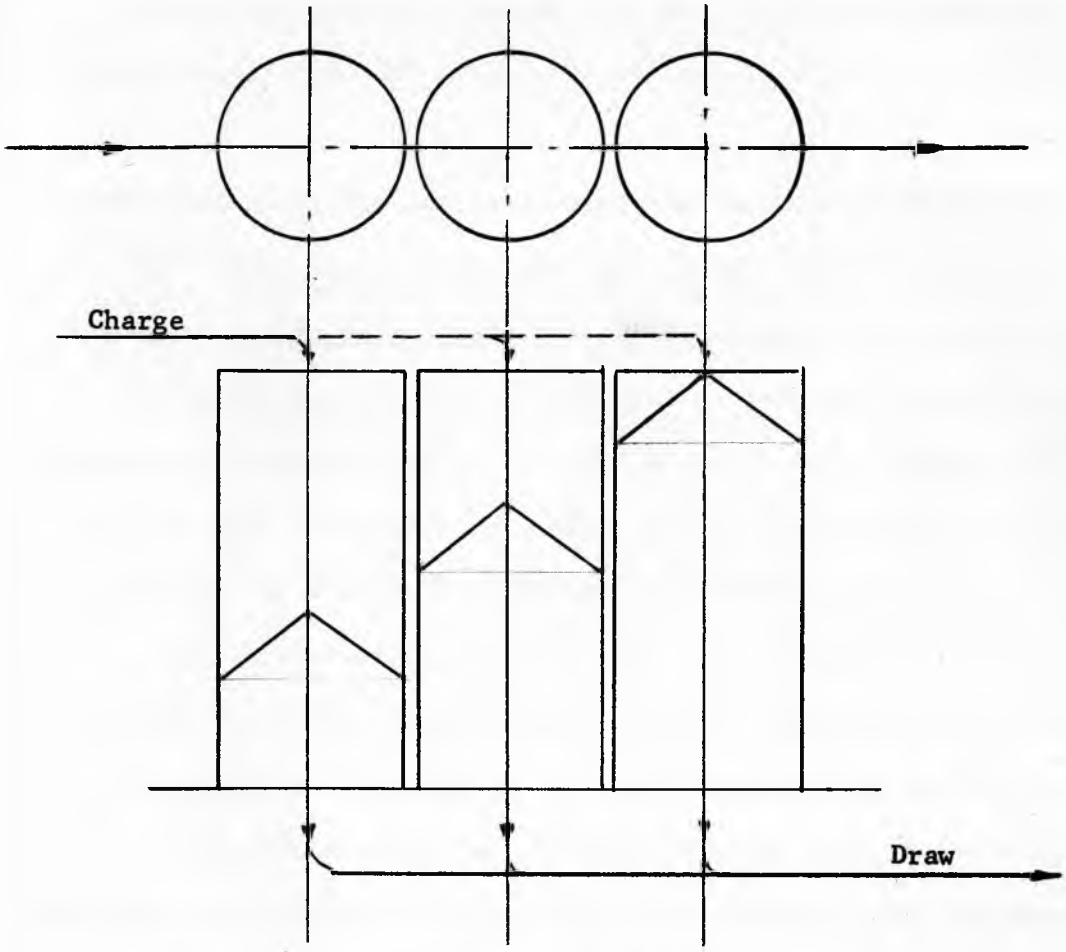

Fig. 149

Blending by means of bins

of gravity and buoys the solid. In a converging channel, the pressure gradient is greatest in the narrowest part of the channel, i.e. at the outlet. The maximum pressure gradient which can be applied without stopping the gravity flow of the solid is about 70% of the bulk weight of the solid.

It is important that the gas pressure at the outlet be maintained at a uniform level without sudden changes, either up or down. When the process is steady, the consolidating pressures in the solid are reduced by the gas pressure gradient in the same ratio as the pressures of failure, and gravity flow is not affected. If gas pressure fluctuates, the solid may consolidate under the pressures of gravity when the gas gradient is low, and dome when the pressures of failure are decreased as the gas gradient becomes high. If the process is intermittent, then during the stoppages of flow the gas pressure gradient vanishes and the solid consolidates under the full pressures of gravity. If the gas gradient is then applied prior to the re-establishment of gravity flow, the gas gradient reduces the pressure of failure and flow may not start. It is better to start gravity flow first, and then gradually apply the gas pressure.

Since the gravity flow of a solid in a vertical channel is unsteady and erratic, vertical channels should not be used as reactors. Vertical spouts connecting sections of a reactor, as shown in Fig. 150, should have by-pass pipes for the gas, otherwise doming in the spouts may occur.

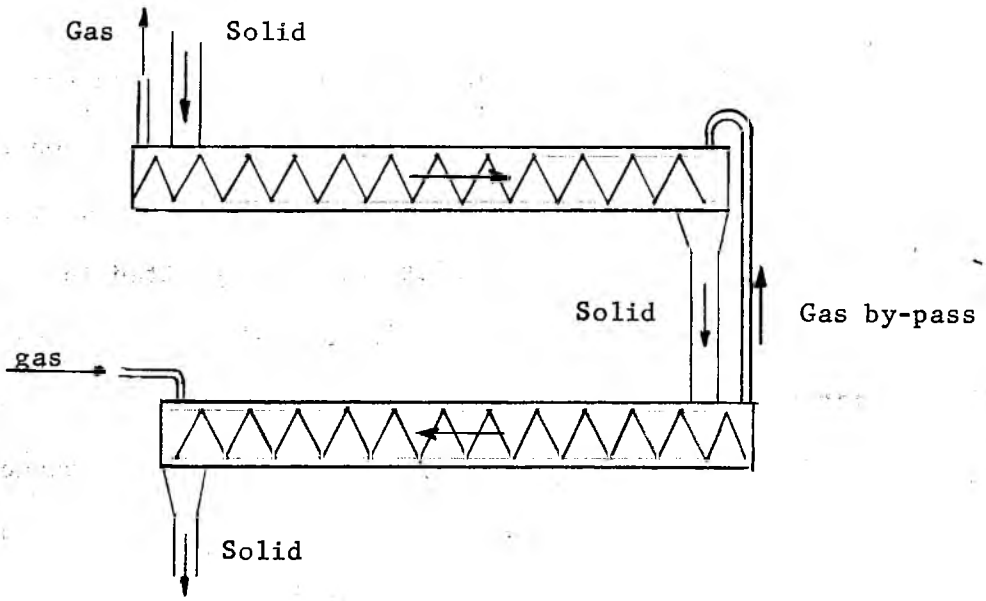

Fig. 150

Gas by-passes of spouts

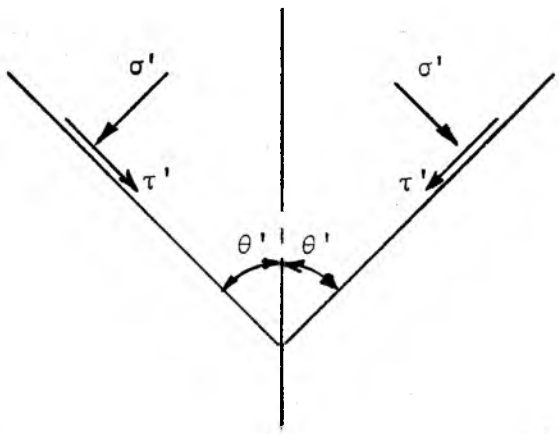

Fig. 151

Stresses acting from a flowing solid on hopper walls

Structural problems

Stresses acting on hopper walls. The normal pressure σ' and the shearing stress τ' which a flowing solid exerts on the wall of a hopper, Fig. 151, have been computed for symmetric hoppers in plane and conical flow. Contours of constant values of these stresses are plotted in Figures 50 to 61 for the values of $\delta = 30°$, $40°$, and $50°$. The stresses for $\delta > 50°$ are less than those for $\delta = 50°$.

It will be observed that these stresses are very low. For instance in plane flow, $\delta = 40°$, $\theta' = 15°$, $\phi' = 23°$, $\gamma = 100$ pcf, B = 2 ft., from Fig. 51, $\sigma' = 1.01 \times 100 \times 2 = 202$ psf, which is equivalent to a static head of the solid of 2.04 ft, or just about the width of the hopper. In conical flow, these stresses are less yet; for instance, for the same θ', ϕ', γ and B, from Fig. 54, $\sigma' = .50 \times 100 \times 2 = 100$ psf.

For easy, and free-flowing, fine solids the above values are acceptable for design purposes. For cohesive solids, which can dome and impose large impact loads upon failure, and for solids containing large particles, a safety factor needs to be used over the computed values.

It should be remembered that these values have been derived for mass flow and in cases of plug flow can only be used as a guide. The stresses on the hopper will also be higher in the vicinity of the transition to the vertical portion.

Bin failures. Failures of bin structures can be divided into two categories. In the first category belong those failures which are due to recognized structural causes, such as: foundation failure, uneven

settlement of footings of a multi-column bin, wind loads, earthquakes. In the second category are the failures caused by irregularities in the flow pattern of the stored solid. Only the latter are of interest in this work.

The most dangerous failures occur when a stored solid domes at or above the transition between the vertical portion of a bin and the hopper while the hopper empties out. A large void then forms under the doming solid. If the whole mass happens to break away simultaneously, it acts like a piston, compresses the air in the hopper, and either splits the hopper open or tears it off its supports. Lives have been lost in such accidents. Solids whose time flow-functions approach a straight line, are most likely to dome at or above the transition. Bins for such solids (many agricultural products belong here) should be built with rounded, smooth transitions. Similar hang-ups have been known to burst large holes in the sides of agricultural concrete silos.

While a break-away of a large doming mass develops a high pressure in the hopper, it also develops a vacuum at the top of an enclosed bin and, unless the top is vented, the roof of the bin may be sucked in. A vent may be closed by a diaphragm to keep the dust in, the diaphragm being designed to fail if the pressure differential exceeds a safe value. Such vents are also recommended to safeguard against dust explosions [33].

Less dangerous failures occur typically in bins of circular horizontal cross-section. In a circular cross-section the hoop stresses are tensile and the walls require no bending reinforcement,

provided the stresses acting on the walls from the solid are uniform all-around. This condition is satisfied if the solid is charged and drawn at the center of the bin. Therefore, the hopper, if any, must be circular and symmetric with respect to the vertical axis: only one outlet is permitted. If the hopper is offset to one side, Fig. 152, the pressures from the solid on the vertical side are decreased and the hoop stresses in the hopper may pull that side in. Bending reinforcement is required to retain the shape of this hopper.

In a cylindrical, flat-bottom bin with two (or more) outlets, Fig. 153, the solid empties out of two craters centered at the outlets and the pressures on the walls at points A fall to zero while, simultaneously, at B the solid presses against the walls. As a result, the walls at A are pulled in. To counteract this effect, the cylinder should be reinforced by rings between the A and B levels.

Ores

Broken rock. From the stand point of flow, the main characteristic of these solids is the large size of the rocks compared to the cross-section of the channels through which the rock has to flow. In most ore passes, chutes, and ore pocket outlets, the dimensions of the apertures are well below those plotted in Fig. 123, hence the probability of interlocking is substantial. However, experience shows that flow is sufficiently reliable provided the smaller dimension of the aperture, a, is

$$a > 2d, \qquad (171)$$

where d is the intermediate dimension of the largest rocks, Fig. 154.

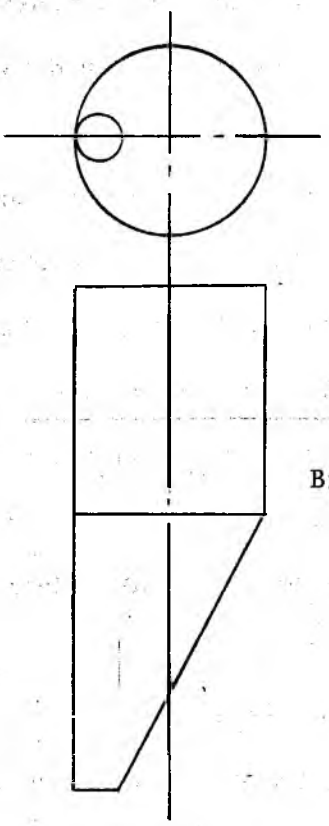

Fig. 152

Bin with offset conical hopper

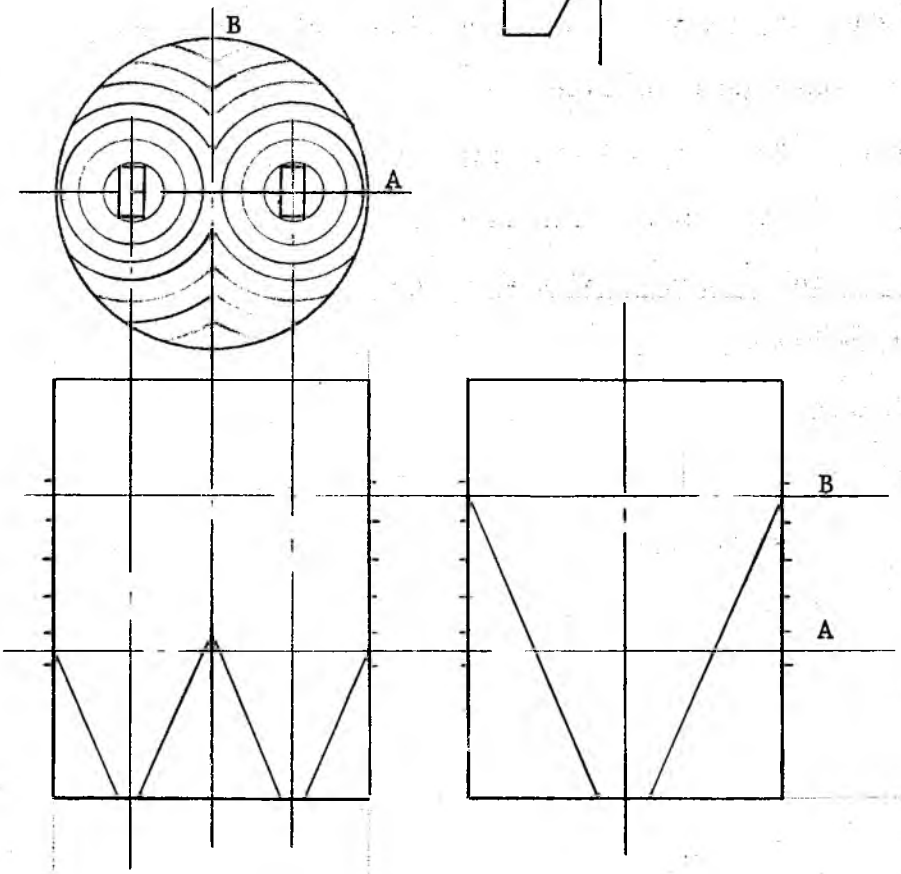

Fig. 153

Cylindrical bin with two outlets

It is interesting to note that the largest dimension of the rocks does not enter into this formula. This is explained by the fact that, whenever a solid flows in an even slightly converging channel, the velocity profile is as shown in Fig. 155. If a rock of length ℓ happens to be positioned as shown at A, its velocity v_1 at one end is greater than v_2 at the other end, and the rock rotates as it flows, until it has aligned in the direction of flow, as shown at B.

From the standpoint of flow, an ore pass should be converging and not straight. Flow in a converging channel is more steady, the pressures in the solid are lower and, hence, the consolidation and the tendency for doming is less.

In a straight channel, flow is non-steady, therefore pressures are higher, the solid does not converge but flows like a rigid plug and, even though it flows, it undergoes consolidation at rest under these higher pressures, resulting in increased tendency for doming. Beside that, flow in a straight channel causes more wear at the walls. This can be illustrated by the consideration of the energy of a flowing mass. As the solid flows down, it dissipates by friction the potential energy due to the gravitational field. In a straight channel, the solid flows like a rigid plug and all the energy is dissipated at the walls, wearing out the wall surfaces. In converging flow, the shape of the flowing mass is continuously changed, and a part of the work is done within the solid itself, reducing the energy spent at the walls.

The pattern of flow in an ore pass is governed by its shape at the outlet and the method of controlling the draw. The principle of the

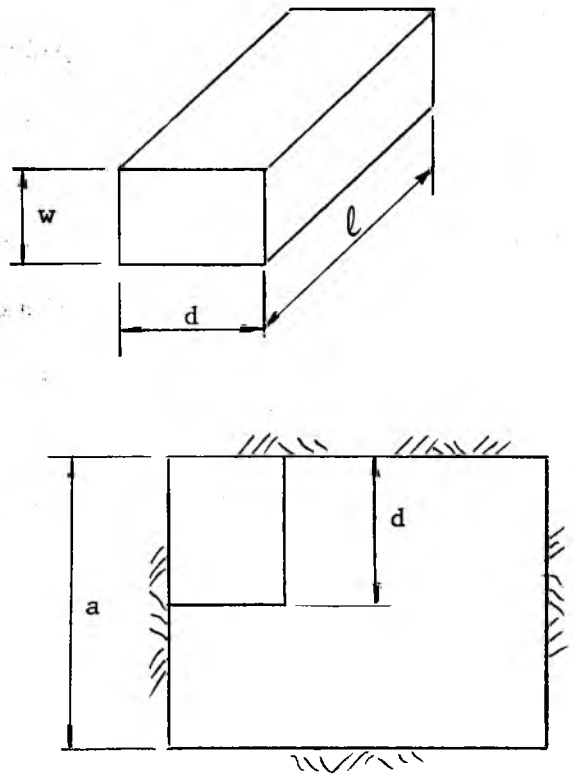

Fig. 154

Cross-section of an ore pass

active outlet, discussed in the section on feeders, applies to ore passes as well as to the other channels. An insight into the behavior of ore in ore pass has been obtained from a study of flow in models. The study was carried out on behalf of the Iron Ore Company of Canada in the process of analyzing 800 foot high and 30 foot diameter ore passes for the Carol Project in Labrador. In order to ensure against obstructions to flow, and to provide storage capacity, it is necessary that the ore flows across the whole horizontal section of the ore pass without piping.

An ore pass with an orthodox outlet is shown in Fig. 156 (a). The vertical channel bends, and flow is controlled, say, by means of chains. At a bend, a channel always tends to narrow down with a narrow pipe extending upward, as shown in the figure. To widen out the channel above the bend, it is necessary to cut a converging channel as shown in Fig. 156 (b). Whether this theoretical shape is practically attainable and can be preserved as ore flows and wears away the walls is another matter. A more positive solution is provided by the split-stream layout, shown in Fig. 157. Here, the ore is drawn along two sides of the channel, two pipes tend to develop and that is sufficient to enforce flow across the whole channel. If one side of the split stream is stopped, Fig. 158, a pipe extends up the ore pass. In the experiment, the ore emptied out of the pipe which remained stable. A white material was fed into the empty pipe to show its extent on the photograph.

In ore pockets, there is a problem of rapid convergence of a

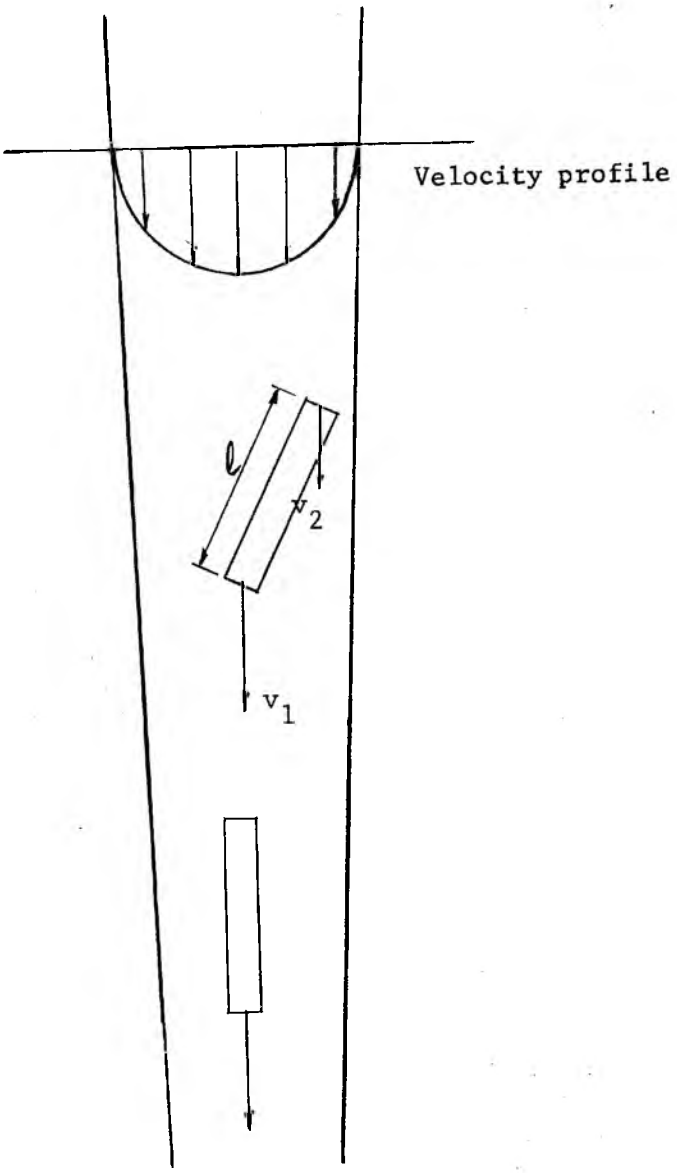

Fig. 155

Alignment of rocks in an ore pass

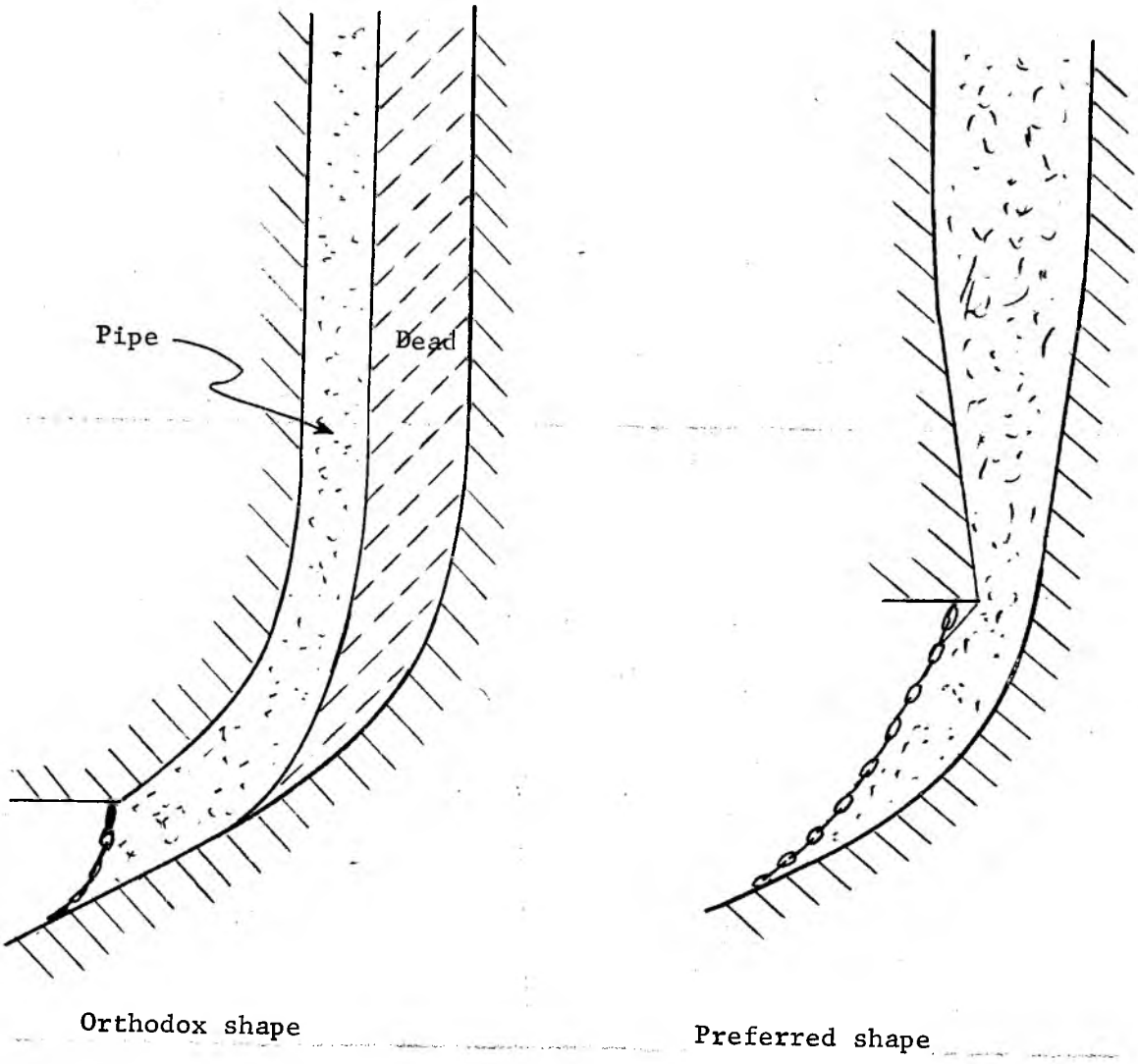

Fig. 156

Outlets of an ore pass

channel toward and within a feeder, as shown in Fig. 159. In this case, a successful operation requires that, at any particular cross-section of the channel, convergence by in one plane only. The walls and the skirts of the ore pocket are so shaped that, within its upper part, flow converges only in plane z - x, in the intermediate part, only in plane y - z, and at the outlet, only in plane x - y. Since the pocket is to handle rock up to a 5 foot intermediate dimension onto a 7 foot apron feeder, it is important that one side wall slopes all the way down to the feeder. This brings the narrow part of the hopper to within the range of action of the feeder and allows it to disturb any large boulders which may tend to interlock.#

Coarse ore (minus 8 inch) which contains fines and a high moisture content is difficult to store and to feed. The difficulties are aggravated when frozen ore is charged into storage and, even more so during fall and spring, when the charged ore is partly thawed out during the day and refreezes in storage at night.

Under these conditions the best solution is to keep as much of the ore as possible in a live, flowing state. The velocities of flow need not be high to prevent the ore from freezing and from consolidation at rest. This solution will be obtained most economically by providing long, active slot-outlets with side-discharge reciprocating feeders, Figures 145 to 147.

The author is indebted to the engineers at Carol who built a model of such an ore pocket, proportioned it for best flow, and demonstrated its advantages. The mining operation is due to start in the summer of 1962.

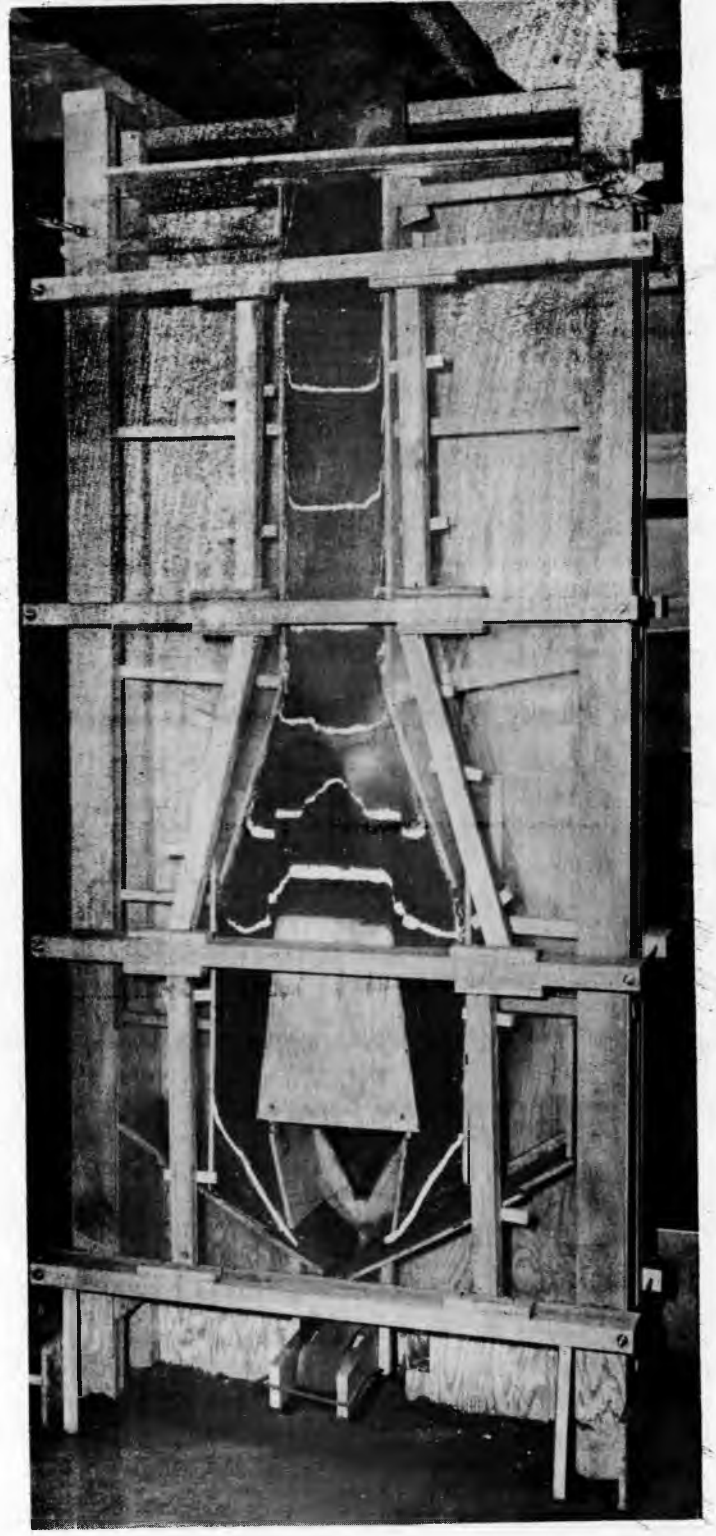

Fig. 157

Model of a split-stream ore pass drawing at both sides

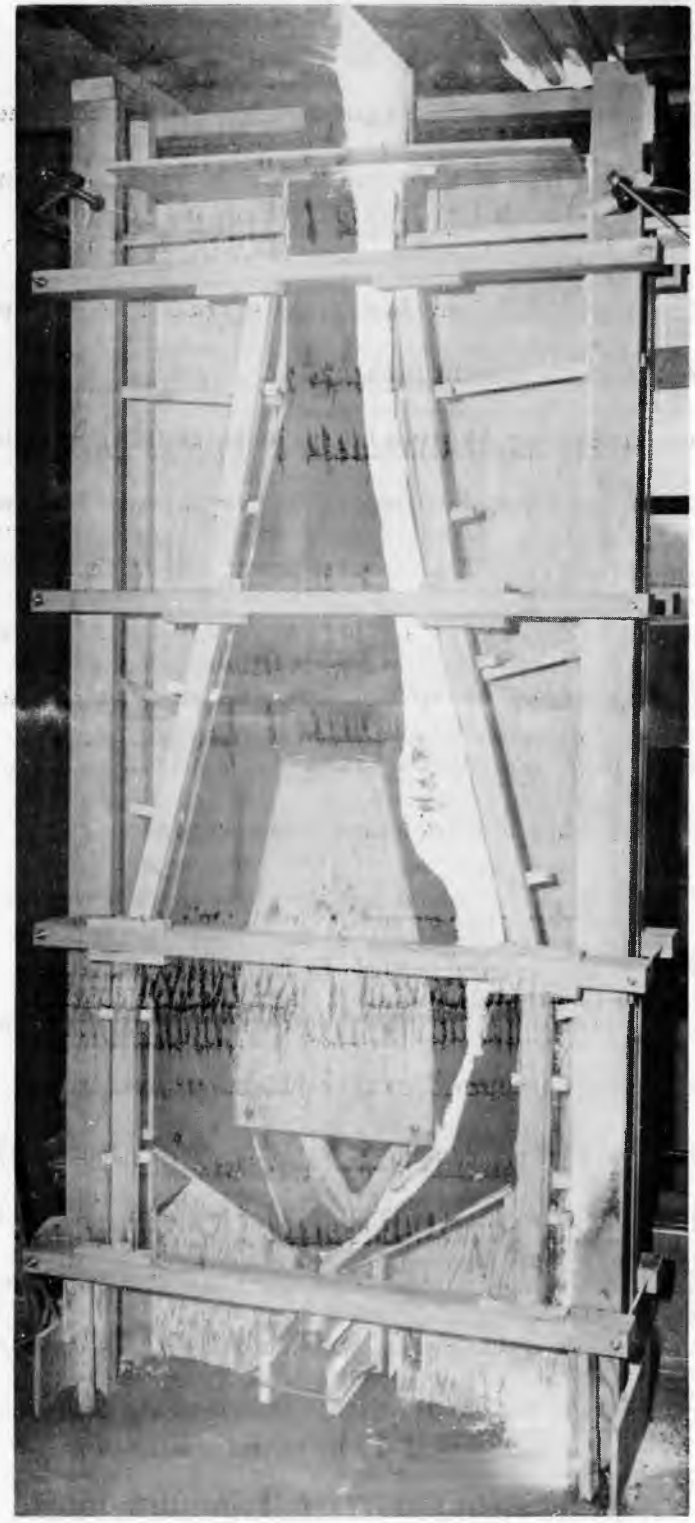

Fig. 158

Piping in a split-stream ore pass drawing on one side only

It should be remembered that, as a coarse ore is charged into storage, the large lumps hit the deposited mass with considerable impact and pack it severely along the trajectory of the falling stream. Unless the ore is free flowing, it is advisable to spread the stream and to distribute the impact over a wide area.

An alternative solution is available when the ore can be screened into a coarse and a fine (say, below 1/2") fraction. The two fractions are then handled separately. The coarse fraction is free flowing and can be stored in flat bottom bins or storage piles and drawn from storage by means of standard reciprocating feeders, apron feeders, or fed directly onto belt conveyors. The fine fraction can be stored in mass flow bins with slot outlets and belt feeders.

Block-caving

In the mining operation of block-caving, a number of draw points is located in tunnels beneath the ore body and a sufficient volume of the ore above the draw points is shattered to cause the whole body to break-up and flow by gravity into the draw points. The ideal flow pattern, which is aimed at, is a uniform drop of the whole ore body without piping. The flow pattern is governed by the location of the draw points, the shape of the crater of the initial shatter, and the sequence of draw.

Considering the flow channel above a draw point, it is evident that the most favorable crater would be a circular cone which would produce a regular channel with weak walls ϕ' and of an included angle $2\theta'$,

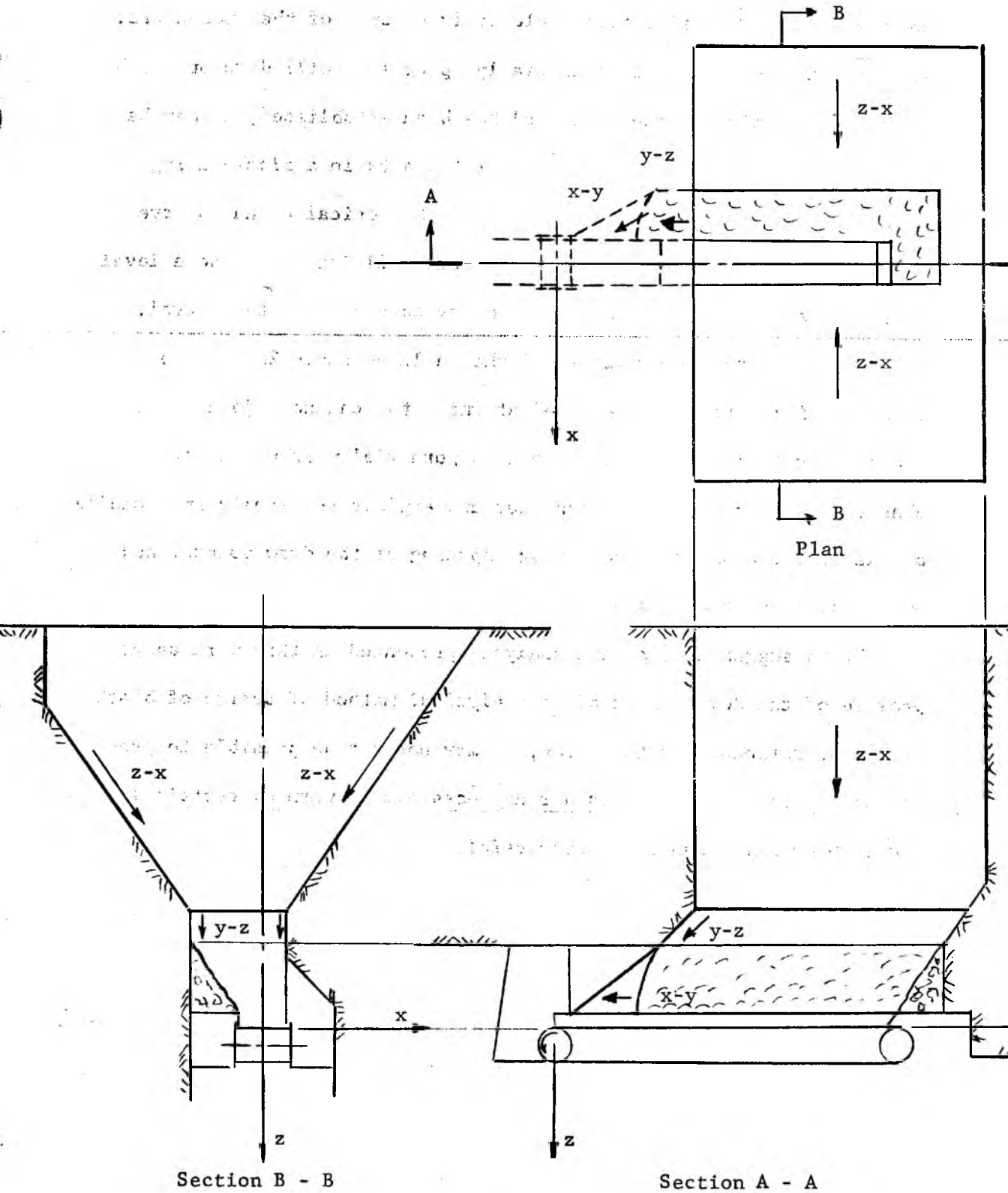

Fig. 159

An ore pocket

appropriate for the effective angle of friction δ of the broken ore. If too much ore is shattered initially, plug flow will develop with inevitable piping. Once a channel has been established, it may be impossible to alter it. Thus, the first blasts in a block-caving operation may decide of its success. If the conical channels have formed above the draw points, the channels will join up at some level within the ore body and uniform flow may obtain above that level. The spacing of the draw points and the included angle $2\theta'$ of the channels will determine the level at which the channels join up. Since every fault in the ore body is a potential weak plane for a channel, it is necessary to consider and exploit the faults in deciding on the most economical location and spacing of the draw points, and on the slope of the channels.

It is suggested that the analysis presented in this work shows promise of the development of an analytical method of design of block-caving operations. At this time, it may not yet be possible to prescribe an optimum layout, but it is already possible to warn of certain layouts and methods which cannot be successful.

REFERENCES

1. Sokolovski, V. V., Theory of Plasticity, Government Printing House of Technical and Theoretical Literature, Moscow, 1946.
2. Prager, W. and Hodge, P. G., Theory of Perfectly Plastic Solids, Wiley, New York, 1951.
3. Hill, R., The Mathematical Theory of Plasticity, Oxford, 1950.
4. Sokolovski, V. V., Prikl. Mat. Mekh., 1950, XIV, 75.
5. Shield, R. T., J. Mech, Phys. Solids, 1955, 3, 246.
6. Von Mises, R., Z. angew. Math. Mech., 1928, 8, 161.
7. Drucker, D. C., Proc. 1st U. S. Nat. Cong. Applied Mechanics, 1951, 487.
8. Haithornthwaite, R. M., J. Soil Mechanics Fndn. Div., Proc. Amer. Soc. Civ. Eng., 1960, 86, 35.
9. Jenike, A. W., and Shield, R. T., J. Appl. Mech., 1959, 81B, 599.
10. Shield, R. T., J. Mech. Phys. Solids, 1955, 4, 10.
11. Drucker, D. C., Gibson, R. E., and Henkel, D. J., Trans. Amer. Soc. Civ. Engr., 1957, 122, 338.
12. Haar, A. and von Karman, Th., Nachr. Ges. Wiss. Göttingen, Math.-Phys., Kl. 1909, 204.
13. DeJosselin DeJong, G., Statics and Kinematics in the Failable Zone of a Granular Material, Uitgeverij, Waltman - Delft, 1959.
14. Jenike, A. W., Elsey, P. J. and Woolley,R. H., Flow Properties of Bulk Solids, Utah Engrg. Exper. Station, University of Utah, Bul. 95, 1958.
15. Sokolovski, V. V., Statics of Soil Media, English translation, Butterworths, London, 1960.

16. Jenike, A. W., Flow of Bulk Solids, Utah Engrg. Exper. Station, University of Utah, Bul. 64, 1954.

17. Jenike, A. W., Chem. Engrg., 1954, 61, 175.

18. Shield, R. T., Quarterly Appl. Math., 1953, XI, 61.

19. Cox, A. D., Eason, H. G. and Hopkins, H. G., Axially-symmetric Plastic Deformations in Soils, A. R. D. E. Report (B) 14/58, Ministry of Supply, Fort Halstead, Kent, England, 1958.

20. Cox, A. D., Axially-symmetric Plastic Deformations in Soils II - Indentation of a Plane Surface by a Circular Cylinder, A. R. D. E. Report (B) 22/59, The War Office, Fort Halstead, Kent, England, 1959.

21. Cox, A. D., Axially-symmetric Plastic Deformations in Soils III - Indentation of Ponderable Soils, A. R. D. E. Report (B) 16/60, The War Office, Fort Halstead, Kent, England, 1960.

22. Jenike, A. W. and Yen Bing Cheng, Slope Stability in Axial Symmetry, Utah Engrg. Exper. Station, Univ. of Utah, Bul. 115, 1962.

23. Johanson, J. R. and Jenike, A. W., Stress and Velocity Fields in Gravity Flow of Bulk Solids, Utah Engrg. Exper. Station, Univ. of Utah, Bul. 116, 1962.

24. Ketchum, M. S., The Design of Walls, Bins and Grain Elevators, Mc-Graw Hill, New York, 1919.

25. Mitchell, D. R., Trans. Amer. Inst. Mining Eng., 1938, 130, 107.

26. J. R. O'Callaghan, J. Agric. Engrg. Research., Wrest Park, Bedfordshire, England, 1959, 4, 200.

27. Colburn, A. P., Industrial and Engineering Chemistry, 1931, 23, 913.

28. Shedd, C. K., Agricultural Engineering, 1951, 32, 493.

29. Shedd, C. K., Agricultural Engineering, 1953, 34, 616.

30. Sinden, A. D., Getting "Difficult" Materials out of Bins", The Amer. Soc. Mech. Engr., paper 61-BSH-8.

31. Jenike, A. W., Elsey, P. J. and Woolley,R. H., Flow of Bulk Solids - Progress Report, Utah Engrg. Exper. Station, Univ. of Utah, Bul. 96, 1959.

32. Jenike, A. W., A Preliminary Study of Segregation, Utah Engrg. Exper. Station, Univ. of Utah, Bul. 107, 1960.

33. Olson R. W., Mechanical Engineering, 1961, 83, 59.